January 2020

Substitution And Oxidation Reactions Of Cyclodiphosph(III)azane Compounds Of The Group 15 Elements

Joseph Tabifor Musongong

SUBSTITUTION AND OXIDATION REACTIONS ON CYCLODIPHOSPH(III)AZANE COMPOUNDS OF THE GROUP 15 ELEMENTS

By

Joseph T. Musongong

Bachelor of Science, University of Dschang, 2003,

Master of Science, University of Yaounde I, 2008.

A dissertation

Submitted to the Graduate School

of the

University of North Dakota

In partial fulfilment of the requirements

for the degree of

Doctor of Philosophy

Grand Forks, North Dakota

May

2020

This dissertation, submitted by Joseph T. Musongong in partial fulfilment of the requirements for the Degree of Doctor of Philosophy from the University of North Dakota, has been read by the Faculty Advisory Committee under whom the work has been done, and is hereby approved.

Dr. Lothar Stahl

Dr. Mark Hoffmann

Dr. Harmon Abrahamson

Dr. Guodong Du

Dr. Edward Kolodka

This dissertation is being submitted by the appointed advisory committee as having met all of the requirements of the Graduate School at the University of North Dakota and is hereby approved.

Chris Nelson

Dean of the Graduate School

Date

PERMISSION

Title **SUBSTITUTION AND OXIDATION REACTIONS ON CYCLODIPHOSPH(III)AZANE COMPOUNDS OF THE GROUP 15 ELEMENTS**

Department Chemistry

Degree Doctor of Philosophy

In presenting this dissertation in partial fulfilment of the requirements for a graduate degree from the University of North Dakota, I agree that the library of this university shall make it freely available for inspection. I further agree that permission for extensive copying for scholarly purposes may be granted by the professor who supervised my dissertation work or, in his absence, by the chairperson of the department or the dean of the Graduate School. It is understood that any copying or publication or other use of this dissertation or part thereof for financial gain shall not be allowed without my written permission. It is also understood that due recognition shall be given to me and to the University of North Dakota in any scholarly use which maybe made of any material in my dissertation.

TABLE OF CONTENTS

TABLE OF FIGURES

LIST OF TABLES

LIST OF SCHEMES

LIST OF SYMBOLS AND ABBREVIATIONS

1. Chemical Symbols and Abbreviations

Ar = Aryl

^{t}Bu = tertiary butyl

Cy = cyclohexyl

E = chalcogen or organic azide

Et = ethyl

HMDS = hexamethyldisilylamide

M = molar

Me = methyl

Ph = phenyl

R = alkyl or aryl

THF = tetrahydrofuran

X = halogen

2 General Symbols and Abbreviations

Å = Angstrom (1×10^{-10} m)

Atm = atmosphere

°C = degree Celsius

d = day

dec = decomposition

Σ = summation

Fw = formula weight

eq. = equivalent

g = gram

h = hour

K = degree Kelvin

μ = bridging

M = metal

mL = milliliter

mmol = millimole

Mp = melting point

R = gas constant (8.314 J/K/mol)

RT = room temperature

s = second

T = temperature

3 Nuclear Magnetic Resonance Symbols and Abbreviations

br = broad

d = doublet

dd = doublet of doublets

dt = doublet of triplets

δ = chemical shift

Hz = hertz (cycles per second)

J = coupling constant

m = multiplet

NMR = nuclear Magnetic Resonance

ppm = parts per million

s = singlet

t = triplet

td = triplet of doublets

{^{1}H} = proton decoupled

4 Infrared Spectroscopic Symbols and Abbreviations

m = medium

s = strong

vs = very strong

vw = very weak

w = weak

5 Crystallographic Symbols and Abbreviations

a = unit cell axis

b = unit cell axis

c = unit cell axis

α = unit cell angle between ***b*** and ***c***

β = unit cell angle between ***a*** and ***c***

γ = unit cell angle between ***a*** and ***b***

λ = wavelength

μ = absorption coefficient

ρ = density

L_P = Lorentz and polarization correction

ORTEP = Oak Ridge Thermal Ellipsoid Program

R = conventional residual factor

V = volume of unit cell

$wR2(F^2)$ = weighted residual factor

Z = number of molecules per unit cell

ACKNOWLEDGEMENTS

My sincere gratitude goes to my advisor, Dr. Stahl, for his relentless efforts and keen supervision in guiding me through my research program. I am equally thankful to Dr. Zeller of the department of Chemistry, Purdue University, for carrying out X-ray studies of some compounds in this dissertation. I am sincerely grateful for the immense technical assistance and feedback from all my graduate committee members.

I would like to extend my profound appreciation to the Graduate School for financial assistance that I received during my stay at UND, in the form of Graduate Teaching Assistant and Tuition Waiver, through the Department of Chemistry. This financial assistance was a big privilege and it enabled me to meet up with my financial challenges and to effectively pursue my research program without hitches.

I am highly indebted to all the staff of the Department of Chemistry at UND for their support and contributions in various forms that provided me with the necessary impetus towards the completion of this work. Special thanks to my former research group member, Dr. Mathew E. Otang, for introducing me to the use of the Schlenk line and other air-sensitive techniques. My deep appreciation also goes to my fellow graduate students for the exchange of ideas and companionship that kept my graduate school experience a memorable one.

Finally, I thank my wife and my entire family for their prayers and love they showed me during my stay at UND.

ABSTRACT

In the first part of this work, the substitution of the chloride ligand on group 15 element bis(*tert*-butylamido)cyclodiphosph(III)azane monochlorides, {[(^{t}BuNP)$_2$(^{t}BuN)$_2$]ECl}, where E = P, As, Sb and Bi, with various monodentate ligands is rerported. The reaction of one equivalent of PhMgCl with {[(^{t}BuNP)$_2$(^{t}BuN)$_2$]ECl}, resulted in the isolation of {[(^{t}BuNP)$_2$(^{t}BuN)$_2$]EPh} **2b** (E = As) or **4b** (E = Bi), while the reaction of LiN(SiMe$_3$)$_2$ with {[(^{t}BuNP)$_2$(^{t}BuN)$_2$]ECl} gave {[(^{t}BuNP)$_2$(^{t}BuN)$_2$]EN(SiMe$_3$)$_2$} **2d** (E = As) or **4d** (E = Bi) in good yields. Compounds {[(^{t}BuNP)$_2$(^{t}BuN)$_2$]AsL} **2c** (L = N_3), **2e** (L = O^{t}Bu) and **2f** (L = OPh) were isolated by treating {[(^{t}BuNP)$_2$(^{t}BuN)$_2$]AsCl} with one equivalent of NaN_3, NaO^{t}Bu and LiOPh, respectively. The non coordinating salt, {[(^{t}BuNP)$_2$(^{t}BuN)$_2$]SbOSO$_2$CF$_3$} **3g**, was isolated by treating AgOSO$_2$CF$_3$ with {[(^{t}BuNP)$_2$(^{t}BuN)$_2$]SbCl} in THF. Similarly, compounds {[(^{t}BuNP)$_2$(^{t}BuN)$_2$]EI} **1h** (E = P), **2h** (E = As) and **3h** (E = Sb) were isolated by treating {[(^{t}BuNP)$_2$(^{t}BuN)$_2$]ECl} with one equivalent of NaI in THF. The structures of **2b**, **2c**, **4d**, **3g**, **1h**, **2h** and **3h** were determined by multi-nuclear NMR spectroscopy and elemental analyses and confirmed by X-ray crystallography.

In the next part of this work, the oxidation of the group 15 element bis(*tert*-butylamido)cyclodiphosph(III)azane compounds to cyclodiphosph(III/V)azane compounds, without elimination, using sulfur and selenium as the oxidizing agent is reported. First, treating {[(^{t}BuNP)$_2$(^{t}BuN)$_2$]EL} with one equivalent of sulfur or selenium furnished the monosulfides or -selenides {[(^{t}BuNP)$_2$(^{t}BuN)$_2$A]EL} **1aSe** (E = P, A = Se, L = Cl), **2aS** (E = As, A = S, L = Cl), **2aSe** (E = As, A = Se, L = Cl) and **2bS** (E = As, A = Se, L = Ph). The treatment of {[(^{t}BuNP)$_2$(^{t}BuN)$_2$]PPh} with one equivalent of selenium gave {[(^{t}BuNP)$_2$(^{t}BuN)$_2$](P=Se)Ph} **1bSe′** in which only the P(III) atom above the P_2N_2 ring is oxidized. Secondly, treating

{[(^{t}BuNP)$_2$(^{t}BuN)$_2$]EL} with two equivalents of sulfur or selenium furnished the disulfides or -selenides, {[(^{t}BuNP=A)$_2$(^{t}BuN)$_2$]EL} **1aSe$_2$** (E = P, A = Se, L = Cl), **2aS$_2$** (E = As, A = S, L = Cl), **2aSe$_2$** (E =As, A = Se, L = Cl), **2bS$_2$** (E = As, A = S, L = Ph), **2bSe$_2$** (E = As, A = Se, L = Ph), **2cSe$_2$** (E = As, A = Se, L = N_3), **3aS$_2$** (E = Sb, A = S, L = Cl), **3bS$_2$** (E = Sb, A = S, L = Ph), **3bSe$_2$** (E = Sb, A = Se, L = Ph), **3cS$_2$** (E = Sb, A = S, L = N_3) and **3cSe$_2$** (E = Sb, A = Se, L = N_3). These compounds were characterized by X-ray crystallography, multi-nuclear NMR spectroscopy and elemental analyses.

The third part of this dissertation covers the oxidation of {[(^{t}BuNP)$_2$(^{t}BuN)$_2$]PL} (L = Cl or Ph) with selenium, in which the post-oxidation product shows the elimination of a molecule, ^{t}BuCl or isobutene. When {[(^{t}BuNP)$_2$(^{t}BuN)$_2$]PCl} and excess selenium were refluxed in toluene {[(^{t}BuNP=Se)$_2$(NH)$_2$(N^{t}Bu(H)P=Se)]} **1aSe$_2$Se′** was obtained with the elimination of ^{t}BuCl and the attachment of NH^{t}Bu group to the P(V) atom above the P_2N_2 ring and all the P(III) atoms being oxidized to P(V) atoms. On the other hand, when {[(^{t}BuNP)$_2$(^{t}BuN)$_2$]PPh} and excess selenium were heated at high temperatures, {[(^{t}BuNP=Se)$_2$(NH)$_2$](P=Se)Ph} **1bSe$_2$Se′** was isolated in which the *tert*-butyl groups on the amino nitrogen atoms are eliminated. The structures of **1aSe$_2$Se′** and **1bSe$_2$Se′** were determined by multi-nuclear NMR spectroscopy and elemental analyses and confirmed by single crystal X-ray analyses.

The final part of this work describes the syntheses and characterization of compounds derived from the reaction of *cis*-[(^{t}BuNP)$_2$(RNLi·thf)$_2$] (R = Cy or ^{t}Bu) with $AsCl_3$, $SbCl_3$ and $PhPCl_2$. The reaction of *cis*-[(^{t}BuNP)$_2$(RNLi·thf)$_2$] with the above electrophiles gave compounds {[(^{t}BuNP)$_2$(CyN)$_2$]ECl} **2aCy** (E = As), **3aCy** (E = Sb) and {[(^{t}BuNP)$_2$(^{t}BuNP)$_2$]Ph_2Cl_2} **1ab**. When **1ab** was refluxed with magnesium powder, compound [(^{t}BuNP)$_2$(^{t}BuN)$_2$]P_2Ph_2 **1bb** was

obtained. These compounds were characterized by X-ray, multi-nuclear NMR spectroscopy and elemental analyses.

CHAPTER I

GENERAL INTRODUCTION

1. BACKGROUND TO CYCLODIPHOPHAZANES

Amines and phosphines are well-established ligands in coordination chemistry.[1–3] Amines, which are harder bases form a great variety of compounds both as anions and neutral molecules with elements across the periodic table.[4–6] On the other hand, the softer phosphines are widely used as neutral monodentate ligands to stabilize a broad range of oxidation states and to promote important catalytic reactions, where oxidation/reduction cycling of the metal occurs in the reaction.[7] In phosphorus-nitrogen compounds, where phosphorus and nitrogen are linked by a direct bond, in their neutral form, metals are coordinated exclusively through phosphorus.[1]

There exists a plethora of compounds in the literature with P–N single bonds and P=N double bonds, but in most cases the molecules are oligomeric or polymeric.[6] Phosphazenes, cyclic and acyclic, contain a P=N double bond and serve as precursors for P–N polymers and hybrid materials.[6, 8–12] Cyclodiphosphazene is a planar molecule with a P–N bond distance of 1.65 Å, indicative of a delocalized π-bond system.[13, 14] The trimeric and tetrameric are the most studied cyclophosphazenes,[15] although larger polymers have also been characterized (Figure 1).[6, 8, 9]

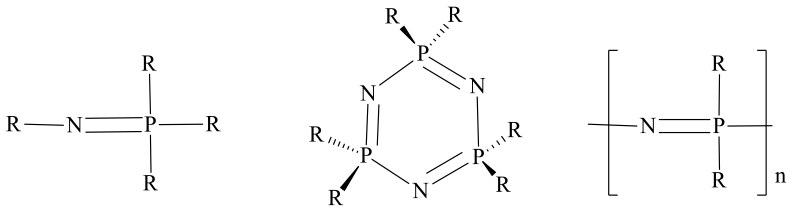

Figure 1. Formulas of linear (**A**), cyclic (**B**) and (**C**) phosphazenes.

Phosphazanes by contrast, both cyclic and acyclic, contain P–N single bonds, with phosphorus and nitrogen atoms formally in their trivalent state.[6, 16] Cyclodiphosphazane is a saturated inorganic ring system with alternating nitrogen and P(III) atoms, with a rigid and almost planar framework **D**.[9, 17–39] Only one of the phosphorus substituents and the lone pair show some degree of flexibility.

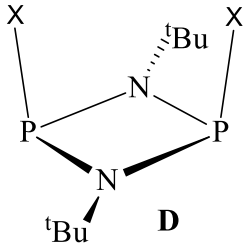

D

X = N-alkyl, N-aryl, chloride
R = alkyl, aryl

Figure 2. Structure of a cyclodiphosphazane (**D**).

First reported in the 19th century[12, 40, 41] by Michaelis and Schroeter, this compound was not fully characterized until the 1960s and the verification of the central $(P–N)_2$ ring by X-ray studies was carried out as late as 1971.[42, 43] This aroused much interest into the chemistry of cyclodiphosphazanes due to the potential application of the saturated P_2N_2 framework as building blocks for the design of a variety of cages, clusters and macrocycles with main group or transition metal centers.[16, 18–22, 25–27, 29–39, 44–70] The coordination behavior of cyclodiphosphazane, both as neutral and anionic ligand towards both main group[66, 71–75] and transition metals[9, 37, 76] is another captivating feature of this compound. Besides, cyclodiphosphazane derivatives have been employed in homogenous catalysis,[35, 54, 56, 70] antitumor studies,[19, 67, 77] in metal organic frameworks to form even sodalite type structures,[78] as well as in the isolation of stable biradicaloids with a rich chemistry.[79–81] Recently, a carbene[82, 83] was synthesized by Wright *et al*. based on cyclodiphosphazanes, underscoring the versatility of cyclodiphosphazane scaffolds in the design of hybrid materials.

Bis(1°-amino)cyclodiphosph(III)azanes are the product of the formal [2 + 2] cycloaddition of amino(imino)phosphines or aminophosphazenes (R(H)P=NR).[45] Their structures are characterized by a central four-membered ring of alternating trivalent phosphorus atoms and nitrogen atoms, with each atom bearing an exocyclic substituent.[9, 45] The substituents on the nitrogen atoms lie approximately in the plane of the ring, while those of the phosphorus atoms (amino-substituents) are orthogonal to it. The arrangement of the substituents gives the molecule an approximate bowl-shaped structure. These compounds exist in *cis*- and *trans*-isomeric forms with a small energy difference, but in the solid state, the thermodynamically preferred *cis* isomer is almost exclusively isolated.[9] Aminocyclodiphosphazanes are neutral molecules of the form **E** which can be deprotonated by a strong base like n-butyllithium to give a dianionic amidocyclodiphosphazanes $\mathbf{E}^{2-}$ (Figure 3).[1]

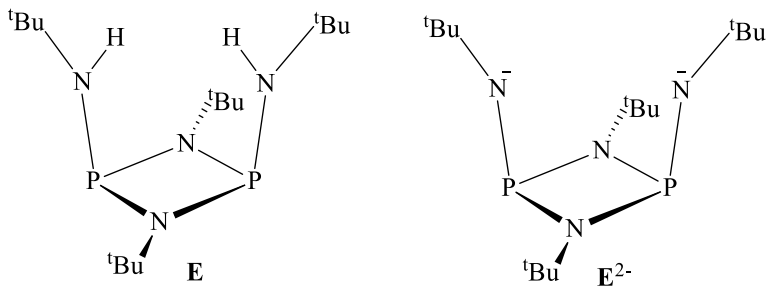

Figure 3. Structure of neutral (**E**) and dianionic ($\mathbf{E}^{2-}$) amidocyclodiphosphazane.

The dianion can serve as a chelating diamide ligand supported by a cyclodiphosph(III)azane base. Their flexible bite angle and multidentate nature make them ideal ligands for main-group- and transition-metals alike. Bis(amino)cyclodiphosph(III)azanes have a trivalent phosphorus in the P_2N_2 heterocycle while bis(amino)cyclodiphosph(V)azane contain P(V) atoms.[9]

2. LITERATURE REVIEW

2.1 Syntheses of Bis(amino)cyclodiphosph(III)azanes

2.1.1 Reactions of Phosphorus(III) Chloride with Primary Amines

This is the first and easiest method for synthesizing symmetrically-monosubstituted bis(amino)cyclodiphosph(III)azanes. It entails the reaction of two molecules of PCl_3 and five-fold excess of a primary amine (Scheme 1).[9, 12, 41] The amine in excess serves as a base to remove hydrogen chloride generated during the reaction. When tris(diethylamino)phosphine or PCl_3 is treated with aniline, the compound **2** is obtained[8, 45] with good yields.

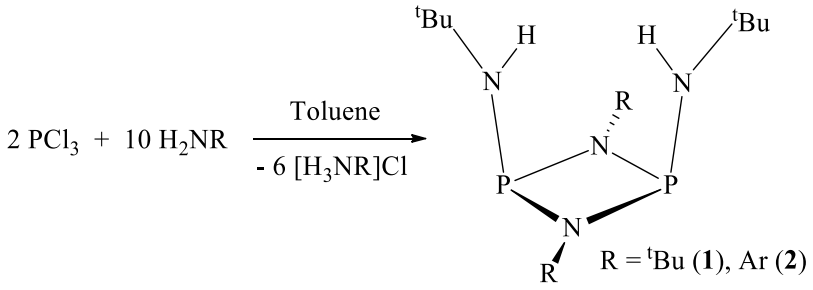

Scheme 1. Syntheses of **1** and **2**.

2.1.2 Reaction of Phosphorus Trichloride with a Primary Amine in the Presence of Triethylamine

Hetero-substituted bis(amino)cyclodiphosph(III)azanes are difficult to synthesize using the above method, so alternative methods have been devised. One efficient method for this synthesis was first advanced by Moser *et al*. (Scheme 2).[63]

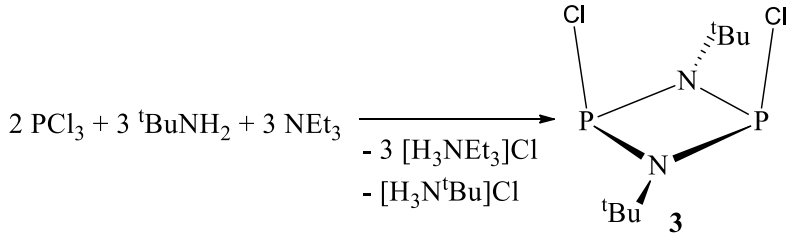

Scheme 2. Synthesis of **3**.

In the absence of a base, PCl_3 can be treated with three-fold excess of the corresponding primary amine to obtain $Cl_2P_2N_2R_2$ (Scheme 3).[30, 84]

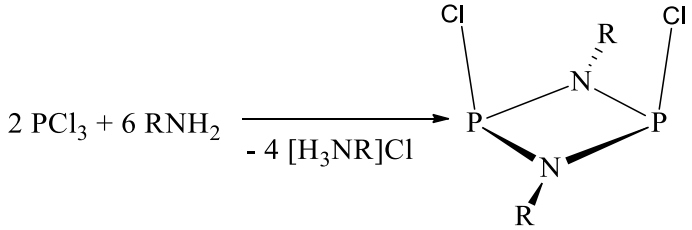

R = alkyl (**4**), aryl (**5**)

Scheme 3. Syntheses of **4** and **5**.

Trimethylsilyl substituted aminodichlorophosphanes, $RN(SiMe_3)PCl_2$ have been used recently by Schultz *et al*. to prepare chlorodiphosphazanes in a one-step reaction. With this method electron-rich, electron-poor, aryl, silyl and disilylamino derivatives are obtained in moderate to good yields (Scheme 4).[23, 69]

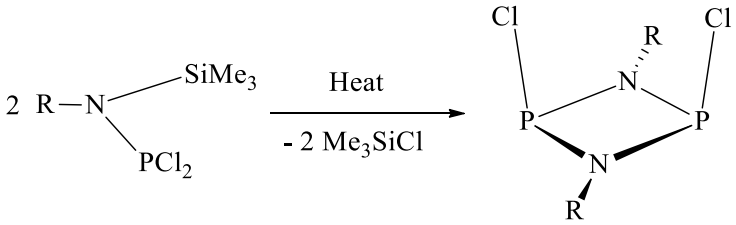

R = $N(SiMe_3)_2$ (**6**), $SiMe_3$ (**7**), 2,6-$^{i}Pr_2C_6H_3$ (**8**), 2,6-$Me_2C_6H_3$ (**9**), 2,4,6-$^{t}Bu_3C_6H_2$ (**10**), CPh_3 (**11**), *p*-tosyl (**12**)

Scheme 4. Syntheses of **6**, **7**, **8**, **9**, **10**, **11** and **12**.

Replacements of the chlorine atoms of dichlorocyclodiphosph(III)azanes with amino groups can be achieved through two principal methods. First, treatment of the dichlorocyclodiphosph(III)azane with two equivalents of a primary amine and two equivalents of trimethylamine. This method is suitable for acidic amines like pyrazoles and anilines, where 1,3-di-*tert*-butyl-*cis*-2,4-dianilinocyclodiphosph(III)azane is obtained in the latter (Scheme 5). Similarly, a wide variety of aromatic amines can be used for the ring substitution.

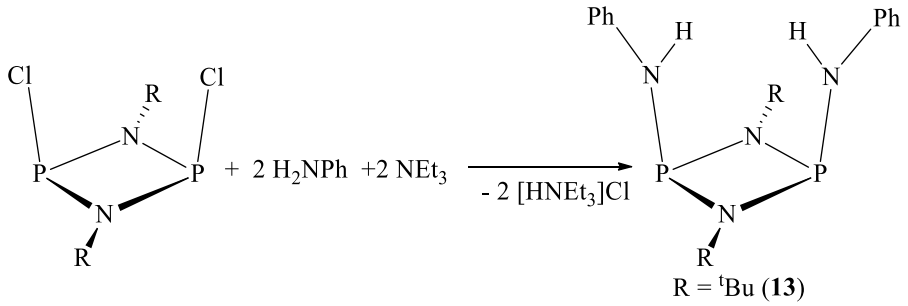

Scheme 5. Synthesis of **13**.

Secondly, a more general method of ring substitution is the treatment of dichlorocyclodiphosph(III)azane with two equivalents of the corresponding lithium amide. Although an additional step is necessary, the cleanest products are obtained using this method (Scheme 6).[45, 63]

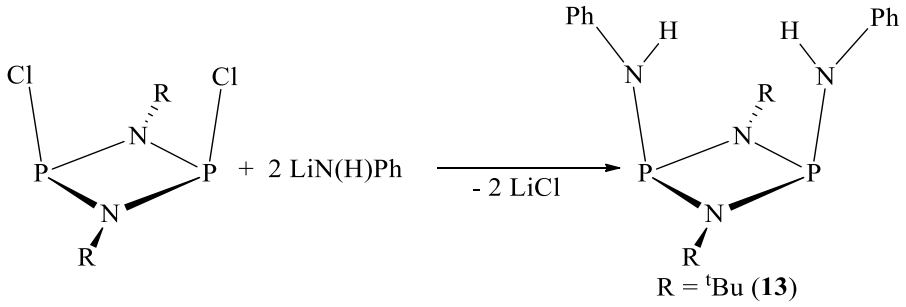

Scheme 6. Synthesis of **13**.

By appropriate stoichiometric adjustments, asymmetrically heterosubstituted bis(amido)cyclodiphosph(III)azanes can be prepared in a one-step reaction (Scheme 7).[9]

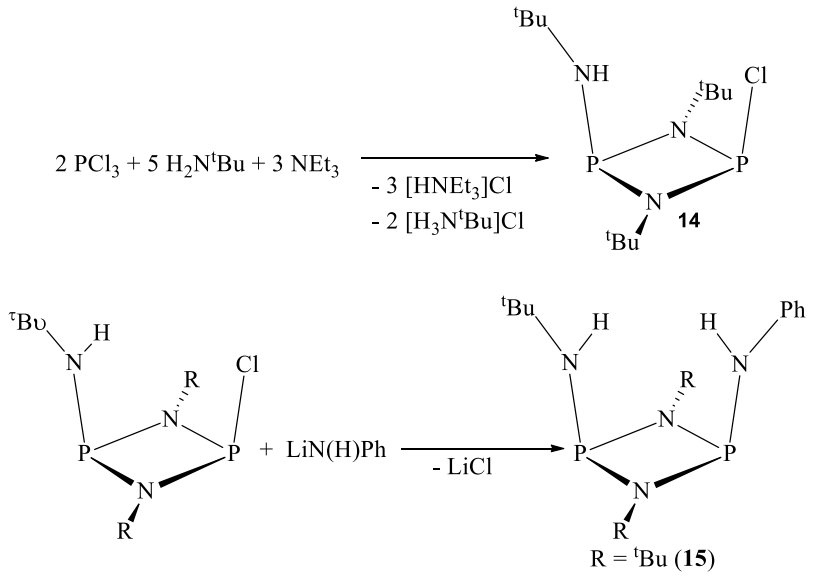

Scheme 7. Synthesis of **14** and **15**.

2.2 Synthesis of Bis(amino)cyclodiphosph(V)azane

There are several ways by which bis(amino)cyclodiphosph(V/V)azanes can be synthesized. Three of these synthetic routes are quite distinct and have been frequently used.

2.2.1 Oxidation of bis(amino)cyclodiphosph(III)azanes

The two ring phosphorus(III) centers in cyclodiphosph(III)azanes are easily oxidized to the corresponding P(V)/P(V) ring system by the chalcogens (O, S, Se and Te) and organic azides (E = NR).[22, 25, 27, 30, 32, 39, 47, 64, 71, 74, 75, 85–88] This oxidation occurs through an S_N2 attack on the oxidizing agent by the lone pair of electrons on the phosphorus, resulting in a retention of configuration at the phosphorus center.[66, 88–90] Exclusively, the *cis*-cyclodiphosph(III/III)azanes are oxidized to the *cis*-cyclodiphosph(V/V)azanes and the *trans*-cyclodiphosph(III/III)azane to the *trans*-cyclodiphosph(V/V)azanes (Scheme 8).

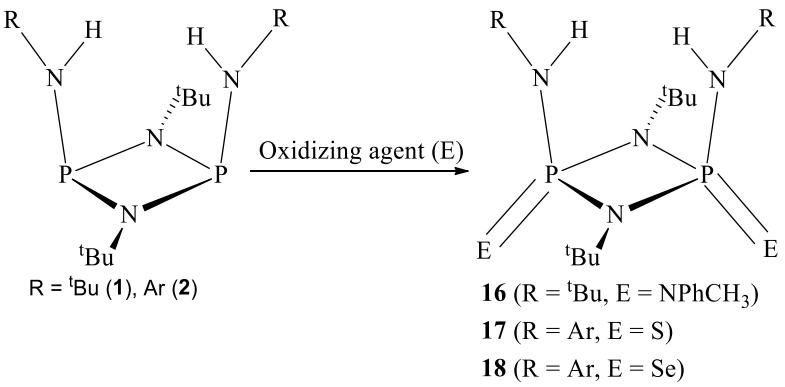

Scheme 8. Syntheses of **16**, **17**, and **18**.

A set of air-stable cyclodiphosph(V/V)azane derivatives has been reported from a single cyclodiphosph(III/III)azane precursor. These cyclodiphosph(V/V)azane derivatives, ([R′(E)P(μ–NR)]$_2$, R′ = amide group) serve as ligands for main group and transition metals with enhanced stability.

2.2.2 Thermolysis (condensation) of tris(amino)phosphates

Bis(amino)cyclodiphosph(V)azanes are obtained via direct condensation by heating tris(amino)phosphates (Scheme 9) and tris(amino)thiophosphates.[66, 91]

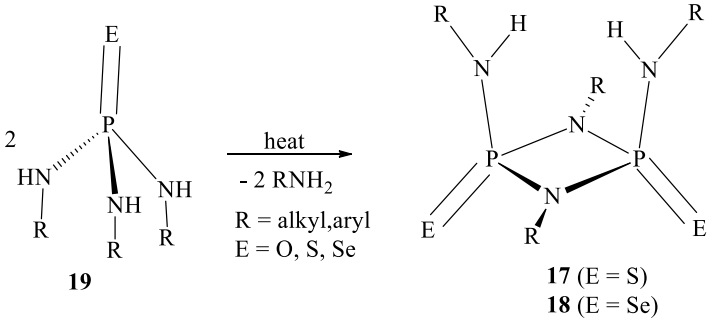

Scheme 9. Syntheses of **17** and **18** by thermolysis.

2.2.3 Condensation/substitution

In this method, trichlorophosphine chalcogenide is condensed with a primary amine *in situ*, and the reaction mixture is then heated to afford a mixture of the tri(amino)thiophosphates and the desired bis(amino)cyclodiphosph(V)azanes at lower temperatures (Scheme 10).[66]

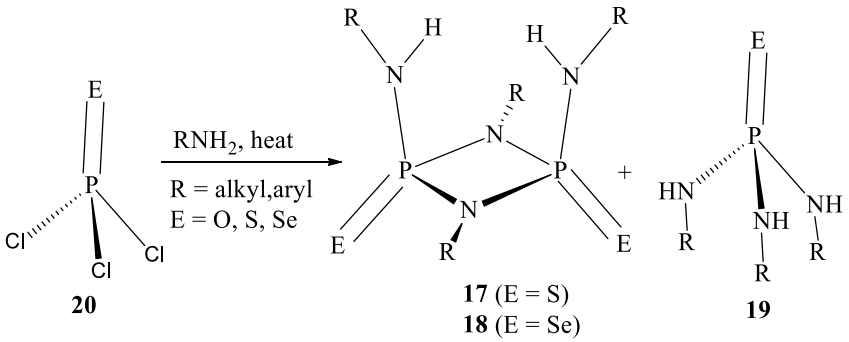

Scheme 10. Syntheses of **17** and **18** by thermolysis.

2.3 Synthetic Methods for Metal Complexes of Bis(amino)cyclodiphosph(V)azanes

The principal methods employed in the syntheses for metal complexes of bis(amino)cyclodiphosph(V)azanes are metalation, methathesis, aminolysis, and oxidation.

2.3.1 Metallation

This method involves the deprotonation of the ligand with a reactive organometallic compound, and a metal amide, or metal alkoxide reagent (Scheme 11).[24, 63, 66, 86]Although this method is most often used for the preparation of alkali-metal salts, it can also be employed for zinc or aluminum derivatives.[64]

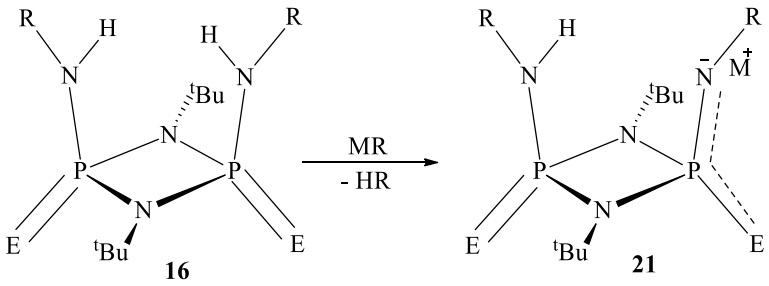

Scheme 11. Synthesis of **21** by metalation.

2.3.2 Metathesis

This involves the reaction between an anionic ligand, as an alkali metal salt and a metal halide. Transition metal complexes are typically synthesized through this method (Scheme 12).[45,

[59, 87, 92, 93] In complex **23**, the Ni^{2+} ion in the bis(*N,S*)-chelated complex is in a tetrahedral environment and exhibits paramagnetic properties.

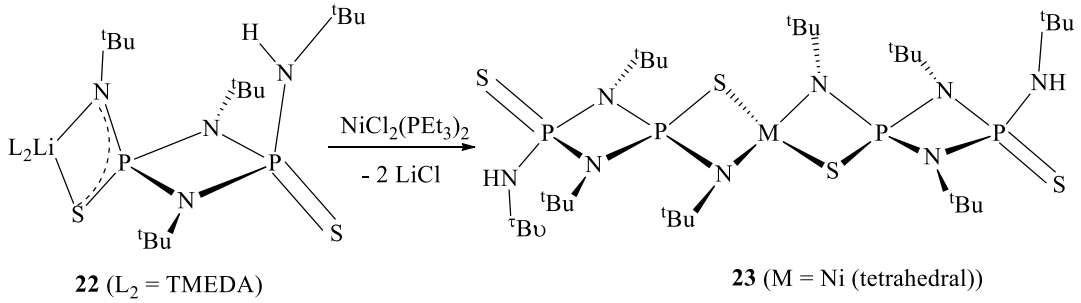

22 (L_2 = TMEDA) **23** (M = Ni (tetrahedral))

Scheme 12. Synthesis of **23** by methathesis.

2.3.3 Aminolysis

In aminolysis a neutral ligand reacts with a metal/element halide and a weak base, where the weak base serves as a proton scavenger (Scheme 13).[47, 54, 63, 87]

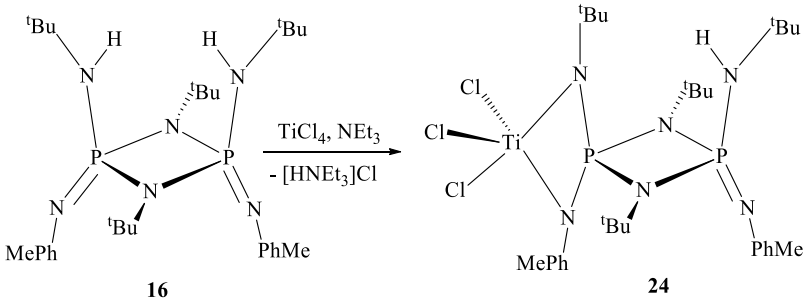

16 **24**

Scheme 13. Synthesis of **24** by aminolysis.

1.3.4 Oxidation

Treating the cyclodiphosph(III/III)azane metal complex with the chalcogens (O, S, Se and Te) or organic azides oxidize the P(III) system to the P(V) system. The coordination mode of the ligand is not altered by the oxidation (Scheme 14).[94]

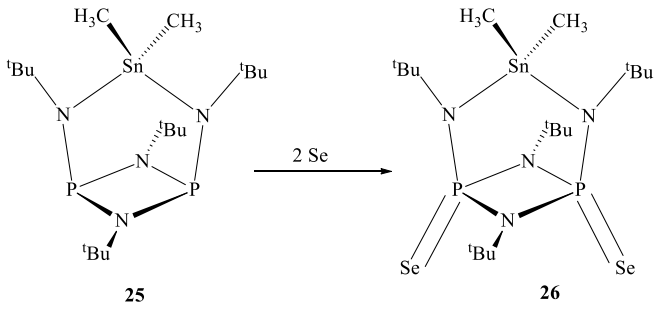

25 26

Scheme 14. Synthesis of **26** by oxidation.

2.4 Application of Cyclodiphosphazanes

Although much work has been done to elucidate the structural, electronic and spectroscopic properties of cyclodiphosphazanes, the catalytic properties and other applications are yet to be fully exploited.

2.4.1 Polymerization of Ethene

When Stahl *et al*.[63]first reported the metal complexes of bis(amido)cyclodiphosphazanes, several group 4 metal complexes of the type [{RNPN^{t}Bu}$_2$Me$_2$] were synthesized some years later and employed in the polymerization of ethene.[54–56, 70, 93, 95] Using methylaluminoxane (MAO) or B(C_6F_5)$_3$ for generating activated species, moderate success was achieved. The catalytic activity and stability of catalysts were found to be greatly influenced by the amido-nitrogen substituents. While bulky substituents have the advantage of preventing the degradation of the catalyst by shielding the metal center from side reactions, and thus enhancing the turnover frequency, they moderately reduced the catalytic efficiency. Titanium complexes produced linear polyethylene with activities of about 2.6 x 10^6 g mol_{cat}^{-1} with the highest activity shown by the N^{t}Bu derivative (231 kg polyethylene mol_{cat}^{-1} bar^{-1} h^{-1}).[69]

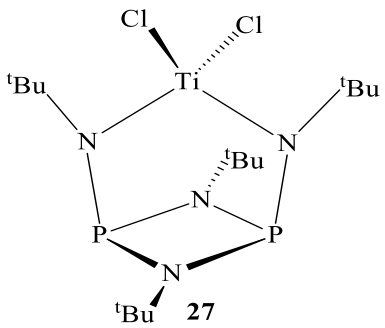

27

Figure 4. Complex of bis(amido)cyclodiphosphazane, **27**.

2.4.1 Scaffolds for Building Clusters, Cages and Macrocycles

Main group inorganic macrocycles, cages and clusters based on *p*-block element backbones other than carbon, are quite challenging to synthesize due to the inherent problems of weaker and more polar bonds present.[25, 29, 58, 61] However, there has been a surging interest, of late, in the application of cyclodiphosphazanes in the synthesis of a wide range of inorganic clusters, cages and macrocycles with both main group and transition elements incorporated. The rigid nature of the P_2N_2 ring of bis(chloro)cyclodiphosphazanes, $[ClP(\mu\text{-}N^tBu)]_2$, coupled with the *cis*-orientation and high reactivity of the P–Cl bond makes this compound a unique building block for P/N macrocycles.[16, 26, 31, 33, 38, 53, 57, 62, 68, 71, 83] Although both *cis*- and *trans*-conformers are present in solution, the *cis*- conformer offers an immediate advantage for building macrocycles by providing favorable pre-orientation for the formation of cyclic structures. Wright *et al*. converted the electrophilic building block, $[ClP(\mu\text{-}N^tBu)]_2$, into nucleophilic building blocks by substitution with H_2O or NH_3, which then reacted with $[ClP(\mu\text{-}N^tBu)]_2$ in a single step to give the corresponding phosph(III)azane macrocycle.[96] A recent development provides a highly versatile approach to hexameric S- or Se-bridged macrocycles containing $(P^{III}/P^V)_2$ backbones and involves the *in situ* formation of the P^V dianions, $[S(E)P(\mu\text{-}N^tBu)]_2^{2-}$ (E = S or Se), from the unstable S-precursor followed by the final cyclization with $[ClP(\mu\text{-}N^tBu)]_2$. The mixed

chalcogenide dianion $[S(Se)P(\mu\text{-}N^tBu)]_2^{2-}$ reacts with $[ClP(\mu\text{-}N^tBu)]_2$ to form the Se-bridged macrocycle $[\{(S{=})P^V([(\mu\text{-}N^tBu)_2(\mu\text{-}Se)_2\{P^{III}(\mu\text{-}N^tBu)\}_2]_3$ instead of the S-bridged alternative, suggesting that steric bulk at the periphery of the macrocycle is a remarkable factor determining the preference for bridging atom within the core.[25, 96, 97] These macrocycles are capable of hosting neutral and ionic molecules in their cavities, similar to crown ethers, calixarenes, cryptands and porphyrins.[53] These metallamacrocycles are essential supramolecular structures that are applicable in gas storage, catalysis, sensors and molecular electronics.[69]

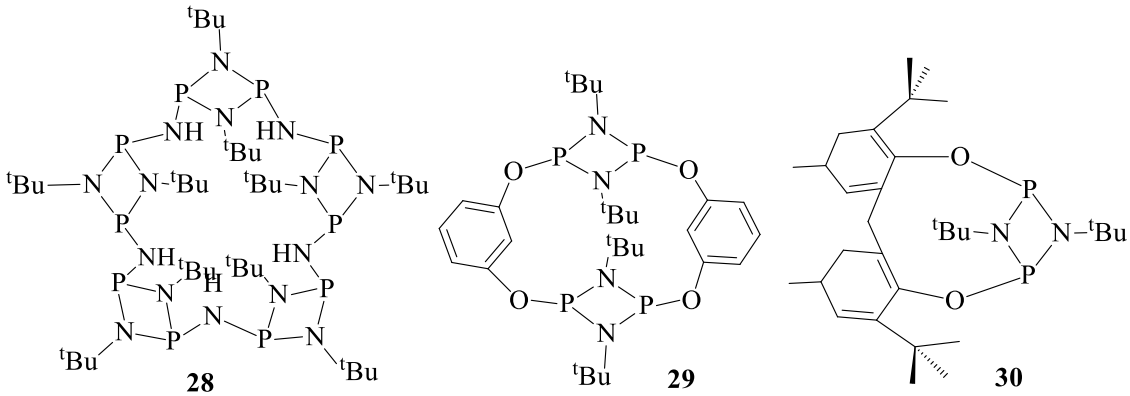

Figure 5. Macrocycles **28**, **29** and 3**0** Based on Cyclodiphosphazanes.

2.4.2 Other Applications of Cyclodiphosphazanes

The versatility of cyclodiphosphazanes makes them suitable for a variety of applications, ranging from medicine,[19, 67, 69, 77, 98] catalysis, to material science.[16, 26, 31, 32, 36, 38, 53, 57, 62, 71, 83] Some dicopper and gold(I) complexes of cyclodiphosphazanes have antiproliferation properties towards cancer cells, while cyclodiphosphazane complexes of Rh and Pd are now being employed in the Suzuki–Muyaura carbon–carbon cross coupling and hydrogenation reactions.[35, 38] Recently, chiral cyclodiphosphazane derivatives containing binol, vanol, vapol and menthol have been synthesized and their catalytic properties studied.[46] Cyclodiphosphazanes with rigid planar structures and moderately stable P–N bonds can serve as 2-connected linkers in metal

organic frameworks.[78] The interested reader on the various applications of cyclodiphosphazanes should consult the relevant references cited herein.

2.5 Cyclodiphosph(III/V)azanes as Versatile Ligands

When compound **E** is deprotonated with ^{n}BuLi,[24] the resulting dilithium salt is an excellent transfer reagent for the ligand to group 4 metals (Zr, Hf) and even main group elements.[47, 63, 98] The reagent has been successfully employed in the synthesis of cyclodiphosph(III)azane compounds of transition metals and main group elements in which the metal or the element is centered above the P_2N_2 ring in a κ^2N,N' chelation mode. Stahl *et al*. treated the above mentioned dilithium salt with MCl_4 (M = Zr, Hf) and ECl_3 (E = P, As, Sb, Bi) to obtain the first cyclodiphosph(III)azane compounds of the group 4 and 15 elements as the dichlorides, $[(^{t}BuNP)_2(^{t}BuN)_2]MCl_2$,[47, 63] and monochlorides, $[(^{t}BuNP)_2(^{t}BuN)_2]ECl$,[92, 98] respectively. These complexes can further be derivatized by substituting the chlorine atom on the newly introduced metal (element) with monodentate ligands, or by oxidizing the central group 15 element above the P_2N_2 heterocycle or the P(III) atoms bearing a lone pair of electrons (Figure 6).

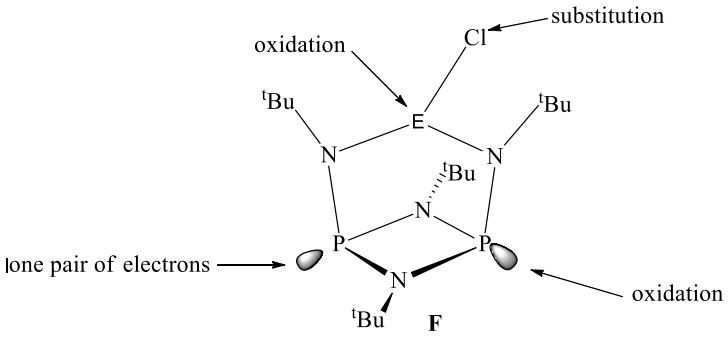

Figure 6. Oxidation and substitution sites in compound **F**.

While the cyclodiphosph(III)azane compounds of the group 4 elements (Zr, Hf) are very active catalysts for ethylene polymerization, the ligand is easily degraded due to complex cations

and cocatalyst coordinating with the lone pair of electrons on the P(III) atoms[93] since the polymerization environment is very Lewis-acidic. To circumvent these unwanted reactions, the P(III) atoms in the ligand are first oxidized with ^{t}BuOOH, S_8 or Se to the corresponding cyclodiphosph(V)azane ligand before deprotonation.[87] Bis(*tert*-butylamino)cyclodiphosph(V)azanes are more acidic than their P(III) analogues.[93] This means that they can be easily deprotonated at RT and below by strong bases. The resulting mono- and dinuclear main group and transition metal complexes of these ligands show a great variety of coordination modes (Figure 7).[47, 74, 85, 87] The κ^2N,N' chelation mode is not achieved when the phosphorus atoms of this ligand are oxidized before deprotonation.

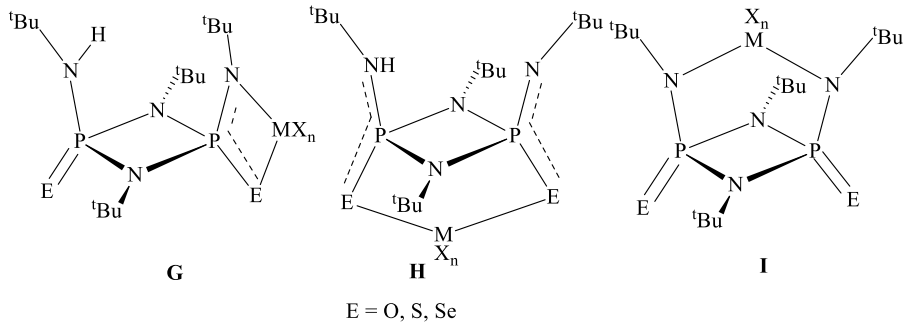

Figure 7. Selected binding modes of bis(amido)cyclodiphosph(V)azanes.

In a number of cases, one or both metal centers were chelated between the exocyclic nitrogen and the chalcogen atom of the cyclodiphosph(V)azanes in a κN, κE fashion (**G**). Soft metal centers preferred the κ^2E, E' coordination (**H**), while other metal ions exhibited a combination of the two.[93] Chivers *et al*. have shown that when cyclodiphosph(III)azanes are first oxidized with the chalcogens to cyclodiphosph(V)azanes before deprotonation, the preferred binding sites are N,E for small ions like Li^+, N,N' and E,E' for the larger alkali metal ions like Na^+ and K^+.[74, 87] These coordination modes offer the possibility of generating metal-containing polymers.

In order to synthesize cyclodiphosph(V)azane complexes of the group 4 elements, in which the metal is chelated in κ^2N,N' fashion (**I**), Otang *et al*. oxidized the P(III) atoms to P(V) of the post-chelation product, $[(^tBuNP)_2(^tBuN)_2]MCl_2$, using excess sulfur.[93] They later extended this idea to the cyclodiphosph(III)azane compounds of the group15 elements by refluxing a mixture of $[(^tBuNP)_2(^tBuN)_2]PCl$ and excess sulfur in toluene. A ^{t}BuCl group was eliminated and the ensuing product was a symmetrical phosphorus(V) nitride compound, whose ^{1}H NMR and $^{31}P\{^1H\}$ NMR spectra depict only a singlet compared to that of the precursor.[93, 99] The structure of this compound is analogous to that of $[(^tBuNP)_2(^tBuN)_2]P^+OSO_2CF_3^-$, which reveals a singlet in the $^{31}P\{^1H\}$ NMR spectra as well.[99] Furthermore, it has been reported that C–N bonds are cleaved to form N–H bonds and a molecule of isobutene when the compound $[\{P(\mu\text{-}N^tBu)\}_2(\mu\text{-}N^tBu)_2]_2$ was oxidized by selenium to $P_4(\mu\text{-}N^tBu)_6Se_4$,[100, 101] an observation that has been attributed to steric congestion.

Spurred by these findings, we decided to extend this study to the cyclodiphosph(III)azane compounds of the group 15 elements. First, we wanted to find out whether we can selectively oxidize the group 15 element above the P_2N_2 heterocycle bearing a lone pair of electrons with sulfur and selenium. Secondly, we were interested in understanding the influence of the various monodentate ligands during the oxidation of the group 15 elements by sulfur and selenium and finally, we were curious to know whether elimination of small molecules and molecular rearrangement is possible when these oxidations are carried out at elevated temperatures. To achieve the above objectives, we started by synthesizing more substrates. The chloride ligand on the compounds $[(^tBuNP)_2(^tBuN)_2]ECl$ (E = P, As, Sb, Bi) was first substituted with a variety of monodentate ligands (HMDS, Ph, N_3, O^{t}Bu, OPh, I, OTf). While some of these compounds (E = P, Sb) have already been synthesized and characterized, those of arsenic and bismuth have not

been reported. We therefore synhesized those of arsenic and bismuth to ensure a greater substrate variety of molecules for our studies.

3. Scope of Dissertation

In this work we investigated the substitution and oxidation reactions of cyclodiphosph(III)azane compounds of the group 15 elements. This dissertation is divided into five chapters. In Chapter I, a general introduction is provided and related literature is reviewed. In the next three chapters, the main topics of this dissertation– substitution, oxidation without elimination and oxidation with elimination are presented. Finally, the metathesis reactions of deprotonated bis(alkylamido)cyclodiphosph(III)azane with $PhPCl_2$, $AsCl_3$ and $SbCl_3$ is reported in Chapter V.

CHAPTER II

SUBSTITUTION REACTIONS ON CYCLODIPHOSPH(III)AZANE COMPOUNDS OF GROUP 15

1. INTRODUCTION

Covering the properties and transformations of virtually all elements and their compounds, inorganic chemistry is perhaps the broadest of the traditional areas of chemistry. It is therefore hardly surprising that attempts have been made to divide it into sub-groups, such as main-group and transition metal chemistry, or molecular- vs. solid-state chemistry. Our interest lies in inorganic molecules whose skeleton consists of mainly N, P and Si with only enough organic groups for stabilization. These compounds are prone to polycyclic and cage formation with bond angles close to 90°[1] and high symmetry.[9] The binding behavior of cyclodiphospazanes are largely influenced by both their steric and electronic properties that can be modified by substituting the substituents on the phosphorus atoms or by changing the oxidation state of the P(III) atoms.[75, 85, 93] Neutral cyclodiphosph(III)azane ligands can readily be converted to the dianionic version by deprotonation with a strong base like *n*-butyllithium (Scheme 15).[9, 24]

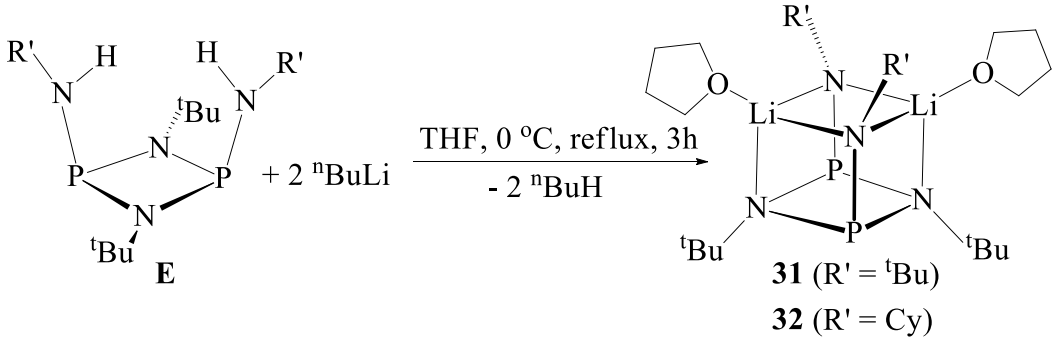

E

31 (R' = ^{t}Bu)

32 (R' = Cy)

Scheme 15. Syntheses of **31** and **32**.

The neutral ligand when deprotonated without oxidation generates three different chelation modes (**I–III**, Figure 8).

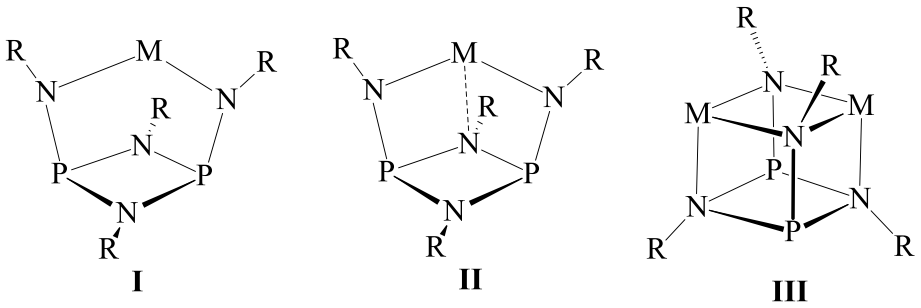

Figure 8. Chelation modes of cyclodiphosph(III)azanes.

These coordination modes are, either through a bridging, or terminal *N*-donor atoms, through which s-, p-, or d-block elements with various atomic parameters (ionic or covalent radii) and oxidation states can bind.[87]

Chelation modes of cyclodiphosphazanes are modulated by a combination of factors: the size of the metal (covalent radius), the bulk of the substituents around the metal and the amido nitrogen substituents, the electron-donating capability of the amido nitrogen and the hard-soft-acid-base (HSAB) property of the metal and ligand fragments.[9] While large metals often bind to the ligand at the amido nitrogen atoms in a κ^2*N*,*N*′ mode, they sometimes bind laterally to the cyclodiphosphazane ligand.[74, 84] An explanation for these observations is that the larger N–N interatomic distance compared to the smaller *N*, *E* lateral binding makes coordination at the bis(amido) nitrogen atoms preferable to larger metals (elements). Large metals possessing sterically congested ancillary ligands, however, will prefer to coordinate to the cyclodiphosphazane laterally to avoid significant repulsion between the amido substituents in the cyclodiphosphazane and the metal ligands.[102]

The reactions of cyclodiphosphazanes have been studied extensively by different investigators in order to develop the above coordination modes. In these complexes, the metal centers used are electrophiles while the *N*- or *E*-donors are nucleophiles. Consequently, metals, metalloids, and nonmetals from across the periodic table have been incorporated into this ligand, and these compounds have been used in diverse applications, ranging from homogeneous catalysts to materials precursors. In one such studies, Stahl *et al*. treated group 4 metals with **31** to obtain a coordination mode in which the metal is centered directly above the P_2N_2 heterocycle ring (**II**, Figure 8).[24, 47, 56, 59, 92] Using a salt elimination method in another study, they treated non-metallic electrophiles, ECl_3 (E = P, As, Sb, and Bi), with **31** to introduce phosphorus, arsenic, antimony and bismuth to obtain the first fully characterized mono-phosphorus, -arsenic, -antimony and -bismuth derivatives of bis(alkylamino)cyclodiphosph(III)azanes (Scheme 16).[92, 98, 103]

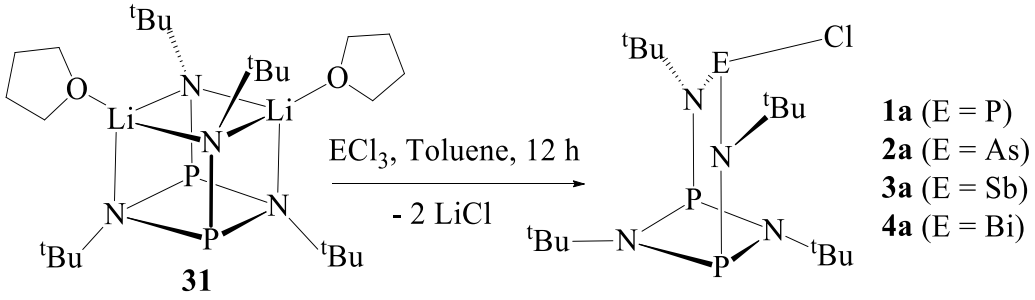

Scheme 16. Syntheses of **1a**, **2a**, **3a** and **4a**. (These compounds are numbered as P = **1**, As = **2**, Sb = **3**, Bi = **4**, while the chloride ligand is labelled **a** for clarity. Ligands used in this work will be labelled as follows: Ph = **b**, N_3 = **c**, $N(SiMe_3)_2$ = **d**, O^{t}Bu = **e**, OPh = **f**, OSO_2CF_3 = **g,** I = **h**).

The incorporation of trivalent group 15 element chlorides affords compounds of structure types **I** or **II** (Figure 8), the exact conformation depending on the nature of the chelated atom.

Thus, in structure type **I** the group 15 element is perfectly centered above P_2N_2 ring in a κ^2N mode, while in structure type **II** the chelated atom is displaced from the central amido posts and rests above one of the ring nitrogen atoms in a κ^3N fashion. This series of compounds (**1a**–**4a**) completes a homologous series of group 15 compounds with formula, $[(^tBuNP)_2(^tBuN)_2]ECl$ (E = P **1a**, As **2a**, Sb **3a** and Bi **4a**).[98, 103] The compounds, **1a**–**4a**, can be further derivatized from the newly incorporated chloride ligand and the lone pairs on the phosphorus atoms.

The homologous series of group 15 compounds with formula, $[(^tBuNP)_2(^tBuN)_2]ECl$, can undergo S_N2 substitution reactions, by replacing the chloride ligand with a more nucleophilic monodentate ligand. The chloride ligand on the Group 15 element can be readily replaced by a *N*- and *O*-centered monodentate ligand like, azide, alkoxide, phenoxide and hexamethyldisilazide. These ligands differ significantly in size, ranging from the compact pseudo-halide N_3 to the very bulky $N(SiMe_3)_2$. While some derivatives of **1a** and **3a** have been characterized (Scheme 17),[92, 98, 103] those of **2a** and **4a** have not been previously reported.

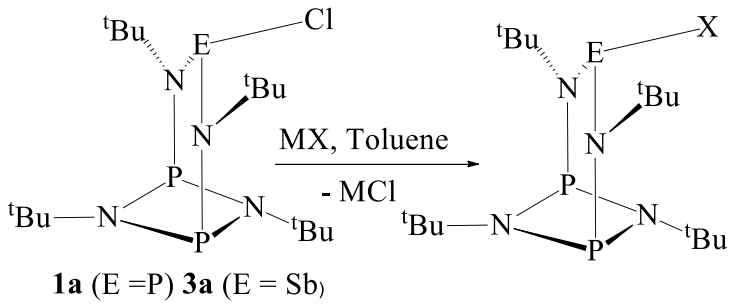

1a (E =P) **3a** (E = Sb)

1b, M = MgCl, X = Ph, E = P
1c, M = Na, X = N_3, E = P
1d, M = Li, X = $N(SiMe_3)_2$, E = P
1e, M = Na, X = O^tBu, E = P
1g, M = Ag, X = OSO_2CF_3, E = P
3b, M = MgCl, X = Ph, E = Sb
3c, M = Na, X = N_3, E = Sb
3d, M = Li, X = $N(SiMe_3)_2$, E = Sb
3e, M = Na, X = O^tBu, E = Sb
3f, M = Li, X = OPh, E = Sb

Scheme 17. The syntheses of **1b–e, g** and **3b–f**.

Such derivatized cyclodiphosph(III)azanes thus also form a bridge between inorganic and organic chemistry, as well as between the molecular and the solid state. Our goal in this study is to compare the relative basicities of the Lewis–basic sites in these molecules.

Here we report the extension of previous work on group 15 elements to the transformation of known and newly synthesized compounds of this type by chloride substitution.

2. EXPERIMENTAL

General Procedures

All experimental procedures were performed under an atmosphere of argon using standard Schlenk techniques. Immediately before use, solvents were dried and freed of molecular oxygen by distillation under a nitrogen atmosphere from sodium- or potassium benzophenone ketyl. PCl_3, ^nBuLi (2.5 M in hexanes), NaN_3, PhMgCl, $LiN(SiMe_3)_2$, LiOPh, $AgOSO_2CF_3$, NaI and NaO^tBu were purchased from Sigma Millipore or Alfa Aesar and used without further purification. The compounds *cis*-$[(^tBuNP)_2(^tBuNH)_2]$, *cis*-$[(^tBuNP)_2(^tBuNLi{\cdot}thf)_2]$ **31**, *cis*-$[(^tBuNP)_2(CyNLi{\cdot}thf)_2]$ **32**, $[(^tBuNP)_2(^tBuN)_2]PCl$ **1a**, $[(^tBuNP)_2(^tBuN)_2]AsCl$ **2a**, $[(^tBuNP)_2(^tBuN)_2]SbCl$ **3a** and $[(^tBuNP)_2(^tBuN)_2]BiCl$ **4a** were synthesized according to published procedures.[24, 98, 103] All fritted filter tubes used were of medium porosity.

Description of Instrumentation

NMR spectra were recorded on a Bruker AVANCE-500 NMR spectrometer. The ^1H and $^{13}C\{^1H\}$ NMR spectra are referenced relative to C_6D_5H (7.16 ppm) and (128.39 ppm), respectively, or $CDCl_3$ (7.27 ppm) and $CDCl_3$ (77.23 ppm), respectively, as internal standards, while the $^{31}P\{^1H\}$ NMR spectra are referenced relative to $P(OEt)_3$ (137.0 ppm) as external standard in C_6D_6 or $CDCl_3$. In all cases positive chemical shift values represented higher frequencies and downfield shifts. Melting points were recorded on a Mel-Temp melting point

apparatus; they are uncorrected. Elemental analyses were performed by ALS Life Sciences Division Environmental, Tucson, AZ.

X-ray Crystallography

Suitable single crystals were coated with Paratone oil, affixed to Mitegen or Litholoop crystal holders and centered on the diffractometer in a stream of cold nitrogen. Reflection intensities were collected with a Bruker Apex Diffractometer equipped with an Oxford Cryosystems, 700 Series Cryostream cooler, operating at 173 K. Data were measured using ω scans of 0.3° per frame for 20 seconds until a complete hemisphere of data had been collected. Cell parameters were retrieved using SMART[104] software and refined with SAINT[105] on all observed reflections. Data were reduced with SAINTplus, which corrects for Lorentz polarization effects and crystal decay. Empirical absorption corrections were applied with SADABS.[106] The structures were solved by direct methods with SHELXS-90[107] program and refined by full-matrix least squares methods on F^2 with SHELXS-97[108] incorporated in SHELXTL Version 5.10.[109]

Single crystals of **1h**, **2h** and **3h** were coated with Paratone oil and quickly transferred to the goniometer head of a Bruker Quest diffractometer with a fixed angle χ, a sealed fine focus X-ray tube, single crystal curved graphite incident beam monochromator, a Photon100 CMOS area detector and an Oxford Cryosystems low temperature device. Examination and data collection were performed with Mo Kα radiation (λ = 0.71073 Å) at 150 K.

Data were collected, reflections were indexed and processed, and the files scaled and corrected for absorption using APEX3.[110] The space groups were assigned and the structures were solved by direct methods using XPREP within SHELXTL suite of programs[105, 111] and refined by full matrix least squares against F^2 with all reflections using Shelxl2018[112, 113] using the graphical interface Shelxle.[114] If not specified otherwise H atoms attached to carbon and

nitrogen atoms were positioned geometrically and constrained to ride on their parent atoms. C–H bond distances were constrained to 0.95 Å for aromatic and CH_2 moieties, and to 1.00, 0.99 and 0.98 Å for aliphatic C–H, CH_2 and CH_3 moieties, respectively. Methyl (CH_3) were allowed to rotate but not to tip to best fit the experimental electron density.

3.0 SYNTHESES OF COMPOUNDS

{[(^{t}BuNP)$_2$(^{t}BuN)$_2$]AsPh} 2b

To a cooled (0 °C) solution of [(^{t}BuNP)$_2$(^{t}BuN)$_2$]AsCl **2a** (1.30 g, 2.85 mmol) in toluene (25 mL) was added dropwise an ethereal solution of PhMgCl (1.60 mL, 3.04 mmol). The mixture was stirred at RT for 24 h and then filtered with a frit. The ensuing pale-yellow solution was concentrated *in vacuo* and stored at –12 °C to furnish colorless, plate-shaped crystals of **2b**. Yield: (1.23 g, 2.48 mmol), 87%. Mp: 140–141 °C. ^{1}H NMR (benzene-d$_6$, 25 °C): 8.36 (d, 2 H, Ph, *ortho*), 7.23 (t, H, *J* = 8.00 Hz, Ph, *meta*), 7.04 (t, H, *J* = 6.80 Hz, Ph, *para*), 1.46 (s, 9 H, N^{t}Bu, amido), 1.39 (s, 9 H, N^{t}Bu, amido), 1.33 (s, 18 H, N^{t}Bu, imido). ^{13}C{^{1}H} NMR (benzene-d$_6$, 25 °C): 152.09 (s, Ph, C$_{ipso}$), 133.32 (s, Ph, *ortho*), 129.97 (s, Ph, *meta*), 57.96 (t, J_{PC} = 9.39 Hz, N*C*(CH$_3$)$_3$, amido), 53.67 (t, J_{PC} = 15.07 Hz, N*C*(CH$_3$)$_3$, imido), 52.05 (t, J_{PC} = 4.89 Hz, N*C*(CH$_3$)$_3$, imido), 32.97 (t, J_{PC} = 5.93 Hz, NC(*C*H$_3$)$_3$, amido), 30.69 (t, J_{PC} = 5.92 Hz, NC(*C*H$_3$)$_3$, imido), 29.72 (t, J_{PC} = 8.24 Hz, NC(*C*H$_3$)$_3$, imido). ^{31}P{^{1}H} NMR (benzene-d$_6$, 25 °C): 172.08 (s). Anal. Calcd. for $C_{22}H_{41}AsN_4P_2$: C, 53.01; H, 8.29; N, 11.24%. Found: C, 52.58; H, 8.01; N, 10.89%.

{[(^{t}BuNP)$_2$(^{t}BuN)$_2$]BiPh} 4b

In a manner analogous to that used for the synthesis of **2b**, [(^{t}BuNP)$_2$(^{t}BuN)$_2$]BiCl **4a** (0.930 g, 1.58 mmol) in toluene (25 mL) was added dropwise to an ethereal solution of PhMgCl (1.17 mL, 1.66 mmol). The ensuing light-yellow solution was concentrated *in vacuo* and stored at –12

°C to yield colorless, needle-like crystals of **4b**. Yield: (0.890 g, 1.40 mmol), 89%. Mp: 168–170 °C. ^{1}H NMR (benzene-d_6, 25 °C): 8.72 (d, J_{PH} = 7.35 Hz, 2 H, Ph, *ortho*), 7.56 (t, J_{PH} = 7.33 Hz, 2 H, Ph, *meta*), 7.20 (t, J_{PH} = 8.40, 1 H, Ph, *para*), 1.53 (s, 9 H, N^{t}Bu, imido), 1.45 (s, 9 H, N^{t}Bu, imido), 1.16 (s, 18 H, N^{t}Bu, amido). ^{13}C{^{1}H} NMR (benzene-d_6, 25 °C): 139.18 (s, Ph, C_{ipso}), 135.00 (s, Ph, *ortho*), 132.12 (s, Ph, *meta*), 130.69 (s, Ph, *para*), 56.49 (d, J_{PC} = 17.03 Hz, N*C*(CH$_3$)$_3$, amido), 54.26 (t, J_{PC} = 15.12 Hz, N*C*(CH$_3$)$_3$, imido), 53.28 (t, J_{PC} = 15.50 Hz, N*C*(CH$_3$)$_3$, imido), 34.78 (d, J_{PC} = 11.44 Hz, NC(*C*H$_3$)$_3$, imido), 31.24 (t, J_{PC} = 7.51 Hz, NC(*C*H$_3$)$_3$, imido), 29.99 (t, J_{PC} = 6.44 Hz, NC(*C*H$_3$)$_3$, imido). ^{31}P{^{1}H} NMR (benzene-d_6, 25 °C): 129.67 (s). Anal. Calcd. for $C_{22}H_{41}BiN_4P_2$: C, 41.78; H, 6.53; N, 8.86%. Found: C, 41.61; H, 6.35; N, 8.23%.

{[(tBuNP)$_2$(tBuN)$_2$]AsN$_3$} 2c

In a 100 mL two-necked flask, equipped with a stir bar and a gas-inlet, **2a** (0.900 g, 1.97 mmol) and NaN_3 (0.140 g, 2.17 mmol) were mixed in THF (12 mL) and then stirred for 24 h at RT. The light-orange suspension slowly turned cloudy due to the formation of a white precipitate of sodium chloride. The THF was removed *in vacuo* and the crystalline residue was extracted with toluene (15 mL) and then filtered with a frit. The filtrate was concentrated to 3 mL and stored at –15 °C. Colorless, plate-like crystals of **2c** were isolated after several days. Yield: (0.770 g, 1.67 mmol), 85%. Mp: 110–111 °C. ^{1}H NMR (benzene-d_6, 25 °C): 1.45 (s, 9 H, N^{t}Bu, imido), 1.38 (s, 18 H, N^{t}Bu, amido), 1.22 (s, 9 H, N^{t}Bu, imido). ^{31}C{^{1}H} NMR (benzene-d_6, 25 °C): 58.04 (t, J_{PC} = 8.47 Hz, N*C*(CH$_3$)$_3$, amido), 53.42 (t, J_{PC} = 13.59 Hz, N*C*(CH$_3$)$_3$, imido), 51.96 (t, J_{PC} = 4.70 Hz, N*C*(CH$_3$)$_3$, imido), 32.59 (t, J_{PC} = 5.30 Hz, NC(*C*H$_3$)$_3$, amido), 29.84 (t, J_{PC} = 7.07 Hz, NC(*C*H$_3$)$_3$, imido), 29.68 (t, J_{PC} = 6.10 Hz, NC(*C*H$_3$)$_3$, imido). ^{31}P{^{1}H} NMR

(benzene-d_6, 25 °C): 183.05 (s). Anal. Calcd. for $C_{16}H_{36}N_7P_2As$: C, 41.47; H, 7.83; N, 21.16%. Found: C, 41.15; H, 7.76; N, 20.18%.

{[(^{t}BuNP)$_2$(^{t}BuN)$_2$]AsN(SiMe$_3$)$_2$} 2d

A sample (0.400 g, 2.38 mmol) of lithium hexamethyldisilylamide was dissolved in THF (8 mL) in a 100 mL two-necked flask, and then cooled to 0 °C. To this cooled solution was added a sample of **2a** (1.00 g, 2.19 mmol) dissolved in 24 mL of toluene. The reaction mixture which turned orange with the formation of lithium chloride, was stirred for 1 day at RT and all volatiles were pumped off and the residue was extracted with toluene (15 mL) and then filtered using a frit. The resulting filtrate was concentrated *in vacuo* to about 5 mL and kept at – 6 °C for two days to furnish colorless crystals of **2d**. Yield: (1.15 g, 1.98 mmol), 91%. Mp: 139–140 °C. ^{1}H NMR (C_6D_6, 25 °C): 1.53 (s, 18 H, N^{t}Bu, amido), 1.40 (s, 9 H, N^{t}Bu, imido), 1.33 (s, 9 H, N^{t}Bu, imido), 0.58 (s, 9 H, CH_3, Si(CH_3)$_3$), 0.40 (s, 9 H, CH_3, Si(CH_3)$_3$). ^{13}C{^{1}H} NMR (C_6D_6, 25 °C): 58.66 (t, J_{PC} = 11.10 Hz, N*C*(CH_3)$_3$, amido), 54.34 (t, J_{PC} = 16.98 Hz, N*C*(CH_3)$_3$, imido), 52.58 (t, J_{PC} = 7.19 Hz, N*C*(CH_3)$_3$, imido), 34.36 (t, J_{PC} = 7.25 Hz, NC(*C*H$_3$)$_3$, amido), 30.85 (t, J_{PC} = 6.11 Hz, NC(*C*H$_3$)$_3$, imido), 29.22 (t, J_{PC} = 9.16 Hz, NC(*C*H$_3$)$_3$, imido), 7.44 (s, Si(CH_3)$_3$), 5.61 (s, Si(CH_3)$_3$). ^{31}P{^{1}H} NMR (C_6D_6, 25 °C): 186.98 (s). Anal. Calcd. for $C_{22}H_{54}N_5P_2Si_2As$: C, 45.42; H, 9.36; N, 12.04%. Found: C, 45.85; H, 9.65; N, 12.04%.

{[(^{t}BuNP)$_2$(^{t}BuN)$_2$]BiN(SiMe$_3$)$_2$} 4d

In a manner similar to that used for the synthesis of **2d**, a crystalline sample (0.250 g, 1.48 mmol) of lithium hexamethyldisilylamide was added to **4a** (0.870 g, 1.48 mmol), dissolved in toluene (24 mL). Upon cooling to –6 °C for 3 days, the solution furnished light-yellow crystals of **4d**. Yield: (0.830 g, 1.15 mmol), 78%. Mp: 211–212 °C. ^{1}H NMR (benzene-d_6, 25 °C): 1.45 (s, 18 H, N^{t}Bu, amido), 1.37 (s, 9 H, N^{t}Bu, imido), 1.29 (s, 9 H, N^{t}Bu, imido), 0.67 (s, 9 H,

$Si(CH_3)_3$), 0.29 (s, 9 H, $Si(CH_3)_3$). $^{13}C\{^1H\}$ NMR (benzene-d_6, 25 °C): 58.08 (d, J_{PC} = 15.44 Hz, $NC(CH_3)_3$, amido), 54.81 (t, J_{PC} = 14.95 Hz, $NC(CH_3)_3$, imido), 54.22 (t, J_{PC} = 17.13 Hz, $NC(CH_3)_3$, imido), 36.24 (d, J_{PC} = 12.63 Hz, $NC(CH_3)_3$, amido), 30.43 (t, J_{PC} = 9.18 Hz, $NC(CH_3)_3$, imido), 28.26 (t, J_{PC} = 6.83 Hz, $NC(CH_3)_3$, imido), 8.25 (s, $Si(CH_3)_3$) and 5.95 (s, $Si(CH_3)_3$). $^{31}P\{^1H\}$ NMR (benzene-d_6, 25 °C): 147.89 (s). Anal. Calcd. for $C_{22}H_{54}N_5P_2Si_2Bi$: C, 36.92; H, 7.60; N, 9.78%. Found: C, 37.02; H, 7.64; N, 9.52%.

{[(^{t}BuNP)$_2$(^{t}BuN)$_2$]AsO^{t}Bu} 2e

Samples of **2a** (0.800 g, 1.75 mmol) and NaO^{t}Bu (0.180 g, 1.83 mmol) were dissolved in toluene (30 mL) and stirred at RT for 24 h. The NaCl formed was filtered off using a frit and the resulting filtrate was concentrated *in vacuo* to about 5 mL and stored at –12 °C for 3 days. This produced colorless, block-shaped crystals of **2e**. Yield: (0.660 g, 1.33 mmol), 76%. Mp: 174–176 °C. ^1H NMR (C_6D_6, 25 °C): 1.58 (s, 9 H, O^{t}Bu), 1.52 (s, 27 H, N^{t}Bu), 1.41 (s, 9 H, imido, N^{t}Bu). $^{13}C\{^1H\}$ NMR (C_6D_6, 25 °C): 75.44 (s, $NC(CH_3)_3$, O^{t}Bu), 57.77 (t, J_{PC} = 8.99 Hz, $NC(CH_3)_3$, amido), 53.27 (t, J_{PC} = 13.65 Hz, $NC(CH_3)_3$, imido), 52.75 (t, J_{PC} = 7.18 Hz, $NC(CH_3)_3$, imido), 33.60 (t, J_{PC} = 5.53 Hz, $NC(CH_3)_3$, amido), 33.28 (s, O^{t}Bu), 30.50 (t, J_{PC} = 6.35 Hz, $NC(CH_3)_3$, imido), 29.95 (t, J_{PC} = 6.08 Hz, $NC(CH_3)_3$, imido). $^{31}P\{^1H\}$ NMR (C_6D_6, 25 °C): 183.08 (s). Anal. Calcd. for $C_{20}H_{45}AsN_4OP_2$: C, 48.58; H, 9.17; N, 11.33%. Found: C, 48.12; H, 8.68; N, 10.74%.

{[(^{t}BuNP)$_2$(^{t}BuN)$_2$]AsOPh} 2f

To a sample of **2a** (1.00 g, 2.19 mmol), dissolved in toluene (10 mL), was added via a syringe, a lithium phenoxide solution (1.00 M, 2.30 mL). The pale-yellow reaction mixture was stirred at RT for 1 day and volatiles were removed *in vacuo* and the crystalline residue extracted with toluene (15 mL). The mixture was filtered with a frit, concentrated to 3 mL and stored at –15 °C.

Colorless, block-shaped crystals of **2f** were collected after several days. Yield: (0.880 g, 1.71 mmol), 78%. Mp: 113–114 °C. ^{1}H NMR (benzene-d_6, 25 °C): 7.20 (t, J_{PH} = 7.61 Hz, 2 H, *meta*), 7.15 (m, 2 H, *ortho*), 6.85 (t, J_{PH} = 7.03 Hz, 1 H, *para*), 1.59 (s, 9 H, N^{t}Bu, imido), 1.40 (s, 18 H, N^{t}Bu, amido), 1.36 (s, 9 H, N^{t}Bu, imido). ^{13}C{^{1}H} NMR (benzene-d_6, 25 °C): 159.60 (s, Ph, C_{ipso}), 130.09 (s, Ph, *ortho*), 120.25 (s, Ph, *meta*), 118.72 (s, Ph, *para*), 57.83 (t, J_{PC} = 9.03 Hz, N*C*(CH$_3$)$_3$, amido), 53.09 (t, J_{PC} = 13.13 Hz, N*C*(CH$_3$)$_3$, imido), 52.07 (t, J_{PC} = 5.75 Hz, N*C*(CH$_3$)$_3$, imido), 33.08 (t, J_{PC} = 5.67 Hz, NC(*C*H$_3$)$_3$, amido), 30.09 (t, J_{PC} = 6.34 Hz, NC(*C*H$_3$)$_3$, imido), 29.87 (t, J_{PC} = 6.34 Hz, NC(*C*H$_3$)$_3$, imido). ^{31}P{^{1}H} NMR (benzene-d_6, 25 °C): 182.18 (s). Anal. Calcd. for $C_{22}H_{41}N_4P_2OAs$: C, 51.36; H, 8.03; N, 10.89%. Found: C, 51.06; H, 8.25; N, 10.39%.

{[(tBuNP)$_2$(tBuN)$_2$]SbOSO$_2$CF$_3$} 3g

A sample of AgOSO$_2$CF$_3$ (0.280 g, 1.09 mmol) in THF (5 ml) was cooled to 0 °C. To this stirred solution was added dropwise [(tBuNP)$_2$(tBuN)$_2$]SbCl **3a** (0.50 g, 0.99 mmol) in chloroform. A white precipitate of AgCl formed instantly. The reaction mixture was stirred at 0 °C for 30 minutes and all volatiles were pumped off, and the residue was extracted with chloroform. The AgCl was removed with a frit and the ensuing colorless solution was concentrated *in vacuo* and stored at –20 °C. Colorless, needle-shaped crystals of **3g** were deposited after 24 h. Yield: (0.56 g, 0.91 mmol), 92%. Alternatively, **3a** and AgOSO$_2$CF$_3$ were combined in a flask, and dissolved in toluene (20 mL) and then the mixture was stirred at RT for 1 h. Yield: (0.60 g, 0.97 mmol), 81%. Mp: 156–158 °C. ^{1}H NMR (C_6D_6, 25 °C): 1.46 (s, 18 H, N^{t}Bu, amido), 1.10 (s, 18 H, N^{t}Bu, imido). ^{13}C{^{1}H} NMR (C_6D_6, 25 °C): 120 (q, J_{CF} = 318.95 Hz, CF$_3$), 57.91 (t, J_{PC} = 5.80 Hz, N*C*(CH$_3$)$_3$, amido), 54.96 (t, J_{PC} = 10.37 Hz, N*C*(CH$_3$)$_3$, imido), 33.61 (t, J_{PC} = 6.63 Hz, NC(*C*H$_3$)$_3$, amido), 27.85 (s, NC(*C*H$_3$)$_3$, imido). ^{31}P{^{1}H} NMR (C_6D_6,

25 °C): 182.73 (s, P(III)). Anal. Calcd. for $C_{17}H_{36}N_4P_2O_3SF_3Sb$: C, 33.08; H, 5.88; N, 9.08%. Found: C, 32.92; H, 5.93; N, 8.60%.

{[(^{t}BuNP)$_2$(^{t}BuN)$_2$]PI} 1h

Samples of [(^{t}BuNP)$_2$(^{t}BuN)$_2$]PCl **1a** (0.500 g, 1.21 mmol) and NaI (0.210 g, 1.40 mmol) were combined in THF (20 mL) and stirred for 24 h at RT. The mixture was then filtered using a frit. The resulting solution was concentrated *in vacuo* and stored at – 6 °C to furnish block-shaped, yellow crystals of **1h** after 24 h. Yield: (0.560 g, 1.10 mmol), 91%. Mp: 212–214 °C. ^{1}H NMR ($CDCl_3$, 25 °C): 1.61 (d, J_{PH} = 4.77 Hz), 18 H, N^{t}Bu, amido), 1.35 (s, 18 H, N^{t}Bu, imido).^{13}C{^{1}H} NMR ($CDCl_3$, 25 °C): 60.84 (m, N*C*$(CH_3)_3$, amido), 53.55 (s, N*C*$(CH_3)_3$, imido), 29.02 (m, NC(*C*$H_3)_3$, imido). ^{31}P{^{1}H} NMR ($CDCl_3$, 25 °C): 196.42 (d, J_{PP} = 28.71 Hz, P(III)), 173.77 (t, J_{PP} = 27.15 Hz, P(III)). Anal. Calcd. for $C_{16}H_{36}N_4P_3I$: C, 38.11; H, 7.19; N, 11.11%. Found: C, 37.72; H, 7.27; N, 10.79%.

{[(^{t}BuNP)$_2$(^{t}BuN)$_2$]AsI} 2h

Like in the synthesis of **1h** above, samples of **2a** (0.600 g, 1.31 mmol) and NaI (0.210 g, 1.40 mmol) were mixed in THF (20 mL) and stirred at RT for 24 h. The ensuing light-yellow solution was concentrated *in vacuo* and stored at –6 °C to afford yellow, block-shaped crystals of **2h** after 24 h. Yield: (0.670 g, 1.22 mmol), 93%. Mp: 186–188 °C. ^{1}H NMR ($CDCl_3$, 25 °C): 1.54 (s, 27 H, N^{t}Bu) 1.33 (br, 9 H, N^{t}Bu, imido). ^{13}C{^{1}H} NMR ($CDCl_3$, 25 °C): 60.38 (t, J_{PC} = 8.58 Hz, N*C*$(CH_3)_3$, amido), 53.30 (s, N*C*$(CH_3)_3$, imido), 30.02 (t, J_{PC} = 4.89 Hz, NC(*C*$H_3)_3$, amido), 29.10 (s, NC(*C*$H_3)_3$, imido). ^{31}P{^{1}H} NMR ($CDCl_3$, 25 °C): 182.44 (s, P(III)). Anal. Calcd. for $C_{16}H_{36}N_4P_2AsI$: C, 35.05; H, 6.62; N, 10.22%. Found: C, 35.12; H, 6.65; N, 9.96%.

{[(^{t}BuNP)$_2$(^{t}BuN)$_2$]SbI} 3h

A sample of **3a** (0.600 g, 1.19 mmol) and NaI (0.190 g, 1.26 mmol) were mixed in THF (20 mL) and stirred at RT for 1 day. The resulting light-yellow solution was concentrated *in vacuo* and stored at –6 °C to furnish yellow, needle-like crystals of **3h** after 3 days. Yield: (0.620 g, 1.05 mmol), 88%. Mp: ^{1}H NMR ($CDCl_3$, 25 °C): 1.55 (s, 27 H, N^{t}Bu), 1.40 (s, 9 H, N^{t}Bu). ^{13}C{^{1}H} NMR ($CDCl_3$, 25 °C): 59.00 (m, N*C*(CH_3)$_3$), 33.56 (m, NC(*C*H$_3$)$_3$). ^{31}P{^{1}H} NMR ($CDCl_3$, 25 °C): 143.70 (s, P(III)). Anal. Calcd. for $C_{16}H_{36}N_4P_2SbI$: C, 32.29; H, 6.10; N, 9.41%. Found. C, 31.52; H, 6.28; N, 8.75%.

4 RESULTS AND DISCUSSIONS

Synthesis and Spectroscopic Analysis of {[(^{t}BuNP)$_2$(^{t}BuN)$_2$]AsPh} 2b

The reaction of **2a** with PhMgCl at RT in toluene afforded compound **2b** in 87% yield as colorless, plate-like crystals (Scheme 18). The P and Sb analogues of **2b** had previously been synthesized and characterized in a similar fashion. The syntheses and characterizations of **2b** and **4b**, therefore completes a homologous series of group 15 compounds with formula [(^{t}BuNP)$_2$(^{t}BuN)$_2$]EPh (E = P, As, Sb and Bi).

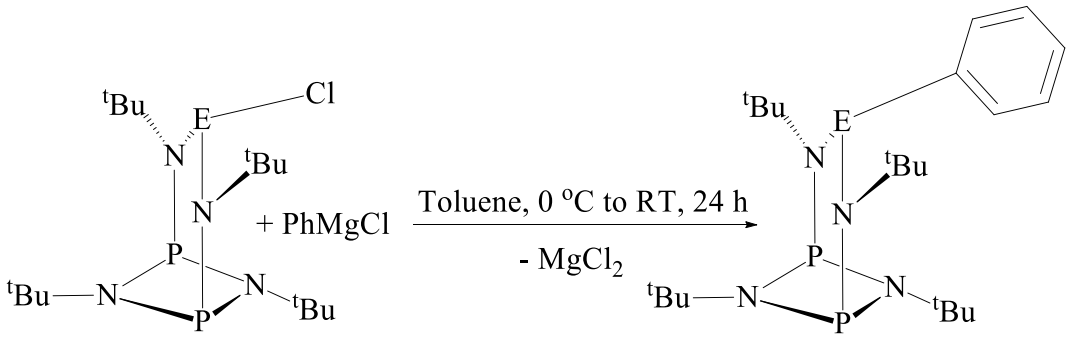

2a (E = As), **4a** (E = Bi) **2b** (E =As), **4b** (E = Bi)

Scheme 18. Synthesis of **2b** and **4b**.

The ^{1}H NMR spectrum of **2b** (Figure 9), shows three singlets at 1.46, 1.39, and 1.33 ppm in the ratio 1:1:2, respectively, representing the different *tert*-butyl protons. Like in the phosphorus analogue,[99] **1b**, the phenyl group is located above the P_2N_2 ring in **2b** making the *tert*-butyl substituents of the imino nitrogen atoms diastereotopic, producing two proton NMR signals. On the other hand, the amino *tert*-butyl protons are in a mirror symmetric plane,[99] making them chemically and magnetically equivalent, hence generating a singlet with intensity 2 at 1.33 ppm. In fact, almost all cyclodiphosph(III)azane compounds of group 15 elements, bearing a monodentate ligand at the E center contain chemically and magnetically equivalent protons at the amino nitrogen, while those at the imino nitrogen are diastereotopic. The three different aromatic protons appear at 8.36 (d), 7.23 (t) and 7.04 ppm (t) corresponding to the *ortho*, *meta*, and *para* protons respectively. The ^{13}C{^{1}H} NMR spectrum of compound **2b** (Figure 11), shows the phenyl carbons as three singlets at 152.09, 133.32 and 129.97 ppm representing the *ipso*, *ortho* and *meta* carbons, respectively. The quaternary *tert*-butylamino and *tert*-butylimino carbons appear as triplets at 57.96, 53.67 and 52.05 ppm, with respective J_{PC} values, 9.39, 15.07 and 4.89 Hz, while the primary *tert*-butylamino and *tert*-butylimino carbons appear as triplets at 32.97 (J_{PC} = 5.93 Hz), 30.69 (J_{PC} = 5.92 Hz) and 29.72 ppm (J_{PC} = 8.24 Hz), respectively, in the ratio 2:1:1. The ^{31}P{^{1}H} NMR spectrum of **2b** (Figure 10), shows a singlet at 172.08 ppm corresponding to the two equivalent phosphorus(III) environments in the P_2N_2 ring.

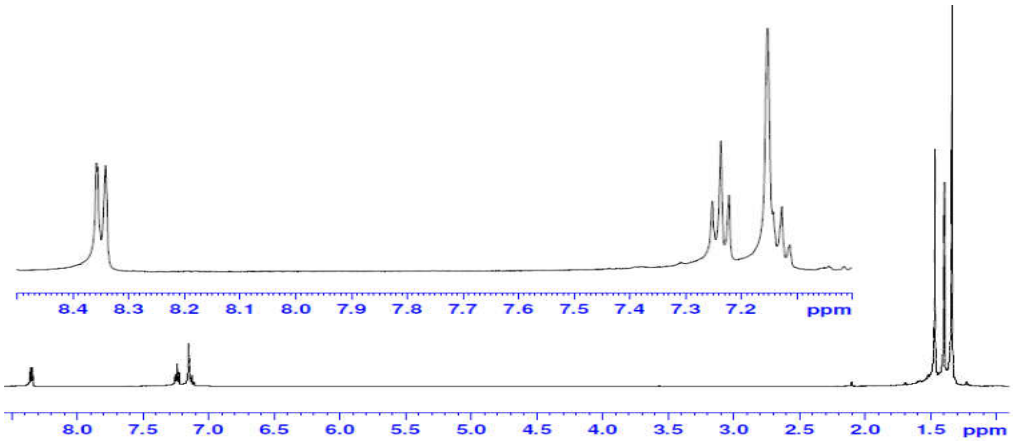

Figure 9. ^{1}H NMR Spectrum for **2b**.

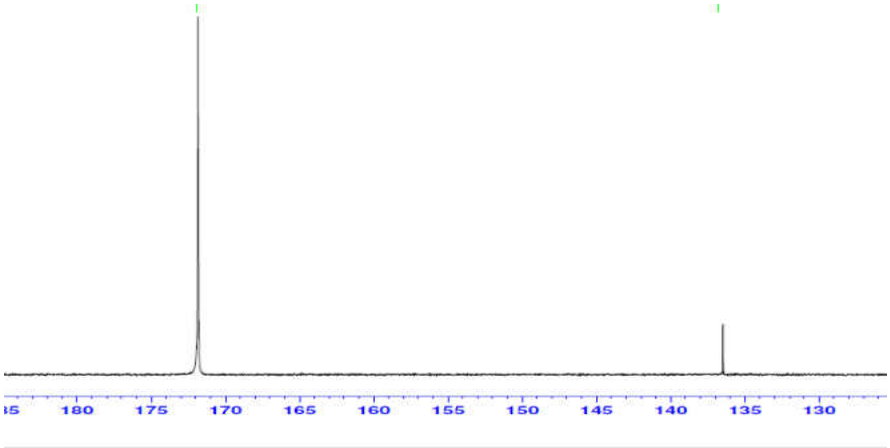

Figure 10. ^{31}P{^{1}H} NMR Spectrum for **2b**.

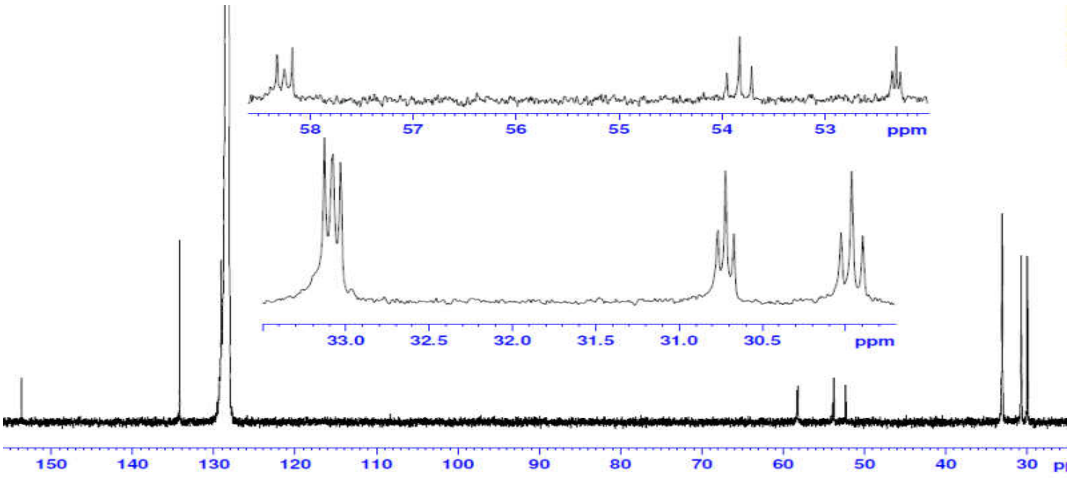

Figure 11. $^{13}C\{^{1}H\}$ NMR Spectrum for **2b**.

Solid-state Structure of {[(^{t}BuNP)$_2$(^{t}BuN)$_2$]AsPh} 2b

Colorless, plate-shaped crystals of **2b**, suitable for single-crystal analysis, were isolated from toluene (–12 °C) solution. The solid-state structure of **2b** with a partial atom numbering scheme is presented in Figure 12 below, while the crystal data and selected bond parameters are listed in Tables 1 and 2 below, respectively. From Figure 12, it is seen that the arsenic atom is perfectly centered above the P_2N_2 ring in a κ^2*N* chelation fashion (Figure 8). Compound **2b** crystallized in the triclinic space group $P\bar{1}$ with two molecules per unit cell. The arsenic center is chelated by two As–N bonds of equal lengths (1.899(2) and 1.908(2) Å), while forming an As–C bond of 1.981(3) Å with the phenyl ligand, which is approximately equal to the value calculated from covalent radii, As–C (1.960 Å).[115] The arsenic atom sits at the top of a trigonal pyramid with an angle sum of 302.24°. The structure of **2b** is analogous to that of **3b**, but because the antimony atom is larger than arsenic, the latter makes bonding contacts with N1 of the P_2N_2 ring and thus adopts a κ^3*N* coordination mode. The As–C bond length (1.981(3) Å) in **2b** is relatively similar to the As–C bond lengths in $As[C(O)]_2CPh_2^-$ (1.925(4) and 1.941(4) Å),[116]

[(IMes)AsP(IDipp)][PF_6] (1.9377(15) and 1.957 Å)[117] and bis(diphenylphosphinomethyl)phenylarsine (1.982(9) Å).[118] The bond angles, N3–P1–N1, N3–P1–N2, and N3–As1–N4 are similar in both **2a** and **2b**, suggesting that the cage is not distorted after the chlorine atom is substituted by the phenyl ligand. It is interesting to note that the N3–As1–Cl1 and N3–As1–C1 bond angles are identical (101.24(6) and 101.37(10)°).[98]

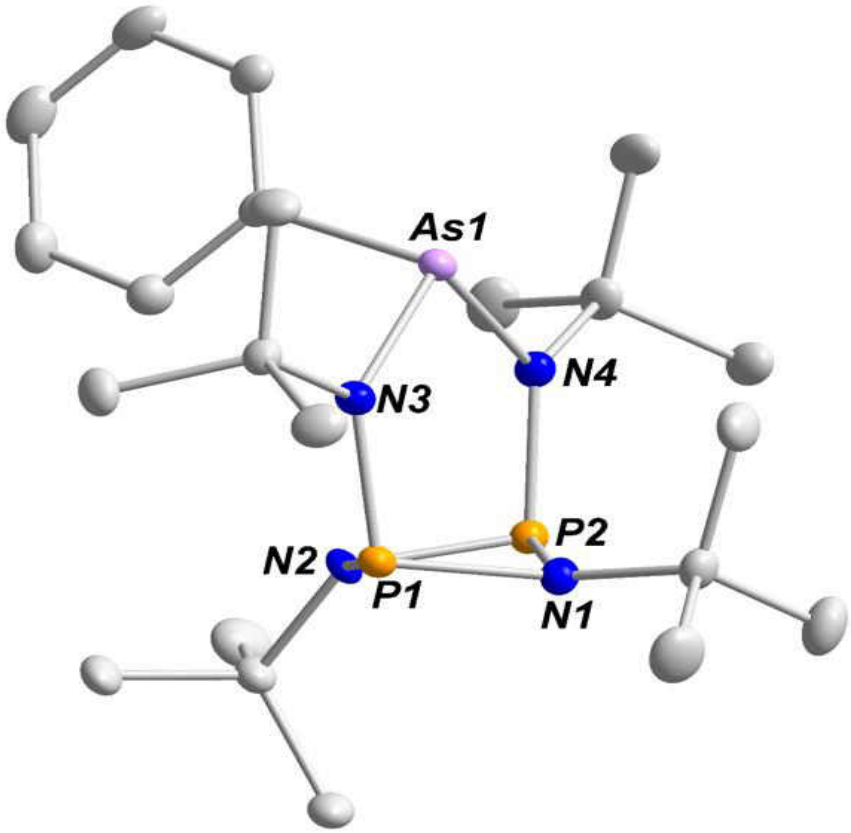

Figure 12. Solid-state structure and partial labelling scheme of **2b**. All atoms are drawn at the 50 % probability level.

Table 1. Crystal data and structure refinement for **2b**.

Chemical formula	$C_{22}H_{41}AsN_4P_2$
fw	498.45
T/K	100(2)
λ/ Å	0.71073
Crystal system	*Triclinic*
Space group	$P\bar{1}$
a/ Å	9.5164(5)
b/ Å	9.9718(5)
c/ Å	15.6775(9)
α/°	79.744(3)
β/°	87.738(3)
γ/°	63.228(3)
V/ Å^3	1305.62(12)
Z	2
ρ(calc) g/m^3	1.268
μ/ mm^{-1}	1.439
F(000)	528
Reflections collected	18771
Independent reflections	5942 [R_{int} = 0.0486]
Completeness (%)	99.6
$Rw(F^2)^b$ [I>2σ(I)]	R_1 = 0.0382, wR_2 = 0.0846
$R(F)^a$ (all data)	R_1 = 0.0537, wR_2 = 0.1020
[a] $R = \sum\|F_o - F_c\| \sum\|F\|_o$. [b] $R_w = \{[\sum w(F_o^2 - F_c^2)] / [\sum w(F_o^2)^2]\}^{1/2}$; $w = 1/[\sigma^2(F_o)^2 + (xP)^2 + yP]$, where $P = (F_o^2 + 2F_c^2)/3$.	

Table 2. Selected bond lengths (Å) and angles (°) for **2b**.

Bond Lengths (Å)			
As1–N3	1.899(2)	P2–N1	1.725(2)
As1–N4	1.908(2)	P2–N2	1.746(2)
As1–C1	1.981(3)	N1–C10	1.477(3)
P1–N3	1.695(2)	N2–C20	1.494(3)
P1–N1	1.722(2)	N3–C30	1.504(3)
P1–N2	1.737(2)	N4–C40	1.508(3)
P2–N4	1.697(2)		
Bond Angles (°)			
N3–As1–N4	101.00(9)	N1–P1–N2	82.85(10)
N3–As1–C1	101.37(10)	N4–P2–N1	102.32(10)
N4–As1–C1	99.86(10)	N4–P2–N2	101.38(11)
N3–P1–N1	104.20(11)	N1–P2–N2	82.49(10)
N3–P1–N2	100.59(10)	N1–P2–N2	82.49(10)

Synthesis and Spectroscopic Analysis of {[(^{t}BuNP)$_2$(^{t}BuN)$_2$]BiPh} 4b

Like in compound **2b**, the reaction of **4a** with PhMgCl, at RT in toluene for a day, produced the phenyl-substituted **4b** (Scheme 18) in 89% yield. Unlike compound **2b** where chelation type I is adopted, the Bi atom in **4b** is chelated in a typical type II chelation style (Figure 8). The large size of Bi, like that of Sb, causes the atom to bond with the N1 atom of the P_2N_2 ring, hence adopting the κ^3*N* chelation mode.

The ^{1}H NMR spectrum of **4b** (Figure 13) shows signals at 8.72, 7.56, and 7.20 ppm representing the *ortho*, *meta*, and *para* protons of the phenyl ligand, respectively. The *tert*-butyl protons of compound **4b** appear as singlets at 1.53, 1.45 and 1.16 ppm with relative intensities 1:1:2, corresponding to the respective *tert*-butylimino protons (1:1) and the *tert*-butylamino protons. As in **2b**, the two imino nitrogen atoms in **4b** are chemically and magnetically non-equivalent, as such two signals with equal intensities (1:1) are generated at 1.53 and 1.45 ppm. The ^{13}C{^{1}H} NMR spectrum of **4b** depicts four signals for the phenyl carbons at 139.18, 138.00, 132.12 and 130.69 ppm attributed to the *ipso*, *ortho*, *meta* and *para* carbons. The quaternary carbons of the *tert*-butyl groups appear as triplets at 56.49, 54.26 and 53.28 ppm. Meanwhile, the primary carbons appear as a doublet at 34.78 ppm (J_{PC} = 11.44 Hz) for the *tert*-butylamino carbons, and as triplets at 31.24 (J_{PC} = 7.51 Hz) and 29.99 ppm (J_{PC} = 6.44 Hz), representing the *tert*-butylimino-carbons. The ^{31}P{^{1}H} NMR spectrum of **4b** (Figure 14) shows a singlet at 129.67 ppm corresponding to the two equivalent P(III) atoms in the P_2N_2 ring of the compound.

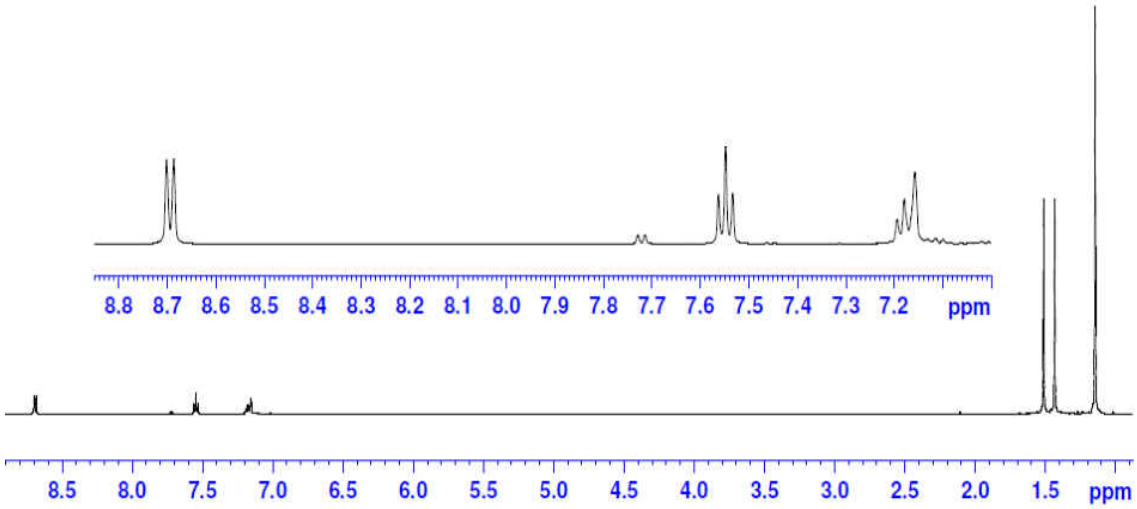

Figure 13. ^{1}H NMR spectrum for **4b**.

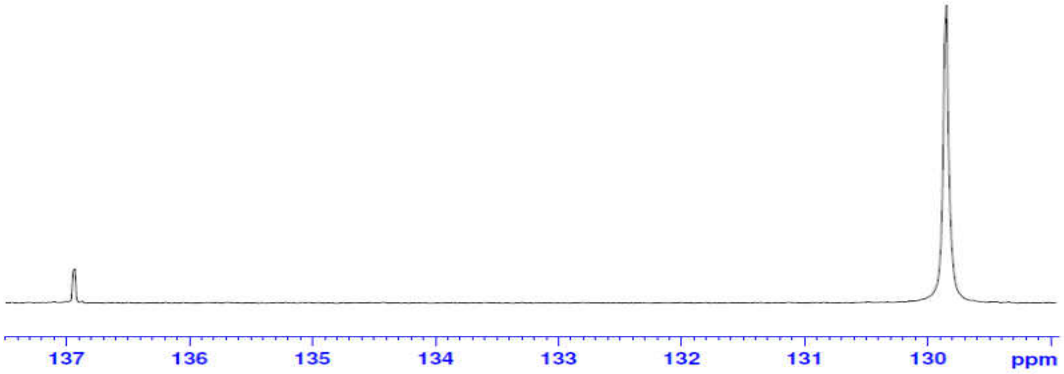

Figure 14. ^{31}P{^{1}H} NMR Spectrum for **4b**.

Synthesis and Spectroscopic Analysis of {[(^{t}BuNP)$_2$(^{t}BuN)$_2$]AsN$_3$} 2c

Like the azide derivatives **1c** and **3c**, **2c** was obtained by the straightforward treatment of the chloride precursor, **2a**, with one equivalent of sodium azide in THF at RT (Scheme 19). When the reaction was completed, THF was removed *in vacuo* and **2c** was extracted from the residue with toluene and a yield of 85% was obtained. While the azide and hexamethyldisilyamide are both *N*-donor monodentate ligands, the azide ligand is less bulky than the latter. However, the

percent yield obtained in **2c** and **2d** are almost equal, indicating that in the presence of an N-donor ligand the chloride is always a better leaving group.

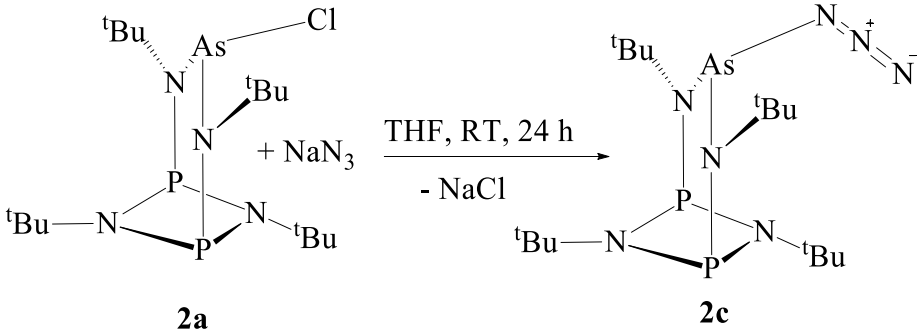

2a **2c**

Equation 19. Synthesis of **2c**.

The ^{1}H NMR spectrum of compound **2c** shows three singlets in the ratio 1:2:1 at 1.45, 1.38 and 1.22 ppm, representing the *tert*-butyl protons. The eighteen *tert*-butylamino protons are equivalent, and therefore appear as a singlet with intensity 2, while those of *tert*-butylimino groups are non-equivalent. The ^{31}P{^{1}H} NMR spectrum for **2c** depicts a singlet at 183.05 ppm attributed to the two phosphorus(III) atoms on the P_2N_2 ring. The ^{13}C{^{1}H} NMR spectrum of **2c** depicts three triplets corresponding to the quaternary carbons of *tert*-butyl groups at 58.04 (J_{PC} = 8.47 Hz), 53.42 (J_{PC} = 13.59 Hz) and 51.96 ppm (J_{PC} = 4,70 Hz). There are triplets resonating at 32.59 (J_{PC} = 5.30 Hz), 29.84 (J_{PC} = 7.07 Hz) and 29.68 ppm (J_{PC} = 6.10 Hz), representing the primary *tert*-butyl carbons of **2c**. The above J_{PC} values are similar to those of compound **2a**.

Solid-state Structure of {[(^{t}BuNP)$_2$(^{t}BuN)$_2$]AsN$_3$} 2c

Colorless, plate-like crystals of **2c**, suitable for single crystal analysis, were isolated in a toluene solution at –15 °C. The solid-state structure of **2c** with a partial atom numbering scheme is presented in Figure 15 below, while the crystal data and selected bond parameters are listed in Tables 3 and 4 below, respectively. Compound **2c** crystallized in the monoclinic space group,

$P2_1/m$, with two molecules per unit cell which has unit cell dimensions of $\boldsymbol{a}$ = 9.613(5), $\boldsymbol{b}$ = 11.6759(6), and $\boldsymbol{c}$ = 10.3557(5) Å, and β = 98.442 (2)°. This C_s-symmetric compound is isomorphous with **1a**, **1c**, and **2a**. Compound **2c** (Figure 15) adopts a κ^2N chelation mode, analogous to that of **1c**, with the arsenic atom centered above the P_2N_2 heterocycle. The molecule also has a mirror plane that contains the arsenic atom, the azide moiety, and the nitrogen atoms of the P_2N_2 ring. While the azide ligand in **1c** and **3c** points upward, that of **2c** points downward. The result is a noticeable bend in the heterocycle, and the *tert*-butyl substituent of N2 is significantly pushed below the heterocycle's plane due to its repulsive interaction with the azide ligand. The As–N bond distance to N3 in **2c** is 1.8505(9) Å, equidistant to that of the precursor **2a** (1.843(2) Å),[98] while the As–N bond (1.9668(17) Å) to the azide ligand is significantly shorter than the As–Cl bond distance (2.3325(11) Å). This is longer than the calculated As–N_{azide} bond length (1.920 Å) by 0.0468(17) Å.[115] Whereas, the bond distance of N5–N6 in **1c** (1.218(5) Å) and **3c** (1.196(6) Å) are almost isometric, that of **2c** (1.175 (2) Å) is significantly shorter and almost equidistant to its N6–N7 bond (1.157(3) Å).[98, 103] The N–N bond distances of the azide ligand in **2c**, therefore, remain symmetrical with a linear N–N–N bond angle (N5–N6–N7 = 176.5 (2)°), compared to $Zn(C_5H_5N)_2(N_3)_2$ (N1–N2 = 1.170 (23) Å, N2–N3 = 1.131(24) Å and N1–N2–N3 = 173.2 (20)°).[119] The sum of the bond angles, N4–As1–N3 = 101.75(6), N4–As1 – N5 = 102.02(4) and N3–As1 –N5 = 102.02(4)°, is 305.79° suggesting that the arsenic atom is situated at the apex of a pyramid in **2c**.

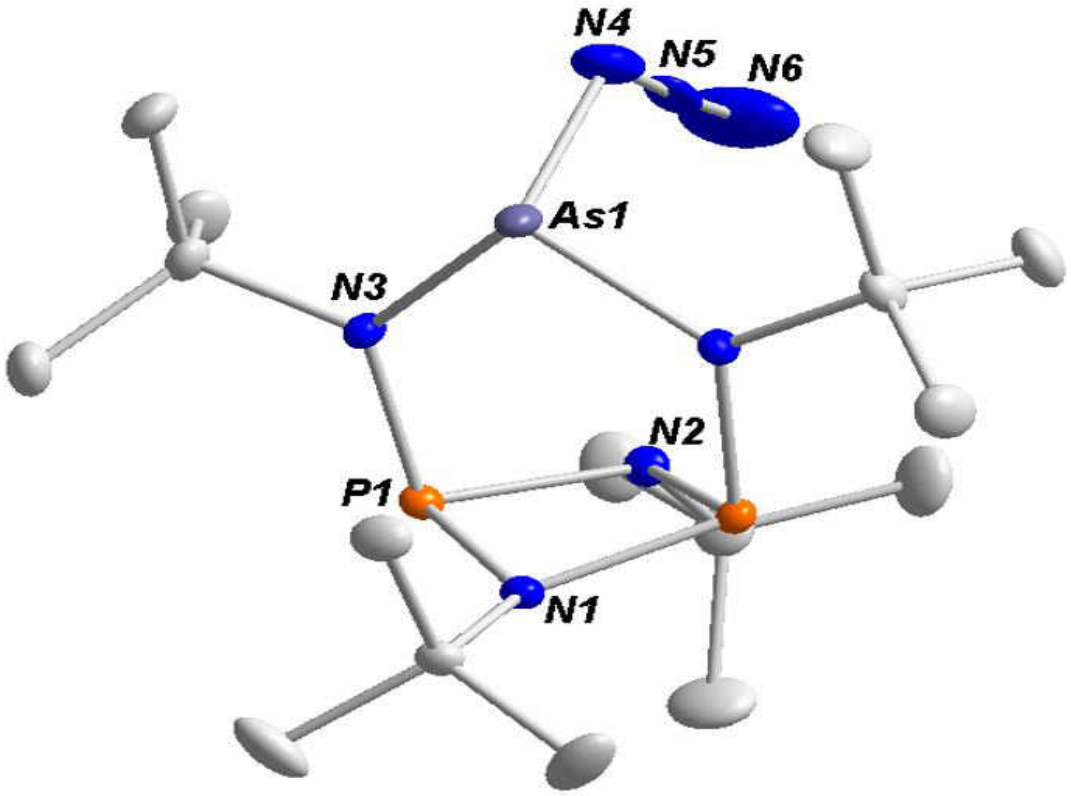

Figure 15. Solid-state structure and partial labelling scheme of **2c**. With the exception of carbon (35 %) all atoms are drawn at the 50 % probability level.

Table 3. Crystal and structure refinement data for **2c**.

Chemical formula	$C_{16}H_{36}AsN_7P_2$
Fw	463.38
T/ K	100(2)
λ/ Å	0.71073
Crystal system	*Monoclinic*
Space group	$P2_1/m$
a/ Å	9.6134(5)
b/ Å	11.6759(6)
c/ Å	10.3557(5)
α/°	90
β/°	98.442(2)
γ/°	90
V/Å^3	1149.78(10)
Z	2
ρ (calc) g/cm^3	1.338
μ/ mm^{-1}	1.632
F(000)	488
Reflections collected	16118
Independent reflections	4279 [R_{int} = 0.0222]
Completeness (%)	99.5 %
$Rw(F^2)^b$ [I>2σ(I)]	R_1 = 0.0252, wR_2 = 0.0683
$R(F)^a$ (all data)	R_1 = 0.0265, wR_2 = 0.0689
[a] $R = \sum\|F_o - F_c\| \sum\|F\|_o$. [b] $R_w = \{[\sum w(F_o^2 - F_c^2)] / [\sum w(F_o^2)^2]\}^{1/2}$; $w = 1/[\sigma^2(F_o)^2 + (xP)^2 + yP]$, where $P = (F_o^2 + 2F_c^2)/3$.	

Table 4. Selected bond lengths (Å) and angles (°) for **2c**.

Bond Lengths (Å)			
As1–N3	1.8505(9)	N5–N6	1.175(2)
As1–N5	1.9668(17)	N6–N7	1.157(3)
P1–N3	1.7154(9)	N1–C10	1.4786(19)
P1–N1	1.7180(9)	N2–C20	1.4910(19)
P1–N2	1.7393(9)	N1–P2	1.7179(9)
N2–P4	1.7393(9)	C10–C11	1.5249(16)
N3–C30	1.5061(14)	C10–C11	1.5249(15)
Bond Angles (°)			
N4–As1–N3	101.75(6)	N1–P1–N2	83.26(5)
N4–As1 –N5	102.02(4)	C30–N3–As1	117.83(7)
N3–As1 –N5	102.02(4)	P1–N3–As1	123.69(5)
N3–P1–N1	102.36(5)	N5–N4–As1	121.29(13)
N3–P1–N2	100.08(5)	N6–N5–N4	176.5(2)

Synthesis and Spectroscopic Analysis of {[(^{t}BuNP)$_2$(^{t}BuN)$_2$]AsN(SiMe$_3$)$_2$} 2d

The treatment of **2a** with LiN(SiMe$_3$)$_2$ at RT for 24 h in toluene/THF furnished compound **2d** in 91% yield, (Scheme 20). Considering that crystalline lithium hexamethyldisilylamide is insoluble in toluene, it was dissolved in THF and after the reaction, volatiles were removed *in vacuo* and **2d** was extracted with toluene. Hexamethyldisilylamide is a bulky, monodentate *N*-donor ligand which is typically employed when low-coordination is desired. Despite the bulk of the ligand, however, the yield for **2d** was above 90%.

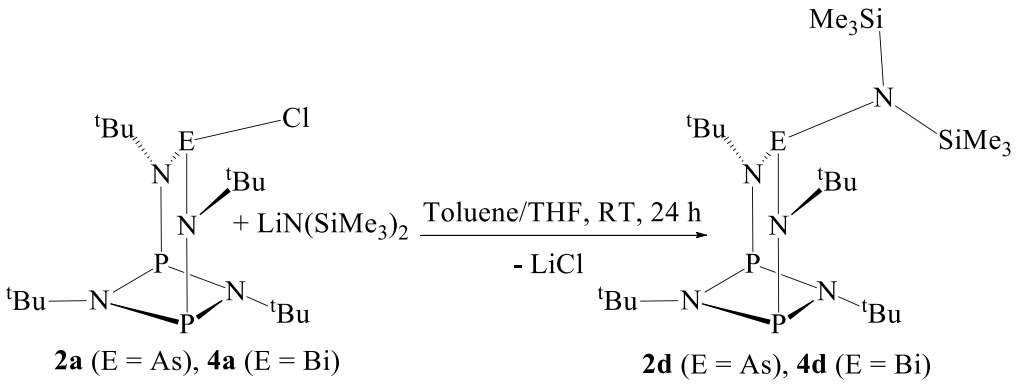

Scheme 20. Synthesis of **2d** and **4d**.

The ^{1}H NMR spectrum of compound **2d** (Figure 16) shows three singlets at 1.53, 1.40, and 1.33 ppm in the ratio 2:1:1, representing the *tert*-butyl protons and two singlets at 0.58 and 0.40 ppm attributed to the methyl protons of the HMDS group. While the signal at 1.53 ppm is attributed to the *tert*-butyl protons, which are spectroscopically equivalent, that at 1.33 ppm is assigned to the *tert*-butylimino group on the same side as the N(SiM$_3$)$_2$ ligand. The ^{13}C{^{1}H} NMR spectrum for **2d** (Figure 17) depicts a triplet (J_{PC} = 11.10 Hz) at 58.08 ppm and two triplets at (54.34 (J_{PC} = 17 Hz) and 52.58 ppm (J_{PC} = 7.19 Hz)) corresponding to the quaternary *tert*-butylamino and *tert*-butylimino carbons, respectively. There are also triplets at 34.36 (J_{PC} = 7.25 Hz), 30.85 (J_{PC} = 6.11 Hz) and 29.22 ppm (J_{PC} = 9,16 Hz) which we assign to the primary *tert*-

butyl carbons, and two singlets upfield at 7.44 and 5.61 ppm assigned to the highly shielded carbons attached to the silicon atoms. As expected, the $^{31}P\{^{1}H\}$ NMR spectrum for **2d** reveals a singlet at 186.98 ppm, for the two P(III) centers in the P_2N_2 ring of the molecule.

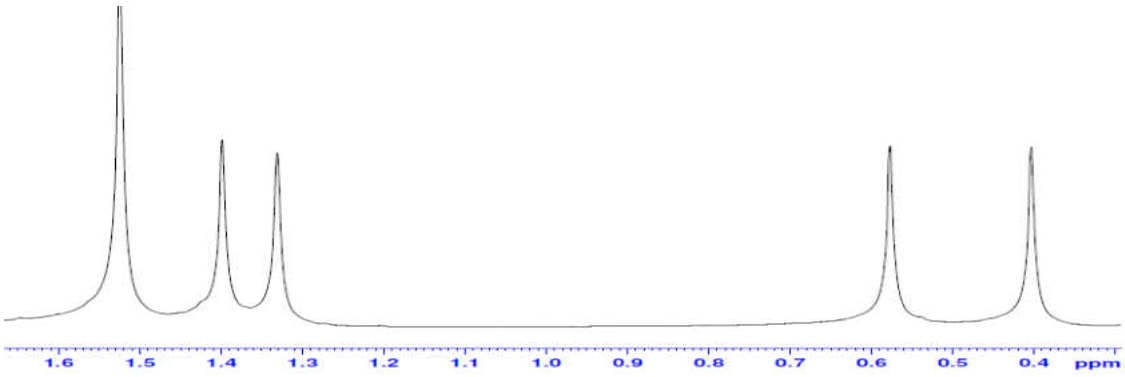

Figure 16. ^{1}H NMR spectrum for **2d**.

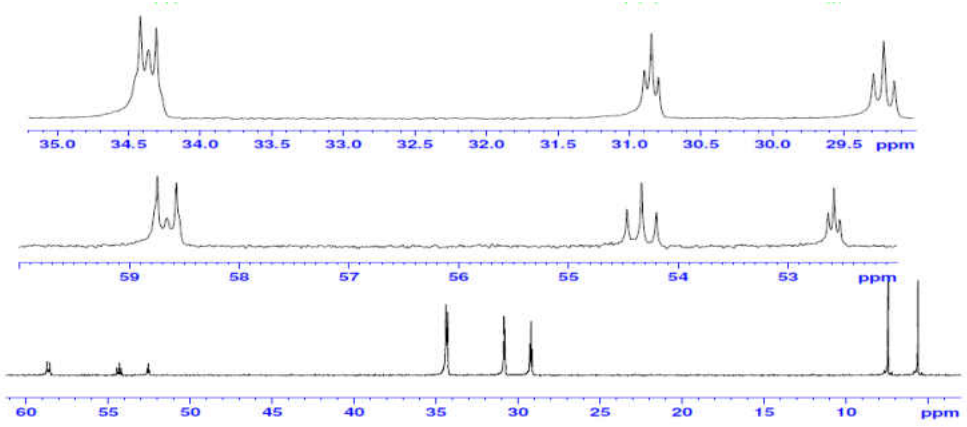

Figure 17. $^{13}C\{^{1}H\}$ NMR Spectrum for **2d**.

Synthesis and Spectroscopic Analysis of {[(^{t}BuNP)$_2$(^{t}BuN)$_2$]BiN(SiMe$_3$)$_2$} 4d

Like in the synthesis of **2d**, a sample of **4a** was treated with LiN(SiMe$_3$)$_2$ in THF at RT for 24 h to furnish compound **4d** (Scheme 20), which was then extracted with toluene. The steric congestion of bismuth in **4a**, and the bulky nature of the monodentate ligand, N(SiMe$_3$)$_2$, still afforded **4d** with a yield of 78% indicating that despite the bulky nature of substituents on the nitrogen atom, it is still available for coordination. The syntheses of **2d** and **4d**, like **2b** and **4b**, completes a homologous series of group 15 compounds with formula [(^{t}BuNP)$_2$(^{t}BuN)$_2$]EN(SiMe$_3$)$_2$, where E = P, As, Sb, and Bi. Compounds **2a**–**4d** are all thermally stable, air-sensitive and colorless, except **4d** that shows a yellow coloration.

As in **2d**, the ^{1}H NMR spectrum of compound **4d** (Figure 18) shows three singlets at 1.45, 1.37 and 1.29 ppm in the ratio 2:1:1, representing the *tert*-butyl protons. The *tert*-butylimino protons are diastereotopic, generating singlets at 1.37 and 1.29 ppm with equal intensities. The signal at 1.29 ppm is attributed to the *tert*-butylimino group on the same side with the N(SiMe$_3$)$_2$ ligand due to steric congestion. Also observed upfield are two singlets at 0.67 and 0.29 ppm representing the methyl protons of the hexamethyldisilylamide ligand. Again, the methyl protons on the more congested side are observed at 0.29 ppm. The ^{13}C{^{1}H} NMR spectrum for **4d** (Figure 19) depicts a doublet at 58.08 (J_{PC} = 15.44 Hz) and two triplets at 54.81 (J_{PC} = 14.95 Hz) and 54.22 ppm (J_{PC} = 17.13 Hz), for the quaternary *tert*-butylamino and *tert*-butylimino carbons, respectively. There are also signals resonating at 36.24 (d, J_{PC} = 12.63 Hz), 30.43 (t, J_{PC} = 9.18 Hz) and 28.26 ppm (t, J_{PC} = 6.83 Hz), attributable to the primary *tert*-butyl carbons, and two singlets upfield at 8.25 and 5.95 ppm representing the highly shielded carbons attached to the silicon atoms. The ^{31}P{^{1}H} NMR spectrum for compound **4d** reveals a singlet at 147.89 ppm, for the two P(III) atoms in the P_2N_2 ring of the molecule.

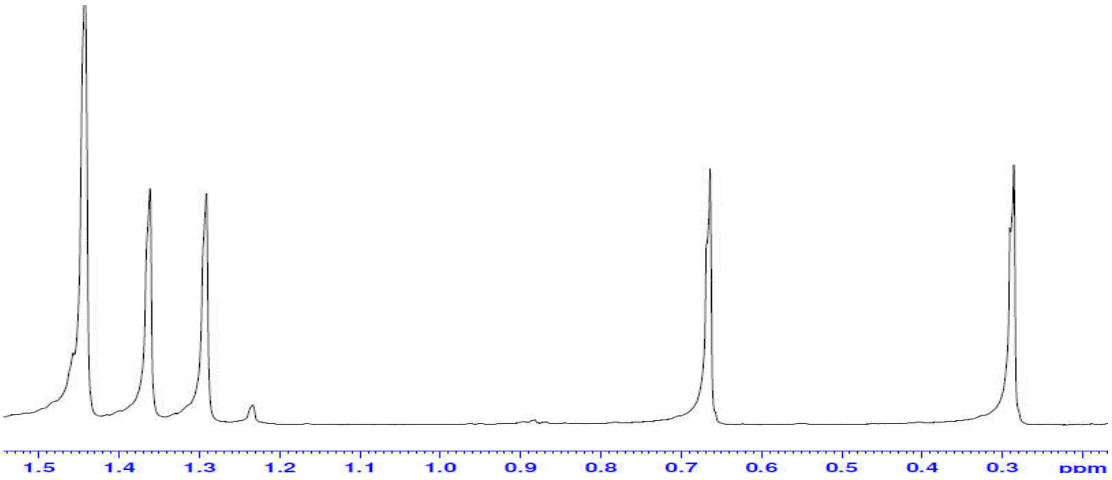

Figure 18. ^{1}H NMR Spectrum for **4d**.

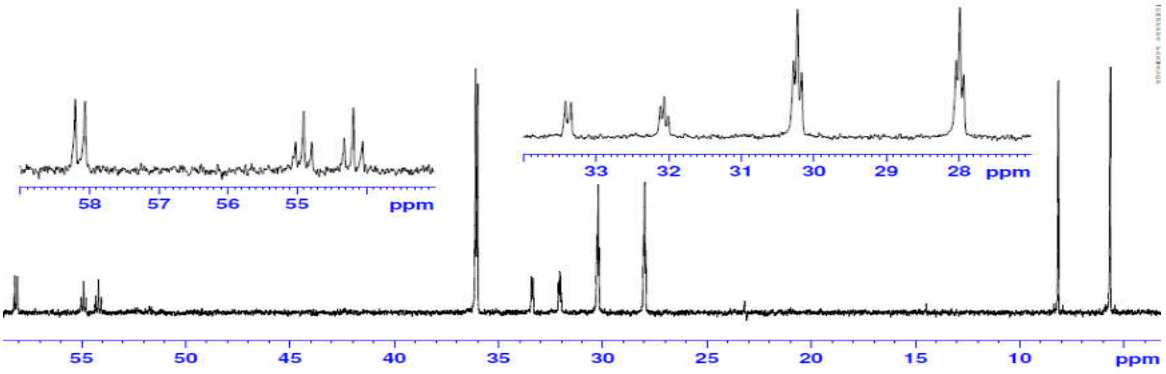

Figure 19. ^{13}C{^{1}H} NMR Spectrum for **4d**.

Solid-state Structure of {[(^{t}BuNP)$_2$(^{t}BuN)$_2$]BiN(SiMe$_3$)$_2$} 4d

X-ray quality crystals of **4d** were isolated as light-yellow, block-shaped crystals from a cold (–6 ℃), concentrated toluene solution. The solid-state structure of **4d** with a partial atom numbering scheme is presented in Figure 20 below, while the crystal data and selected bond parameters are listed in Tables 5 and 6 below, respectively. Compound **4d** crystallized in the monoclinic space group, $P2_1/c$, containing four molecules per unit cell. The bismuth atom

bearing the $N(SiMe_3)_2$ ligand is above the P_2N_2 heterocycle ring, making a bonding contact with N1 of the ring in a κ^3*N* binding mode. The sum of the covalent radius of Bi and N, ($R_{BiN} = r_N + r_{Bi} = 0.71 + 1.51 = 2.22$ Å), giving a theoretical Bi–N bond distance of 2.22 Å. The actual Bi1–N5 bond distance in **4d** from crystallographic data is 2.217(2) Å, showing a difference of 0.003 Å.[115, 120, 121] Thus, the newly formed Bi–N bond distance is quite close to the theoretical value. This is significantly shorter than the $Bi–N_{azide}$ bond distance (2.277 (3) Å)[121] in $Py_2–Bi(N_3)_3$ (Py = pyridine), but more elongated than the Sb–N5 bond distance (2.099(2) Å)[92] in the antimony analogue **3d** due to the difference in covalent radius. The exo-P–N bond distances (P1–N3 = 1.682(2) and P2–N4 = 1.675(2) Å) in **4d** are almost identical to the same bonds in **3d** (1.685(3) and 1.686(3) Å). Similarly, the endocyclic P–N bond distances in **3d** and **4d** are all equidistant. On the contrary, the Bi–N1, Bi–N3 and Bi–N4 bond distances in **4d**, 2.733(2), 2.222(2) and 2.236(2) Å, respectively, are more elongated than the corresponding bond lengths in **3d** (Sb1–N1 = 2.656(2), Sb–N3 = 2.123(2), Sb–N4 = 2.120(2) Å).[92] This observation is expected as the covalent radius of the pnictogens increases down the group. The three bond angles around Bi atom in **4d**, N3–Bi1–N4 = 98.90(8), N3–Bi1–N5 = 101.09(8) and N4–Bi1–N5 = 101.88(8)° (sum = 301.87°), are identical to the same bond angles in **3d** (sum = 302.04°).[92]

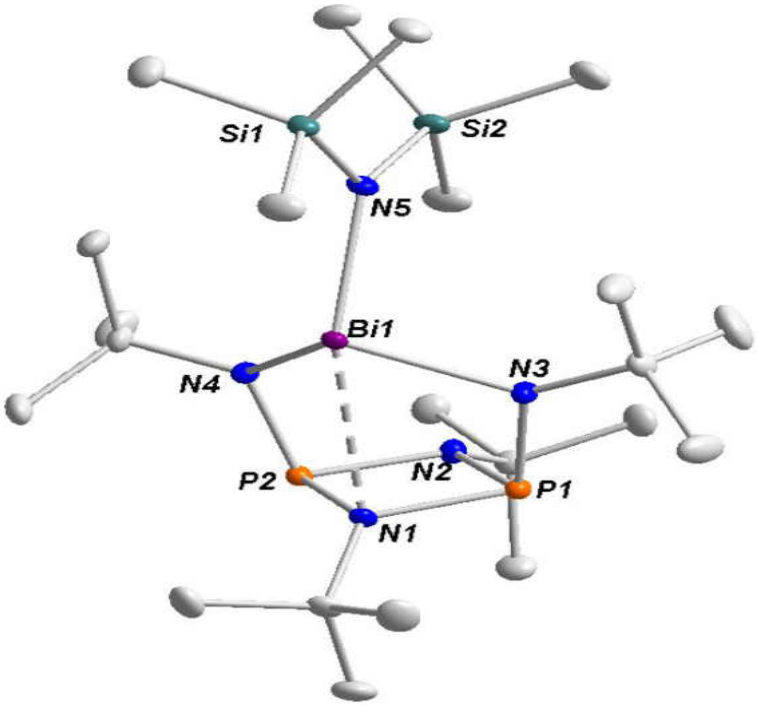

Figure 20. Solid-state structure and partial labelling scheme of **4d**. With the exception of carbon (35 %) all atoms are drawn at the 50 % probability level.

Table 5. Crystal data and structure refinement for **4d**.

Chemical formula	$C_{22}H_{54}BiN_5P_2Si_2$
Fw	715.80
T/K	100.04
λ/Å	0.71073
Crystal system	*monoclinic*
Space group	$P2_1/c$
a/Å	16.4218(12)
b/Å	10.8323(8)
c/Å	18.0205(14)
α/°	90
β/°	96.409(3)
γ/°	90
V/Å^3	3185.6(4)
Z	4
ρ (calc.) g cm^{-3}	1.493
μ/mm^{-1}	5.729
F(000)	1448.0
Reflections collected	38050
Independent reflections	12023 [R_{int} = 0.0344, R_σ = 0.0376]
$Rw(F^2)^b$ [I>2σ(I)]	R1 = 0.0291, wR2 = 0.0772
$R(F)^a$ (all data)	R1 = 0.0344, wR2 = 0.085

[a] $R = \sum|F_o - F_c| \sum |F|_o$. [b] $R_w = \{[\sum w(F_o^2 - F_c^2)] / [\sum w(F_o^2)^2]\}^{1/2}$; $w = 1/[\sigma^2(F_o)^2 + (xP)^2 + yP]$, where $P = (F_o^2 + 2F_c^2)/3$.

Table 6. Selected bond lengths (Å) and angles (°) for **4d**.

Bond Lengths (Å)			
Bi1–N3	2.222(2)	P2–N4	1.675(2)
Bi1–N4	2.236(2)	P1–N1	1.757(2)
Bi1–N1	2.733(2)	P1–N2	1.735(2)
Bi1–N5	2.217(2)	P2–N1	1.759(2)
P1–N3	1.682(2)	P2–N2	1.730(2)
Bond Angles (°)			
N3–Bi1–N4	98.90(8)	N1–P1–N2	82.86(11)
N3–Bi1–N5	101.09(8)	N1–P2–N2	82.48(10)
N4–Bi1–N5	101.88(8)		

Synthesis and Spectroscopic Analysis of {[(^{t}BuNP)$_2$(^{t}BuN)$_2$]AsO^{t}Bu} 2e

In a manner analogous to that used for the syntheses of **1e** and **3e**, **2a** was treated with NaO^{t}Bu in toluene at RT for one day to obtain compound **2e** in 76% yield (Scheme 21) as colorless, block-shaped crystals. The compound is thermally stable and air-sensitive with a melting point of 174–176 °C.

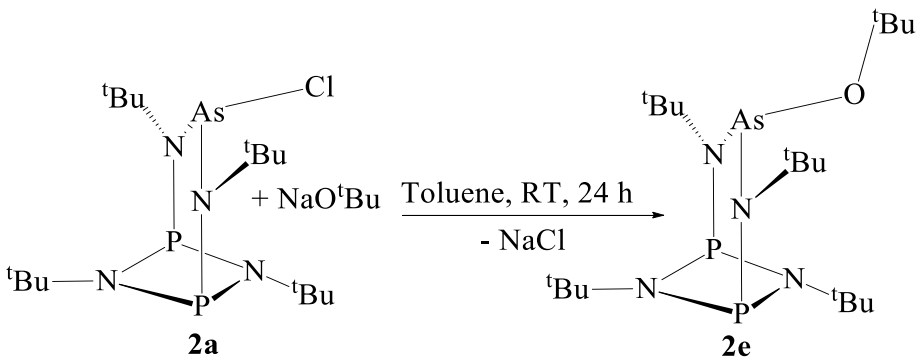

Scheme 21. Synthesis of **2e**.

The ^{1}H NMR spectra of **2e** shows three singlets in the ratio 1: 3: 1 at 1.58, 1.52 and 1.41 ppm, representing the *tert*-butoxide, amino- and imino-*tert*-butyl protons. While the singlet at 1.52 ppm represents the protons of the *tert*-butoxide and *tert*-butylamino groups, those at 1.58 and 1.41 ppm are attributed to the imino *tert*-butyl groups. The signal upfield at 1.41 ppm is assigned to the *tert*-butylimino group on the same side with the *tert*-butoxide ligand. In the ^{13}C{^{1}H} NMR spectrum of **2e** (Figure 21) the quaternary carbon of the *tert*-butoxide ligand is found downfield at 75.44 ppm as a singlet, while those of the *tert*-butylamino and *tert*-butylimino carbons are shown as triplets at 57.77, 53.27 and 52.75 ppm with J_{PC} of 8.99, 13.65 and 7.18 Hz, respectively. The primary carbons of the *tert*-butoxide ligand appear as a singlet at 33.28 ppm, while those of the *tert*-butyl groups are shown as triplets at 33.60 (J_{PC} = 5.53 Hz), 30.50 (J_{PC} = 6.35 Hz) and 29.95 ppm (J_{PC} = 6.08Hz). The triplet at 33.60 ppm is attributed to the primary carbons of the *tert*-butylamino carbons. The ^{31}P{^{1}H} NMR spectrum of **2e** show a singlet at 183.08 ppm representing the two phosphorus(III) atoms of the P_2N_2 heterocycle.

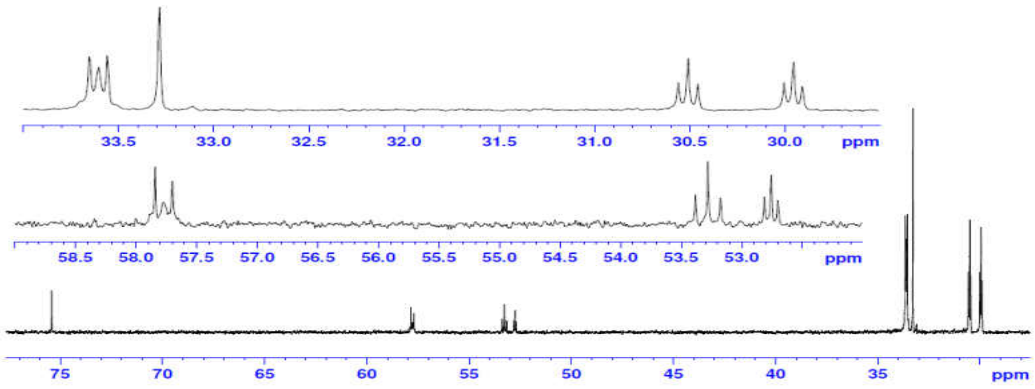

Figure 21. $^{13}C\{^{1}H\}$ NMR Spectrum for **2e**.

Synthesis and Spectroscopic Analysis of {[(^{t}BuNP)$_2$(^{t}BuN)$_2$]AsOPh} 2f

When a sample of **2a**, dissolved in toluene, was treated at RT with a solution of lithium phenoxide for 24 h compound **2f** was obtained (Scheme 22). A yield of 78% of this colorless, air-sensitive and thermally stable solid was obtained.

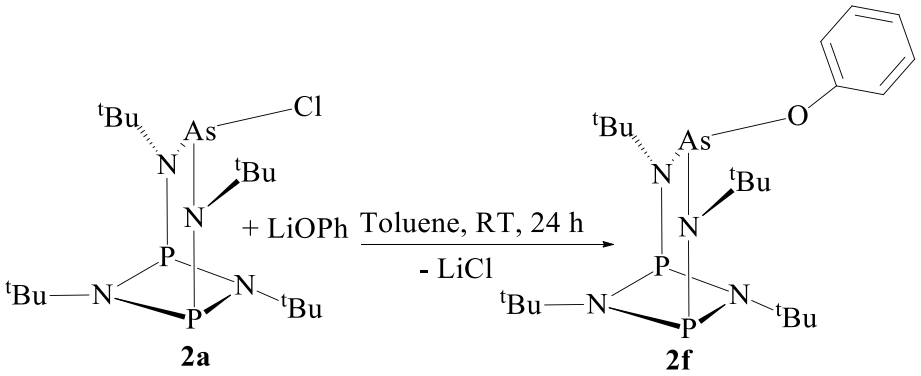

Scheme 22. Synthesis of **2f**.

The ^{1}H NMR spectrum of **2f** depicts a doublet at 7.20 ppm (J_{PH} = 7.61 Hz), multiplets at 7.15 ppm and a triplet at 6.85 ppm (J_{PH} = 7.03 Hz), these being the respective signals for *ortho*, *meta*, and *para* protons of the phenyl group attached to the phenoxide ligand. Due to the presence of the electronegative oxygen atom, the phenyl protons moved more upfield than those in **2b**. The signals of the *tert*-butyl protons are found at 1.59, 1.40 and 1.36 ppm in the ratio 1:2:1

representing the protons of *tert*-butylimino and *tert*-butylamino, those of the former being diastereotopic. The $^{13}C\{^{1}H\}$ NMR spectrum for **2f** (Figure 22) shows phenyl carbon signals at 159.60, 130.09, 120.25 and 118.72 ppm, these being the respective signals for the *ipso*, *ortho*, *meta*, and *para* carbons. The quaternary *tert*-butylamino carbons appear as a triplet at 57.83 ppm (J_{PC} = 9.03 Hz), while those of *tert*-butylimino carbons appear as triplets at 53.09 (J_{PC} = 13.13 Hz) and 52.07 ppm (J_{PC} = 5.75 Hz). The signals at 33.08 (t, J_{PC} = 5.67 Hz), and 30.00 (t, J_{PC} = 6.34 Hz) and 29.87 ppm (t, J_{PC} = 6.34 Hz), represent the primary carbons of the *tert*-butylamino and *tert*-butylimino carbons, respectively. The $^{31}P\{^{1}H\}$ NMR spectrum for **2f** is a singlet at 182.18 ppm depicting the phosphorus(III) centers in the P_2N_2 heterocycle.

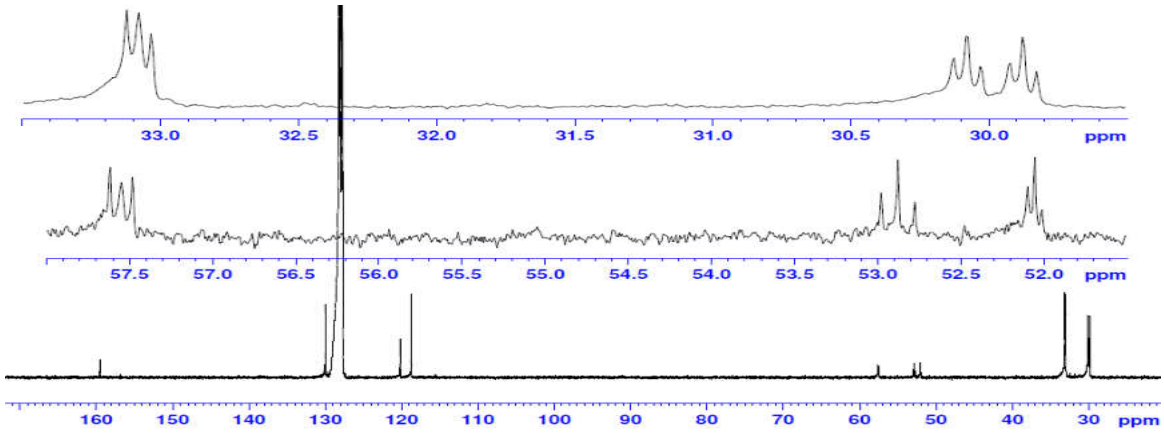

Figure 22. $^{13}C\{^{1}H\}$ NMR Spectrum for **2f**.

Synthesis and Spectroscopic Analysis of {[(^{t}BuNP)$_2$(^{t}BuN)$_2$]SbOSO$_2$CF$_3$} 3g

When compound **3a** was treated with silver triflate in THF for 30 minutes, **3g** was obtained in 92% yield (Scheme 23). To avoid the photo-reduction of Ag(I) to Ag(s), the flask containing the reaction mixture was wrapped with aluminum foil. In this reaction, there is the possibility of THF polymerization due to the presence of the positive charge on the Sb cation. The THF was pumped off immediately after the reaction was completed and then the residue was extracted

with chloroform to obtain **3g**. An alternative route for this synthesis, however, is to combine **3a** and the silver triflate in toluene and then stir at RT for 1 h, thus avoiding the possibility of THF polymerization.

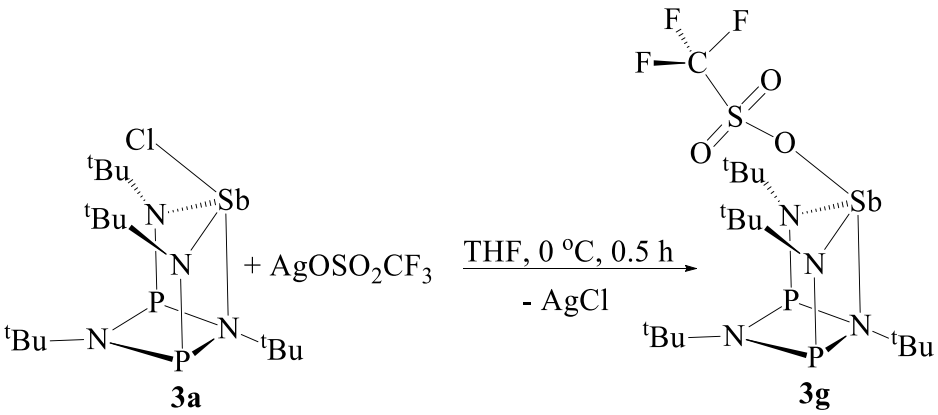

Scheme 23. Synthesis of **3g**.

The ^{1}H NMR spectrum of **3g** (Figure 23) shows two singlets at 1.46 and 1.10 ppm in the ratio 1: 1 for the *tert*-butyl protons. The introduction of the triflate ion into the molecule causes the non-equivalent *tert*-butylimino groups in **3g** to become equivalent and these are, therefore, observed as a singlet at 1.46 ppm. The ^{13}C{^{1}H} NMR spectrum of **3g** (Figure 24) depicts a quartet at 120.67 ppm with a J_{CF} = 319 Hz, which we attribute to the fluorinated carbon, while the quaternary carbons of the *tert*-butyl groups are observed as triplets at 57.91 (J_{PC} = 5.80 Hz) and 54.96 ppm (J_{PC} = 10.37 Hz). The primary *tert*-butyl carbons resonate at 33.61 ppm as a triplet (J_{PC} = 6.63 Hz) and at 27.85 ppm as a singlet. There is only one singlet observed at 182.73 ppm on the ^{31}P{^{1}H} NMR spectrum for **3g** representing the two P(III) centers on the P_2N_2 heterocycle.

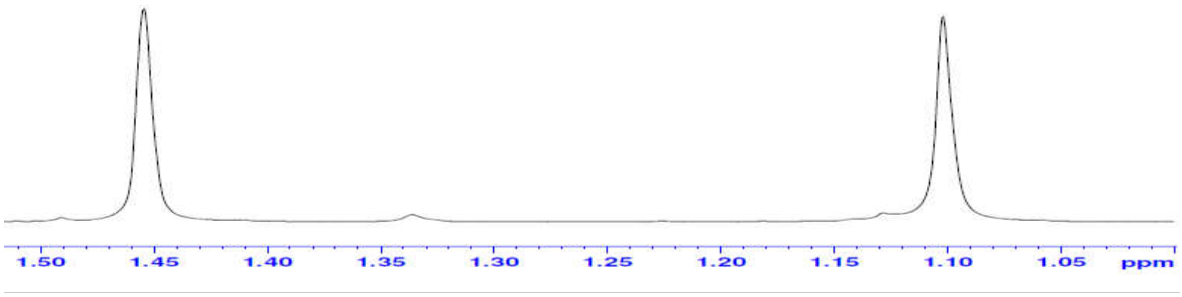

Figure 23. ^{1}H NMR Spectrum for **3g**.

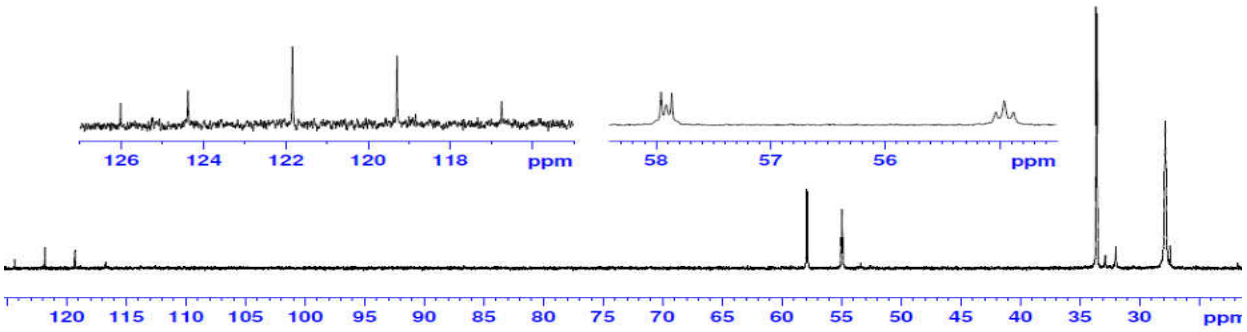

Figure 24. ^{13}C{^{1}H} NMR Spectrum for **3g**.

Solid-state Structure of {[(^{t}BuNP)$_2$(^{t}BuN)$_2$]SbOSO$_2$CF$_3$} 3g

From a cold (–6 °C), concentrated chloroform solution was isolated colorless, needle-like crystals of **3g** suitable for X-ray studies. The solid-state structure of **3g** with a partial atom numbering scheme is presented in Figure 25 below, while the crystal data and selected bond parameters are listed in Tables 7 and 8 below, respectively. The compound crystallizes in the monoclinic space group, $P2_1/n$, with four molecules per unit cell. Unlike the phosphorus analogue where there is no bond formed between the cation and the anion, there is an Sb–O (2.3652(14) Å) bond formed between the triflate and the antimony atom in **3g**. The solid-state structure of **3g** (Figure 25) shows it to be a *seco*-heterocubic since the larger antimony atom makes bonding contact with N1 of the P_2N_2 ring. The metalloid is symmetrically chelated by the

two amido groups, forming the long bond to O3 of the triflate moiety mentioned above. The endocyclic (1.716(16)–1.7971(6) Å) and exocyclic (1.675(2) Å) bonds of **3g** are almost identical to those of **3a**. Experimentally determined Sb–O bond distances in Sb(III) systems, $K[Sb(C_4H_4O_6)_2].H_2O$ 2.193(13) Å and $K_2[Sb_2C_4H_4O_6)_2].3H_2O$[122] 2.163(28) Å reported by Palenik *et al*., are significantly shorter than the Sb–O bond in **3g**. Also, the Sb–O bond in **3g** is longer than that in **3f** (2.031(8) Å)[103]because the triflate is a non-coordinating ligand and therefore bonds poorly to the metalloid.

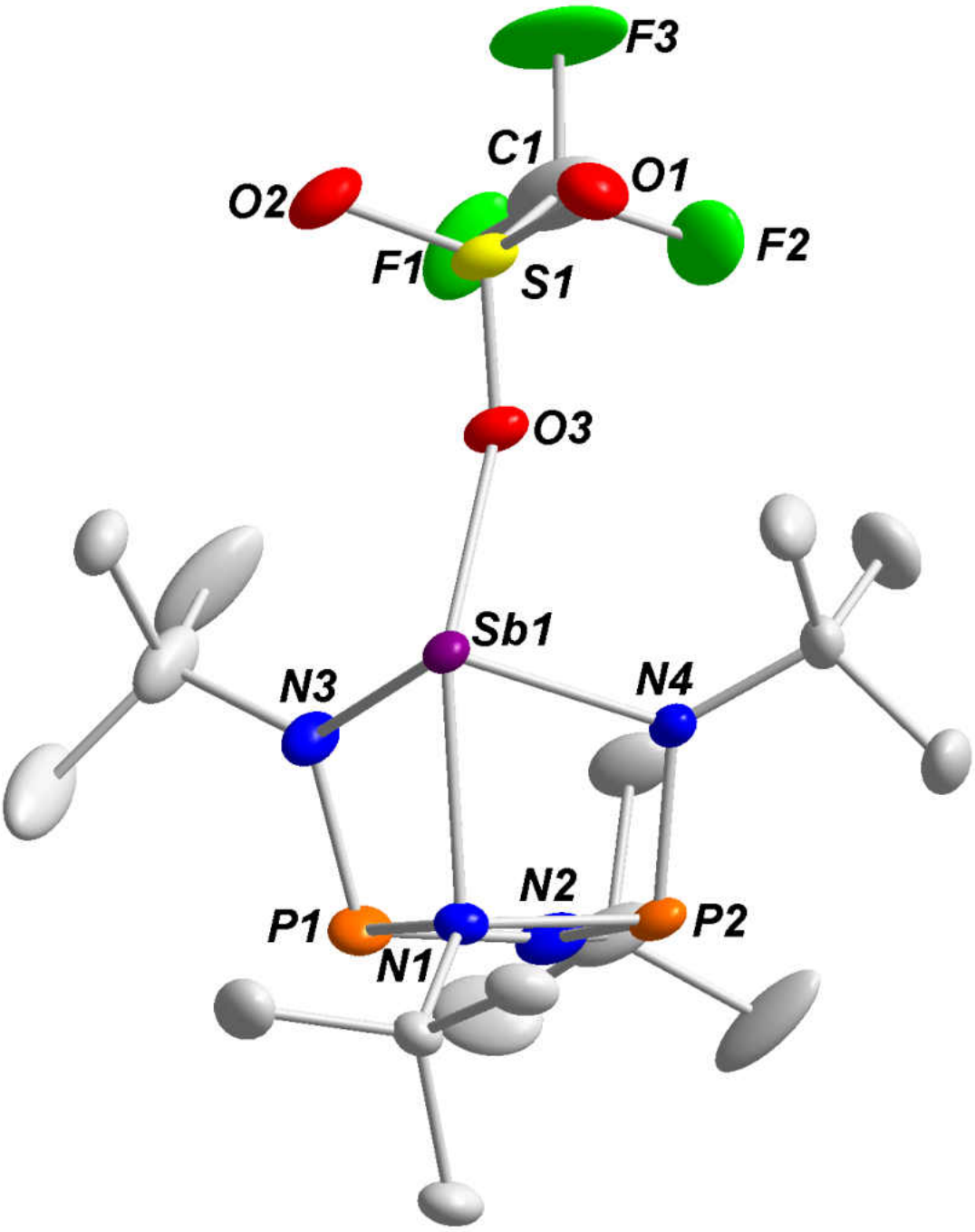

Figure 25. Solid-state structure and partial labelling scheme of **3g**. All atoms are drawn at the 50 % probability level.

Table 7. Crystal data and structure refinement for **3g**.

Chemical formula	$C_{17}H_{36}F_3N_4O_3P_2SSb$
Fw	617.25
T/K	100(2)
λ/Å	0.71073
Crystal system	*Monoclinic*
Space group	$P2_1/n$
a/Å	9.7212(3)
b/Å	18.6010(5)
c/Å	15.2849(4)
α/°	90
β/°	100.5301(12)
γ/°	90
V/Å^3	2717.33(13)
Z	4
ρ (calc.) g cm^{-3}	1.509
μ/mm^{-1}	1.254
F(000)	1256
Completeness (%)	99.9
Reflections collected	49097
Independent reflections	14692 [R_{int} = 0.0241]
$Rw(F^2)^b$ [I>2σ(I)]	R_1 = 0.0427, wR_2 = 0868
$R(F)^a$ (all data)	R_1 = 0.0517, wR_2 = 0.0907

[a] $R = \sum|F_o - F_c| \sum |F|_o$. [b] $R_w = \{[\sum w(F_o^2 - F_c^2)] / [\sum w(F_o^2)^2]\}^{1/2}$; $w = 1/[\sigma^2(F_o)^2 + (xP)^2 + yP]$, where $P = (F_o^2 + 2F_c^2)/3$.

Table 8. Selected Bond Lengths (Å) and Angles (°) for **3g**.

Bond Lengths (Å)			
Sb1–O3	2.3652(14)	P2—N1	1.8009(16)
Sb1–N1	2.3029(14)	P2—N2	1.7177(19)
Sb1–N3	2.0613(16)	S1—O1	1.436(2)
Sb1—N4	2.0662(15)	S1—O2	1.437(18)
P2—N4	1.675(2)	S1—O3	1.4702(14)
P1—N1	1.7971(16)	C—F(avg)	1.321(5)
P1—N2	1.716(2)	S1—C1	1.823(3)
Bond Angles (°)			
N3—Sb1—N4	104.34(7)	Sb1—O3—S1	136.42(8)
N3—Sb1—O3	87.14(6)	O1—S1—O2	116.68(11)
N4—Sb1—O3	86.99(6)	O1—S1—O3	113.92(10)
N1—P1—N2	80.73(8)	O2—S1—O3	113.98(11)
N1—P2—N2	80.58(8)		

Synthesis and Spectroscopic Analysis of {[(^{t}BuNP)$_2$(^{t}BuN)$_2$]PI} 1h

The treatment of compound **1a** with NaI in THF at RT for 1 day gave compound **1h** with a yield of 91% (Scheme 24). To avoid unwanted side reactions between EI_3 (E = P, As, Sb) and **31**, NaI is used to substitute the chloride ligand with iodide in **1a**–**3a**. This reaction is consistent with a typical S_N2 reaction in which the stronger nucleophile, I^-, displaces the weaker one, Cl^-, to form NaCl with a higher lattice energy than NaI. An attempt to substitute the chloride nucleophile with a bromide failed because the reaction, though feasible, was too slow.

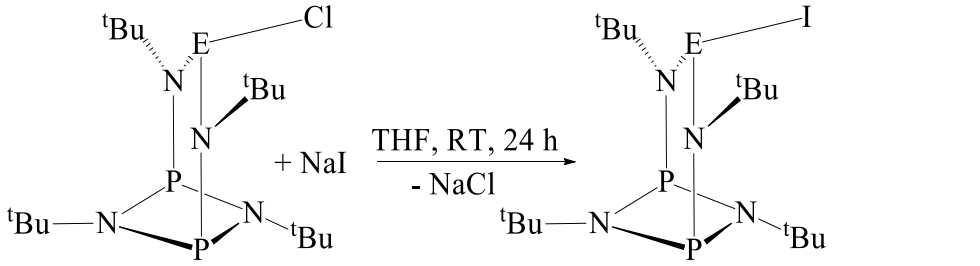

1a (E = P), **2a** (E = As), **3a** (E = Sb) **1h** (E = P), **2h** (E = As), **3h** (E = Sb)

Scheme 24. Synthesis of **1h**, **2h** and **3h**.

The ^{1}H NMR spectrum for **1h** in deuterated chloroform shows two signals: a doublet at 1.61 ppm with a J_{PH} = 4.77 Hz and a singlet at 1.35 ppm. **1h** ^{13}C{^{1}H} NMR spectrum (Figure 26) depicts a multiplet at 60.84 ppm and a singlet at 53.55 ppm, corresponding to the quaternary carbons of the *tert*-butylamino and *tert*-butylimino carbons, respectively. Meanwhile, the primary carbons of the *tert*-butyl groups appear upfield at 29.02 ppm as a multiplet. Two signals are observed on the ^{31}P{^{1}H} NMR spectrum for **1h** (Figure 27) at 196.42 ppm (t, J_{PP} = 29 Hz) and 173.77 ppm (d, J_{PP} = 27 Hz), representing the P(III) center at the apex of the cage and the two P(III) centers of the P_2N_2 ring, respectively. This shows that the two P(III) atoms on the P_2N_2 ring coupled with the P(III) atom above the P_2N_2 ring to generate a doublet, while the latter in turn coupled with the former to give the triplet. This observation is analogous to what is seen in **1a**.

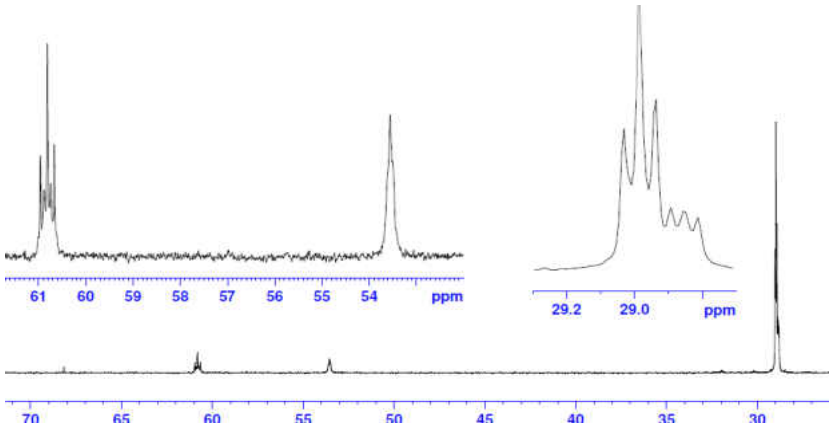

Figure 26. $^{13}C\{^{1}H\}$ NMR Spectrum for **1h**.

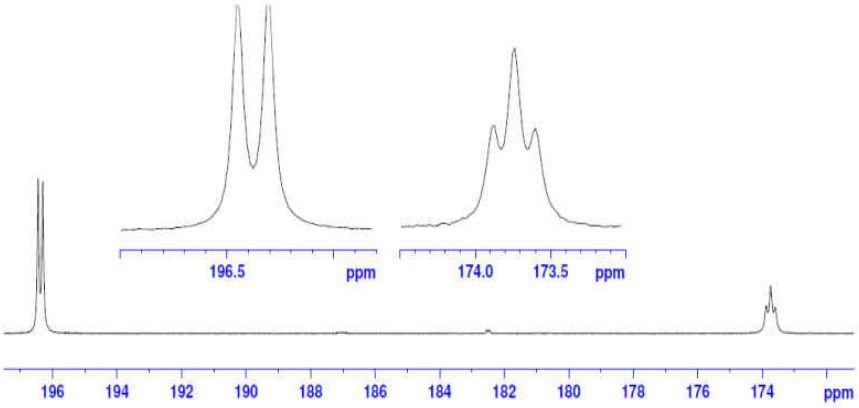

Figure 27. $^{31}P\{^{1}H\}$ NMR Spectrum for **1h**.

Solid-state Structure of {[(^{t}BuNP)$_2$(^{t}BuN)$_2$]PI} 1h

Yellow, block-shaped single crystals of **1h**, of excellent quality, were obtained from a cold concentrated THF solution, thus offering the opportunity for an X-ray structural investigation for this compound. The solid-state structure of **1h** with a partial atom numbering scheme is presented in Figure 28 below, while the crystal data and selected bond parameters are listed in Tables 9 and 10 below, respectively. Compound **1h** crystallized in the centrosymmetric space group, $P2_1/m$, with dimensions, **a** (9.5405(7) Å) ≠ **b** (11.8694(8) Å) ≠ **c** (10.3274(7) Å) and α =

$\gamma = 90° \neq \beta = 96.573(2)°$, containing two molecules per unit cell. The molecule, therefore, belongs to the point group, C_s, with the mirror plane containing the P–I bond and the two nitrogen atoms of the P_2N_2 ring. In Figure 28, it is observed that the phosphorus(III) atom bearing the iodine atom is centered above the P_2N_2 heterocycle in a typical κ^2N chelation mode, just as in **1a**. The P–I bond length in **1h** is 2.7339(3) Å, ca. 10% (0.2939(3) Å) longer than the theoretical value (2.440 Å). Meanwhile, the P–I bond distance in PI_3 (2.463(5) Å) differs from the theoretical value (2.440 Å) by 0.023 Å. The P–I bond length in **1h** (2.7339(3) Å) is 0.4899 Å longer than the P–Cl bond in **1a** (2.244(3) Å), as expected. This is attributed to the large size of the iodine ligand which prevents the formation of a purely covalent but forms a partial covalent and partial ionic bond. This explanation is justified by the equidistant bond length in **1h** (P–I = 2.7339(3) Å) and **2h** (As–I = 2.7374(4) Å), despite the difference in covalent radii of P and As. The theoretical difference between the P–I and As–I bond distances is 0.100 Å. Compound, PI_3, with bond parameters (2.463(5) Å and 102.0(3)°)[123] shows a marked difference between the P–I bond length in **1h** but the same bond angle for I–P–I =102.0(3)° and N1–P–I = 102.67(4)°. However, the bond length of the P–I bond in $[(Ph_3P)\cdot(sym\text{-}C_6F_3I_3)]$ (3.376(1) Å)[124] is much longer than the same bond in **1h**. The bonds, P–N3, P1–N1, P1–N2, and P1–N3 with respective lengths, 1.6783(10), 1.7183(10), 1.7170(10), and 1.7531(10) Å in **1h** perfectly match those of **1a** in value indicating that there was no distortion in the bicyclic cage after the chloride ligand was replaced by the iodide.[98] While the bond angle, P1–N3–P3 = 124.57(6)°, in **1h** is exactly equal to the same angle in **1a** (124.9(3)°), the angle, N–P– Hal, shows a difference of less than 1° between the two compounds.

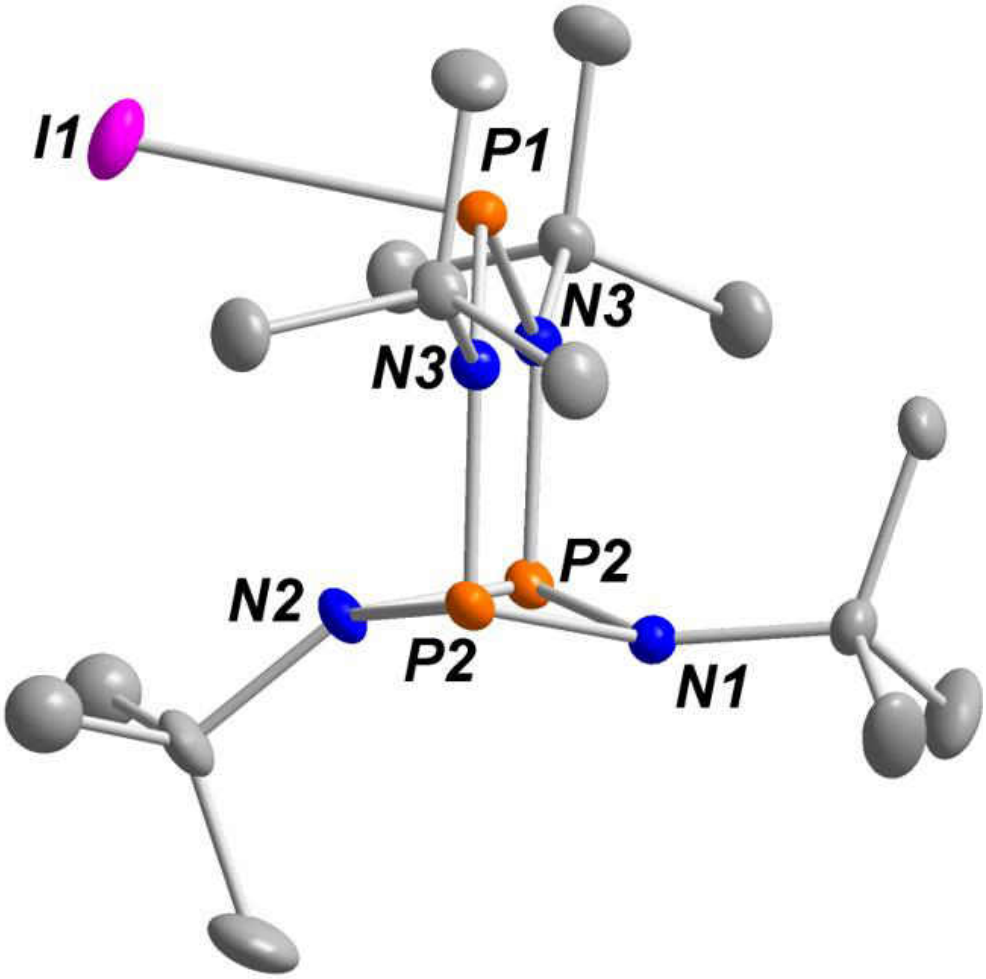

Figure 28. Solid-state structure and partial labelling scheme of **1h**. Hydrogen atoms have been omitted for clarity. All atoms are drawn at the 50 % probability level.

Table 9. Crystal data and structure refinement for **1h**.

Chemical formula	$C_{16}H_{36}IN_4P_3$
Fw	504.32
T/K	149.99
λ/Å	0.71073
Crystal system	monoclinic
Space group	$P2_1/m$
a/Å	9.5405(7)
b/Å	11.8694(8)
c/Å	10.3274(7)
α/°	90
β/°	96.573(2)
γ/°	90
V/Å^3	1161.79(14)
Z	2
ρ (calc.) g cm^{-3}	1.4415
μ/mm^{-1}	1.591
F(000)	515.9
Reflections collected	26788
Independent reflections	4626 [R_{int} = 0.0261, R_σ = 0.0163]
$Rw(F^2)^b$ [I>2σ(I)]	R_1 = 0.0241, wR_2 = 0.05531
$R(F)^a$ (all data)	R_1 = 0.0276, wR_2 = 0.0551

[a] $R = \sum||F_o| - |F_c|| \sum |F|_o$. [b] $R_w = \{[\sum w(F_o^2 - F_c^2)] / [\sum w(F_o^2)^2]\}^{1/2}$; $w = 1/[\sigma^2(F_o)^2 + (xP)^2 + yP]$, where $P = (F_o^2 + 2F_c^2)/3$.

Table 10. Selected Bond Lengths (Å) and Angles (°) for **1h**.

Bond Lengths (Å)			
I1–P2	2.7339(5)	P3–P3[1]	2.5236(6)
N1–P2	1.6783(10)	P3–N3	1.7170(10)
N1–P3	1.7531(10)	N3–C13	1.481(2)
N2–P3[1]	1.7183(10)	C8–C9	1.531(2)
N2–P3	1.7183(10)	C8–C11[1]	1.5234(17)
N1–C2	1.5173(15)	C8–C11	1.5234(17)
N2–C8	1.481(2)	C13–C15	1.528(3)
Bond Angles (°)			
C2–N1–P2	118.00(7)	N2–P3–N1	100.98(6)
P3–N1–P2	124.57(6)	P3[1]–P3–N1	92.18(3)
P3–N1–C2	116.60(7)	P3[1]–P3–N2	42.75(3)
N1[1]–P2–I1	102.67(4)	N3–P3–N1	98.18(6)
N1–P2–I1	102.67(4)	N3–P3–N2	83.24(5)
N1[1]–P2–N1	104.67(7)	P3[1]–N3–P3	94.59(7)
P3[1]–N2–P3	94.50(7)	C13–N3–P3[1]	125.48(6)

Synthesis and Spectroscopic Analysis of {[(^{t}BuNP)$_2$(^{t}BuN)$_2$]AsI} 2h

Like in the synthesis of **1h**, compound **2a** was treated with sodium iodide in THF at RT for 24 h to furnish compound **2h** in a yield of 93% (Scheme 24).

The NMR data for compound **2h** were collected in deuterated chloroform. The ^{1}H NMR spectrum for **2h** shows two singlets in the ratio 3:1 at 1.54 and 1.33 ppm corresponding to the *tert*-butyl protons. In the ^{13}C{^{1}H} NMR spectrum of **2h**, two signals are observed at 60.38 (t, J_{PC} = 8.58 Hz) and 53.30 ppm (s), corresponding to the quaternary carbons of the *tert*-butyl groups, while two other signals are observed at 30.02 and 29.10 ppm representing the primary carbons. As expected, the ^{31}P{^{1}H} NMR spectrum for **2h** reveals a singlet resonating at 182.44 ppm corresponding to the two P(III) centers of the P_2N_2 cycle.

Solid-state Structure of {[(^{t}BuNP)$_2$(^{t}BuN)$_2$]AsI} 2h

Yellow, block-shaped crystals of **2h**, suitable for single crystal study, were isolated after recrystallization, from a cold (– 6 °C) concentrated THF solution after one day. The solid-state structure of **2h** with a partial atom numbering scheme is presented in Figure 29 below, while the crystal data and selected bond parameters are listed in Tables 11 and 12 below, respectively. Compound **2h** like **1h**, crystallized in the monoclinic space group, $P2_1/m$, with two molecules per unit cell and dimensions, **a** = 9.5274(8), **b** = 11.9897(9) and **c** = 10.3478(7) Å and β = 96.533(3)°. An interesting feature of **2h** and **1h** is the equality in the E–I bond lengths (As–I = 2.7374(4) and P–I = 2.7339(5) Å). This anomalous bond length observation is attributable to the fact that the P–I and As–I bonds have more ionic character than covalent character. Compound **2h** is analogous to **1h** in all respects, therefore a detailed discussion will not be given here.

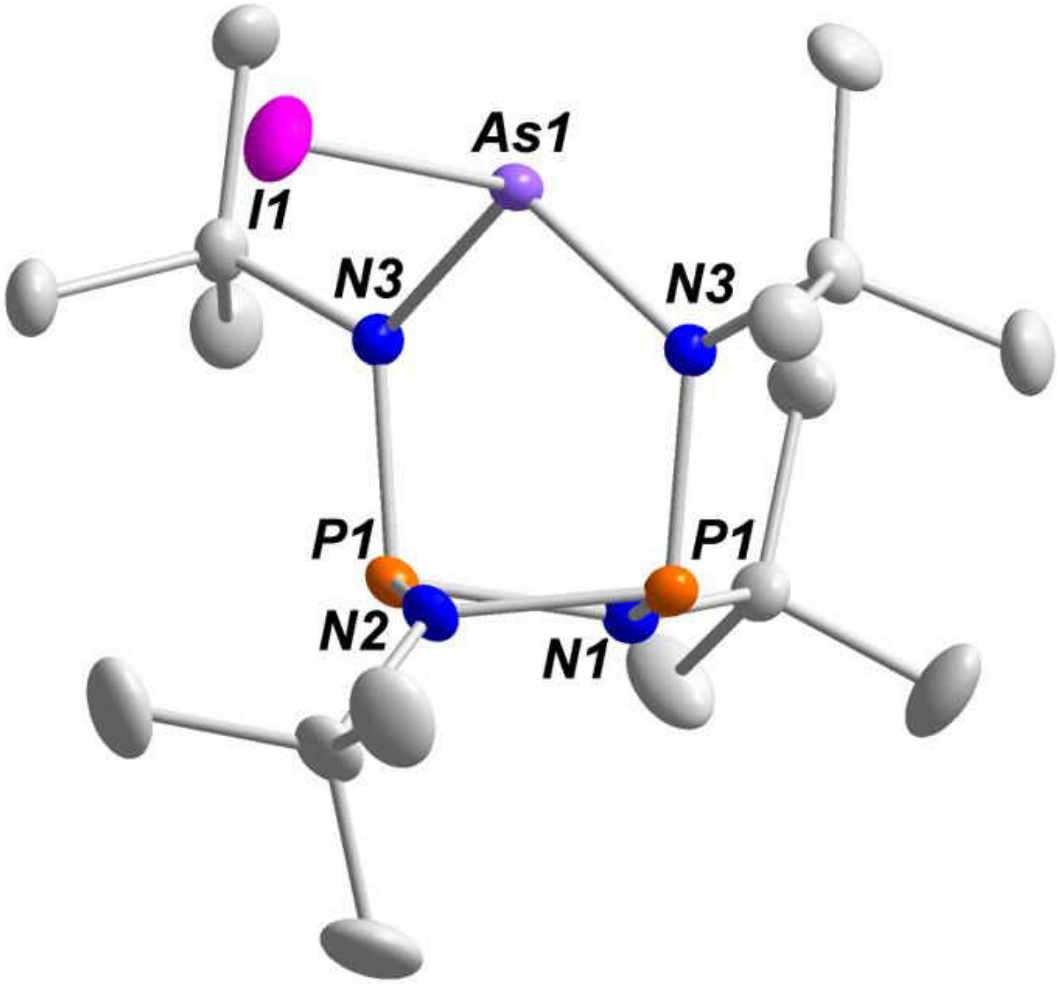

Figure 29. Solid-state structure and partial labelling scheme of **2h**. All atoms are drawn at the 50 % probability level. Hydrogen atoms have been omitted for clarity.

Table 11. Selected Bond Lengths (Å) and Angles (°) for **1h**.

Chemical formula	$C_{16}H_{36}AsIN_4P_2$
Fw	511.98
T/K	149.99
λ/Å	0.71073
Crystal system	*monoclinic*
Space group	$P2_1/m$
a/Å	9.5274(8)
b/Å	11.9897(9)
c/Å	10.3478(7)
α/°	90
β/°	96.533(3)
γ/°	90
V/Å^3	1174.36(15)
Z	2
ρ (calc.) g cm^{-3}	1.4478
μ/mm^{-1}	2.901
F(000)	479.9
Reflections collected	28533
Independent reflections	4681 [R_{int} = 0.0307, R_σ = 0.0196]
$Rw(F^2)^b$ [I>2σ(I)]	R_1 = 0.0327, wR_2 = 0.0984
$R(F)^a$ (all data)	R_1 = 0.0393, wR_2 = 0.1037
[a] $R = \sum\|F_o - F_c\| \sum\|F\|_o$. [b] $R_w = \{[\sum w(F_o^2 - F_c^2)] / [\sum w(F_o^2)^2]\}^{1/2}$; $w = 1/[\sigma^2(F_o)^2 + (xP)^2 + yP]$, where $P = (F_o^2 + 2F_c^2)/3$.	

Table 12. Selected Bond Lengths (Å) and Angles (°) for **2h**.

Bond Lengths (Å)			
I1–As1	2.7374(4)	C2–C12	1.527(3)
N1–As1	1.8383(17)	C13–C15	1.531(6)
N1–P3	1.7255(17)	C6–C4	1.531(3)
P3–P3[1]	2.5471(11)	N1–C4	1.508(3)
P3–N3	1.7178(17)	C2–N3	1.481(4)
N2–P3[1]	1.7248(17)	N2–C13	1.482(4)
N2–P3	1.7248(17	C2–C11	1.527(4)
Bond Angles (°)			
P3–N1–As1	122.70(9)	N2–P3–N1	99.61(10)
C4–N1–As1	117.39(13)	P3[1]–P3–N2	42.41(6)
C4–N1–P3	118.96(13)	N3–P3–N1	101.95(10)
N1–As1–I1	101.96(50	N3–P3–N2	82.92(90
N1[1]–As1–I1	101.96(5)	P3[1]–N3–P3	95.70(12)

Synthesis and Spectroscopic Analysis of {[(^{t}BuNP)$_2$(^{t}BuN)$_2$]SbI} 3h

When compound **3a** was treated with NaI in THF for 1 day at RT, **3h** was obtained in about 88% yield (Scheme 24). Like **1h** and **2h**, the reaction follows an S_N2 mechanism, but much faster

than the former. While **1h** and **2h** produced block-shaped crystals, **3h** afforded tiny needle-like crystals.

The ^{1}H NMR spectrum of **3h** in chloroform shows two singlets at 1.55 and 1.40 ppm in the ratio 3:1 representing the *tert*-butyl protons in the molecule. Probably, because of the large size and repulsive interaction of the iodine atom with the nitrogen atoms of the *tert*-butylamino groups, one of the *tert*-butylimino groups becomes magnetically equivalent to the *tert*-butylamino groups, thus generating the singlet at 1.55 ppm. The ^{13}C{^{1}H} NMR spectrum for **3h**, on the other hand depicts a triplet at 59.00 ppm (J_{PC} = 6.30 Hz) representing the quaternary carbons of the *tert*-butyl groups, while the primary carbons are seen as a triplet upfield at 33.56 ppm (J_{PC} = 5.99 Hz). The two phosphorus(III) atoms of the P_2N_2 ring are shown as a singlet at 143.70 ppm on the ^{31}P{^{1}H} NMR spectrum of **3h**.

Solid-state Structure of {[(^{t}BuNP)$_2$(^{t}BuN)$_2$]SbI} 3h

Yellow, needle-like crystals of **3h**, suitable for single crystal study, were isolated from a cold (– 6 °C) THF solution after 3 days. The solid-state structure of **3h** with a partial atom numbering scheme is presented in Figure 30 below, while the crystal data and selected bond parameters are listed in Tables 13 and 14 below, respectively. This compound crystallized in the monoclinic space group, $P2_1/c$, with four molecules per unit cell. While **1h**, **2h** and **3h** are isomorphs of the centrosymmetric space groups ($P2_1/m$, and $P2_1/c$), **3h** adopts a κ^3N chelation mode, in which the Sb atom makes a bonding contact with N1 of the P_2N_2 heterocycle. The Sb–I bond length in **3h** (2.9131(3) Å) differs from the calculated Sb–I bond length (2.730 Å) by 0.183(3) Å. Apart from the Sb–I (2.9131(3) Å) bond in **3h** that is longer than the Sb–Cl (2.492(3) Å) bond in **3a**, all

other bond parameters are the same. A similar bond distance (Sb–I = 2.928(6) Å) is seen in {[(NETU)SbI_2(μ_2-I)$_2$(μ_2-S-NETU)SbI_2(NETU)]} (NETU = *N*-ethylthiourea).[125]

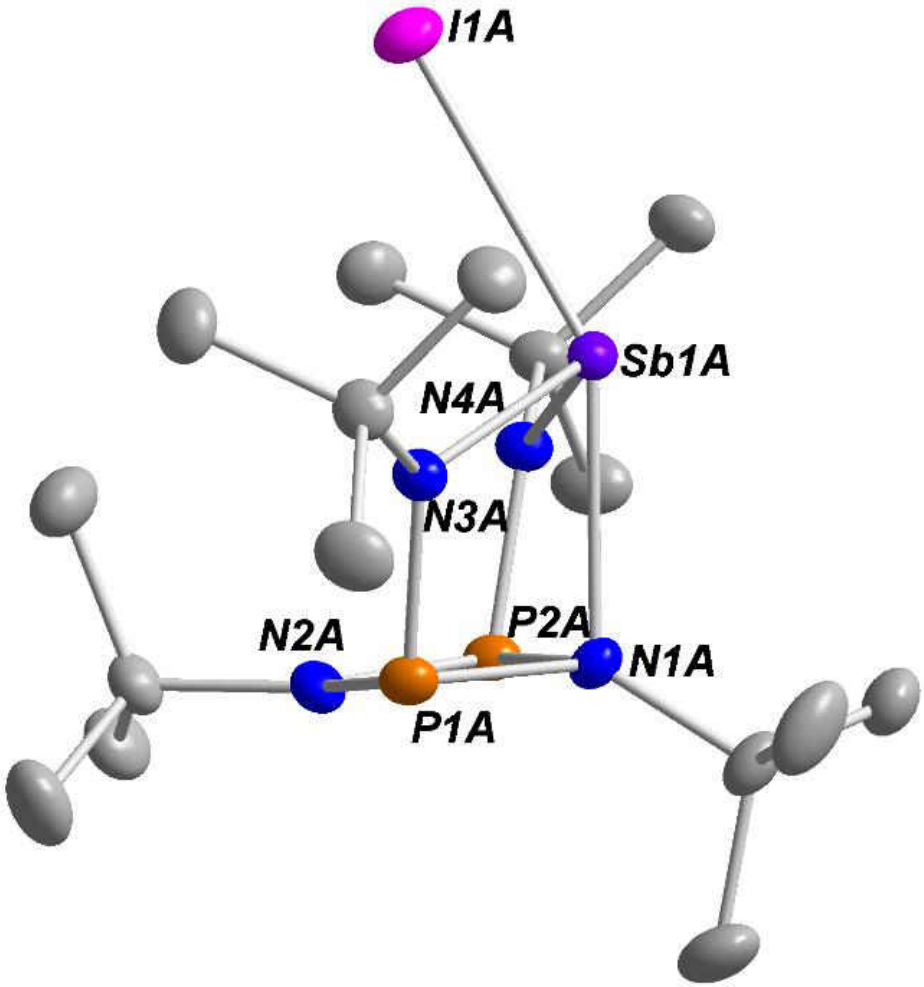

Figure 30. Solid-state structure and partial labelling scheme of **3h**. All atoms are drawn at the 50 % probability level. Hydrogen atoms have been omitted for clarity.

Table 13. Crystal and structure refinement data for **3h**.

Chemical formula	$C_{16}H_{36}IN_4P_2Sb$
Fw	595.10
T/K	150.0
λ/Å	0.71073
Crystal system	*monoclinic*
Space group	$P2_1/c$
a/Å	9.6060(6)
b/Å	18.7374(12)
c/Å	26.7135(18)
α/°	90
β/°	93.325(3)
γ/°	90
V/Å^3	4800.1(5)
Z	8
ρ (calc.) g cm^{-3}	1.6468
μ/mm^{-1}	2.576
F(000)	2346.0
Reflections collected	68044
Independent reflections	14615 [R_{int} = 0.0482, R_σ = 0.0373]
$Rw(F^2)^b$ [I>2σ(I)]	R_1 = 0.0333, wR_2 = 0.0729
$R(F)^a$ (all data)	R_1 = 0.0501, wR_2 = 0.0803

[a] $R = \sum|F_o - F_c| \sum |F|_o$. [b] $R_w = \{[\ \sum w(F_o^2 - F_c^2\ )]\ /[\sum w(F_o^2)^2]\}^{1/2}$; $w = 1/[\sigma^2(F_o)^2 + (xP)^2 + yP]$, where $P = (F_o^2 + 2F_c^2)/3$.

Table 14. Selected Bond Lengths (Å) and Angles (°) for **3h**.

Bond Lengths (Å)			
Sb1–I1	2.9131(3)	P2–N2	1.719(3)
N1–Sb1	2.107(2)	P2–N4	1.679(2)
N4–Sb1	2.431(2)	P2–N1	1.773(2)
N3–Sb1	2.095(2)	P1–N2	1.722(2)
P1–N3	1.685(3)	P1–N1	1.774(2)
		N10–C14	1.491(4)
Bond Angles (°)			
N3–P1–N2	92.60(12)	N1–P2–N4	107.01(12)
N1–P1–N2	107.03	Sb1–N3–P1	106.76(12)
N1–P1–N3	80.58(11)	P2–N3–P1	97.25(12)
N4–P2–N3	92.88(12)	Sb1–N3–P1	91.39(10)
N1–P2–N3	80.68(11)	Sb1–N3–P2	91.47(9)
I1–Sb1–N2	96.33(7)	I1–Sb1–N3	149.61(6)
N4–Sb1–N2	104.21(9)	I1–Sb1–N4	95.93(7)

5. SUMMARY AND CONCLUSIONS

The substitution of the chloride ligand in [(^{t}BuNP)$_2$(^{t}BuN)$_2$]ECl (E = P, As, Sb, Bi) by some monodentate ligands has been investigated. The reaction of {[(^{t}BuNP)$_2$(^{t}BuN)$_2$]PCl **1a**, with NaI furnished **1h** in 91% yield, and the compound crystallized in the monoclinic space group, $P2_1/m$. The reaction of [(^{t}BuNP)$_2$(^{t}BuN)$_2$]AsCl **2a**, with PhMgCl, NaN_3, $LiN(SiMe_3)_2$, NaO^tBu, LiOPh and NaI gave compounds [(^{t}BuNP)$_2$(^{t}BuN)$_2$]AsPh **2b**, [(^{t}BuNP)$_2$(^{t}BuN)$_2$]AsN_3 **2c**, [(^{t}BuNP)$_2$(^{t}BuN)$_2$]$AsN(SiMe_3)_2$ **2d**, [(^{t}BuNP)$_2$(^{t}BuN)$_2$]AsO^tBu **2e**, [(^{t}BuNP)$_2$(^{t}BuN)$_2$]AsOPh **2f** and [(^{t}BuNP)$_2$(^{t}BuN)$_2$]AsI **2h**, respectively. While **2b** crystallized in the triclinic space group, $P\bar{1}$, the analogous compounds **2c** and **2h** crystallized in the monoclinic space group, $P2_1/m$. Compound **1h** and **2h** show structural similarities in all respects, including the E–I bond that is equidistant in both compounds.

Treating [(^{t}BuNP)$_2$(^{t}BuN)$_2$]SbCl **3a**, with $AgOSO_2CF_3$ and NaI, afforded [(^{t}BuNP)$_2$(^{t}BuN)$_2$]$SbOSO_2CF_3$ **3g** and [(^{t}BuNP)$_2$(^{t}BuN)$_2$]SbI **3h** in about 92 and 88% yield, respectively. Compound **3g** crystallized in the monoclinic space group, $P2_1/n$, with a Sb–O bond distance of 2.3652(14) Å, while **3h** crystallized in the space group, $P2_1/c$. Similarly, the reaction of [(^{t}BuNP)$_2$(^{t}BuN)$_2$]BiCl **4a**, with PhMgCl and $LiN(SiMe_3)_2$, afforded [(^{t}BuNP)$_2$(^{t}BuN)$_2$]BiPh **4b** and [(^{t}BuNP)$_2$(^{t}BuN)$_2$]$BiN(SiMe_3)_2$ **4d**, respectively. Compound **2c** and **4d** are isostructural and they both crystallized in the monoclinic space group, $P2_1/c$. The synthesis of **2b**, **4b**, **2d** and **4d** completes a homologous series of group 15 compounds [(^{t}BuNP)$_2$(^{t}BuN)$_2$]EPh (E = P, As, Sb, Bi) and [(^{t}BuNP)$_2$(^{t}BuN)$_2$]$EN(SiMe_3)_2$ (E = P, As, Sb, and Bi). These newly synthesized compounds, **2b**, **4b**, **2d**, **4d**, **2c**, **2e**, **2f**, **3g**, **1h**, **2h** and **3h** are all air- and moisture-sensitive and except for **3g**, which is only slightly soluble in toluene, they are all soluble in organic solvents like toluene and hexanes.

CHAPTER III

OXIDATION REACTIONS OF CYCLODIPHOSPH(III)AZANE COMPOUNDS OF THE GROUP 15 ELEMENTS

1. INTRODUCTION

In addition to the lone-pairs on the nitrogen atoms which encapsulate the central element, the exterior of **E** features two lone-pairs of electrons on the phosphorus atoms that are not involved in chelation. These latter atoms allow further derivatization by oxidation with, for example, chalcogens and azides.[64, 87, 90] There are many examples of bis(amino)cyclodiphosph(III)azanes that were oxidized in this manner, but these reactions were usually performed on pristine bis(amino)cyclodiphosph(III)azanes. When these phosphorus(III) species are oxidized prior[22, 64, 75, 87] to deprotonation and incorporation of the chelated elements, the ligand exhibits decidedly different modes of chelation and entirely different structures from those shown above.

Stahl *et al*. had previously oxidized Group 4 and 14 bis(amido)cyclodiphos(III)azane compounds with chalcogens and discovered that although oxidation of the heterocycle's P(III) centers becomes significantly more difficult after the introduction of a metalloid or metal, the skeleton of the cyclodiphosph(III)azane remains unchanged.[93, 99] This is true irrespective if the incorporated element is sensitive to oxidation, as in the case of Sn(II)[60] or not, as the case of Zr(IV).[93, 99] Importantly, the post-chelation oxidations render the complexes more robust, because the very Lewis-basic P(III) centers are now capped with less Lewis-basic chalcogens.

The oxidizing agents, sulfur and selenium have standard electrode potentials of –0.48 V and –0.92 V, respectively, meaning that sulfur is a better oxidizing agent than selenium.[126] However, when the P(III) centers in cyclodiphosph(III)azane compounds are treated with these elements,

selenium reacts faster than sulfur. This anomalous behavior can be rationalized from the molecular structures of these elements. In the yellow allotrope of sulfur (S_8), for example, sulfur atoms are locked in an eight membered ring with S–S bond distances of ca. 206 pm and bond dissociation energy, S–S = 429(6) kJ mol^{-1}. On the other hand, gray selenium (Se_8) is an infinite helical chain of Se atoms (Se–Se = 237 pm) and bond dissociation energy, Se–Se = 332.6(6) kJ mol^{-1}, with their axes parallel to each other.[126–130] During a chemical reaction the bonds in selenium are easily broken to release Se atoms, whereas more energy is needed to break the stronger S–S bonds in S_8. Apart from the fast reactivity of Se with P(III) atoms, the element offers another advantage over sulfur as an oxidizing agent. The selenium isotope, ^{77}Se, has a nuclear spin of $I = ½$, and a relative abundance of 7.6%,[72, 87] as such couples with ^{31}P atoms and generates satellite peaks in a $^{31}P\{^1H\}$ NMR spectrum with typical J_{PSe} values in the range 400–1000 Hz, which help to elucidate the structure of the post–oxidation product.[34] While high J_{PSe} values (> 750 Hz) are often attributed to the P=Se bond, values of ca. 450 Hz are characteristic of P–Se bonds.[87] Thus, J_{PSe} and J_{PP} values of oxidized cyclodiphosph(III/V)azane compounds can be used to identify them.

Group 15 elements have two important oxidation states, the +3 and the +5 states. While the +3 is very stable throughout the group, the +5 state becomes less stable as one moves down the group. The +5 state is very stable in nitrogen and phosphorus, while very few arsenic(V) compounds exists. Antimony and bismuth are rarely found in the +5 state.[37, 126] The less stable +5 state as we move down the group means that most of the oxidation is carried out at the phosphorus(III) center. The metalloids and metal centers are hardly oxidized by the chalcogens. In this regard, we anticipate molecular rearrangements and possible decomposition products

from the oxidation of phosphorus(III) to phosphorus(V) in compounds of cyclodiphosph(III)azanes, where the +5 oxidation state is very stable.

Here we report on the chalcogen oxidation of known and newly-synthesized Group 15 compounds of cyclodiphosph(III)azanes. These reactions will show that the post-chelation oxidations of *bis*(amido)cyclodiphosph(III)azanes create compounds not accessible from pristine cyclodiphosph(III)azanes as demonstrated by the improbable transformation of an amide to a nitride under comparatively mild conditions. The numbering of the compounds below will be as follows: phosphorus = **1**, arsenic = **2**, antimony = **3**, bismuth = **4**, chloride = **a**, phenyl = **b**, azide = **c**, **S** or **Se** for the mono-sulfide or mono-selenide, if one of the P(III) atoms of the P_2N_2 ring is oxidized, respectively; **S′** or **Se′**, if the central group 15 atom is oxidized by sulfur or selenium; disulfide (**S_2**) or diselenide (**Se_2**) if the two P(III) centers in the P_2N_2 ring are oxidized. e.g. **1aS_2** = $[(^tBuNP{=}S)_2(^tBuN)_2]PCl$.

2 EXPERIMENTAL

General Procedures

All experimental procedures were performed under an atmosphere of argon using standard Schlenk techniques. Immediately before use, solvents were dried and freed of molecular oxygen by distillation under a nitrogen atmosphere from sodium- or potassium benzophenone ketyl. Sulfur and selenium were purchased from Sigma Millipore or Alfa Aesar; while sulfur was purified by sublimation before being used, selenium was used as obtained. The compounds, $[(^tBuNP)_2(^tBuN)_2]PCl$ **1a**, $[(^tBuNP)_2(^tBuN)_2]PPh$ **1b**, $[(^tBuNP)_2(^tBuN)_2]AsCl$ **2a**, $[(^tBuNP)_2(^tBuN)_2]SbCl$ **3a**, $[(^tBuNP)_2(^tBuN)_2]SbPh$ **3b** and $[(^tBuNP)_2(^tBuN)_2]SbN_3$ **3c**,[98, 99, 103] were synthesized according to published procedures. All fritted filter tubes used were of medium porosity.

Description of Instrumentation

NMR spectra were recorded on a Bruker AVANCE-500 NMR spectrometer. The ^{1}H, ^{13}C NMR spectra are referenced relative to C_6D_5H (7.16 ppm) and (128.39 ppm), respectively, or $CHCl_3$ (7.27 ppm) and $CDCl_3$ (77.23 ppm), respectively, as internal standards, while the $^{31}P\{^{1}H\}$ spectra are referenced relative to $P(OEt)_3$ (137.0 ppm) as external standard in C_6D_6 or $CDCl_3$. In all cases positive chemical shift values represent higher frequencies and downfield shifts. Melting points were recorded on a Mel-Temp melting point apparatus; they are uncorrected. Elemental analyses were performed by ALS Life Sciences Division Environmental, Tucson, AZ.

X-ray Crystallography

A suitable single crystal of **2aS** was coated with Paratone oil, affixed to Mitegen or Litholoop crystal holders and centered on the diffractometer in a stream of cold nitrogen. Reflection intensities were collected with a Bruker Apex Diffractometer equipped with an Oxford Cryosystems, 700 Series Cryostream cooler, operating at 173 K. Data were measured using ω scans of 0.3° per frame for 20 seconds until a complete hemisphere of data had been collected. Cell parameters were retrieved using SMART[104] software and refined with SAINT[105] on all observed reflections. Data were reduced with SAINTplus, which corrects for Lorentz polarization effects and crystal decay. Empirical absorption corrections were applied with SADABS.[106] The structures were solved by direct methods with SHELXS-90[107] program and refined by full-matrix least squares methods on F^2 with SHELXS-97[108] incorporated in SHELXTL Version 5.10.[109]

Single crystals were coated with Paratone oil and quickly transferred to the goniometer head of a Bruker Quest diffractometer with a fixed angle χ, a sealed fine focus X-ray tube, single crystal curved graphite incident beam monochromator, a Photon100 CMOS area detector and an

Oxford Cryosystems low temperature device. Examination and data collection were performed with Mo Kα radiation (λ = 0.71073 Å) at 150 K.

Data were collected, reflections were indexed and processed, and the files scaled and corrected for absorption using APEX3.[110] The space groups were assigned and the structures were solved by direct methods using XPREP within SHELXTL suite programs[105, 111] and refined by full matrix least squares against F^2 with all reflections using Shelxl2018[112, 113] using the graphical interface Shelxle.[114] If not specified otherwise, H atoms attached to carbon and nitrogen atoms were positioned geometrically and constrained to ride on their parent atoms. C–H bond distances were constrained to 0.95 Å for aromatic and CH_2 moieties, and to 1.00, 0.99 and 0.98 Å for aliphatic C–H, CH_2 and CH_3 moieties, respectively. Methyl groups (CH_3) were allowed to rotate but not to tip to best fit the experimental electron density.

3 SYNTHESES OF COMPOUNDS

{[(^{t}BuNP)$_2$(^{t}BuN)$_2$Se]PCl} 1aSe

Selenium (0.140 g, 1.77 mmol) and [(^{t}BuNP)$_2$(^{t}BuN)$_2$]PCl **1a** (0.700 g, 1.70 mmol) were combined in a 100 mL two-necked flask equipped with a stir bar and a gas inlet. Toluene (25 mL) was added, and the mixture was stirred at 50 °C for 12 h. After the reaction mixture had been allowed to cool to RT, it was filtered using a frit. The resulting filtrate was concentrated *in vacuo* to about 4 mL and then stored at –6 °C to furnish colorless crystals of **1aSe** after 2 days. Yield: (0.780 g, 1.58 mmol), 93%. Mp: 160–162 °C. ^{1}H NMR (C_6D_6, 25 °C): 1.92 (d, J_{PH} = 4.90 Hz, 9 H, N^{t}Bu, imido), 1.73 (s, 9 H, N^{t}Bu, imido), 1.37 (d, J_{PH} = 3.90 Hz, 18 H, N^{t}Bu, amido). ^{13}C{^{1}H} NMR (C_6D_6, 25 °C): 64.83 (d, J_{PC} = 21.20 Hz, N*C*(CH$_3$)$_3$, amido), 59.83 (m, N*C*(CH$_3$)$_3$, amido), 57.97 (d, J_{PC} = 13.24 Hz, N*C*(CH$_3$)$_3$, imido), 55.87 (m, N*C*(CH$_3$)$_3$, imido), 31.92 (m, NC(*C*H$_3$)$_3$, amido), 30.57 (t, J_{PC} = 5.64 Hz, NC(*C*H$_3$)$_3$, imido), 30.25 (t, J_{PC} = 5.64 Hz,

NC(CH_3)$_3$, imido). $^{31}P\{^1H\}$ NMR (C_6D_6, 25 °C): 161.17 (s, P(III)), 135.98 (d, J_{PP} = 17.05 Hz, P(III)), 64.07 (d, J_{PSe} = 909.66 Hz, J_{PP} = 9.25 Hz, P(V)) Anal. Calcd. for $C_{16}H_{36}N_4P_3ClSe$: C, 39.07; H, 7.38; N, 11.39%. Found: C, 38.94; H, 7.37; N, 10.98%.

{[(^{t}BuNP=Se)$_2$(^{t}BuN)$_2$]PCl} 1aSe$_2$

In a 100 mL two-necked flask, samples of [(^{t}BuNP)$_2$(^{t}BuN)$_2$]PCl **1a** (0.750 g, 1.82 mmol) and excess selenium (0.320 g, 4.05 mmol) were dissolved in toluene (30 mL) and stirred at 60 °C for 24 h. After cooling to RT, unreacted selenium was removed with a frit. The resulting filtrate was concentrated *in vacuo* to about 4 mL and stored at –6 °C to furnish colorless, needle-like crystals of **1aSe$_2$** after 3 days. Yield: (0.910 g, 1.60 mmol), 88%. Mp: 148–150 °C. ^1H NMR (C_6D_6, 25 °C): 1.97 (s, 9 H, N^{t}Bu, imido), 1.79 (s, 9 H, N^{t}Bu, amido), 1.78 (s, 9 H, N^{t}Bu, imido), 1.49 (s, 9 H, N^{t}Bu, imido). $^{13}C\{^1H\}$ NMR (C_6D_6, 25 °C): 65.55 (s, N*C*(CH_3)$_3$, amido), 65.36 (s, N*C*(CH_3)$_3$, amido), 62.39 (s, N*C*(CH_3)$_3$, imido), 59.66 (s, N*C*(CH_3)$_3$, imido), 31.93 (s, NC(*C*H_3)$_3$, imido), 31.77(s, NC(*C*H_3)$_3$, imido), 30.73 (t, J_{PC} = 4.60 Hz, NC(*C*H_3)$_3$, amido). $^{31}P\{^1H\}$ NMR (C_6D_6, 25 °C): 142.18 (s, P(III)), 43.93 (d, P(V), J_{PSe} = 955.71 Hz, J_{PP} = 14.78 Hz). IR (cm^{-1}): 600.47 (P=Se), 694.13, 716.89, 791.00, 849.75, 881.89, 922.14, 955.54, 1025.62, 1040.45, 1172.08, 1223.63, 1237.96, 1363.78, 1393.52, 1462.99, 2966.53. Anal. Calcd. for $C_{16}H_{36}N_4P_3ClSe_2$: C, 33.67; H, 6.36; N, 9.82%. Found: C, 33.85; H, 6.39; N, 9.75%.

{[(^{t}BuNP)$_2$(^{t}BuN)$_2$](P=Se)Ph} 1bSe′

A sample of [(^{t}BuNP)$_2$(^{t}BuN)$_2$]PPh **1b** (0.480 g, 1.06 mmol) and one equivalent of selenium (0.090 g, 1.14 mmol) were combined in toluene (25 mL) and stirred for 12 h at RT. Excess selenium was filtered off and the resulting solution was concentrated *in vacuo* and stored at –12 °C to afford colorless, rod-shaped crystals of **1bSe′** after 2 days. Yield: (0.51 g, 0.95 mmol), 90%. Mp: 150–152 °C. ^1H NMR (C_6D_6, 25 °C): 8.68 (m, 2 H, Ph, *ortho*), 7.16 (s, 2 H, Ph, *meta*),

7.08 (m, H, Ph, *para*), 1.58 (s, 9 H, N^{t}Bu, imido), 1.43 (s, 18 H, N^{t}Bu, amido), 1.38 (s, 9 H, N^{t}Bu, imido). ^{13}C{^{1}H} NMR (C_6D_6, 25 °C): 145.08 (s, C_{ipso}), 144.42 (s, Ph, *ortho*), 133.31 (s, Ph, *meta*), 130.63 (s, Ph, *para*), 62.30 (m, N*C*(CH$_3$)$_3$, amido), 54.40 (t, J_{PC} = 12.93 Hz, N*C*(CH$_3$)$_3$, imido), 54.02 (t, J_{PC} = 8.00 Hz, N*C*(CH$_3$)$_3$, imido), 32.99 (m, NC(*C*H$_3$)$_3$, amido), 30.56 (t, J_{PC} = 5.70 Hz, NC(*C*H$_3$)$_3$, imido). ^{31}P{^{1}H} NMR (C_6D_6, 25 °C): 194.12 (d, J_{PP} = 21.36 Hz, P(III)), 46.41 (t, J_{PP} = 20.76 Hz, J_{PSe} = 842.38 Hz, P(V)). IR (cm^{-1}): 599.44 (P=Se), 634.32, 703.41, 739.29, 787.19, 867.03, 910.63, 935.77, 1007.55, 1044.34, 1093.81, 1171.45, 1237.80, 1222.02, 1359.95, 1389.30, 1435.96, 1460.29, 2960.68. Anal. Calcd. for $C_{22}H_{41}N_4P_3Se$: C, 49.53; H, 7.75; N, 10.50%. Found: C, 49.50; H, 7.85; N, 10.20%.

{[(tBuNP)$_2$(tBuN)$_2$S]AsCl} 2aS

Samples of **2a** (0.46 g, 1.00 mmol) and excess sublimed sulfur (0.15 g, 4.69 mmol) were combined in a 100 mL two-necked flask. Toluene (20 mL) was added and the mixture was stirred for 48 h at 70 °C. After cooling to RT, excess sulfur was filtered off and the filtrate was concentrated *in vacuo* to about 4 mL and stored at –6 °C. Needle-like crystals of **2aS** were obtained after several days. Yield: (0.43 g, 0.88 mmol), 88%. Mp: 179–181 °C. ^{1}H NMR (benzene-d$_6$, 25 °C): 1.81 (s, 9 H, N^{t}Bu, amido), 1.72 (s, 9 H, N^{t}Bu, amido), 1.36 (s, 9 H, N^{t}Bu, imido), 1.33 (s, 9 H, N^{t}Bu, imido). ^{13}C{^{1}H} NMR (benzene-d$_6$, 25 °C): 63.86 (s, N*C*(CH$_3$)$_3$, amido), 59.50 (d, J_{PC} = 16.73 Hz, N*C*(CH$_3$)$_3$, amido), 57.02 (d, J_{PC} = 15.17 Hz, N*C*(CH$_3$)$_3$, imido), 55.13 (m, N*C*(CH$_3$)$_3$, imido), 32.68 (d, J_{PC}= 10.36 Hz, NC(*C*H$_3$)$_3$, amido), 31.96 (d, J_{PC} = 4.38 Hz, NC(*C*H$_3$)$_3$, amido), 30.79 (t, J_{PC} = 5.34 Hz, NC(*C*H$_3$)$_3$, imido), 30.40 (t, J_{PC} = 6.70 Hz, NC(*C*H$_3$)$_3$, imido). ^{31}P{^{1}H} NMR (benzene-d$_6$, 25 °C): 122.81 (s, P(III)), 68.26 (s, P(V)). IR (cm^{-1}): 537.88, 592.06, 726.71, 758.76, 787.34, 839.65, 883.65, 929.31 (s, P=S), 965.30,

1036.86, 1178.35, 1221.49, 1242.73, 1259.63, 1361.68, 1388.95, 1466.95, 2960.99. Anal. Calcd. for $C_{16}H_{36}N_4P_2AsClS$: C, 39.31; H, 7.42; N, 11.46%. Found: C, 39.57; H, 7.40; N, 11.39%.

{[(^{t}BuNP)$_2$(^{t}BuN)$_2$Se]AsCl} 2aSe

Samples of **2a** (0.500 g, 1.09 mmol) and selenium (0.100 g, 1.27 mmol) were mixed in a 100 mL two-necked flask. Toluene (24 mL) was added and the mixture was stirred at 50 °C for 12 h. Excess selenium was removed with a frit and the filtrate was concentrated *in vacuo* to about 4 mL and stored at –6 °C. Block-shaped crystals of **2aSe** were obtained after several days. Yield: (0.52 g, 0.98 mmol), 89%. Mp: 181–182 °C (dec). ^{1}H NMR (C_6D_6, 25°C): 1.86 (s, 9 H, N^{t}Bu, amido), 1.75 (s, 9 H, N^{t}Bu, amido), 1.39 (s, 9 H, N^{t}Bu, imido), 1.32 (s, 9H, N^{t}Bu, imido). ^{13}C{^{1}H} NMR (C_6D_6, 25 °C): 64.50 (s, N*C*(CH$_3$)$_3$, amido), 60.02 (d, J_{PC} = 17.59 Hz, N*C*(CH$_3$)$_3$, amido), 57.41 (d, J_{PC} = 12.17 Hz, N*C*(CH$_3$)$_3$, imido), 55.57 (m, N*C*(CH$_3$)$_3$, imido), 32.77 (d, J_{PC} = 10.14 Hz, NC(*C*H$_3$)$_3$, amido), 32.19 (d, J_{PC} = 3.99 Hz, NC(*C*H$_3$)$_3$, amido), 30.64 (t, J_{PC} = 5.43 Hz, NC(*C*H$_3$)$_3$, imido), 30.52 (t, J_{PC} = 5.97 Hz, NC(*C*H$_3$)$_3$, imido). ^{31}P{^{1}H} NMR (C_6D_6, 25 °C): 130.18 (s, P(III)), 61.81(d, J_{PP} = 8.89 Hz, J_{PSe} = 891.44 Hz, P(V)). IR (cm^{-1}): 545.05, 568.84 (s, P=Se), 597.79, 667.85, 748.62, 783.19, 833.68, 883.02, 966.61, 1040.29, 1179.83, 1219.42, 1359.88, 1388.76, 1464.33, 2958.10. Anal. Calcd. for $C_{16}H_{36}N_4P_2AsClSe$: C, 35.87; H, 6.77; N, 10.46%. Found: C, 35.99; H, 6.82; N, 10.26%.

{[(^{t}BuNP=S)$_2$(^{t}BuN)$_2$]AsCl} 2aS$_2$

In a 100 mL two-necked flask, **2a** (0.700 g, 1.53 mmol) and excess sulfur (0.15 g, 4.69 mmol) were dissolved in toluene (30 mL). The reaction mixture was stirred at 80 °C for 48 h. Excess sulfur was filtered off, and the filtrate was concentrated *in vacuo* to about 4 mL and stored at –6 °C for several days to obtain colorless, rod-shaped crystals of **2aS$_2$**. Yield: (0.570 g, 1.09 mmol), 71%. Mp: 206–208 °C. ^{1}H NMR (C_6D_6, 25 °C): 1.90 (s, 9 H, N^{t}Bu, imido), 1.68 (s, 18

H, N^{t}Bu, amido), 1.43 (s, 9 H, N^{t}Bu, imido). ^{13}C{^{1}H} NMR (C_6D_6, 25 °C): 64.18 (s, N*C*(CH$_3$)$_3$, amido), 60.72 (s, N*C*(CH$_3$)$_3$, imido), 58.40 (s, N*C*(CH$_3$)$_3$, imido), 32.22 (s, NC(*C*H$_3$)$_3$, amido), 30.62 (m, NC(*C*H$_3$)$_3$, imido). ^{31}P{^{1}H} NMR (C_6D_6, 25 °C): 52.46 (s, P(V)). IR (cm^{-1}): 603.95, 668.92, 757.68, 791.49, 840.74, 888.76, 930.11(s, P=S), 977.99, 1034.38, 1169.43, 1190.99, 1221.15, 1259.19, 1362.75, 1392.52, 2972.08. Anal. Calcd. for $C_{16}H_{36}N_4P_2AsClS_2$: C, 36.89; H, 6.97; N, 10.76 %. Found: C, 36.92; H, 7.09; N, 10.30%.

{[(tBuNP=Se)$_2$(tBuN)$_2$]AsCl} 2aSe$_2$

A sample of **2a** (1.00 g, 2.19 mmol) and excess selenium (0.440 g, 5.57 mmol) were placed in a 100 mL two-necked flask. Toluene (30 mL) was added to dissolve the reactants, and the reaction mixture was stirred at 75 °C for 24 h. Excess selenium was filtered off after cooling to RT and the filtrate was concentrated to about 5 mL and stored at –6 °C for 3 days to obtain colorless, rod-shaped crystals of **2aSe$_2$**. Yield: (1.25 g, 2.04 mmol), 93%. Mp: 196–198 °C (dec). ^{1}H NMR (C_6D_6, 25 °C): 1.97 (s, 9 H, N^{t}Bu, imido), 1.71 (s, 18 H, N^{t}Bu, amido), 1.51 (s, 9 H, N^{t}Bu, imido). ^{13}C{^{1}H} NMR (C_6D_6, 25 °C): 65.03 (s, N*C*(CH$_3$)$_3$, amido), 61.47 (s, N*C*(CH$_3$)$_3$, imido), 59.17 (s, N*C*(CH$_3$)$_3$, imido), 32.08 (s, NC(*C*H$_3$)$_3$, amido), 30.94 (t, J_{PC} = 4.68 Hz, NC(*C*H$_3$)$_3$, imido), 30.59 (t, J_{PC} = 4.68 Hz, NC(*C*H$_3$)$_3$, imido). ^{31}P{^{1}H} NMR (C_6D_6, 25 °C): 43.68 (s, J_{PSe} = 933.16 Hz, P(V)). IR (cm^{-1}): 581.44 (m, P=Se), 606.72, 703.58, 750.03, 776.92, 826.45, 873.65, 929.55, 972.49, 1025.45, 1169.04, 1236.88, 1362.53, 1392.57, 1465.35, 2970.08. Anal. Calcd. for $C_{16}H_{36}N_4P_2AsClSe_2$: C, 31.26; H, 5.90; N, 9.11%. Found: C, 31.43; H, 6.04; N, 8.66%.

{[(tBuNP)$_2$(tBuN)$_2$S]AsPh} 2bS

In a 50 mL two-necked flask, (0.33 g, 0.67 mmol) of {[(tBuNP)$_2$(tBuN)$_2$]AsPh} **2b** and excess freshly sublimed sulfur (0.07 g, 2.19 mmol) were mixed and toluene (20 mL) was added.

The mixture was stirred at 50 °C for 48 h, after which the unreacted sulfur was filtered, and then the filtrate was concentrated *in vacuo* to about 4 mL and stored at – 15 °C. Colorless crystals of **2bS** were isolated after several days. Yield: (0.30 g, 0.57 mmol), 85%. Mp: 178–180 °C. ^{1}H NMR (C_6D_6, 25 °C): 8.15 (m, 2 H, *ortho*), 7.18 (m, 2 H, *meta*), 7.11 (m, 1 H, *para*), 1.67 (s, 9 H, N^{t}Bu, amido), 1.64 (s, 9 H, N^{t}Bu, amido), 1.59 (s, 9 H, N^{t}Bu, imido), 1.18 (s, 9 H, N^{t}Bu, imido). ^{13}C{^{1}H} NMR (benzene-d_6, 25 °C): 152.05 (s, C_{ipso}), 133.39 (s, Ph, *ortho*), 129.93 (s, Ph, *meta*), 126.04 (s, Ph, *para*), 61.97 (s, N*C*(CH$_3$)$_3$, amido), 58.37 (d, J_{PC} = 19.05 Hz, N*C*(CH$_3$)$_3$, amido), 57.06 (d, J_{PC} = 14.29 Hz, N*C*(CH$_3$)$_3$, imido), 55.62 (d, J_{PC} = 7.62 Hz, N*C*(CH$_3$)$_3$, imido), 33.20 (d, J_{PC} =11.87 Hz, NC(*C*H$_3$)$_3$, amido), 32.60 (d, J_{PC} = 4.87 Hz, NC(*C*H$_3$)$_3$, amido), 31.31 (t, J_{PC} = 5.40, NC(*C*H$_3$)$_3$, imido), 30.70 (m, NC(*C*H$_3$)$_3$, imido). ^{31}P{^{1}H} NMR (benzene-d_6, 25 °C): 115.30 (s, P(III)), 69.38 (s, P(V)). IR (cm^{-1}): 588.92, 601.39, 665.35, 696.18, 710.26, 738.27, 752.32, 781.19, 802.23, 841.97, 873.99, 990.52(s, P=S), 1041.36, 1074.38, 1177.78, 1221.34, 1259.30, 1360.30, 1388.56, 1433.56, 1458.32, 2359.78, 2961.11. Anal. Calcd. for $C_{22}H_{41}N_4P_2AsS$: C, 49.81; H, 7.79; N, 10.56%. Found: C, 49.46; H, 8.02; N, 10.71%.

{[(tBuNP=S)$_2$(tBuN)$_2$]AsPh} 2bS$_2$

A sample of **2b** (0.800 g, 1.61 mmol) and excess sulfur (0.150 g, 4.69 mmol) were mixed and dissolved in toluene (30 mL). The mixture was stirred at 75 °C for 48 h. After the resulting solution had been kept at –12 °C for 3 days, colorless, rod-shaped crystals of **2bS$_2$** were obtained. Yield: (0.860 g, 1.23 mmol), 95%. Mp: 176–178 °C. ^{1}H NMR (C_6D_6, 25 °C): 8.04 (d, J_{PH}= 7.56 Hz, 2 H, Ph, *ortho*), 7.13 (m, 2 H, Ph, *meta*), 7.08 (m, 1 H, Ph, *para*), 2.01 (s, 9 H, N^{t}Bu, imido), 1.75 (s, 9 H, N^{t}Bu imido), 1.46 (s, 18 H, N^{t}Bu, amido). ^{13}C{^{1}H} NMR (C_6D_6, 25 °C): 152.02 (s, C_{ipso}), 133.11 (s, Ph, *ortho*), 130.62 (s, Ph, *meta*), 126.14 (s, Ph, *para*), 62.49 (s, N*C*(CH$_3$)$_3$, amido), 60.72 (s, N*C*(CH$_3$)$_3$, imido), 58.45 (s, N*C*(CH$_3$)$_3$, imido), 31.08 (d, J_{PC} = 4.87 Hz ,

NC(CH_3)$_3$, amido), 30.82 (t, J_{PC} = 4.87 Hz , NC(CH_3)$_3$, imido). $^{31}P\{^1H\}$ NMR (C_6D_6, 25 °C): 50.50 (s, P(V)). IR (cm^{-1}): 598.28, 647.79, 665.12, 693.57, 734.95, 747.21, 839.22, 880.85 (s, P=S), 927.81, 998.58, 1011.48, 1044.62, 1172.17, 1232.76, 1259.39, 1361.68, 1390.11. Anal. Calcd. for $C_{22}H_{41}N_4P_2AsS_2$: C, 46.97; H, 7.35; N, 9.96%. Found: C, 46.96; H, 7.29; N, 9.71%.

{[(^{t}BuNP=Se)$_2$(^{t}BuN)$_2$]AsPh} 2bSe$_2$

In a manner analogous to the synthesis of **2bS$_2$**, (0.560 g, 1.13 mmol) of **2b** and excess selenium (0.200 g, 2.53 mmol) were combined and dissolved in toluene (30 mL) and then stirred at 70 °C for 24 h. The ensuing solution was kept at –12 °C to furnish colorless, block-shaped crystals of **2bSe$_2$** after several days. Yield: (0.690 g, 1.05 mmol), 93%. Mp: 142–144 °C. ^1H NMR (C_6D_6, 25 °C): 7.95 (m, 2 H, Ph, *ortho*), 7.10 (m, 2 H, Ph, *meta*), 7.06 (m, 1 H, Ph, *para*), 2.07(s, 9 H, N^{t}Bu, imido), 1.82 (s, 9 H, N^{t}Bu, imido), 1.44 (s, 18 H, N^{t}Bu, amido). $^{13}C\{^1H\}$ NMR (C_6D_6, 25 °C): 152.70 (s, C_{ipso}), 133.11 (s, Ph, *ortho*), 130.79 (s, Ph, *meta*), 126.01 (s, Ph, *para*), 63.52 (s, NC(CH_3)$_3$, amido), 60.63 (s, NC(CH_3)$_3$, imido), 59.24 (s, NC(CH_3)$_3$, imido), 32.75 (s, NC(CH_3)$_3$, amido), 30.94 (t, J_{PC} = 4.92 Hz, NC(CH_3)$_3$, imido), 30.82 (t, J_{PC} = 4.36 Hz, NC(CH_3)$_3$, imido). $^{31}P\{^1H\}$ NMR (C_6D_6, 25 °C): 37.52 (s, P(V), J_{PSe} = 910.89 Hz). IR (cm^{-1}): 570.89 (m, P=Se), 603.50, 696.24, 739.06, 765.21, 794.91, 869.39, 925.17, 1009.82, 1074.02, 1172.29, 1235.32, 1258.87, 1363.39, 1391.76, 1457.42, 2962.77. Anal. Calcd. for $C_{22}H_{41}N_4P_2AsSe_2$: C, 40.26; H, 6.30; N, 8.54%. Found: C, 40.20; H, 6.33; N, 8.23%.

{[(^{t}BuNP=Se)$_2$(^{t}BuN)$_2$]AsN$_3$} 2cSe$_2$

In a 100 mL two-necked flask, exactly (0.35 g, 0.75 mmol) of [(^{t}BuNP)$_2$(^{t}BuN)$_2$]AsN$_3$ **2c** and excess selenium, (0.130 g, 1.65 mmol) were combined and toluene (20 mL) was added. The mixture was stirred for 24 h at 70 °C and unreacted selenium was removed with a frit after cooling to RT. The resulting filtrate was concentrated *in vacuo* to about 2 mL and stored at –12

°C. Colorless crystals of **2cSe$_2$** were obtained after several days. Yield: (0.41 g, 0.66 mmol), 88%. Mp: 168 – 170 °C. ^{1}H NMR (C_6D_6, 25 °C): 1.89 (s, 9 H, N^{t}Bu, imido), 1.61 (s, 18 H, N^{t}Bu, amido), 1.51 (s, 9 H, N^{t}Bu, imido). ^{13}C{^{1}H} NMR (C_6D_6, 25 °C): 63.80 (s, N*C*(CH$_3$)$_3$, amido), 60.80 (s, N*C*(CH$_3$)$_3$, imido), 59.12 (s, N*C*(CH$_3$)$_3$, imido), 32.87 (s, NC(*C*H$_3$)$_3$, amido), 31.01 (t, J_{PC} = 4.84 Hz, NC(*C*H$_3$)$_3$, imido), 30.53 (t, J_{PC} = 4.28 Hz, NC(*C*H$_3$)$_3$, imido). ^{31}P{^{1}H} NMR (C_6D_6, 25 °C): 43.31 (s, P(V), J_{PSe} = 930.49 Hz). IR (cm^{-1}): 580.17 (m, P=Se), 603.94, 661.86, 699.29, 754.62, 777.46, 875.10, 926.72, 942.94, 984.47, 1027.94, 1167.86, 1236.38, 1258.21, 1366.37, 1392.89, 1457.63, 2062.05, 2962.12. Anal. Calcd. for $C_{16}H_{36}N_7P_2AsSe_2$: C, 30.93; H, 5.84; N, 15.78%. Found: C, 31.57; H, 6.03; N, 15.31 %.

{[(tBuNP=S)$_2$(tBuN)$_2$]SbCl} 3aS$_2$

A sample of **3a** (0.600 g, 1.19 mmol) and excess sulfur (0.130 g, 4.06 mmol) were dissolved in toluene (35 mL) and stirred for 48 h at 80 °C. The resulting solution furnished block-shaped, colorless crystals of **3aS$_2$** after several days. Yield: (0.580 g, 1.02 mmol), 86%. Mp: 208–210 °C. ^{1}H NMR (C_6D_6, 25 °C): 1.84 (s, 9 H, N^{t}Bu, imido), 1.59 (s, 18 H, N^{t}Bu, amido), 1.52 (s, 9 H, N^{t}Bu, imido). ^{13}C{^{1}H} NMR (C_6D_6, 25 °C): 62.58 (s, N*C*(CH$_3$)$_3$, amido), 59.37 (s, N*C*(CH$_3$)$_3$, imido), 59.12 (s, N*C*(CH$_3$)$_3$, imido), 32.94 (d, J_{PC} = 3.33 Hz, NC(*C*H$_3$)$_3$, amido), 30.68 (t, J_{PC} = 4.57 Hz, NC(*C*H$_3$)$_3$, imido), 30.54 (t, J_{PC} = 4.77 Hz, NC(*C*H$_3$)$_3$, imido). ^{31}P{^{1}H} NMR (C_6D_6, 25 °C): 47.53 (s, P(V)). IR (cm^{-1}): 596.96, 701.89, 745.50, 786.19, 893.08, 931.10 (s, P=S), 1017.38, 1184.05, 1258.42, 1363.16, 1390.49, 1463.04, 2963.62. Anal. Calcd. for $C_{16}H_{36}N_4P_2SbClS_2$: C, 33.85; H, 6.39; N, 9.87%. Found: C, 34.27; H, 6.49; N, 9.65%.

{[(tBuNP=S)$_2$(tBuN)$_2$]SbN$_3$} 3cS$_2$

A sample of [(tBuNP)$_2$(tBuN)$_2$]SbN$_3$ **3c** (0.780 g, 1.52 mmol) and excess sulfur (0.130 g, 4.06 mmol) were dissolved in toluene (24 mL) and placed in a 100 mL two-necked flask. The

mixture was then stirred at 75 °C for 48 h and after cooling to RT, unreacted sulfur was filtered off and the ensuing filtrate was concentrated to about 4 mL and stored at –12 °C. After several days colorless, cubic crystals of **3cS$_2$** were obtained. Yield: (0.640 g, 1.11 mmol), 73%. Mp: 188 – 190 °C. ^{1}H NMR (C_6D_6, 25 °C): 1.80 (s, 9 H, N^{t}Bu, imido), 1.52 (s, 18 H, N^{t}Bu, amido), 1.51 (s, 9 H, N^{t}Bu, imido). ^{13}C{^{1}H} NMR (C_6D_6, 25 °C): 61.03 (s, N*C*(CH$_3$)$_3$, amido), 60.84 (s, N*C*(CH$_3$)$_3$, imido), 59.06 (s, N*C*(CH$_3$)$_3$, imido), 33.08 (d, J_{PC} = 6.38 Hz, NC(*C*H$_3$)$_3$, amido), 30.99 (t, J_{PC} = 4.52 Hz, NC(*C*H$_3$)$_3$, imido), 29.40 (t, J_{PC} = 4.79 Hz, NC(*C*H$_3$)$_3$, imido). ^{31}P{^{1}H} NMR (C_6D_6, 25 °C): 45.72 (s, P(V)). IR (cm^{-1}): 550.25, 592.01, 606.08, 643.60, 694.42, 740.51, 782.89, 805.68, 833.72, 931.14 (s, P=S), 989.32, 1023.89, 1175.91, 1227.82, 1260.09, 1309.75, 1362.42, 1392.00, 1461.84, 2078.34, 2965.23. Anal. Calcd. for $C_{16}H_{36}N_7P_2SbS_2$: C, 33.46; H, 6.32; N, 17.07%. Found: C, 34.35; H, 6.66; N, 16.73%.

{[(tBuNP=Se)$_2$(tBuN)$_2$]SbN$_3$} 3cSe$_2$

Selenium (0.280 g, 3.55 mmol) and **3c** (0.731 g, 1.42 mmol) were placed in a 100 mL two-necked flask. Toluene (24 mL) was added to dissolve the reaction mixture, which was then stirred at 70 °C for 24 h. Unreacted selenium was removed with a frit, and the filtrate was then concentrated *in vacuo* to about 5 mL and stored at –12 °C to obtain colorless crystals of **3cSe$_2$**. Yield: (0.770 g, 1.16 mmol), 81%. Mp: 186–188 °C. ^{1}H NMR (C_6D_6, 25 °C): 1.85 (s, 9 H, N^{t}Bu, imido), 1.57 (s, 9 H, N^{t}Bu, imido), 1.53 (s, 18 H, N^{t}Bu, amido). ^{13}C{^{1}H} NMR (C_6D_6, 25 °C): 61.71 (s, N*C*(CH$_3$)$_3$, amido), 61.65 (s, N*C*(CH$_3$)$_3$, imido), 59.78 (s, N*C*(CH$_3$)$_3$, imido), 32.91 (m, NC(*C*H$_3$)$_3$, amido), 31.05 (m, NC(*C*H$_3$)$_3$, imido), 29.22 (m, NC(*C*H$_3$)$_3$, imido). ^{31}P{^{1}H} NMR (C_6D_6, 25 °C): 32.77 (s, P(V), J_{PSe} = 922.84 Hz). IR (cm^{-1}): 536.71, 553.15, 563.25 (s, P=Se), 641.88, 669.43, 727.03, 760.22, 812.42, 829.45, 862.34, 931.54, 980.71, 1018.78, 1047.92,

1173.45, 1230.76, 1260.72, 1307.74, 1362.01, 1392.32, 1468.50, 2079.12, 2963.98. Anal. Calcd. for $C_{16}H_{36}N_7P_2SbSe_2$: C, 28.76; H, 5.43; N, 14.67%. Found: C, 29.05; H, 6.13; 13.97%.

{[(^{t}BuNP=S)$_2$(^{t}BuN)$_2$]SbPh} 3bS$_2$

In a 100 mL two-necked flask, a sample of [(^{t}BuNP)$_2$(^{t}BuN)$_2$]SbPh **3b** (1.00 g, 1.99 mmol) and excess sulfur (0.130 g, 4.06 mmol) were dissolved in toluene (30 mL). The mixture was stirred at 80 °C for 36 h after which time unreacted sulfur was removed with a frit. The resulting solution was concentrated *in vacuo* and kept at –12 °C to furnish **3bS$_2$** as colorless, cubic crystals after several days. Yield: (0.980 g, 1.61 mmol), 88%. Mp: 188–190 °C. ^{1}H NMR (C_6D_6, 25 °C): 7.83 (d, J_{PH} = 7.90 Hz, 2 H, Ph, *ortho*), 7.19 (t, J_{PH} =7.93 Hz, 2 H, Ph, *meta*), 7.06 (m, 1 H, Ph, *para*), 1.99 (s, 9 H, N^{t}Bu, imido), 1.77 (s, 9 H, N^{t}Bu, imido), 1.32 (s, 18 H, N^{t}Bu, amido). ^{13}C{^{1}H} NMR (C_6D_6, 25 °C): 160.06 (s, C_{ipso}), 133.69 (s, Ph, *ortho*), 130.45 (s, Ph, *meta*), 126.07 (s, Ph, *para*), 61.35 (s, N*C*(CH$_3$)$_3$, amido), 59.65 (s, N*C*(CH$_3$)$_3$, imido), 58.81 (s, N*C*(CH$_3$)$_3$, imido), 33.00 (d, J_{PC} = 6.65 Hz, NC(*C*H$_3$)$_3$, amido), 31.03 (t, J_{PC} = 4.78 Hz, NC(*C*H$_3$)$_3$, imido), 30.04 (t, J_{PC} = 4.50 Hz, NC(*C*H$_3$)$_3$, imido). ^{31}P{^{1}H} NMR (C_6D_6, 25 °C): 46.33 (s, P(V)). IR (cm^{-1}): 544.55, 595.29, 642.78, 693.44, 727.67, 743.69, 777.86, 806.71, 834.52, 874.53 (s, P=S), 926.73, 1015.66, 1044.70, 1175.95, 1230.95, 1260.01, 1360.96, 1390.88, 1430.89, 2960.77. Anal. Calcd. for $C_{22}H_{41}N_4P_2SbS_2$: C, 43.56; H, 6.78; N, 9.19%. Found: C, 44.40; H, 7.00: N, 8.81%.

{[(^{t}BuNP=Se)$_2$(^{t}BuN)$_2$]SbPh} 3bSe$_2$

In a similar manner to that used for the synthesis of **3bS$_2$**, samples of **3b** (0.410 g, 0.920 mmol) and selenium (0.140 g, 1.77 mmol) were combined in toluene (30 mL) and stirred at 70 °C for 24 h. The ensuing solution furnished **3bSe$_2$** as needle-shaped crystals after standing at –6 °C for 3 days. Yield: (0.50 g, 0.71 mmol), 94%. Mp: 216–218 °C. ^{1}H NMR (C_6D_6, 25 °C):

7.81 (d, J_{PH} = 8.25 Hz, 2 H, Ph, *ortho*), 7.18 (m, 2 H, Ph, *meta*), 7.06 (m, 1 H, Ph, *para*), 2.05 (s, 9 H, N^{t}Bu, imido), 1.84 (s, 9 H, N^{t}Bu, imido), 1.34 (s, 18 H, N^{t}Bu, amido). $^{13}C\{^1H\}$ NMR (C_6D_6, 25 °C): 160.13 (s, C_{ipso}), 133.64 (s, Ph, *ortho*), 130.30 (s, Ph, *meta*), 129.57 (s, Ph, *para*), 62.02 (s, N*C*$(CH_3)_3$, amido), 60.44 (s, N*C*$(CH_3)_3$, imido), 59.58 (s, N*C*$(CH_3)_3$, imido), 33.06 (s, NC(*C*$H_3)_3$, amido), 31.06 (t, J_{PC} = 4.32 Hz, NC(*C*$H_3)_3$, imido), 29.72 (t, J_{PC} = 4.59 Hz, NC(*C*$H_3)_3$, imido). $^{31}P\{^1H\}$ NMR (C_6D_6, 25 °C): 32.80(s, P(V), J_{PSe} = 894 Hz). IR (cm^{-1}): 564.65 (m, P=Se), 697.54, 730.05, 754.28, 795.21, 830.53, 867.63, 929.60, 1014.79, 1043.14, 1175.19, 1224.03, 1259.02, 1362.78, 1390.79, 1430.78, 2964.30. Anal. Calcd. for $C_{22}H_{41}N_4P_2SbSe_2$: C, 37.58; H, 5.88; N, 7.97%. Found: C, 37.71; H, 6.26; N, 7.09%.

4 RESULTS AND DISCUSSIONS

Synthesis and Spectroscopic Analysis of {[(tBuNP)2(tBuN)2Se]PCl} 1aSe

When compound **1a** was oxidized with one equivalent of selenium in toluene at 60 °C, for 12 h, **1aSe** was obtained in 93% yield (Scheme 25). Due to the presence of the electronegative chlorine atom on the P(III) atom at the apex of the bicycle, oxidation is directed to the P(III) centers on the P_2N_2 ring of **1aSe**.

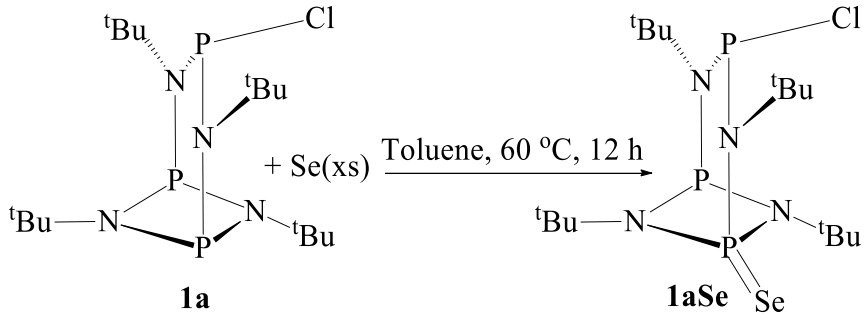

Scheme 25. Synthesis of **1aSe**.

The ^1H NMR spectrum of **1aSe** shows three signals with relative intensities 1:1:2: a doublet at 1.92 ppm (J_{PH} = 4.90 Hz) and a singlet at 1.73 ppm representing the *tert*-butylimino protons,

and a doublet at 1.37 ppm (J_{PH} = 3.90 Hz), attributable to the *tert*-butylamino protons. Four signals are observed at 64.83, 59.83, 57.97 and 55.87 ppm in the $^{13}C\{^{1}H\}$ NMR spectrum of **1aSe** (Figure 31), representing the quaternary carbons of the *tert*-butyl groups. The primary carbons are observed at 31.92 ppm as multiplets representing the *tert*-butylamino carbons and as triplets at 30.57 (J_{PC} = 5.64 Hz) and 30.25 ppm (J_{PC} = 5.64 Hz) attributable to the *tert*-butylimino carbons. The $^{31}P\{^{1}H\}$ NMR spectrum of **1aSe** (Figure 32) depicts three signals: a singlet at 161.17 ppm, and two doublets at 135.98 and 64.07 ppm. The singlet at 161.17 ppm represents the P(III) atom bearing the chlorine atom, while the doublet at 135.98 ppm (J_{PP} = 17.05 Hz) represents the P(III) atom in the P_2N_2 ring. The P(V) atom in the P_2N_2 ring bearing the selenium atom, is observed as a doublet at 64.07 ppm (J_{PP} = 9.25 Hz) flanked by a pair of ^{77}Se satellites attributable to the AA′X spin system with J_{PSe} = 909 Hz. The J_{PP} = 9.25 Hz value falls within the range reported by Keat *et al*. for the cyclic systems $[R_2N(Se)P(\mu\text{-}N^tBu)_2PNR_2]$[131] ($J_{PP}$ = 7–10 Hz), while Balakrishna and coworkers reported A–X (J_{PSe} = 953 Hz) and A–A′ (J_{PP} = 6.7 Hz) values for *cis*-$[^tBuNP(Se)(OCH_2CH_2OMe)]_2$.[32]

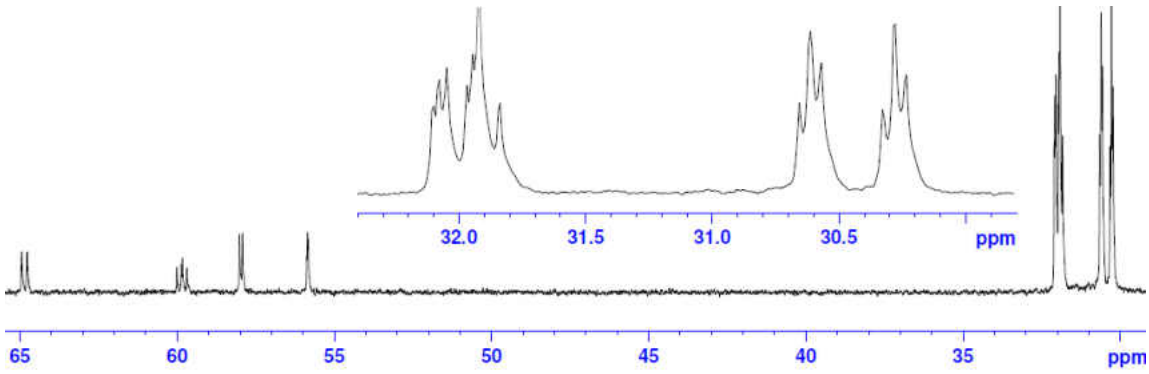

Figure 31. $^{13}C\{^{1}H\}$ NMR Spectrum for **1aSe**.

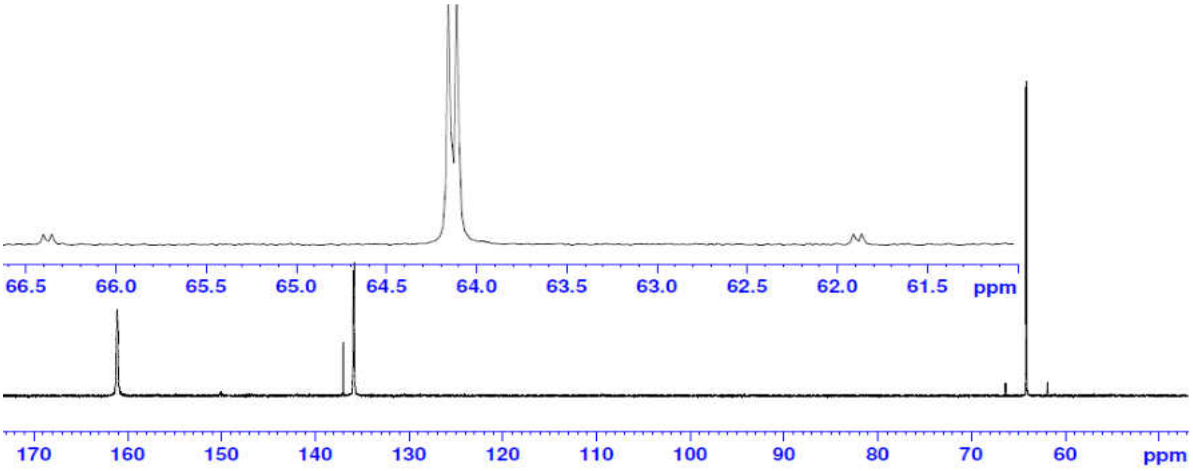

Figure 32. $^{31}P\{^{1}H\}$ NMR Spectrum for **1aSe**.

Synthesis and Spectroscopic Analysis of {[(^{t}BuNP=Se)$_2$(^{t}BuN)$_2$]PCl} 1aSe$_2$

Like compound **1aSe** above, **1aSe$_2$** was obtained by treating **1a** with two equivalents of selenium in toluene at 60 °C for 24 h (Scheme 26). The yield was 88%. The oxidation, as in **1aSe**, is directed to the P_2N_2 ring due to the electron withdrawing chlorine atom attached to the central P(III) atom above the P_2N_2 heterocycle.

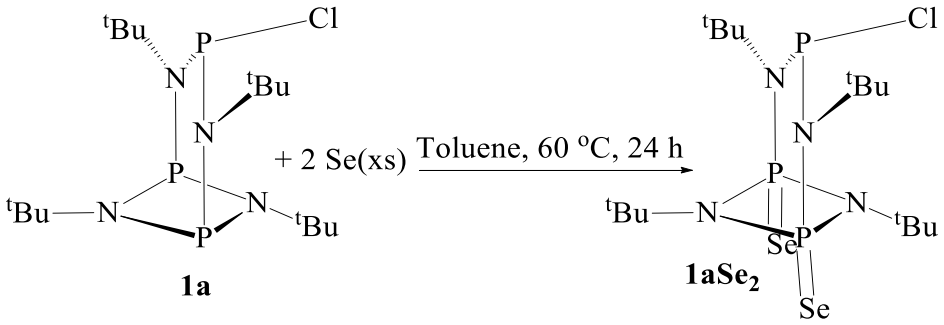

Scheme 26. Synthesis of **1aSe$_2$**.

The ^{1}H NMR spectrum of **1aSe$_2$** (Figure 33) shows four singlets at 1.97, 1.79, 1.78 and 1.49 ppm. We attribute the signals at 1.79 and 1.78 ppm to the *tert*-butylamino protons, while those at 1.97 and 1.49 ppm are due to the *tert*-butylimino protons. The quaternary carbons are observed as four singlets in the ^{13}C{^{1}H} NMR spectrum of **1aSe$_2$** at 65.55, 65.36, 62.39 and 59.66 ppm. While the two singlets at 65.66 and 65.36 ppm represent the quaternary carbons of the *tert*-butylamino carbons, the other two, at 62.39 and 59.66 ppm, are attributed to those of *tert*-butylimino carbons. The primary carbons of the *tert*-butylamino carbons appear as singlets at 31.93 and 31.77 ppm, while those of the *tert*-butylimino carbons are observed as a triplet (J_{PC} = 4.60 Hz) at 30.73 ppm. Two signals are observed in the ^{31}P{^{1}H} NMR spectrum of **1aSe$_2$** (Figure 34) at 142.18 (s) and 43.93 ppm (d, J_{PP} = 14.78 Hz). The singlet corresponds to the P(III) atom to which the chlorine atom is attached, while the doublet (J_{PP} = 14.78 Hz) at 43.93 ppm with a pair of ^{77}Se satellite peaks (J_{PSe} = 955.71 Hz) represents the P(V) atoms of the P_2N_2 ring bearing the selenium atoms. While the P(V) atoms couple with each other to give a doublet, the absence of *J*[P(V)–P(III)] coupling in **1aSe$_2$** is noticeable. Chivers *et al*. have noted the absence of *J*[P(V)–P(III)] coupling in [^{t}Bu(H)N(Se)P(μ-N^{t}Bu)$_2$PN(H)^{t}Bu].[74]The IR spectrum of **1aSe$_2$** shows an absorption band at 600.5 cm^{-1} attributable to the P=Se double bonds of the compound, which can be further confirmed by the high value of J_{PSe} = 955.7 Hz.

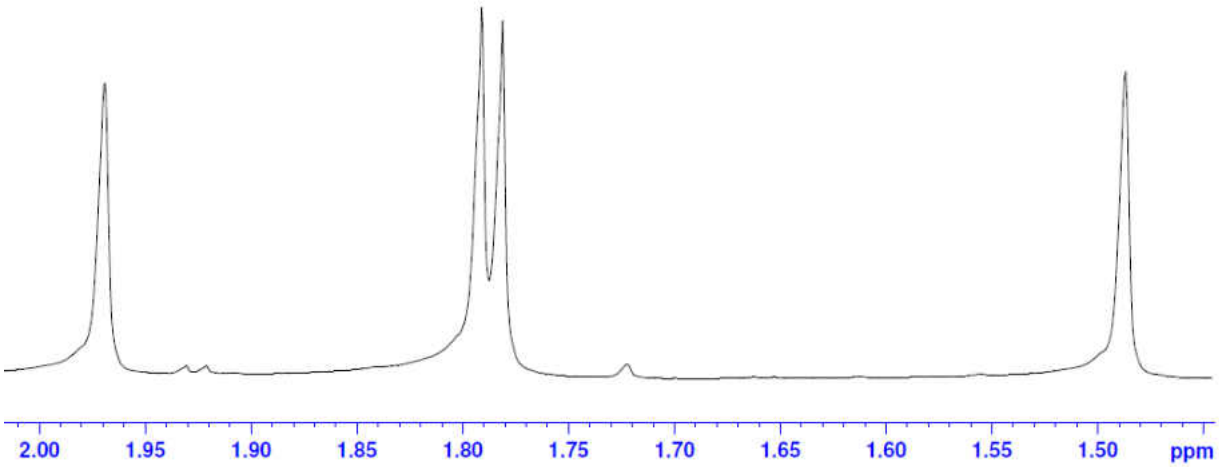

Figure 33. ^{1}H NMR Spectrum for **1aSe$_2$**.

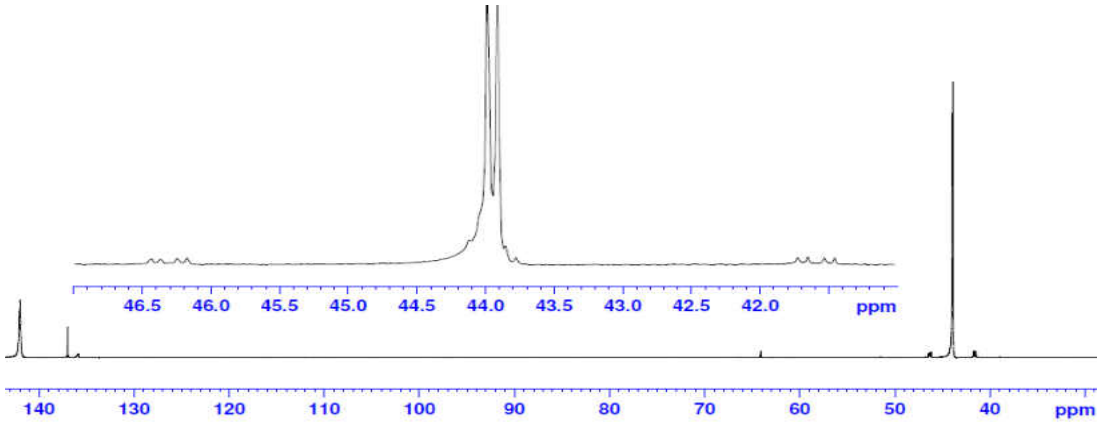

Figure 34. ^{31}P{^{1}H} NMR Spectrum for **1aSe$_2$**.

Solid-state Structure of {[(^{t}BuNP=Se)$_2$(^{t}BuN)$_2$]PCl} 1aSe$_2$

Colorless, needle-like crystals of **1aSe$_2$** were isolated from a cold, concentrated toluene solution after recrystallization. The solid-state structure of **1aSe$_2$**, with a partial numbering scheme is shown in Figure 35, while the crystal data and selected bond parameters are listed in Tables 15 and 16 below, respectively. Compound **1aSe$_2$** crystallized in the monoclinic space

group, $P2_1/c$, with four molecules per unit cell. The P–Cl bond in **1aSe$_2$** (2.1780(6) Å) is shorter than that of **1a** (2.244(3) Å), while its P–N3 bond distance (1.7219(14) Å) is more elongated than that of the latter. The mean exocyclic and endocyclic P–N bond distances in **1aSe$_2$** are 1.711(14) and 1.692(15) Å, respectively. The endocyclic P–N bonds show a marked decrease compared to those of **1a** (1.720(4) Å).[98] This is probably due to the presence of the P(V) atoms that tend to pull in the nitrogen atoms, thereby decreasing the ring size compared to **1a**. The average P=Se bond length in **1aSe$_2$** (2.0675(5) Å) is comparable to those found in [(Se=)P(μ-N^{t}Bu)$_2$P(μ-Se)]$_6$ (2.063(8)–2.081(2) Å) but shorter than those in *cis*-[Ph(H)N(Se=PN^{t}Bu)$_2$N(H)Ph] (2.0826(8) Å).[64, 97] The sum of the angles around the P(V) atoms (359.97°) depicts a distorted pseudo-tetrahedral environment for the P(V) atoms.

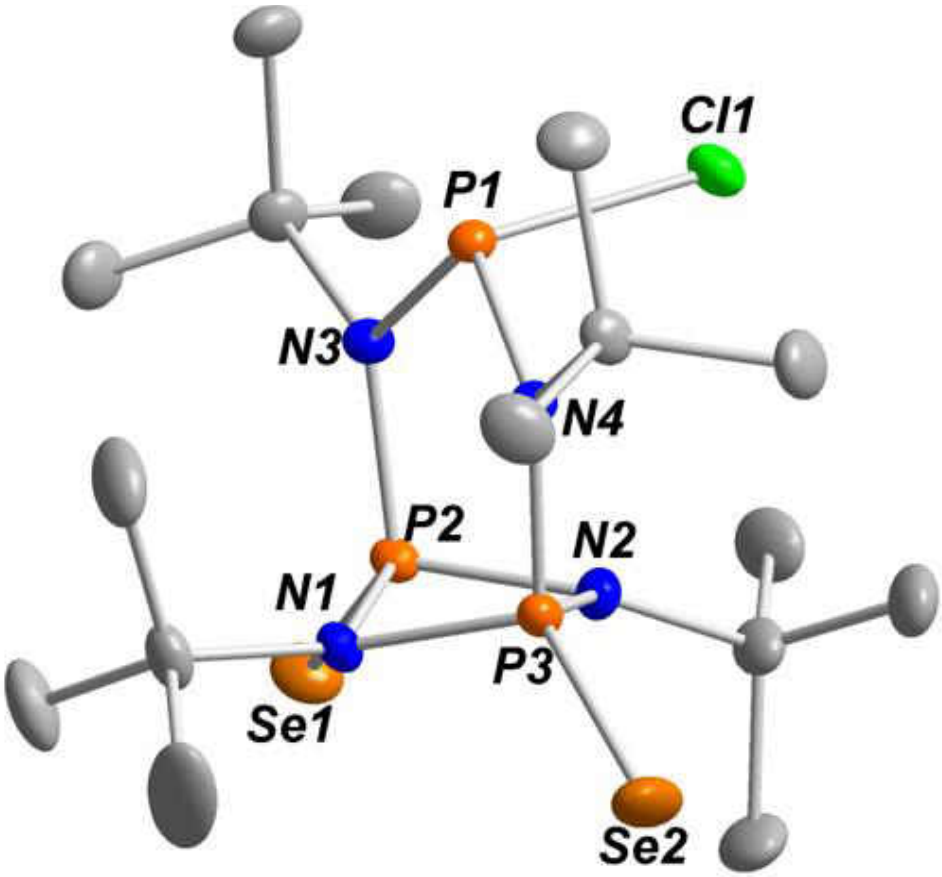

Figure 35**.** Solid-state structure and partial labelling scheme of **1aSe**2. All atoms are drawn at the 50% probability level.

Table 15. Crystal and structure refinement data for **1aSe$_2$**.

Chemical formula	$C_{16}H_{36}ClN_4P_3Se_2$
Formula weight	570.78
Temperature/K	149.99
Crystal system	*monoclinic*
Space group	$P2_1/c$
a/Å	10.0896(7)
b/Å	11.0353(7)
c/Å	21.8574(15)
α/°	90
β/°	95.547(3)
γ/°	90
Volume/Å^3	2422.2(3)
Z	4
ρ_{calc}g/cm^3	1.5651
μ/mm^{-1}	3.371
F(000)	1161.5
Crystal size/mm^3	0.45 × 0.43 × 0.33
Radiation	Mo Kα (λ = 0.71073)
Index ranges	-15 ≤ h ≤ 11, -16 ≤ k ≤ 15, -32 ≤ l ≤ 30
Reflections collected	33421
Independent reflections	8630 [R_{int} = 0.0357, R_σ = 0.0327]
Data/restraints/parameters	8630/0/247
Goodness-of-fit on F^2	0.999
$Rw(F^2)^b$ [I>2σ(I)]	R_1 = 0.0315, wR_2 = 0.0843
$R(F)^a$ (all data)	R_1 = 0.0450, wR_2 = 0.0900
[a] $R = \sum\|F_o - F_c\| \sum \|F\|_o$. [b] $R_w = \{[\sum w(F_o^2 - F_c^2)] / [\sum w(F_o^2)^2]\}^{1/2}$; $w = 1/[\sigma^2(F_o)^2 + (xP)^2 + yP]$, where $P = (F_o^2 + 2F_c^2)/3$.	

Table 16. Selected bond lengths (Å) and angles (°) for **1aSe$_2$**.

Bond Lengths (Å)			
Se2–P3	2.0670(5)	N4–P1	1.7145(14)
Se1–P2	2.0680(5)	N4–P3	1.7116(14)
Cl1–P1	2.1780(6)	N2–P2	1.6839(15)
N3–P1	1.7219(14)	N2–P3	1.6869(15)
N3–P2	1.7104(14)	N1–P2	1.6979(13)
N1–P3	1.6999(14)	P2–P3	2.4474(6)
Bond Angles (°)			
P2–N3–P1	119.63(8)	N2–P2–Se1	120.36(5)
P3–N4–P1	120.14(8)	N1–P2–N3	102.67(7)
P3–N2–P2	93.11(7)	N1–P2–Se1	119.73(5)
P3–N1–P2	92.16(7)	N1–P2–N3	102.96(7)
N3–P1–Cl1	101.52(5)	N1–P2–N2	84.72(7)
N4–P1–Cl1	101.63(50	N4–P3–Se2	119.40(5)
N4–P1–N3	106.98(7)	N2–P3–Se2	121.87(6)
N3–P2–Se1	119.88(5)	N1–P3–Se2	119.35(5)

Synthesis and Spectroscopic Analysis of {[(^{t}BuNP)$_2$(^{t}BuN)$_2$](P=Se)Ph} 1bSe′

When **1b** was treated with excess selenium at RT for 12 h, in toluene, **1bSe′** was obtained in a yield of 90%, (Scheme 27). Unlike in compound **1aSe** and **1aSe$_2$** where oxidation is orientated

towards the P(III) atoms of the P_2N_2 ring, oxidation in **1bSe′** is directed towards the central P(III) atom bearing the phenyl (electron-donor) ligand.

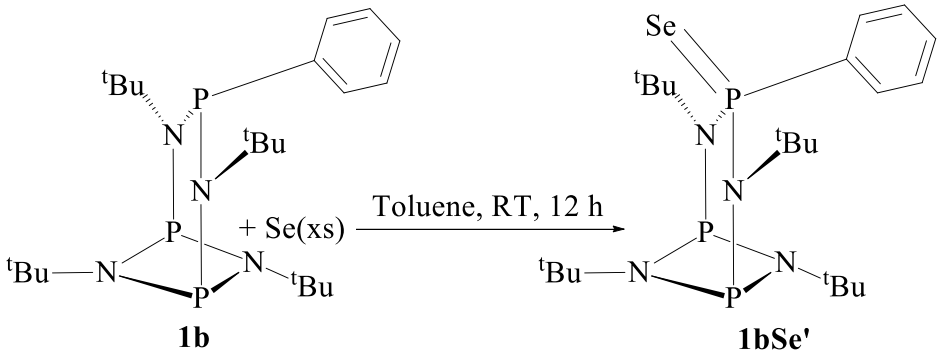

Scheme 27. Synthesis of **1bSe′**.

The ^{1}H NMR spectrum of **1bSe′** depicts three signals at 8.68 (m), 7.16 (s) and 7.08 ppm (m) representing the *ortho*, *meta* and *para* protons on the phenyl ligand. Three singlets are observed at 1.58, 1.43 and 1.38 ppm with relative intensities 1:2:1 attributable to the *tert*-butyl protons. Those with unit intensities represent the *tert*-butylimino protons, while the one with intensity two belongs to the *tert*-butylamino groups. The ^{13}C{^{1}H} NMR spectrum of **1bSe′** reveals four signals at 145.08, 144.42, 133.81 and 130.63 ppm assigned to the *ipso*, *ortho*, *meta* and *para* carbons of the phenyl ligand, respectively. Three other signals–multiplets and two triplets are observed at 62.30 (m), 54.40 (J_{PC} = 12.93 Hz) and 54.02 (J_{PC} = 8.00 Hz) assigned to the quaternary carbons of the *tert*-butyl groups. The primary carbons of the *tert*-butylamido and *tert*-butylimido groups are shown as multiplets and a triplet (J_{PC} = 5.70 Hz) at 32.99 (m) and 30.56 ppm (t), respectively. Two distinct phosphorus environments are revealed by two signals at 194.12 (d, J_{PP} = 21.36 Hz) and 46.41 ppm (t, J_{PP} = 20.76 Hz) in the ^{31}P{^{1}H} NMR spectrum of **1bSe′** (Figure 36). The doublet downfield represents the two P(III) atoms on the P_2N_2 ring while the triplet upfield is assigned to the P(V) atom bearing the selenium atom and the phenyl ligand. Pairs of ^{77}Se satellite peaks of ^{31}P–^{77}Se coupling (J_{PSe} = 842.38 Hz) are also revealed in this

NMR spectrum between 50.00 and 40.00 ppm. The IR spectrum of **1bSe′** shows an absorption band at 599.4 cm^{-1} attributable to the P=Se stretching mode. The presence of the P=Se bond can also be confirmed by the values of the J_{pp} and J_{PSe} coupling constants.

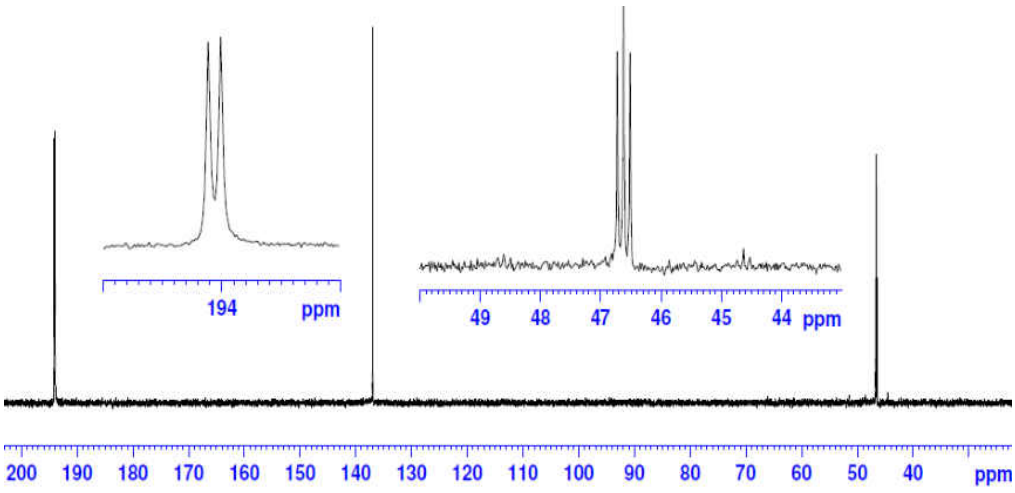

Figure 36. $^{31}P\{^{1}H\}$ NMR Spectrum for **1aSe′**.

Synthesis and Spectroscopic Analysis of {[(^{t}BuNP)$_2$(^{t}BuN)$_2$S]AsCl} 2aS

The treatment of **2a** with freshly sublimed sulfur, in toluene for 2 days at 70 °C, gave compound **2aS** in 71% yield (Scheme 28).

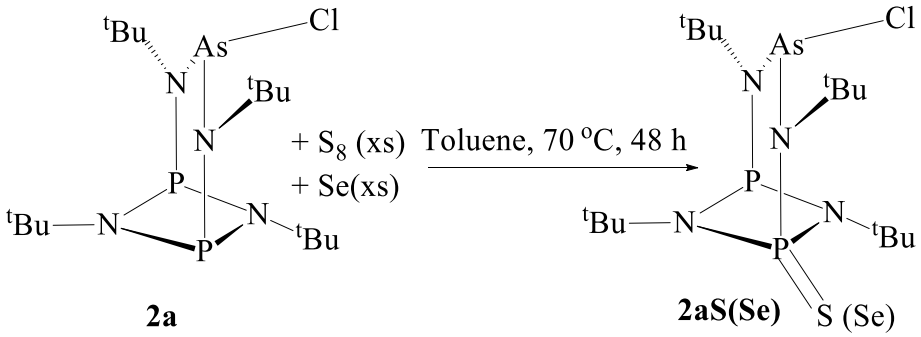

Scheme 28. Synthesis of **2aS** and **2aSe**.

The ^{1}H NMR spectrum of compound **2aS** depicts four singlets at 1.81, 1.72, 1.36 and 1.33 ppm, in the ratio 1:1:1:1, corresponding to the *tert*-butyl protons. The $^{13}C\{^{1}H\}$ NMR spectrum of **2aS** consists of eight signals, representing the four different types of carbon found in the molecule. The quaternary *tert*-butyl carbons appear as multiplets at 63.86, 59.50, 57.02 and 55.13 ppm, while the primary carbons are observed at 32.68, 31.96, 30.79 and 30.40 ppm as doublets in the ratio 1:1:1:1. From the ratio of the protons and carbon signals, it can be concluded that all the *tert*-butyl groups in **2aS** are magnetically different from each other. The $^{31}P\{^{1}H\}$ NMR spectrum of **2aS** depicts two signals at 122.81 and 68.26 ppm, representing phosphorus (III) and phosphorus(V) in the P_2N_2 ring of the compound. The IR spectrum of **2aS** indicates a strong stretching absorption band at 929.3 cm^{-1} corresponding to the vibrational modes of the P=S bond.[11, 32]

Solid-state Structure of {[(^{t}BuNP)$_2$(^{t}BuN)$_2$S]AsCl} 2aS

Colorless, needle-like crystals of **2aS**, suitable for X-ray studies, were isolated from a cold (–6 °C) toluene solution. The solid-state structure of **2aS**, with a partial numbering scheme is shown in Figure 37, while the crystal data and selected bond parameters are listed in Tables 17 and 18 below, respectively. Compound **2aS** crystallized in the monoclinic space group, *P2$_1$/n*, with 4 molecules per unit cell. While there is a crystallographic mirror plane, containing the central group 15 atom and the chlorine atom, bisecting the molecule and its puckered P_2N_2 ring in **2a**, such a mirror plane is absent in **2aS**.[98] The solid-state structure of **2aS**, therefore, depicts a chiral molecule with C_1-symmetry.

Compared to **2a**, the As–Cl bond is shorter in **2aS** (2.3005(6) Å) than in the former (2.3325(11) Å).[98] The exocyclic P–N bond, 1.7292(18) Å, in **2aS** is almost identical to that in

2a, 1.727(2) Å. By contrast, the endocyclic bond distances, 1.6780(19) and 1.675(2) Å in **2aS** are shorter than those in **2a** (1.718(2) and 1.717(2) Å).[98] The **2aS** P=S bond length, 1.9213(9) Å, is similar to that in [(^{t}BuNP=S)$_2$(^{t}BuN)$_2$]Zr(O^{t}Bu)$_2$,[93] 1.9284(7) Å and [Me$_2$Si(μ-N^{t}Bu)$_2$P=S(NHPh)], 1.938(2) Å,[85] but longer than those in [(^{t}BuNP=S)$_2$(^{t}BuN)$_2$]HfCl$_2$, 1.9094(7) Å, and [(^{t}BuNP=S)$_2$(^{t}BuN)$_2$]ZrCl$_2$, 1.9080(5) Å.[93] Compound **2aS**, like **2a**, contains a similar puckered structure, with angle sum = 355.69°, heterocycle P$_2$N$_2$ ring compared to that in [(^{t}BuNP=S)$_2$(^{t}BuN)$_2$]HfCl$_2$ (357°).[93] The exo-S–P–N angles in **2aS** are 120.71, 118.96 and 116.40°, (sum = 356.07°), indicating that the P(V) atom is found in a distorted pseudo-tetrahedral environment, in agreement with those found in [(C$_6$H$_5$NH)P(S)NC$_6$H$_5$]$_2$ (121.8(2), 119.5(2) and 111.6(2)° = 352.9°).[132]

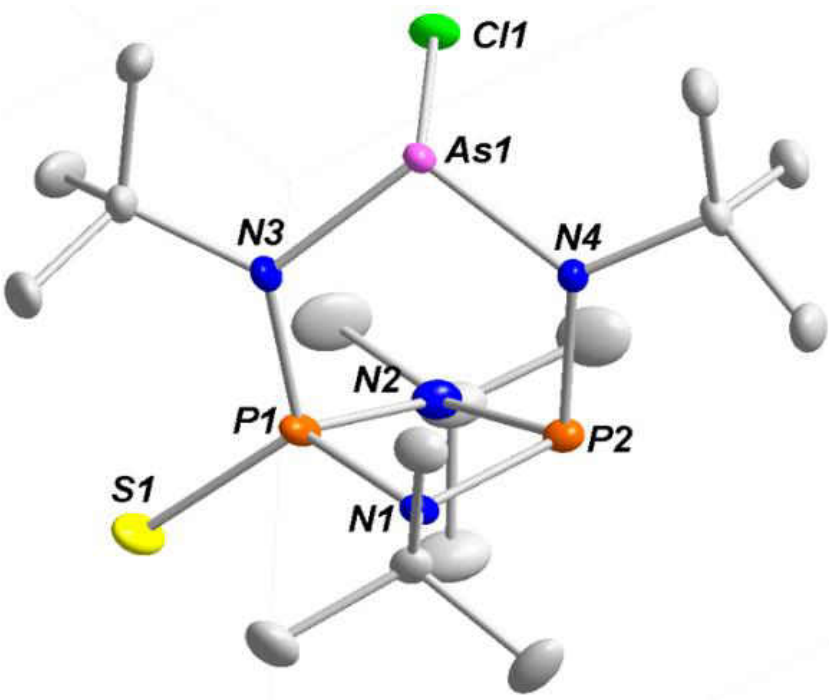

Figure 37. Solid-state structure and partial labelling scheme of **2aS**. All atoms are drawn at the 50% probability level.

Table 17. Crystal data and structure refinement for **2aS**.

Chemical formula	$C_{16}H_{36}AsClN_4P_2S$
Formula weight	488.86
Temperature/K	100(2)
Crystal system	*monoclinic*
Space group	$P2_1/n$

a/Å	9.9227(6)
b/Å	20.7738(14)
c/Å	11.5985(7)
α/°	90
β/°	97.481(3)
γ/°	90
Volume/Å^3	2370.5(3)
Z	4
ρ_{calc}g/cm^3	1.370
μ/mm^{-1}	1.778
F(000)	1024
Reflections collected	19334
Independent reflections	5856[R_{int} = 0.0334, R_σ = 0.0327]
Completeness (%)	100.0
$Rw(F^2)^b$ [I>2σ(I)]	R_1 = 0.0293, wR_2 = 0.0869
$R(F)^a$ (all data)	R_1 = 0.0395, wR_2 = 0.1069

[a] $R = \sum|F_o - F_c| \sum |F|_o$. [b] $R_w = \{[\sum w(F_o^2 - F_c^2)] / [\sum w(F_o^2)^2]\}^{1/2}$;

$w = 1/[\sigma^2(F_o)^2 + (xP)^2 + yP]$, where $P = (F_o^2 + 2F_c^2)/3$.

Table 18. Selected bond lengths (Å) and angles (°) for **2aS**.

Bond Lengths (Å)			
As1–N4	1.8453(16)	P1–P2	2.4979(8)
As1–N3	1.8712(18)	P2–N2	1.722(2)
As1–Cl1	2.3005(6)	P2–N4	1.7292(18)
P1–N2	1.675(2)	P2–N1	1.7378(19)
P1–N1	1.6780(19)	N1–C20	1.485(3)
P1–N3	1.6945(18)	N2–C10	1.485(3)
P1–S1	1.9213(9)	N3–C30	1.530(3)
Bond Angles (°)			
N4–As1–N3	103.02(8)	N2–P1–S1	120.71(7)
N4–As1–Cl1	100.87(6)	N1–P1–S1	118.96(7)
N3–As1–Cl1	99.77(6)	N3–P1–S1	116.40(7)
N2–P1–N1	85.13(9)	N2–P2–N4	100.27(9)
N2–P1–N3	104.84(9)	N2–P2–N1	81.92(9)
N1–P1–N3	105.94(9)	N4–P2–N1	100.63(8)
P1–N3–As1	118.23(10)	P2–N4–As1	123.05(10)

Synthesis and Spectroscopic Analysis of {[(^{t}BuNP)$_2$(^{t}BuN)$_2$Se]AsCl} 2aSe

Like in **2aS**, the treatment of **2a** with one equivalent of selenium at 50 °C in toluene for 12 h, afforded compound **2aSe** in 89% yield (Scheme 28). While the reaction with sulfur took about

2 days to produce the mono-sulfide **2aS**, it took only 12 h using selenium to attain the mono-selenide **2aSe** in good yield, showing that gray selenium is a better oxidizing agent than sulfur. Like all mono-sulfides and mono-selenides, compound **2aSe** is chiral.

The ^{1}H NMR spectrum of **2aSe** (Figure 38), like that of **2aS**, shows four singlets at 1.86, 1.75, 1.39 and 1.32 ppm with equal relative intensities of 1:1:1:1, representing the *tert*-butyl protons. The ^{13}C{^{1}H} NMR spectrum of **2aSe** reveals four signals at 64.50 (s), 60.02 (d, J_{PC} = 17.59 Hz), 57.41 (d, J_{PC} = 12.17 Hz) and 55.57 ppm (m) corresponding to the quaternary carbons of the *tert*-butyl carbons. Four signals of equal intensities are also observed at 32.77 (d, J_{PC} = 10.14 Hz), 32.19 (d, J_{PC} = 3.99 Hz), 30.64 (t, J_{PC} = 5.43 Hz) and 30.52 ppm (t, J_{PC} = 5.97 Hz) attributable to the primary carbons of the *tert*-butyl groups. The ^{31}P{^{1}H} NMR spectrum of **2aSe** (Figure 39) shows two signals at 130.18 and 61.81 ppm. The signal at 130.18 ppm represents the phosphorus(III) atom on the P_2N_2 ring, while the doublet (J_{PP} = 8.89 Hz) at 61.81 ppm corresponds to the phosphorus (V) atom bearing the selenium atom. Two pairs of ^{77}Se satellite peaks are also seen on either side of the 61.81 ppm signal due to ^{31}P–^{77}Se coupling (J_{PSe} = 891.44 Hz). The J_{PSe} = 891.44 Hz clearly indicates the presence of a P=Se bond.

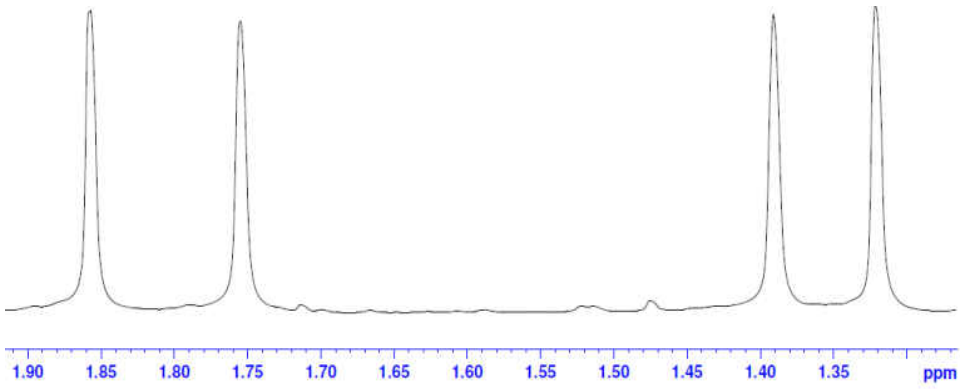

Figure 38. ^{1}H NMR Spectrum for **2aSe**.

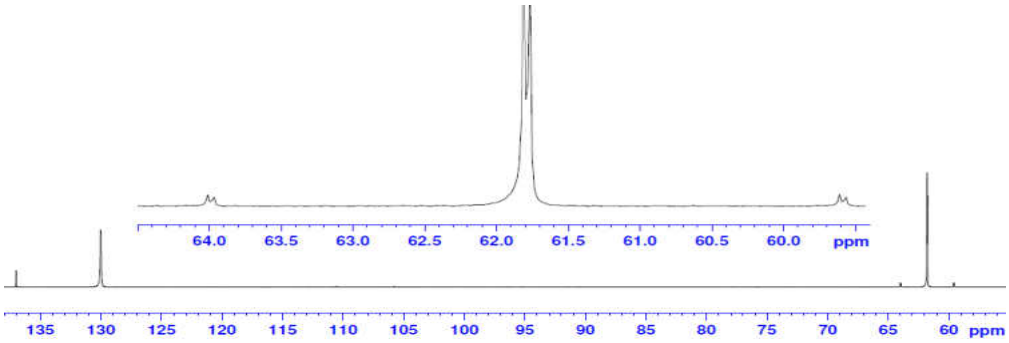

Figure 39. $^{31}P\{^{1}H\}$ NMR Spectrum for **2aSe**.

Solid-state Structure of {[(^{t}BuNP)$_2$(^{t}BuN)$_2$Se]AsCl} 2aSe

Block-shaped single crystals of **2aSe**, suitable for X-ray analysis, were isolated from a cold (–6 °C) concentrated toluene solution. The solid-state structure of **2aSe**, with a partial numbering scheme is shown in Figure 40, while the crystal data and selected bond parameters are listed in Tables 19 and 20, respectively. Compound **2aSe** crystallized in the orthorhombic space group, $P2_12_12_1$, with four molecules per unit cell. Compared to the P=S bond (1.9213(9) Å) in **2aS**, the P=Se bond (2.0756(5) Å) in **2aSe** is longer as expected but almost identical to the same bond distances in [^{t}Bu(H)N(Se)P(μ-N^{t}Bu)$_2$P(Se)N(H)^{t}Bu] (2.078(1) and 2.070(1) Å).[74]The endocyclic P–N bond distances in **2aSe** range from 1.6775(17)–1.7354(17) Å whereas those of **2a** are 1.718(4) Å. The P–N bond bearing the Se atom in **2aSe** is reduced to 1.6775(17) Å. The exocyclic P–N and the As–Cl bonds in **2aSe** are the same as those of **2a**, meaning that the precursor cage remains almost unaltered after the oxidation. The sum of the three Se–P–N angles in **2aSe** is 356.01° indicating that the P(V) atom is situated at the apex of a distorted pseudo-tetrahedron as in **2aS**.

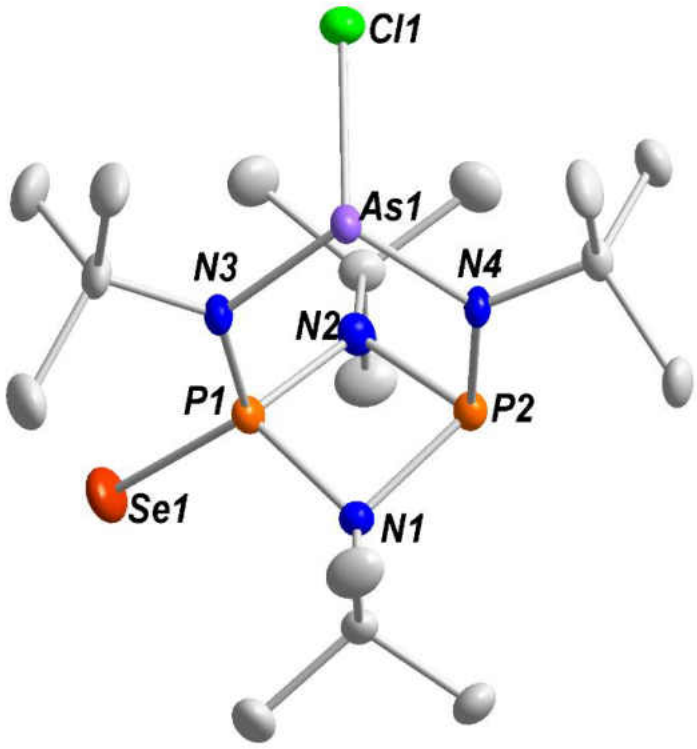

Figure 40. Solid-state structure and partial labelling scheme of **2aS**. All atoms are drawn at the 50 % probability level.

Table 19 . Crystal and structure refinement data for **2aSe**.

Chemical formula	$C_{16}H_{36}N_4P_2AsClSe$
Fw	535.77
T/K	150.0
λ/Å	0.71073
Crystal system	*orthorhombic*
Space group	$P2_12_12_1$

a/Å	10.0427(4)
b/Å	10.8838(5)
c/Å	21.9464(10)
α/°	90
β/°	90
γ/°	90
V/Å^3	2398.80
Z	4
ρ (calc.) g cm^{-3}	1.4834
μ/mm^{-1}	3.187
F(000)	1097.6
Reflections collected	43322
Independent reflections	7328 [R_{int} = 0.0340, R_σ = 0.0350]
$Rw(F^2)^b$ [I>2σ(I)]	R_1 = 0.0245, wR_2 = 0.0632
$R(F)^a$ (all data)	R_1 = 0.0285, wR_2 = 0.0643

[a] $R = \sum|F_o - F_c| \sum |F|_o$. [b] $R_w = \{[\ \sum w(F_o^2 - F_c^2)]\ /[\sum w(F_o^2)^2]\}^{1/2}$; $w = 1/[\sigma^2(F_o)^2 + (xP)^2 + yP]$, where $P = (F_o^2 + 2F_c^2)/3$.

Table 20. Selected bond lengths (Å) and angles (°) for **2aSe**.

Bond Lengths (Å)			
N1–P1	1.6775(17)	P1–Se1	2.0756(5)
N1–P2	1.7354(17)	N3–As1	1.8798(16)
N2–P2	1.7242(16)	As1–Cl1	2.3132(5)

N4–As1 P1–N3	1.8411(15) 1.6908(17)	P2–N4	1.7263(17)
Bond Angles (°)			
P2–N1–P1 As1–N2–P2 N3–P1–N1 N4–P1–N1 N4–P1–N3 Se1–P1–N1 Cl1–As1–N2	94.06(8) 122.85(9) 105.56(8) 85.42(8) 104.48(8) 118.51(6) 101.15(5)	Se1–P1–N3 Se1–P1–N4 N2–P2–N1 N4–P2–N1 N4–P2–N2 N3–As1–N2 Cl1–As1–N3	118.23(6) 119.27(6) 100.85(8) 82.11(8) 99.83(8) 103.35(7) 99.93(5)

Synthesis and Spectroscopic Analysis of {[(^{t}BuNP=S)$_2$(^{t}BuN)$_2$]AsCl} 2aS$_2$

Compound **2aS$_2$** was isolated in about 71% yield when **2a** was treated with excess elemental sulfur in toluene for two days at 80 °C (Scheme 29). Both **2aS** and **2aS$_2$** took two days for the

reaction to go to completion, however, the latter was achieved at a much higher temperature (80 °C).

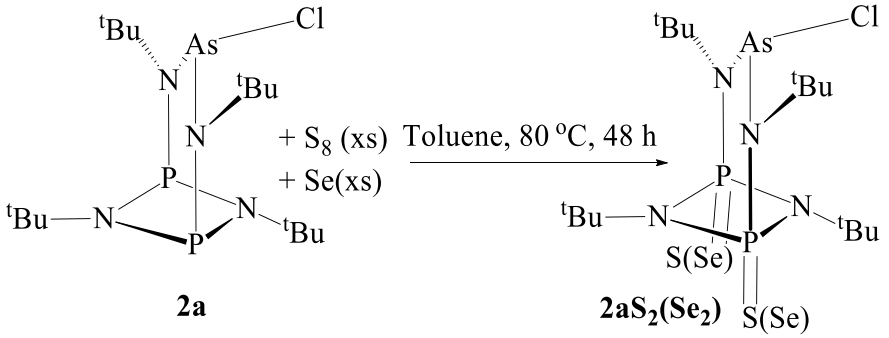

Scheme 29. Synthesis of **2aS2** and **2aSe2**.

The ^{1}H NMR spectrum of **2aS2** reveals three singlets resonating at 1.90, 1.68 and 1.43 ppm with relative intensities of 1:2:1, correspond to the protons of the *tert*-butyl groups. In the ^{13}C{^{1}H} NMR spectrum of **2aS2** are found five signals: four singlets and multiplets at 64.18, 60.72, 58.40, 32.22 and 30.62 ppm (m). While the three singlets, 64.18, 60.72 and 58.40 ppm are attributable to the quaternary carbons of the *tert*-butyl groups, the signals upfield at 32.22 and 30.62 ppm represent the primary carbons. The ^{31}P{^{1}H} NMR spectrum of **2aS2** shows only one singlet at 52.46 ppm representing the two phosphorus(V) atoms bearing the sulfur atoms.

Solid-state Structure of {[(tBuNP=S)2(tBuN)2]AsCl} 2aS2

Colorless crystals of **2aS2**, suitable for single crystal analysis were obtained from a cold concentrated toluene solution. The solid-state structure of **2aS2**, with a partial numbering scheme is shown in Figure 41, while the crystal data and selected bond parameters are listed in Tables 21 and 22, respectively. Compound **2aS2** crystallized in the orthorhombic space group, *Cmca*, with four molecules per unit cell. The P=S bond distances range from 1.9138(10)–1.9211(19) Å,

similar to those in [(^{t}BuNP=S)$_2$(^{t}BuN)$_2$]Zr(O^{t}Bu)$_2$,[93] 1.9284(7) Å and **2aS** (1.9213(9) Å), but longer than P=S bonds in [(^{t}BuNP=S)$_2$(^{t}BuN)$_2$]HfCl$_2$, 1.9094(7) Å, and [(^{t}BuNP=S)$_2$(^{t}BuN)$_2$]ZrCl$_2$, 1.9080(5) Å.[93]The As–Cl bond in **2aS$_2$** (2.2800(9) Å) is about 0.0525 Å shorter than the same bond in **2a** (2.3325(11) Å) suggesting that there is a distortion in the bicycle after oxidation. Both the endocyclic (1.684(2)–1.685(2) Å) and exocyclic (1.694(2)–1.699(4)Å) P–N bonds show significant contraction compared to those of **2a**. The As–N3 bond distance (1.876(2) Å) is also elongated compared to the same bond in **2a** (1.843(2) Å).[98]The sum of the N–P–S angles around the P(V) atom is 357.97° depicting a distorted pseudo-tetrahedral geometry for the P(V) centers.

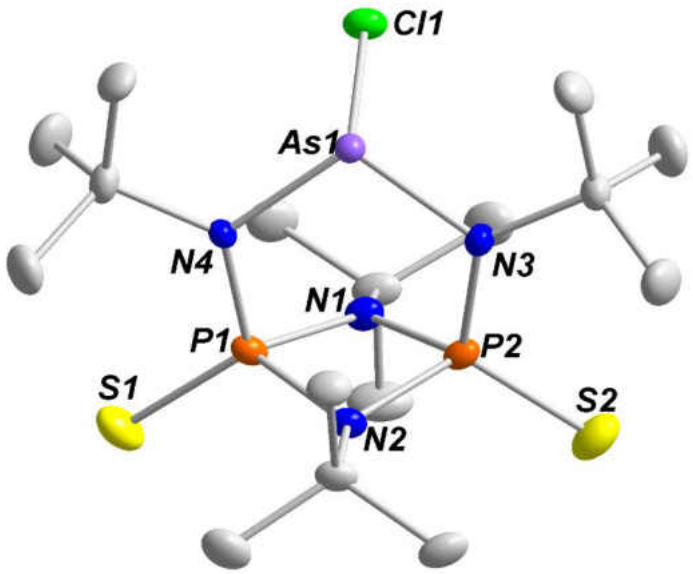

Figure 41. Solid-state structure and partial labelling scheme of **2aS$_2$**. All atoms are drawn at the 50 % probability level.

Table 21. Crystal and structure refinement data for **2aS$_2$**.

Chemical formula	$C_{16}H_{36}N_4P_2S_2ClAs$
Formula weight	520.95
Temperature/K	150.02
Crystal system	*orthorhombic*
Space group	*Cmca*
a/Å	33.7176(17)
b/Å	28.5899(15)
c/Å	9.9383(5)
α/°	90
β/°	90
γ/°	90
Volume/Å^3	9580.4(9)
Z	16
ρ_{calc}g/cm^3	1.4446
μ/mm^{-1}	1.848
F(000)	4363.5
Crystal size/mm^3	0.45 × 0.45 × 0.24
Radiation	Mo Kα (λ = 0.71073)
2Θ range for data collection/°	4.5 to 66.44
Index ranges	$-51 \leq h \leq 51$, $-44 \leq k \leq 44$, $-11 \leq l \leq 15$
Reflections collected	101414
Independent reflections	9295 [R_{int} = 0.0453, R_{sigma} = 0.0227]
Data/restraints/parameters	9295/168/384
Goodness-of-fit on F^2	1.272
Final R indexes [I > = 2σ(I)]	R_1 = 0.1104, wR_2 = 0.2722
Final R indexes [all data]	R_1 = 0.1294, wR_2 = 0.3140
Largest diff. peak/hole / e Å^{-3}	3.66/-16.33

Table 22. Selected bond lengths (Å) and angles (°) for **2aS$_2$**.

Bond Lengths (Å)			
As1–Cl1	2.2800(9)	P1–N2	1.685(2)
As1–N3	1.876(2)	P1–N3	1.694(2)
As1–N4	1.876(2)	P2–S2	1.9211(19)
P1–S1	1.9138(10)	P2–N4	1.699(4)
P1–N1	1.684(2)	N1–C1	1.492(4)
Bond Angles (°)			
N4–As1–Cl1	100.27(7)	N2–P1–N1	104.74(14)
N3–As1–Cl1	100.27(7)	N3–P1–S1	120.17(9)
N3–As1–N4	104.66(14)	N3–P1–N1	84.85(10)
N1–P1–S1	119.25(10)	N3–P1–N2	103.47(13)
N2–P1–S1	118.55(9)		

Synthesis and Spectroscopic Analysis of {[(^{t}BuNP=Se)$_2$(^{t}BuN)$_2$]AsCl} 2aSe$_2$

The treatment of **2a** with two equivalents of selenium in toluene at 75 °C for 24 h afforded **2aSe$_2$** with a yield of 93% (Scheme 29). Unlike the monoselenide **2aSe** that took 12 h at 50 °C for the reaction to be completed, the diselenide **2aSe$_2$** took one day at 75 °C to be formed. This is probably due to the first selenium atom pulling electrons from the P(III) atom making it harder to oxidize.

The ^{1}H NMR spectrum of **2aSe$_2$** (Figure 42), like that of **2aS$_2$**, shows three singlets at 1.97, 1.71 and 1.51 ppm in the ratio 1:2:1 corresponding to the *tert*-butyl protons. The quaternary carbons of the *tert*-butyl groups are represented on the ^{13}C{^{1}H} NMR spectrum of **2aSe$_2$** by three singlets at 65.03, 61.47 and 59.17 ppm. Three other signals, one singlet and two triplets, are found further upfield at 32.08 (s), 30.94 (t, J_{PC} = 4.68 Hz) and 30.59 ppm (t, J_{PC} = 4.68 Hz) attributable to the primary carbons. While the singlet at 32.08 ppm represents the primary carbons of the *tert*-butylamino groups, the triplets at 30.94 and 30.59 ppm correspond to those of the *tert*-butylimino groups. The ^{31}P{^{1}H} NMR spectrum of **2aSe$_2$** (Figure 43) reveals only one singlet at 43.68 ppm with two pairs of ^{77}Se satellite peaks due to ^{31}P–^{77}Se coupling (J_{PSe} = 933.16 Hz). This ^{31}P–^{77}Se coupling constant, 933.16 Hz, confirms the presence of a P=Se bond. The signal at 43.68 ppm is attributed to the two phosphorus (V) atoms of the P_2N_2 ring bearing the selenium atoms. The IR spectrum of **2aSe$_2$** shows an absorption band at 581.4 cm^{-1}, which we assign to the P=Se double bonds.[87]

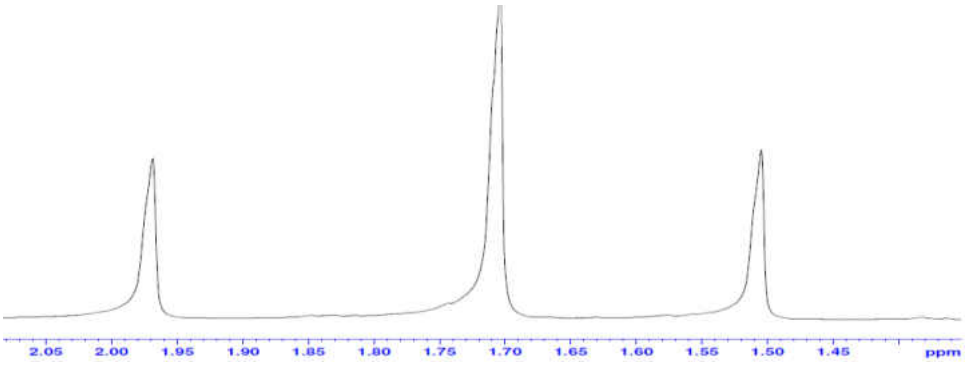

Figure 42. ^{1}H NMR Spectrum for **2aSe$_2$**.

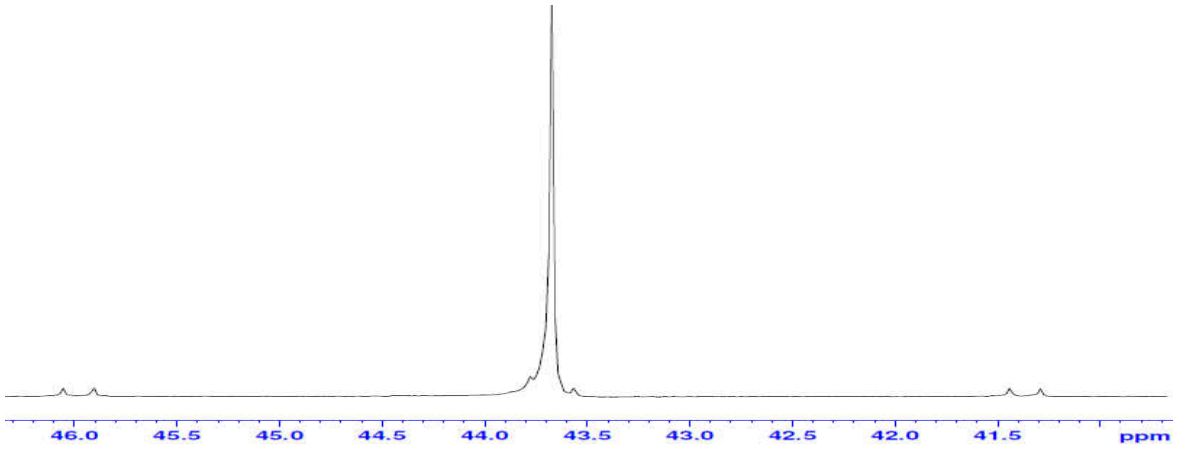

Figure 43. $^{31}P\{^{1}H\}$ NMR Spectrum for **2aSe$_2$**.

Solid-state Structure of {[(^{t}BuNP=Se)$_2$(^{t}BuN)$_2$]AsCl} 2aSe$_2$

Like in **2aS$_2$** above, good quality crystals of **2aSe$_2$** were isolated from a cold (–6 °C) concentrated toluene solution after recrystallization. The solid-state structure of **2aSe$_2$**, with a partial numbering scheme is shown in Figure 44, while the crystal data and selected bond parameters are listed in Tables 23 and 24, respectively. Compound **2aSe$_2$** crystallized in the orthorhombic space group, *Pnma*, with four molecules per unit cell. Like in **2aSe**, the bond lengths of P=Se (2.0709(5) Å) are almost identical with those reported in [^{t}Bu(H)N(Se)P(μ-N^{t}Bu)$_2$P(Se)N(H)^{t}Bu] (2.078(1) and 2.070(1) Å).[74] Compared to **2aSe** and **2a**, the As–Cl bond in **2aSe$_2$** is reduced to 2.2932(5) Å.

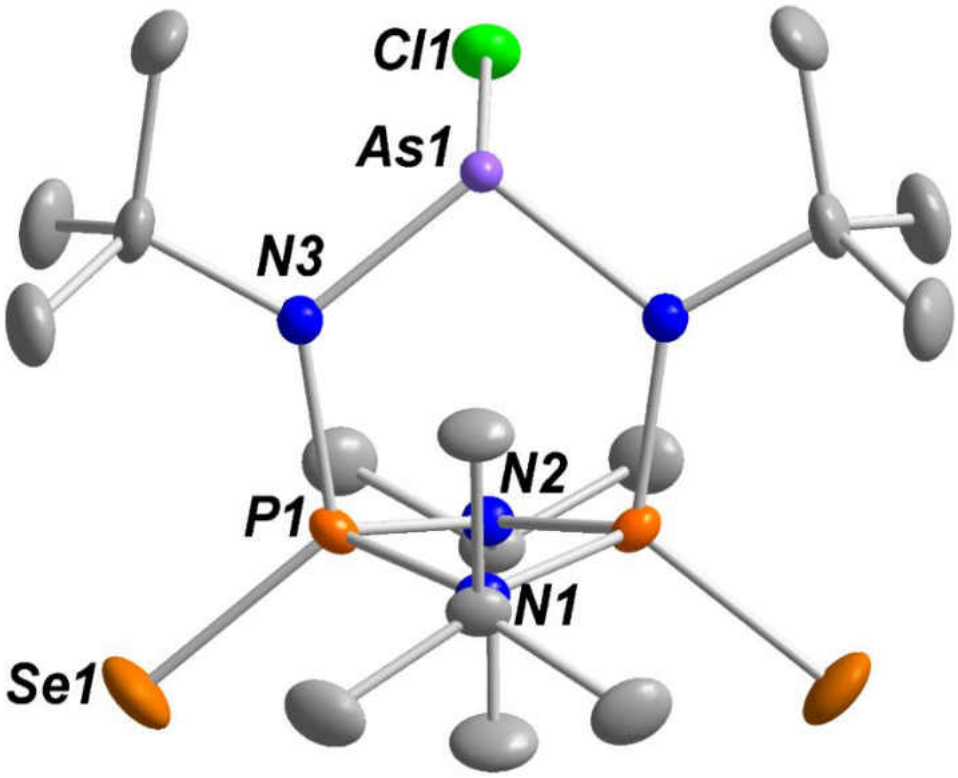

Figure 44. Solid-state structure and partial labelling scheme of **2aSe$_2$**. All atoms are drawn at the 50% probability level.

Table 23. Crystal and structure refinement data for **2aSe$_2$**

Chemical formula	$C_{16}H_{36}AsClN_4P_2Se_2$
Fw	614.73
T/K	150.01
λ/Å	0.71073
Crystal system	orthorhombic
Space group	*Pnma*
a/Å	9.8842(4)
b/Å	17.1670(7)
c/Å	14.6283(7)
α/°	90
β/°	90
γ/°	90
V/Å^3	2482.16(19)
Z	4
ρ (calc.) g cm^{-3}	1.6449
μ/mm^{-1}	4.548
F(000)	1233.4
Reflections collected	33362
Independent reflections	4680 [R_{int} = 0.0388, R_σ = 0.0366]
Rw(F^2)^b [I>2σ(I)]	R_1 = 0.0318, wR_2 = 0.0719
R(*F*)^a (all data)	R_1 = 0.0554, wR_2 = 0.0786

[a] $R = \sum|F_o - F_c| \sum |F|_o$. [b] $R_w = \{[\sum w(F_o^2 - F_c^2)] / [\sum w(F_o^2)^2]\}^{1/2}$; $w = 1/[\sigma^2(F_o)^2 + (xP)^2 + yP]$, where $P = (F_o^2 + 2F_c^2)/3$.

Table 24. Selected bond lengths (Å) and angles (°) for **2aSe$_2$**.

Bond Lengths (Å)			
P1–N3	1.7003(14)	N4–As1	1.8752(14)
P2–N4	1.7003(14)	P1–Se1	2.0709(5)
P1–N1	1.6838(14)	As1–Cl1	2.2932(7)
P1–N2	1.6838(14)	C11–N3	1.503(3)
P2–N2	1.6917(15)	C2–N4	1.507(3)
Bond Angles (°)			
P1–N1–P2	92.87(10)	N3–P1–N2	103.75(9)
P1–N2–P2	94.06(10)	N1–P1–N3	104.22(9)
As1–N3–P1	117.96(8)	Se1–P1–N1	119.54(6)
N1–P1–N2	84.56(7)	Se1–P1–N3	119.48(7)
N4–P2–N1	103.75(9)	Se2–P2–N4	119.20(5)
N4–As1–N3	105.48(9)	Cl20–As1–N4	100.49(5)
Cl20–As1–N4	100.49(5)	P1–N3–C2	132.04(6)

Synthesis and Spectroscopic Analysis of {[(ᵗBuNP)$_2$(ᵗBuN)$_2$S]AsPh} 2bS

When **2b** was treated with excess sulfur at 50 °C in toluene for 48 h, **2bS** was isolated in a yield of 85% (Scheme 30) and as in **2aS** above, only one of the P_2N_2 ring phosphorus (III) was

oxidized by sulfur. Despite the presence of the phenyl ligand on the arsenic atom, it was not oxidized by sulfur, showing that arsenic is difficult to oxidize to the +5 oxidation state.

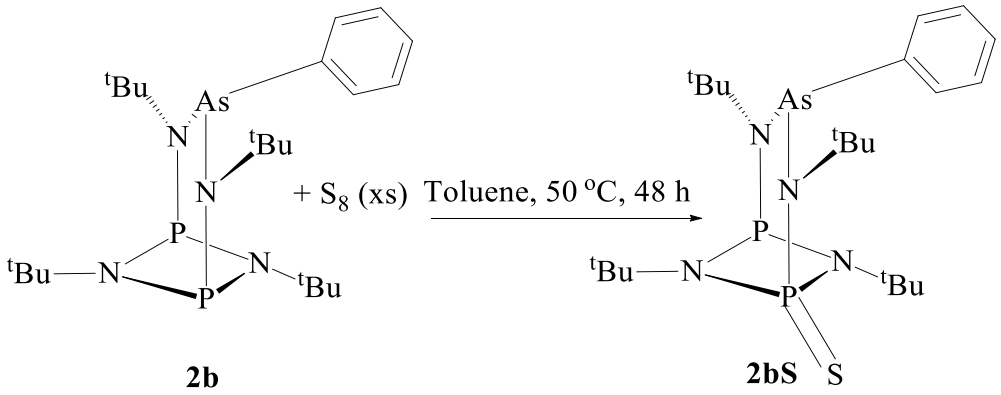

Scheme 30. Synthesis of **2bS**.

The ^{1}H NMR spectrum of **2bS** (Figure 45) shows four singlets at 1.16, 1.59, 1.64 and 1.67 ppm in the ratio 1:1:1:1, corresponding to the four different *tert*-butyl protons. The three different aromatic protons appear at 8.15, 7.18, and 7.11 ppm representing the *ortho*, *meta* and *para* protons, respectively. The ^{13}C{^{1}H} NMR spectrum of **2bS** shows peaks at 151.72, 133.00, and 129.96 ppm, corresponding to the *ipso*, *ortho* and *meta* carbons of the benzene ring, in that order. The quaternary *tert*-butylamino and *tert*-butylimino carbons appear as doublets at 62.75, 57.98, 56.56 and 55.52 ppm, while the corresponding primary carbons appear upfield at 32.93, 32.28, 30.99 and 30.34 ppm as triplets. The primary carbons and the protons appear in a simple ratio of 1:1:1:1 showing that the four *tert*-butyl groups in this compound are all magnetically different. The ^{31}P{^{1}H} NMR spectrum of **2bS** (Figure 46) shows two peaks: a singlet at 114.81 ppm corresponding to P(III) and another singlet at 69.50 ppm for the P(V) in the P_2N_2 ring of the compound. Very unusual is the absence of $J_{AA'}$ coupling between the ^{31}P(V) and ^{31}P(III) systems in the P_2N_2 heterocycle. Chivers *et al*. have reported a $J_{P(III)-P(V)} = 19$ Hz for two mutually coupled doublets for ^{31}P(III) and ^{31}P(V) atoms in the P_2N_2 heterocycle.[87]

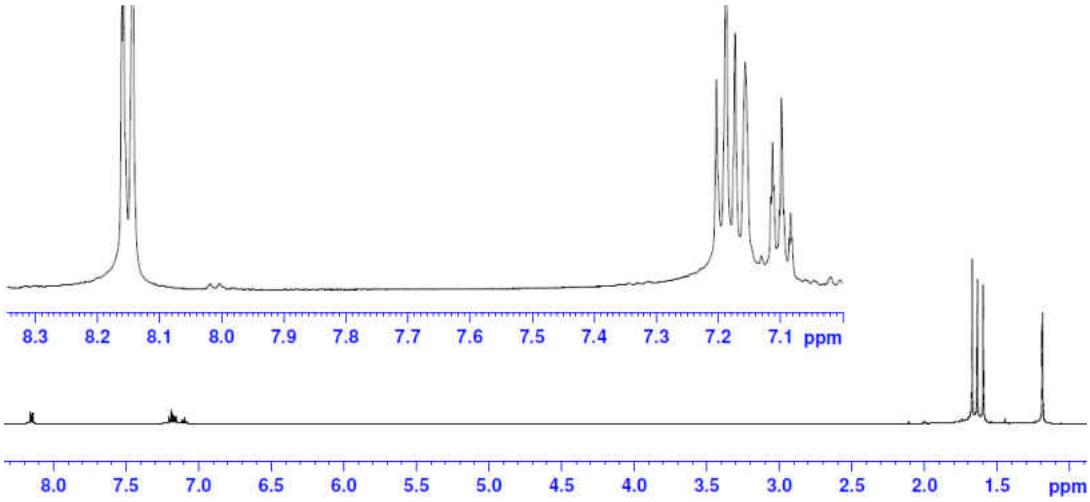

Figure 45. ^{1}H NMR Spectrum for **2bS**.

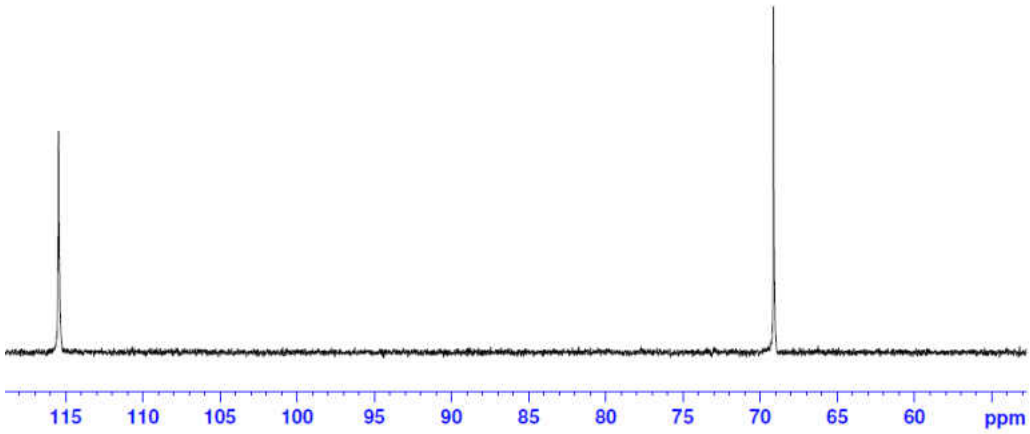

Figure 46. ^{31}P{^{1}H} NMR Spectrum for **2bS**.

Synthesis and Spectroscopic Analysis of {[(^{t}BuNP=S)$_2$(^{t}BuN)$_2$]AsPh} 2bS$_2$

The reaction of **2b** with excess sulfur at 80 °C, in toluene for 48 h furnished **2bS$_2$** in a 95% yield (Scheme 31).

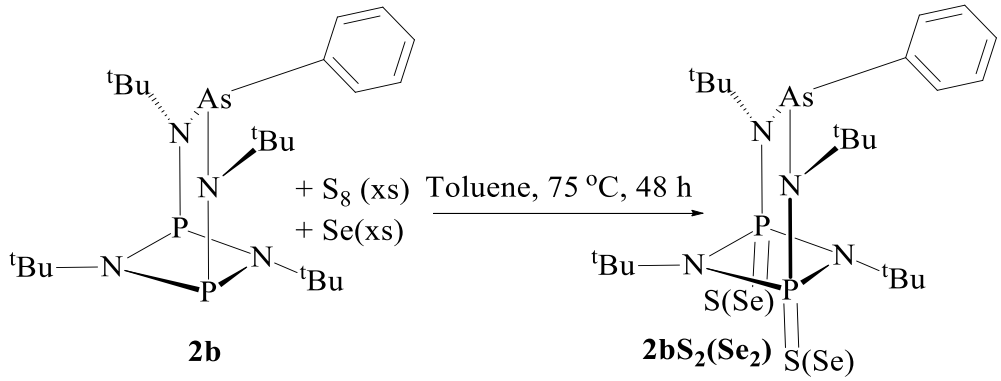

Scheme 31. Synthesis of **2bS$_2$** and **2bSe$_2$**.

The ^{1}H NMR spectrum of **2bS$_2$** shows multiplets at 8.04, 7.13 and 7.08 ppm attributed to the *ortho*, *meta* and *para* protons of the phenyl group and three singlets at 2.01, 1.75 and 1.46 ppm in the ratio 1:1:2 corresponding to the *tert*-butyl protons. The ^{13}C{^{1}H} NMR spectrum of **2bS$_2$** reveals three signals for the phenyl carbons at 152.02, 133.11 and 130.62 ppm assigned to the *ipso*, *ortho* and *meta* carbons, respectively. The signals of the quaternary carbons of the *tert*-butyl groups are shown as singlets at 62.49, 60.72 and 58.45 ppm, while the primary carbons are observed as triplets at 31.08 (J_{PC} = 4.87 Hz) and 30.82 ppm (J_{PC} = 4.87 Hz). Only one singlet is observed at 50.50 ppm in the ^{31}P{^{1}H} NMR spectrum of **2bS$_2$** attributed to the two phosphorus(V) atoms bearing sulfur in the P_2N_2 ring. The IR spectrum of **2bS$_2$** shows a stretching frequency for the P=S bonds at 880.9 cm^{-1}, a decrease of about 49 cm^{-1} from 928 cm^{-1}, the normal P=S stretching frequency.

Solid-state Structure of {[(^{t}BuNP=S)$_2$(^{t}BuN)$_2$]AsPh} 2bS$_2$

Single crystals of **2bS$_2$**, satisfactory for X-ray studies were collected from a cold (–12 °C), concentrated toluene solution after recrystallization. The solid-state structure of **2bS$_2$**, with a partial numbering scheme is shown in Figure 47, while the crystal data and selected bond parameters are listed in Tables 25 and 26 below, respectively. Compound **2bS$_2$** crystallized in the monoclinic space group, $P2_1/n$, with four molecules per unit cell, and it is isomorphous to **2aS**. The P=S bond distance of **2aS$_2$** is 1.9257(6) Å, identical to the same bond in **2aS** (1.9213(9) Å). While there is no change in the As–C bond distance in **2b** and **2bS$_2$**, there is a decrease in the endocyclic bond distances in **2bS$_2$** (1.670(3) and 1.633 (4) Å). The exocyclic bond lengths (1.696(2) Å are almost identical to those in **2b** (1.7070(13) Å). Thus, there is a slight distortion in the molecular cage after the introduction of the sulfur atoms.

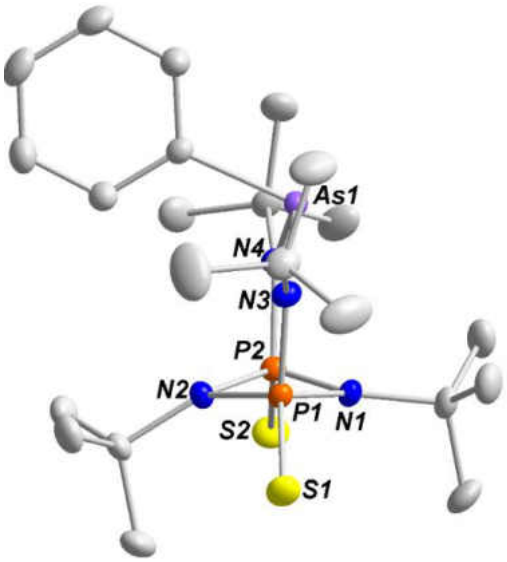

Figure 47. Solid-state structure and partial labelling scheme of **2bS$_2$**. All atoms are drawn at the 50 % probability level.

Table 25. Crystal and structure refinement data for **2bS$_2$**.

Chemical formula	$C_{22}H_{41}AsN_4P_2S_2$
Fw	562.60
T/K	149.98
λ/Å	0.71073
Crystal system	*monoclinic*
Space group	$P2_1/n$
a/Å	9.6812(5)
b/Å	19.0152(8)
c/Å	15.3993(8)
α/°	90
β/°	100.345(2)
γ/°	90
V/Å^3	2788.8(2)
Z	4
ρ (calc.) g cm^{-3}	1.3399
μ/mm^{-1}	1.500
F(000)	1186.3
Reflections collected	57507
Independent reflections	10650[R_{int} = 0.0553, $R_σ$ = 0.0446]
$Rw(F^2)^b$ [I>2σ(I)]	R_1 = 0.0345, wR_2= 0.0806
$R(F)^a$ (all data)	R_1 = 0.0611, wR_2 = 0.0924

[a] $R = \sum||F_o| - |F_c|| \sum |F|_o$. [b] $R_w = \{[\sum w(F_o^2 - F_c^2)] / [\sum w(F_o^2)^2]\}^{1/2}$; $w = 1/[\sigma^2(F_o)^2 + (xP)^2 + yP]$, where $P = (F_o^2 + 2F_c^2)/3$.

Table 26. Selected bond lengths (Å) and angles (°) for **2bS$_2$**.

Bond Lengths (Å)			
As1–C21	1.9721(16)	P1–N2	1.7001(14)
As1–N4	1.9549(14)	S2–P2	1.9257(6)
As1–N3	1.9430(13)	P2–N1	1.6809(14)
P1–S1	1.9278(6)	P2–N2	1.6571(14)
P1–N1	1.6839(13)	P2–N4	1.7070(13)
P1–N3	1.6563(14)	C12–C14	1.535(3)
Bond Angles (°)			
N3–As1–C21	98.80(6)	N2–P1–S1	119.65(5)
N4–As1–C21	97.73(6)	N4–P1–N1	84.84(7)
N4–As1–N3	105.67(5)	N2–P1–N33	105.65(7)
N1–P1–S1	119.09(5)	N1–P2–S2	119.92(5)
N3–P1–S1	118.54(5)	N2–P2–S2	119.35(5)
N3–P1–N1	103.30(7)	N2–P2–N1	102.19(7)
N4–P2–S2	118.39(5)	N4–P2–N2	106.23(7)

Synthesis and Spectroscopic Analysis of {[(^{t}BuNP=Se)$_2$(^{t}BuN)$_2$]AsPh} 2bSe$_2$

The reaction of **2b** with two equivalents of selenium in toluene at 70 °C for 24 h produced compound **2bSe$_2$** in 93% (Scheme 31). Unlike **2bS$_2$** that took 2 days at a higher temperature to go to completion, **2bSe$_2$** was isolated in a high yield with milder reaction conditions, showing again that gray selenium is a better oxidizing agent than elemental sulfur.

The ^{1}H NMR spectrum of **2bSe$_2$** (Figure 48) shows a doublet at 7.95 ppm and two multiplets at 7.10 and 7.06 ppm corresponding to the *ortho*, *meta* and *para* protons of the phenyl ligand, respectively. Like in **2bS$_2$** above, three singlets are observed at 2.07, 1.82 and 1.44 ppm in the ratio 1:1:2 attributable to the *tert*-butyl protons. The *tert*-butylimino protons being diastereotopic, appear as two signals with relative intensities 1:1 at 2.07 and 1.82 ppm. Four singlets are observed in the ^{13}C{^{1}H} NMR spectrum of **2bSe$_2$** at 152.70, 133.11, 130.79 and 126.01 ppm corresponding to the *ipso*, *ortho*, *meta* and *para* carbons of the phenyl ligand. The quaternary carbons of the *tert*-butyl groups in this compound are observed as three singlets at 63.53, 60.63 and 59.24 ppm, while the primary carbons appear at 32.75 (s), 30.94 (t, J_{PC} = 4.92 Hz) and 30.82 ppm (t, J_{PC} = 4.36 Hz). The ^{31}P{^{1}H} NMR spectrum of **2bSe$_2$** (Figure 49) depicts one singlet at 37.52 ppm with two pairs of ^{77}Se satellites as a result of ^{31}P–^{77}Se and ^{31}P–^{31}P coupling (J_{PSe} = 910.89 Hz). The ^{31}P–^{77}Se coupling constant value (J_{PSe} = 910.89 Hz), indicates the presence of a P=Se double bond. The singlet at 37.52 ppm is assigned to the two phosphorus(V) atoms in the P_2N_2 ring. The IR spectrum of **2aSe$_2$** shows a band at 570.9 cm^{-1} which we assign to the P=Se bond stretching.

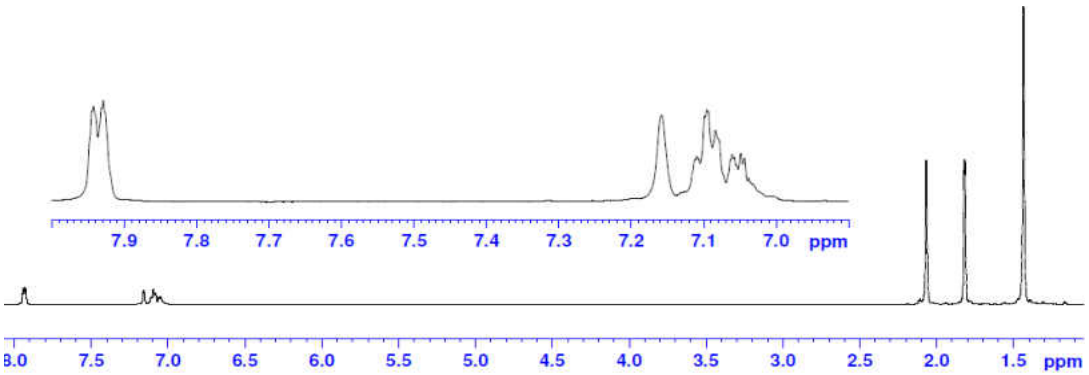

Figure 48. ^{1}H NMR Spectrum for **2bSe$_2$**.

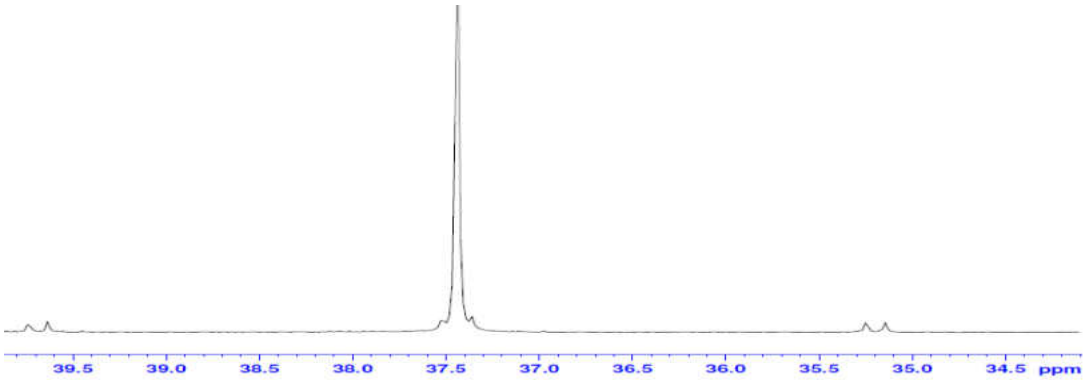

Figure 49. ^{31}P{^{1}H} NMR Spectrum for **2bSe$_2$**.

Solid-state Structure of {[(^{t}BuNP=Se)$_2$(^{t}BuN)$_2$]AsPh} 2bSe$_2$

Colorless, block-shaped crystals of **2bSe$_2$**, suitable for X-ray analysis, were collected from a cold (–12 °C), concentrated toluene solution. The solid-state structure of **2bSe$_2$**, with a partial numbering scheme is shown in Figure 50, while the crystal data and selected bond parameters are listed in Tables 27 and 28 below, respectively. Compound **2bSe$_2$** like **2b** crystallized in the triclinic space group, $P\bar{1}$, with two molecules per unit cell. The P=Se bond distances in **2bSe$_2$**

(2.0859(5) and 2.0789(6) Å) are comparable to those of **2aSe$_2$** (2.0709(5) Å) and **2aSe** (2.0756(5) Å). Similar bond lengths are found in the diselenide derivative, *cis*-[Cy(H)N(Se)P(μ-NCy)]$_2$ (2.093(1) and 2.088(1) Å).[30] While the exocyclic bond distances in **2bSe$_2$** are identical to those in **2b**, the endocyclic bonds (1.6553(16) and 6840(17) Å) are shorter than those in the latter.

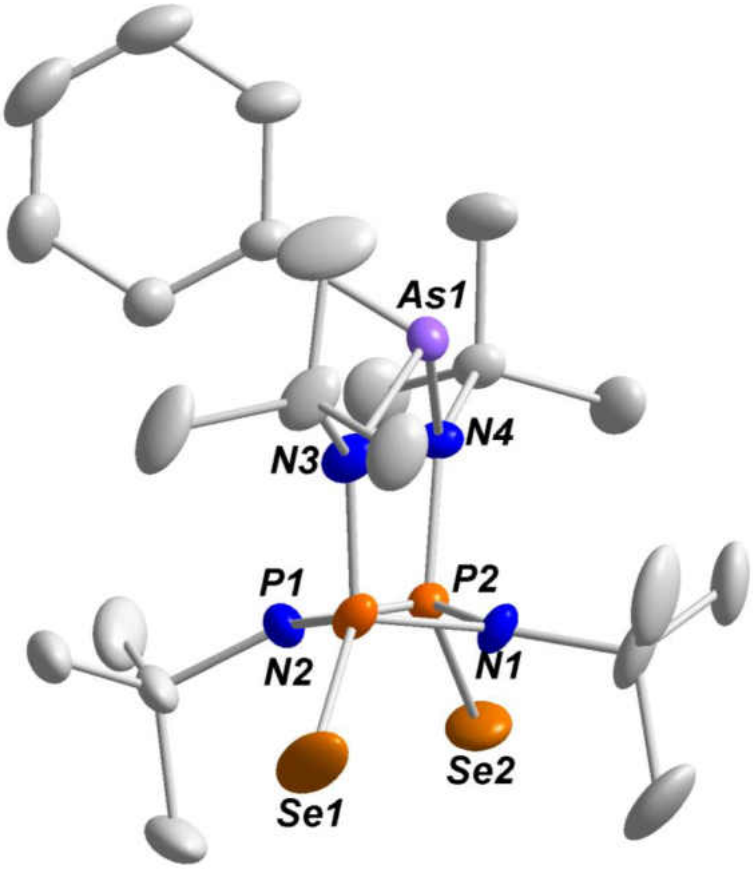

Figure 50. Solid-state structure and partial labelling scheme of **2bSe$_2$**. All atoms are drawn at the 50% probability level.

Table 27. Crystal and structure refinement data for **2bSe$_2$**.

Chemical formula	$C_{25.5}H_{45}AsN_4P_2Se_2$
Fw	702.46
T/K	150.15
λ/Å	0.71073
Crystal system	*triclinic*
Space group	$P\bar{1}$
a/Å	9.8651(8)
b/Å	10.1930(8)
c/Å	15.8869(13)
α/°	97.766(3)
β/°	91.402(3)
γ/°	96.635(3)
V/Å^3	1570.9(2)
Z	2
ρ (calc.) g cm^{-3}	1.4849
μ/mm^{-1}	3.521
F(000)	714.4
Reflections collected	38533
Independent reflections	10474 [R_{int} = 0.0381, R_σ = 0.0398]
$Rw(F^2)^b$ [I>2σ(I)]	R_1 = 0.0350, wR_2 = 0.0815
$R(F)^a$ (all data)	R_1 = 0.0568, wR_2 = 0.0902

[a] $R = \sum|F_o - F_c| \sum |F|_o$. [b] $R_w = \{[\sum w(F_o^2 - F_c^2)] / [\sum w(F_o^2)^2]\}^{1/2}$; $w = 1/[\sigma^2(F_o)^2 + (xP)^2 + yP]$, where $P = (F_o^2 + 2F_c^2)/3$.

Table 28. Selected bond lengths (Å) and angles (°) for **2bSe$_2$**.

Bond Lengths (Å)			
Se1–P1	2.0859(5)	P1–N1	1.6553(16)
Se2–P2	2.0789(6)	P1–N2	1.6803(18)
As1–N4	1.9518(15)	P1–N3	1.6961(17)
As1–N3	1.9461(17)	P2–N2	1.6840(17)
As1–C1	1.963(2)	P2–N4	1.6574(19)
Bond Angles (°)			
N3–As1–N4	105.68(7)	N4–P2–Se2	119.66(6)
C1–As1–N4	98.19(8)	N4–P2–N2	84.50(9)
C1–As1–N3	96.62(8)	N2–P2–Se2	118.24(6)
N1–P1–Se1	119.29(6)	N3–P1–Se1	120.94(7)
N2–P1–Se1	118.59(6)	N3–P1–N2	102.84(9)
N2–P1–N1	103.77(8)	N4–P2–Se2	118.92(6)
N4–P2–N1	104.96(8)	N4–P2–N2	84.31(9)

Synthesis and Spectroscopic Analysis of {[(^{t}BuNP=Se)$_2$(^{t}BuN)$_2$]AsN$_3$} 2cSe$_2$

Compound **2cSe$_2$** was isolated in 88% yield by treating **2c** with two equivalents of selenium in toluene at 70 °C for 24 h (Scheme 32). After the reaction was complete, the solution was

cooled to RT, and then unreacted selenium was filtered using a frit to obtain a clear solution, from which crystals were obtained.

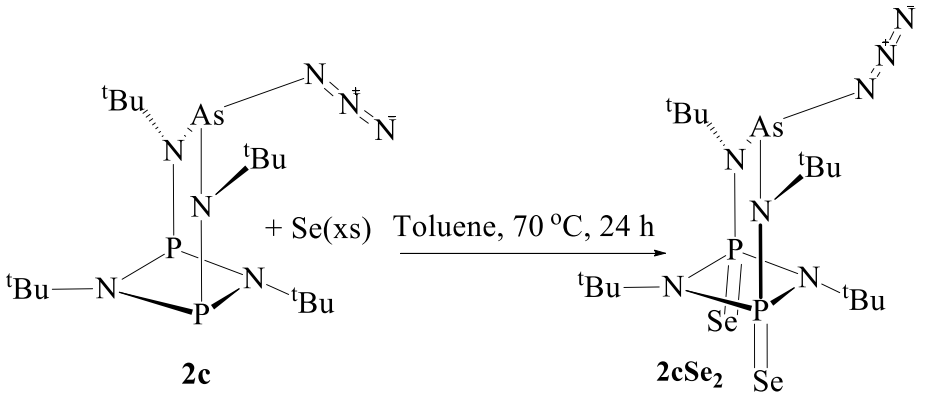

Scheme 32. Synthesis of **2cSe2**.

The ^{1}H NMR spectrum of **2cSe2** depicts three singlets in the ratio 1:2:1 at 1.89, 1.61 and 1.51 ppm representing the *tert*-butyl protons. Because the azide ligand above the P_2N_2 ring is bent towards one of the imino nitrogen atoms, the protons of the *tert*-butyl group on this nitrogen are chemically and magnetically different from those of the other imino *tert*-butyl group. As such, two different signals of equal intensities are generated at 1.89 and 1.51 ppm. The ^{13}C{^{1}H} NMR spectrum of **2cSe2** shows six signals at 63.80, 60.80, 59.12, 32.87, 31.01 (t) and 30.53 ppm (t) representing the *tert*-butyl carbons. The quaternary and primary carbons of the *tert*-butylamino groups are observed as singlets at 63.80 and 32.87 ppm, respectively. Meanwhile, the quaternary carbons of the *tert*-butylimino groups appear as singlets at 60.80 and 59.12 ppm, while the primary carbons appear as triplets at 31.01 and 30.53 ppm, with respective, ^{31}P–^{13}C coupling constants of 4.84 and 4.28 Hz. The ^{31}P{^{1}H} NMR spectrum of **2cSe2** (Figure 51) shows a singlet at 43.31 ppm attributable to the phosphorus(V) atoms on the P_2N_2 ring and a pair of ^{77}Se satellite peaks due to ^{31}P–^{77}Se coupling (J_{PSe} = 930.49 Hz). The coupling constant falls within the range 750–1000 Hz, indicating the presence of a P=Se bond. The IR spectrum of **2cSe2** depicts a band at 580.2 cm^{-1} attributable to the P=Se stretching mode of the compound.

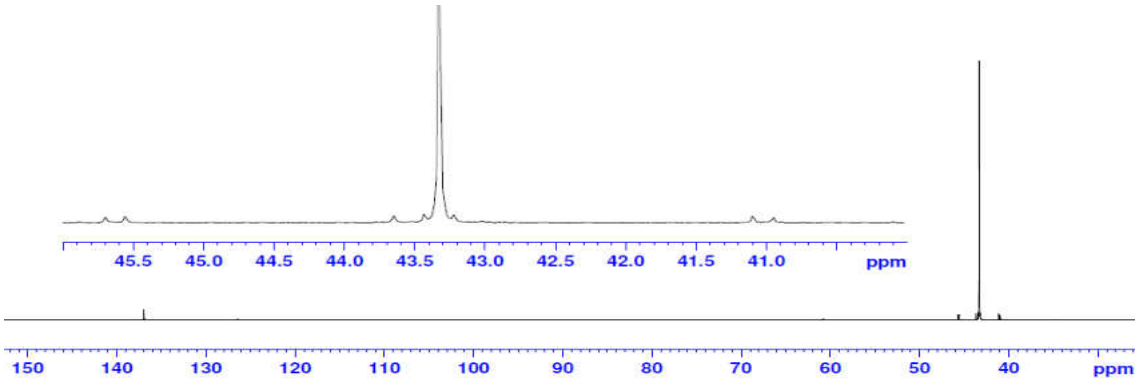

Figure 51. $^{31}P\{^{1}H\}$ NMR Spectrum for **2cSe$_2$**.

Solid-state Structure of {[(^{t}BuNP=Se)$_2$(^{t}BuN)$_2$]AsN$_3$} 2cSe$_2$

Colorless crystals of **2cSe$_2$**, suitable for X-ray analysis, were isolated from a cold (–12 °C) concentrated toluene solution after recrystallization. The solid-state structure of **2cSe$_2$**, with a partial numbering scheme is shown in Figure 52, while the crystal data and selected bond parameters are listed in Tables 29 and 30 below, respectively. Compound **2cSe$_2$** like **2c** crystallized in the monoclinic space group, $P2_1/n$, with four molecules per unit cell. While the azide ligand in **2c** points downwards, that of **2cSe$_2$** is flipped and points upward as in **1c** and **3c** with N2–N1–As bond angle of 116.17(16)°. The P=Se bond distances of **2cSe$_2$** are 2.0762(5) and 2.0768(5) Å, comparable to those of **2aSe**, **2aSe$_2$** and **2bSe$_2$**. The mean ring P–N and exocyclic P–N distances are 1.6972(15) and 1.6899(15) Å, respectively, indicating a contraction in the bicycle compared to **2c** as selenium atoms are introduced. However, the As–N$_{azide}$ bond distances in **2c** (1.9668(17) Å) and **2cSe$_2$** (1.9578(18) Å) are almost identical.

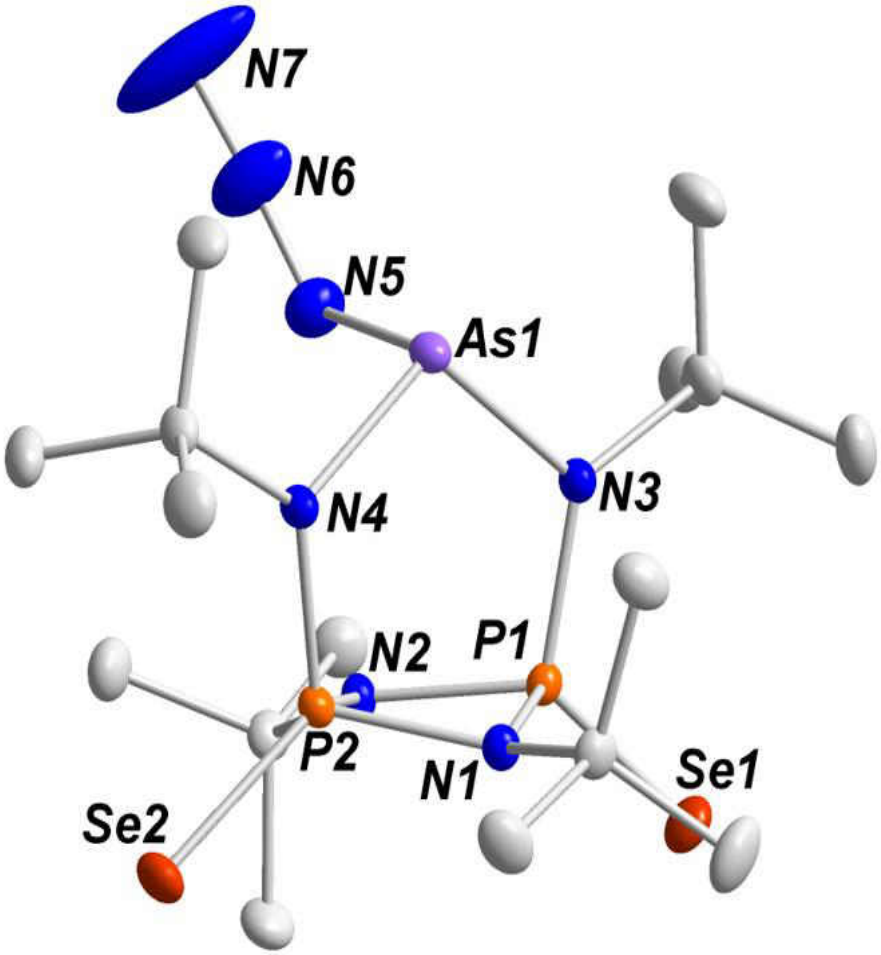

Figure 52. Solid-state structure and partial labelling scheme of **2cSe2**. All atoms are drawn at the 50% probability level.

Table 29. Crystal data and structure refinement for **2cSe$_2$**.

Chemical formula	$C_{16}H_{36}AsN_7P_2Se_2$
Fw	621.30
T/K	149.99
λ/Å	0.71073
Crystal system	monoclinic
Space group	$P2_1/n$
a/Å	9.4999(7)
b/Å	15.4372(10)
c/Å	17.4134(10)
α/°	90
β/°	98.480(3)
γ/°	90
V/Å^3	2525.8(3)
Z	4
ρ (calc.) g cm^{-3}	1.6338
μ/mm^{-1}	4.371
F(000)	1248.8
Reflections collected	43070
Independent reflections	9624 [R_{int} = 0.0343, R_σ = 0.0344]
$Rw(F^2)^b$ [I>2σ(I)]	R_1 = 0.0309, wR_2 = 0.0733
$R(F)^a$ (all data)	R_1 = 0.0493, wR_2 = 0.0801

[a] $R = \sum|F_o - F_c| \sum |F|_o$. [b] $R_w = \{[\sum w(F_o^2 - F_c^2)] / [\sum w(F_o^2)^2]\}^{1/2}$; $w = 1/[\sigma^2(F_o)^2 + (xP)^2 + yP]$, where $P = (F_o^2 + 2F_c^2)/3$.

Table 30. Selected bond lengths (Å) and angles (°) for **2cSe$_2$**.

Bond Lengths (Å)			
Se1–P1	2.0762(5)	P2–N1	1.6972(15)
As1–N1	1.9578(18)	P2–N4	1.6806(15)
As1–N4	1.8823(14)	P2–N2	1.6899(15)
As1–N5	1.8879(14)	N3–P1	1.6766(15)
N1–N2	1.187(3)	P1–N1	1.6976(15)
Se2–P2	2.0768(5)	P1–N2	1.6852(14)
N2–N3	1.135(3)	N3–C12	1.498(2)
Bond Angles (°)			
N4–As1–N1	95.30(7)	N2–P1–N1	84.45(7)
N3–As1–N1	98.39(7)	P1–N1–P2	93.30(7)
N3–As1–N4	105.52(6)	P2–N4–As1	117.56(8)
N6–N5–As1	116.17(16)	N1–P2–Se2	119.41(5)
N2–P1–N1	84.32(7)	N2–P2–Se2	119.66(5)
N5–N6–N7	175.0(3)	N4–P2–Se2	119.36(5)
N2–P2–N4	104.70(7)	N4–P1–Se1	118.60(5)
N1–P1–Se1	119.90(5)	N3–P1–Se1	119.23(5)

Synthesis and Spectroscopic Analysis of {[(^{t}BuNP=S)$_2$(^{t}BuN)$_2$]SbCl} 3aS$_2$

Treatment of **3a** with excess sulfur in toluene for 48 h at 80 °C gave compound **3aS$_2$** with a yield of 86% (Scheme 33). Unreacted sulfur was removed using a frit and the resulting filtrate was concentrated to afford colorless crystals.

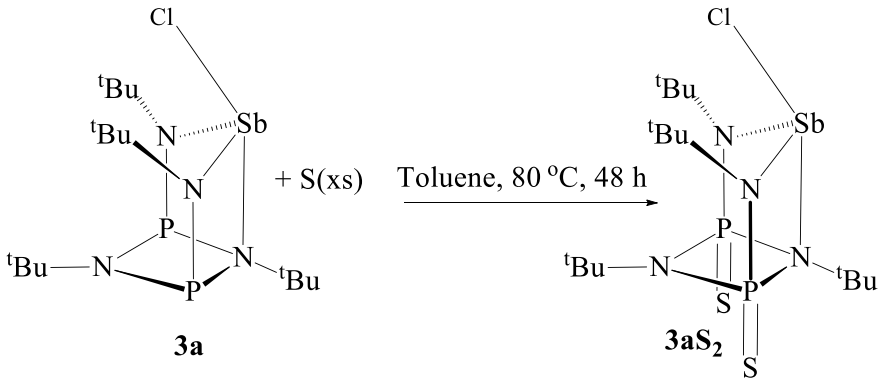

Scheme 33. Synthesis of **3aS$_2$**.

The ^{1}H NMR spectrum of compound **3aS$_2$** reveals three singlets in the ratio 1:2:1 corresponding to the *tert*-butyl protons at 1.84, 1.52 and 1.21 ppm. Like in **2cSe$_2$**, the chemically and magnetically non-equivalent nature of the two imino *tert*-butyl groups generates two singlets at 1.84 and 1.21 ppm. The ^{13}C{^{1}H} NMR spectrum of **3aS$_2$** (Figure 53) reveals six signals resonating between 62.58 and 30.54 ppm which we assign to the quaternary and primary carbons of the *tert*-butyl groups. The quaternary amino carbons are exhibited as a singlet at 62.58 ppm, while those of the imino groups are observed as two singlets at 59.37 and 59.12 ppm. While the primary *tert*-butylamino carbons are observed as a doublet (J_{PC} = 3.33 Hz) at 32.94 ppm, those of the *tert*-butylimino carbons exhibit two triplets at 30.68 and 30.54 ppm with ^{31}P–^{13}C coupling constants of 4.57 and 4.77 Hz, respectively. The coupling constant, J_{PC} = 3.33 Hz, is as a result of the small coupling between the amino *tert*-butyl carbons and one of the P(V) atoms of the P_2N_2 ring. The ^{31}P{^{1}H} NMR spectrum of **3aS$_2$** (Figure 54) shows one singlet at 47.53 ppm

corresponding to the two phosphorus (V) atoms in the P_2N_2 ring. The IR spectrum of **3aS$_2$** depicts a strong band at 931.1 cm^{-1} representing a stretching vibrationa for the P=S bond.

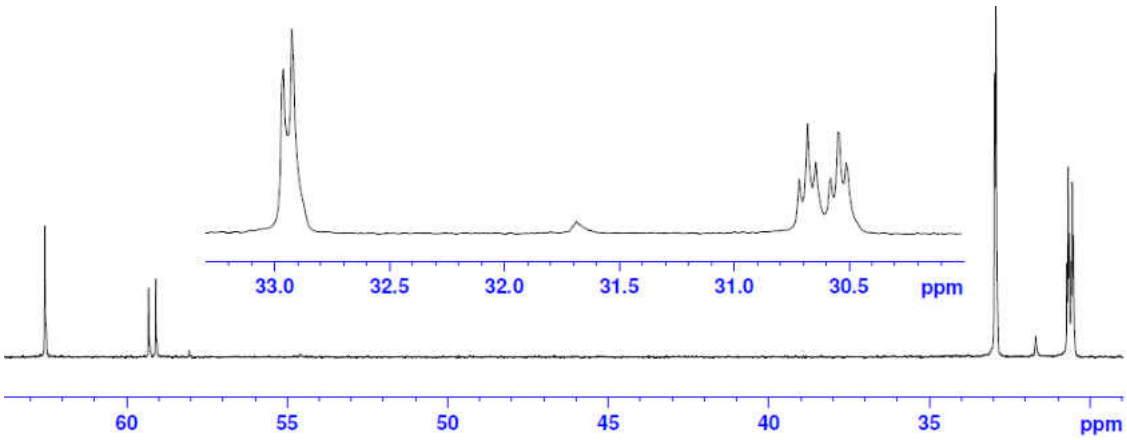

Figure 53. $^{13}C\{^1H\}$ NMR Spectrum for **3aS$_2$**.

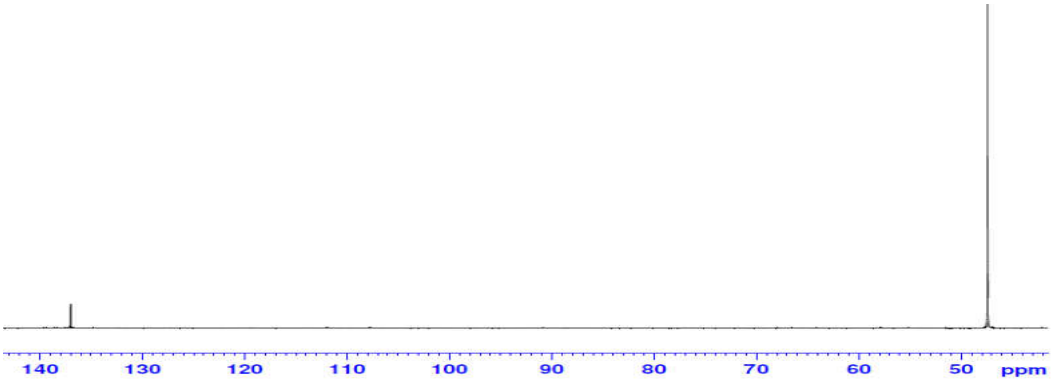

Figure 54. $^{31}P\{^1H\}$ NMR Spectrum for **3aS$_2$**.

Solid-state Structure of {[(^{t}BuNP=S)$_2$(^{t}BuN)$_2$]SbCl} 3aS$_2$

Block-shaped, colorless crystals of **3aS$_2$** were obtained from a cold (–6 °C), concentrated toluene solution after recrystallization. The solid-state structure of **3aS$_2$**, with a partial numbering scheme is shown in Figure 55, while the crystal data and selected bond parameters are listed in Tables 31 and 32 below, respectively. Compound **3aS$_2$** crystallized in the monoclinic space group, $P2_1/n$, with four molecules per unit cell. Contrary to **3a** where the antimony atom makes

bonding contacts with N1 in a κ^3*N* chelation mode, this bonding contact is absent in **3aS₂**. The antimony atom bearing the chloride ligand is chelated above the P_2N_2 ring in a κ^2*N* binding mode. An explanation for this observation is the fact that the electron density from the P_2N_2 ring is reduced by the two sulfur atoms and the inductive effect of the chlorine atom on antimony, therefore, reducing the possibility of bonding between N1 and the Sb atom. The newly formed P=S bonds are 1.9265(7) Å long, consistent with typical bond lengths in similar compounds. For example, Stahl *et al*. found that the bond distances for P=S in *cis*-[Ph(H)N(S=PN^{t}Bu)$_2$N(H)Ph] were 1.9216(11) and 1.9264(9) Å.[64] While the exocyclic bond distances in **3a** and **3aS₂** remain the same, there is a significant reduction in the endocyclic bond lengths of **3aS₂** after the sulfur atoms are introduced.[92] The Sb–Cl bond in **3aS₂** is reduced to 2.3921(7) Å compared to 2.492(3) Å in **3a**.

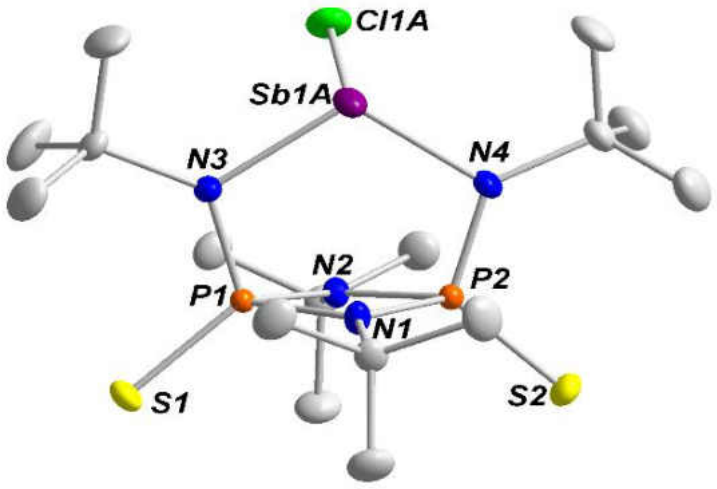

Figure 55. Solid-state structure and partial labelling scheme of **3aS₂**. All atoms are drawn at the 50% probability level. Hydrogen atoms are omitted for clarity.

Table 31. Crystal and structure refinement data for **3aS$_2$**.

Chemical formula	$C_{16}H_{36}ClN_4P_2S_2Sb$
Fw	567.78
T/K	149.98
λ/Å	0.71073
Crystal system	*monoclinic*
Space group	$P2_1/n$
a/Å	13.1879(8)
b/Å	12.3998(7)
c/Å	15.3864(9)
α/°	90
β/°	105.414(2)
γ/°	90
V/Å^3	2425.6(3)
Z	4
ρ (calc.) g cm^{-3}	1.5547
μ/mm^{-1}	1.561
F(000)	1160.2
Reflections collected	56276
Independent reflections	8106 [R_{int} = 0.0296, R_σ = 0.0185]
$Rw(F^2)^b$ [I>2σ(I)]	R_1 = 0.0299, wR_2 = 0.0682
$R(F)^a$ (all data)	R_1 = 0.0377, wR_2 = 0.0742

[a] $R = \sum|F_o - F_c| \sum |F|_o$. [b] $R_w = \{[\sum w(F_o^2 - F_c^2)] / [\sum w(F_o^2)^2]\}^{1/2}$; $w = 1/[\sigma^2(F_o)^2 + (xP)^2 + yP]$, where $P = (F_o^2 + 2F_c^2)/3$.

Table 32. Selected bond lengths (Å) and angles (°) for **3aS$_2$**.

Bond Lengths (Å)			
Sb–Cl1	2.3921(7)	P1–S1	1.9265(6)
Sb–N3	2.0949(17)	P1–N1	1.6920(16)
Sb–N4	2.1007(16)	P2–N4	1.6590(17)
Sb–Cl1	2.355(18)	P1–N3	1.6541(17)
Sb–N4	2.062(4)	P2–N2	1.6904(16)
P2–N2	1.6923(16)	P2–N1	1.6948(16)
P2–S2	1.9265(7)		
Bond Angles (°)			
N4–Sb1–N3	106.86(6)	N2–P1–S1	121.42(6)
N4–Sb–N3	106.73(18)	N2–P1–N1	83.83(8)
N1–P1–S1	118.97(6)	N2–P1–N4	101.29(8)
N2–P1–S1	118.46(6)	N1–P2–S2	118.46(6)
N4–P1–N1	106.79(8)	N3–P2–S2	119.13(6)
N3–P2–N1	106.80(8)	N2–P2–S2	121.17(6)
N2–P2–N1	83.80(8)	N2–P2–N3	101.21(8)

Synthesis and Spectroscopic Analysis of {[(^{t}BuNP=S)$_2$(^{t}BuN)$_2$]SbN$_3$} 3cS$_2$

The treatment of **3c** with excess sulfur in toluene at 75 °C for 48 h yielded compound **3cS$_2$** (Scheme 34). When the reaction was completed, it was cooled to RT and unreacted sulfur was removed using a frit. The concentrated filtrate gave compound **3cS$_2$** in 73% yield.

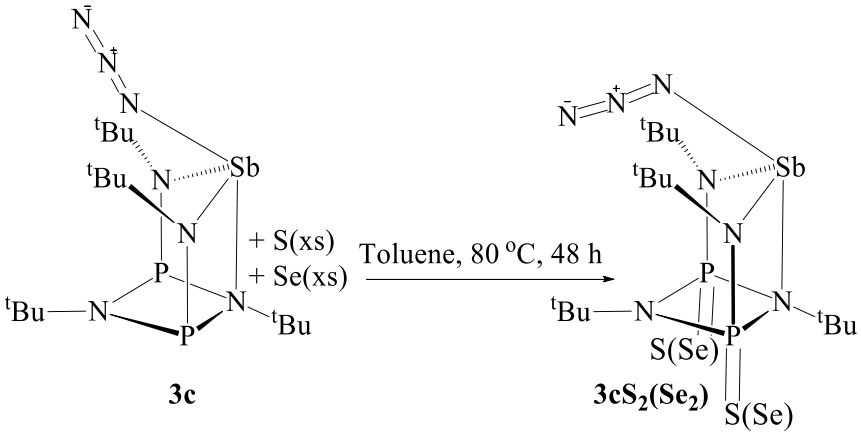

3c **3cS$_2$(Se$_2$)**

Scheme 34. Synthesis of **3cS$_2$** and **3cSe$_2$**.

In the ^{1}H NMR spectrum of **3cS$_2$** are observed three singlets at 1.80, 1.52 and 1.51 ppm in the ratio 1:2:1, representing the protons of the *tert*-butyl groups. The imino *tert*-butyl protons being diastereotopic, exhibit two singlets of equal intensities at 1.80 and 1.51 ppm. The ^{13}C{^{1}H} NMR spectrum of **3cS$_2$** shows six signals between 61.03 and 29.40 ppm representing the *tert*-butyl carbons in the compound. The quaternary and primary carbons of the amino *tert*-butyl groups are exhibited as a singlet and a doublet (J_{PC} = 6.38 Hz) at 61.03 and 33.08 ppm, respectively. The coupling constant, J_{PC} = 6.38 Hz, is about twice the value in **3aS$_2$**. This may be attributed to the greater repulsion between the azide ligand and the amino nitrogen of the *tert*-butyl group compared to that of the chloride ligand. Meanwhile, the quaternary carbons of the imino *tert*-butyl carbons exhibit two singlets at 60.84 and 59.06 ppm, while the primary carbons are observed as triplets at 30.99 and 29.40 ppm with ^{31}P–^{13}C coupling constants of 4.52 and 4.79 Hz, respectively. The ^{13}P{^{1}H} NMR spectrum of **3cS$_2$** shows a singlet at 45.72 ppm

corresponding to the two P(V) atoms on the P_2N_2 ring. The IR spectrum of **3cS₂** shows a strong absorption band at 931.1 cm^{-1} attributed to the stretching vibration of the P=S bond.

Solid-state Structure of {[(^{t}BuNP=S)$_2$(^{t}BuN)$_2$]SbN$_3$} 3cS$_2$

Colorless, cubic crystals of **3cS₂**, excellent for X-ray analysis were obtained from a cold (–12 °C) concentrated toluene solution. The solid-state structure of **3cS₂**, with a partial numbering scheme is shown in Figure 56, while the crystal data and selected bond parameters are listed in Tables 33 and 34 below, respectively. Compound **3cS₂** crystallized in the orthorhombic space group, $P2_12_12_1$, with four molecules per unit cell. The newly formed P=S bonds in **3cS₂** are 1.9208(5) and 1.9269(5) Å, in agreement with those of similar compounds, like [(^{t}BuNP=S)$_2$(^{t}BuN)$_2$]Zr(O^{t}Bu)$_2$,[93] 1.9284(7) Å and [Me$_2$Si(μ-N^{t}Bu)$_2$P=S(NHPh)], 1.938(2) Å.[85] There is a decrease in the Sb–N_{azide} bond distance from 2.492(3) Å in **3c** to 2.1235(14) Å in **3cS₂**. While the endocyclic P–N bonds (1.6878(13) and 1.6398(12) Å) in **3cS₂** are decreased, the exocyclic P–N bonds (1.7160(12) Å) are increased compared to those in **3c** (endo = 1.772(4) and 1.719(4) Å, exo = 1.680(5) Å).[92]As in **3c**, the Sb–N1–N2 and N1–N2–N3 bond angles are maintained at 117.3 and 176.4°, respectively.

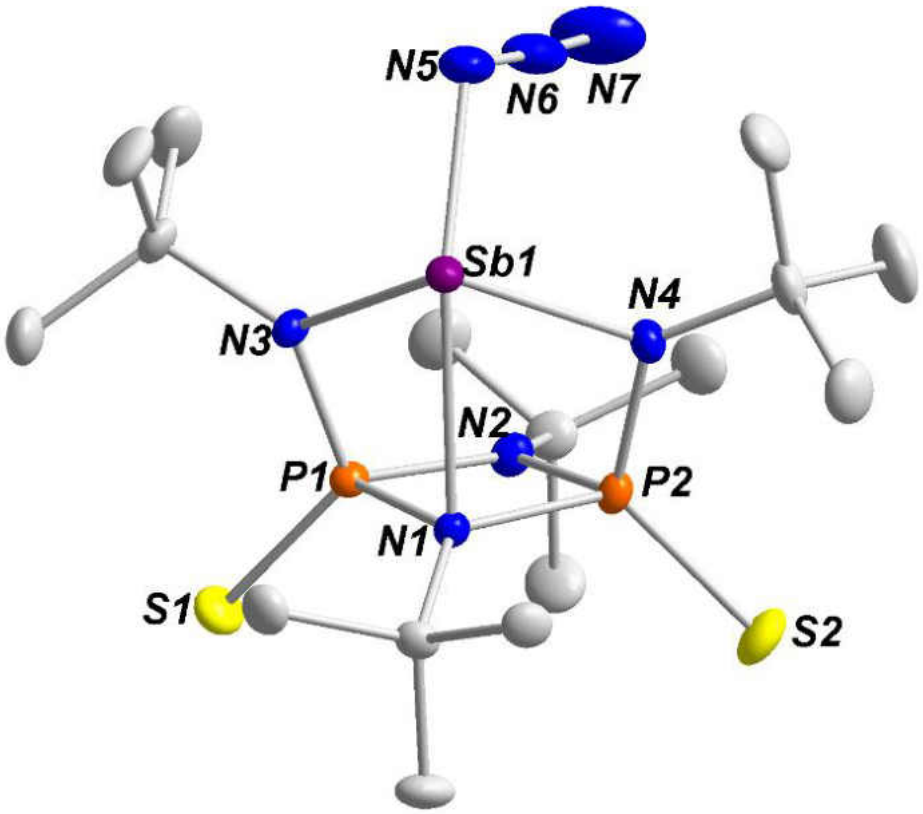

Figure 56. Solid-state structure and partial labelling scheme of **3cS$_2$**. All atoms are drawn at the 50% probability level. Hydrogen atoms are omitted for clarity.

Table 33. Crystal and structure refinement data for **3cS$_2$**.

Chemical formula	$C_{16}H_{36}N_7P_2S_2Sb$
Fw	574.35
T/K	150.01
λ/Å	0.71073
Crystal system	*orthorhombic*
Space group	$P2_12_12_1$
a/Å	9.9533(5)
b/Å	14.3290(7)
c/Å	17.5011(9)
α/°	90
β/°	90
γ/°	90
V/Å^3	2496.0(2)
Z	4
ρ (calc.) g cm^{-3}	1.5283
μ/mm^{-1}	1.418
F(000)	1175.6
Reflections collected	58740
Independent reflections	8354 [R_{int} = 0.0300, $R_σ$ = 0.0203]
$Rw(F^2)^b$ [I>2σ(I)]	R_1 = 0.0168, wR_2 = 0.0464
$R(F)^a$ (all data)	R_1 = 0.0177, wR_2 = 0.0468

[a] $R = \sum|F_o - F_c| \sum |F|_o$. [b] $R_w = \{[\sum w(F_o^2 - F_c^2)] / [\sum w(F_o^2)^2]\}^{1/2}$; $w = 1/[\sigma^2(F_o)^2 + (xP)^2 + yP]$, where $P = (F_o^2 + 2F_c^2)/3$.

Table 34. Selected bond lengths (Å) and angles (°) for **3cS$_2$**.

Bond Lengths (Å)			
Sb1–N5	2.1260(12)	N1–P2	1.6993(13)
Sb1–N3	2.1219(12)	P1–N3	1.6481(13)
Sb1–N4	2.4970(11)	P2–N4	1.7328(12)
Sb1–N1	2.1235(14)	P2–S2	1.9208(5)
N1–P1	1.6878(13)	N2–P1	1.6398(12)
P2–N4	1.7314(12)	P1–S1	1.9269(5)
N1–N2	1.213(2)		
Bond Angles (°)			
N3–Sb1–N2	106.75(5)	S2–P2–N1	118.05(5)
N4–Sb1–N2	64.88(4)	S2–P2–N3	120.74(5)
N4–Sb1–N3	65.82(4)	S2–P2–N4	121.85(5)
N1–Sb1–N2	90.58(5)	S1–P1–N1	116.73(5)
N1–Sb1–N3	92.83(6)	S1–P1–N2	120.86(5)
N1–Sb1–N4	138.47(5)	S1–P1–N4	122.22(4)
P3–N1–P2	97.65(6)	N6–N5–Sb1	117.32(12)
N3–P2–N1	108.33(6)	N5–N6–N7	176.38(19)

Synthesis and Spectroscopic Analysis of {[(^{t}BuNP=Se)$_2$(^{t}BuN)$_2$]SbN$_3$} 3cSe$_2$

When **3c** was treated with two equivalents of selenium at 70 °C for 24 h in toluene **3cSe$_2$** was isolated in 81% yield (Scheme 34). It took longer for **3cS$_2$** to be synthesized than **3cSe$_2$**, illustrating the fact that selenium (Se_n) is more easily converted to atoms during a reaction than molecular sulfur (S_8).

The ^{1}H NMR spectrum of **3cSe$_2$** reveals three singlets at 1.85, 1.57 and 1.53 ppm in the ratio 1:1:2 for the protons of the *tert*-butyl groups. The imino *tert*-butyl protons are chemically and magnetically non-equivalent, and as such they exhibit two singlets at 1.85 and 1.57 ppm. Meanwhile, the ^{13}C{^{1}H} NMR spectrum of **3cSe$_2$** depicts three singlets at 61.71, 61.65 and 59.78 ppm being the quaternary carbons of the *tert*-butyl groups. Three multiplets are also shown at 32.91, 31.05 and 29.22 ppm, attributed to the primary carbons of the *tert*-butyl groups. The ^{31}P{^{1}H} NMR spectrum of **3cSe$_2$** (Figure 57) shows a singlet at 32.77 ppm, which we assign to the two P(V) atoms of the P_2N_2 ring. There are also two pairs of ^{77}Se satellite peaks with a ^{31}P–^{77}Se coupling constant of 922.84 Hz. The coupling constant confirms the presence of a P=Se bond. The IR spectrum of **3cSe$_2$** shows a strong absorption at 563.3 cm^{-1} attributable to the stretching mode of the P=Se double bonds.

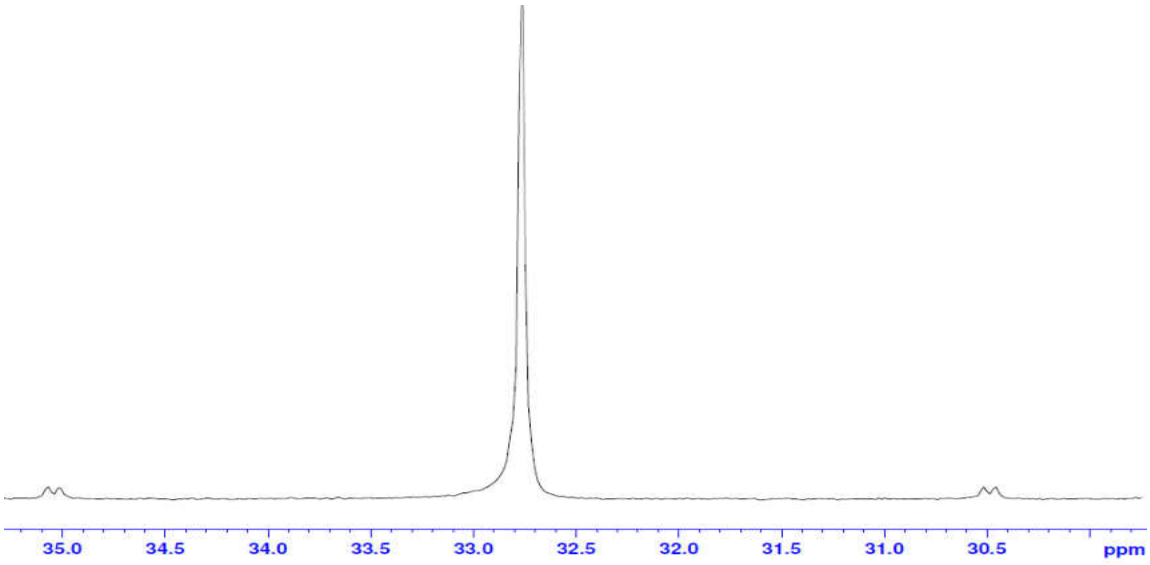

Figure 57. $^{31}P\{^{1}H\}$ NMR Spectrum for **3cSe$_2$**.

Solid-state Structure of {[(^{t}BuNP=Se)$_2$(^{t}BuN)$_2$]SbN$_3$} 3cSe$_2$

Colorless crystals of **3cSe$_2$** were collected from a cold (–12 °C) concentrated toluene solution after recrystallization. The solid-state structure of **3cSe$_2$**, with a partial numbering scheme is shown in Figure 58, while the crystal data and selected bond parameters are listed in Tables 35 and 36 below, respectively. Compound **3cSe$_2$** crystallized in the orthorhombic space group, $P2_12_12_1$, with four molecules in the unit cell. The P=Se bond lengths in **3cSe$_2$** range from 2.0758(6) to 2.0813(6) Å. They are thus similar to the P=Se bond distances in [(Se=)P(μ-N^{t}Bu)$_2$P(μ-Se)]$_6$ (2.063(8)–2.081(2) Å) reported by Wright *et al.*[97] Compounds **3cSe$_2$** and **3cS$_2$** have identical bond parameters, and therefore a detailed description of **3cSe$_2$** will not be given.

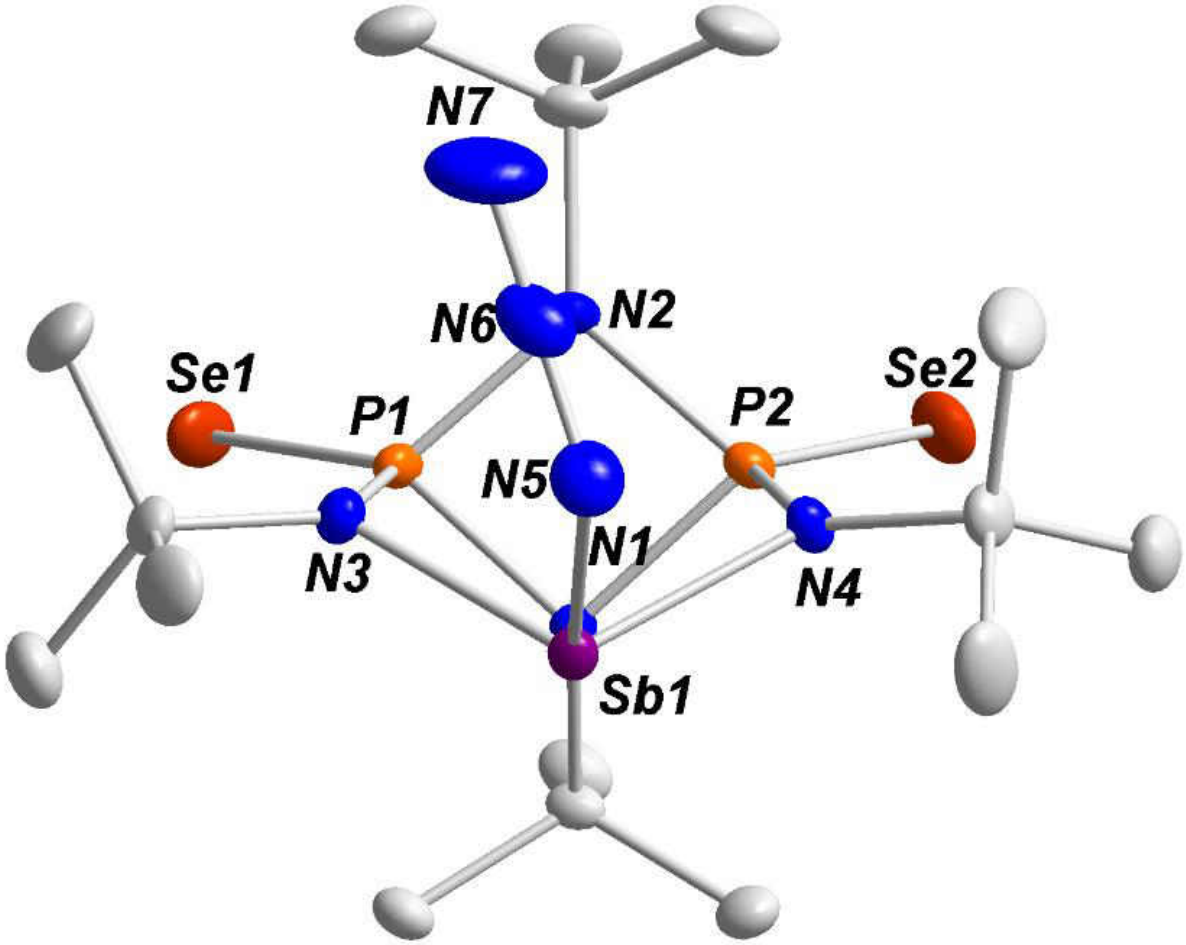

Figure 58. Solid-state structure and partial labelling scheme of **3cSe$_2$**. All atoms are drawn at the 50% probability level.

Table 35. Crystal and structure refinement data for **3cSe$_2$**.

Chemical formula	$C_{16}H_{36}N_7P_2Se_2Sb$
Fw	668.14
T/K	149.99
λ/Å	0.71073
Crystal system	*orthorhombic*
Space group	$P2_12_12_1$
a/Å	10.0095(4)
b/Å	14.4687(6)
c/Å	17.5756(7)
α/°	90
β/°	90
γ/°	90
V/Å^3	2545.38(18)
Z	4
ρ (calc.) g cm^{-3}	1.7434
μ/mm^{-1}	4.086
F(000)	1318.1
Reflections collected	59308
Independent reflections	7782 [R_{int} = 0.0321, R_σ = 0.0261]
$Rw(F^2)^b$ [I>2σ(I)]	R_1 = 0.0185, wR_2 = 0.0400
$R(F)^a$ (all data)	R_1 = 0.0210, wR_2 = 0.0405

[a] $R = \sum|F_o - F_c| \sum |F|_o$. [b] $R_w = \{[\sum w(F_o^2 - F_c^2)] / [\sum w(F_o^2)^2]\}^{1/2}$; $w = 1/[\sigma^2(F_o)^2 + (xP)^2 + yP]$, where $P = (F_o^2 + 2F_c^2)/3$.

Table 36. Selected bond lengths (Å) and angles (°) for **3cSe$_2$**.

Bond Lengths (Å)			
Sb1–N1	2.1251(18)	P1–N2	1.7362(17)
Sb1–N2	2.5111(17)	P1–N3	1.6907(18)
Sb1–N4	2.1367(17)	Se2–P2	2.0813(6)
Sb1–N5	2.121(2)	N2–P2	1.7403(17)
P1–Se1	2.0758(6)	P2–N3	1.6997(19)
P2–N4	1.6399(18)	N6–N7	1.146(3)
N5–N6	1.218(3)	N1–P1	1.6476(19)
Bond Angles (°)			
N2–Sb1–N1	65.58(6)	Se1–P1–N1	121.44(7)
N4–Sb1–N1	106.79(7)	N2–P1–Se1	121.50(60
N4–Sb1–N2	64.75(6)	N3–P1–Se1	117.48(6)
N5–Sb1–N1	93.27(8)	N2–P2–Se2	121.90(6)
N3–P2–N2	83.32(8)	N3–P2–Se2	116.34(6)
N5–Sb1–N4	90.56(8)	N4–P2–Se2	121.22(7)
Sb1–N5–N6	118.22(16)	N7–N6–N5	176.0(3)

Synthesis and Spectroscopic Analysis of {[(^{t}BuNP=S)$_2$(^{t}BuN)$_2$]SbPh} 3bS$_2$

Compound **3bS$_2$** was isolated in 88% yield when **3b** was treated with excess sulfur at 80 °C in toluene for 36 h (Scheme 35). Unreacted sulfur was removed with a frit and the filtrate was concentrated to obtain colorless crystals of **3bS$_2$** after several days.

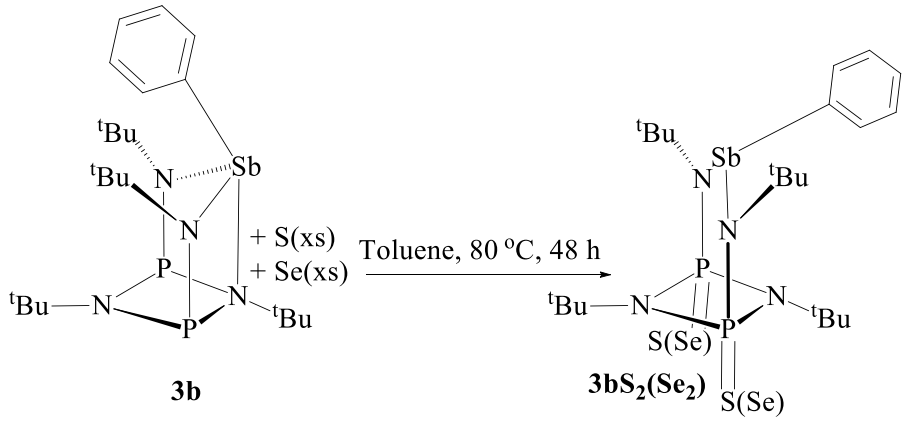

3b **3bS$_2$(Se$_2$)**

Scheme 35. Synthesis of **3bS$_2$** and **3bSe$_2$**.

The ^{1}H NMR spectrum of **3bS$_2$** reveals three signals at 7.83 (d, J_{PH} = 7.90 Hz), 7.19 (t, J_{PH} = 7.93 Hz) and 7.06 ppm (m) representing the *ortho*, *meta* and *para* protons of the phenyl ligand, respectively. Also shown in this spectrum are three singlets at 1.99, 1.77 and 1.32 ppm with relative intensities 1:1:2 corresponding to the *tert*-butylimino protons (1.99 and 1.77 ppm) and *tert*-butylamino protons (1.32 ppm). The ^{13}C{^{1}H} NMR spectrum of **3bS$_2$** depicts four singlets at 160.06, 133.69, 130.45 and 126.07 ppm corresponding to the *ipso*, *ortho*, *meta* and *para* carbons of the phenyl ligand, respectively. The quaternary carbons of the *tert*-butylamino carbons exhibit a singlet at 61.35 ppm, while those of the *tert*-butylimino carbons are observed at 59.65 and 58.81 ppm. Further upfield three signals are observed: a doublet (J_{PC} = 6.65 Hz) at 33.00 ppm attributed to the amino *tert*-butyl primary carbons and two triplets at 31.03 and 30.04 ppm with carbon–phosphorus coupling constants of 4.78 and 4.50 Hz, respectively, corresponding to the imino *tert*-butyl primary carbons. The ^{31}P{^{1}H} NMR spectrum (Figure 59)

of **3bS$_2$** shows a singlet at 46.33 ppm assigned to the two P(V) atoms in the P_2N_2 ring bearing the sulfur atoms. The IR spectrum of **3bS$_2$** shows an absorption band at 874.5 cm^{-1} which we assign to the stretching frequency of the compound. This strong band is shifted from 928 cm^{-1}, which is the typical absorption band for a P=S bond.

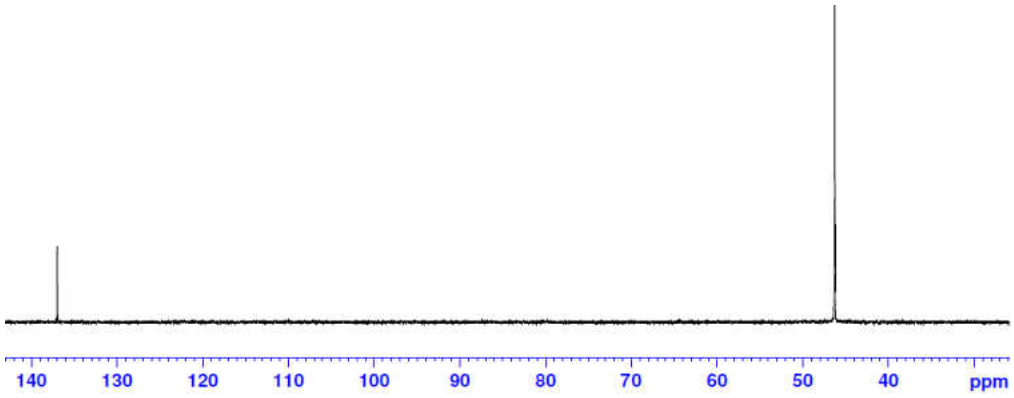

Figure 59. $^{31}P\{^{1}H\}$ NMR Spectrum for **3bS$_2$**.

Solid-state Structure of {[(^{t}BuNP=S)$_2$(^{t}BuN)$_2$]SbPh} 3bS$_2$

Colorless, needle-shaped crystals of **3bS$_2$**, suitable for crystallographic studies were obtained from a cold (–12 °C) concentrated toluene solution after recrystallization. The solid-state structure of **3bS$_2$**, with a partial numbering scheme, is shown in Figure 60, while the crystal data and selected bond parameters are listed in Tables 37 and 38 below, respectively. Compound **3bS$_2$** crystallized in the monoclinic space group, $P2_1/n$, with two molecules per unit cell. Like in 3**aS$_2$**, the Sb atom in **3bS$_2$** makes no bonding contact with N1 and so, the chelation mode is κ^2N where the Sb atom is held above the P_2N_2 heterocycle. The P=S bond lengths in **3bS$_2$** are 1.9283(6) and 1.9320(6) Å, identical to those obtained in [(^{t}BuN)(S)P(μ-N^{t}Bu)$_2$P(S)(NH^{t}Bu)]CuI (1.939(3) Å) and $TeCl_3$[HcddS$_2$][H$_2$cddS$_2$] (1.927(3) Å), (cddS$_2$ = ^{t}Bu(S)P(μ-N^{t}Bu)$_2$P(S)N^{t}Bu) by Chivers and coworkers.[87, 88] The mean endocyclic P–N bonds lengths in **3bS$_2$** (1.6441(15) Å) show a

decrease from those of **3b** (1.7371(9)–1.7416(10) Å) while the mean exocyclic P–N bonds (1.7079(15) Å) show an increase. The phenyl–antimony bond distance (2.1659(17) Å) in **3bS$_2$** is identical to that in **3b**.[99]The sum of the angles N–P–S in **3bS$_2$** is 357°, typical of all P=S bonds, in which the P(V) atom is coordinated in a distorted pseudo-tetrahedral structure.

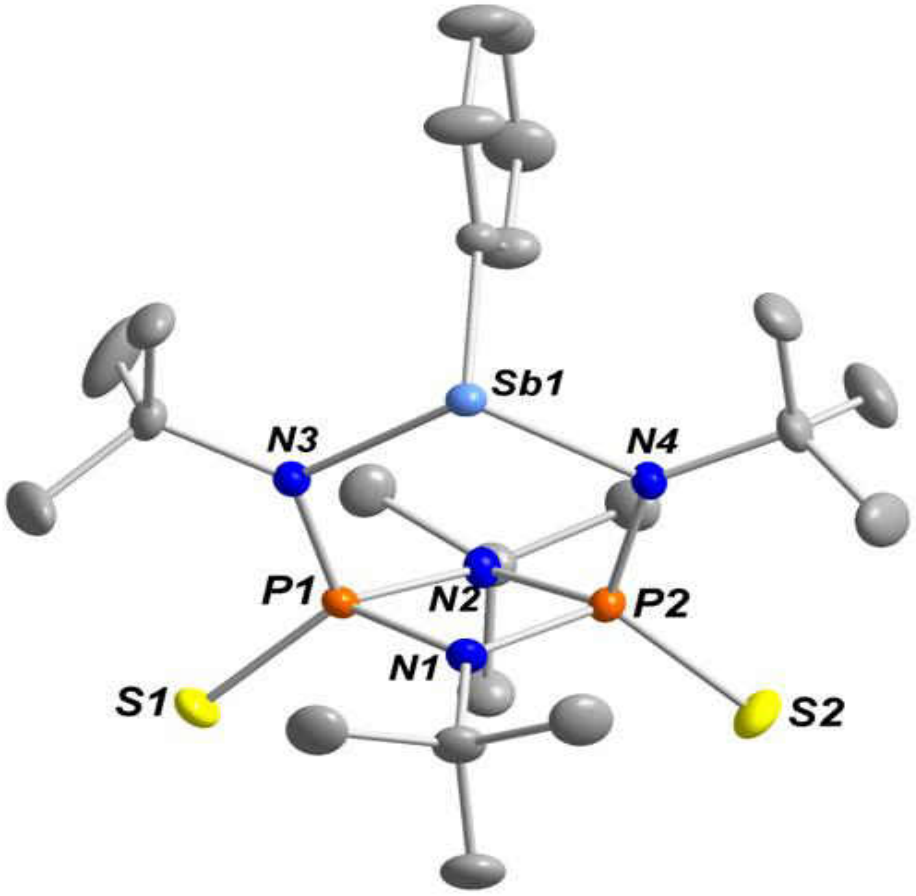

Figure 60. Solid-state structure and partial labelling scheme of **3bS$_2$**. All atoms are drawn at the 50 % probability level.

Table 37. Crystal and structure refinement data for **3bS$_2$**

Chemical formula	$C_{44}H_{82}N_8P_4S_4Sb_2$
Fw	1218.87
T/K	150.01
λ/Å	0.71073
Crystal system	*monoclinic*
Space group	$P2_1/n$
a/Å	9.7946(4)
b/Å	19.1127(8)
c/Å	15.3440(7)
α/°	90
β/°	101.1387(17)
γ/°	90
V/Å^3	2818.3(2)
Z	2
ρ (calc.) g cm^{-3}	1.4362
μ/mm^{-1}	1.258
F(000)	1255.7
Reflections collected	36512
Independent reflections	8342 [R_{int} = 0.0430, R_σ = 0.0328]
$Rw(F^2)^b$ [I>2σ(I)]	R_1 = 0.0249, wR_2 = 0.0541
$R(F)^a$ (all data)	R_1 = 0.0375, wR_2 = 0.0587

[a] $R = \sum|F_o - F_c| \sum |F|_o$. [b] $R_w = \{[\sum w(F_o^2 - F_c^2)] / [\sum w(F_o^2)^2]\}^{1/2}$; $w = 1/[\sigma^2(F_o)^2 + (xP)^2 + yP]$, where $P = (F_o^2 + 2F_c^2)/3$.

Table 38. Selected bond lengths (Å) and angles (°) for **3bS$_2$**.

Bond Lengths (Å)			
Sb1–N3	2.1298(14)	P1–N1	1.6925(15)
Sb1–N4	2.1410(14)	P1–N3	1.7079(15)
Sb1–C24	2.1659(17)	S2–P2	1.9320(6)
P1–N2	1.6441(15)	N1–P2	1.6433(15)
P1–S1	1.9283(6)	P2–N2	1.6910(15)
Bond Angles (°)			
N4–Sb1–N3	103.91(5)	N1–P2–N2	108.25(7)
C24–Sb1–N3	93.73(6)	N1–P1–S1	117.33(5)
C24–Sb1–N4	95.42(6)	N2–P2–N1	84.01(7)
S2–P1–N2	119.50(6)	N1–P2–S2	118.68(6)
N2–P1–N1	100.73(8)	N4–P2–S2	119.89(6)
N2–P1–S1	120.81(5)	N1–P2–S2	118.39(6)

Synthesis and Spectroscopic Analysis of {[(^{t}BuNP=Se)$_2$(^{t}BuN)$_2$]SbPh} 3bSe$_2$

Compound **3bSe$_2$** was isolated in 94% yield by treating **3b** with two equivalents of gray selenium in toluene at 70 °C for 24 h (Scheme 35). Excess selenium was removed with a frit, after the reaction mixture had been cooled to RT. The filtrate was concentrated and allowed to furnish colorless crystals after 3 days.

The ^{1}H NMR spectrum of **3bSe$_2$** depicts six signals resonating between 8.00 and 1.33 ppm. A doublet (J_{PH} = 8.25 Hz) at 7.81 ppm and two multiplets at 7.18 and 7.06 ppm, are assigned to the *ortho*, *meta* and *para* protons of the phenyl ligand, in that order. Also observed in this spectrum are three singlets with relative intensities 1:1:2 corresponding to the protons of the *tert*-butyl groups. The ^{13}C{^{1}H} NMR spectrum for **3bSe$_2$** reveals four singlets at 160.13, 133.64, 130.30 and 129.57 ppm assigned to the *ipso*, *ortho*, *meta* and *para* carbons of the phenyl ligand, respectively. The quaternary carbons of the *tert*-butyl groups appear as three singlets at 62.02, 60.44 and 59.58 ppm. As we move upfield, three more signals are observed as a singlet at 33.06 ppm and two triplets at 31.06 (J_{PC} = 4.32 Hz) and 29.72 ppm (J_{PC} = 4.59 Hz). While the singlet at 33.06 ppm is assigned to the primary carbons of the *tert*-butylamino groups, the triplets at 31.06 and 29.72 ppm are assigned to those of the *tert*-butylimino groups. The primary carbons of the *tert*-butylimino groups are coupled with P(V) atoms of the P_2N_2 ring generating the triplets at 31.06 and 29.72 ppm with carbon–phosphorus coupling constants of 4.32 and 4.59 Hz, respectively. On the ^{31}P{^{1}H} NMR spectrum of **3bSe$_2$** (Figure 61) is observed a singlet at 32.80 ppm with two pairs of ^{77}Se satellite peaks at 30.58 and 35.04 ppm due to ^{31}P–^{77}Se coupling (J_{PSe} = 894 Hz). The singlet at 32.80 ppm is assigned to the P(V) atoms of the P_2N_2 ring bearing the selenium atoms. The IR spectrum of **3bSe$_2$** depicts an absorption band at 564.7 cm^{-1} attributed to the stretching mode of the P=Se bond.

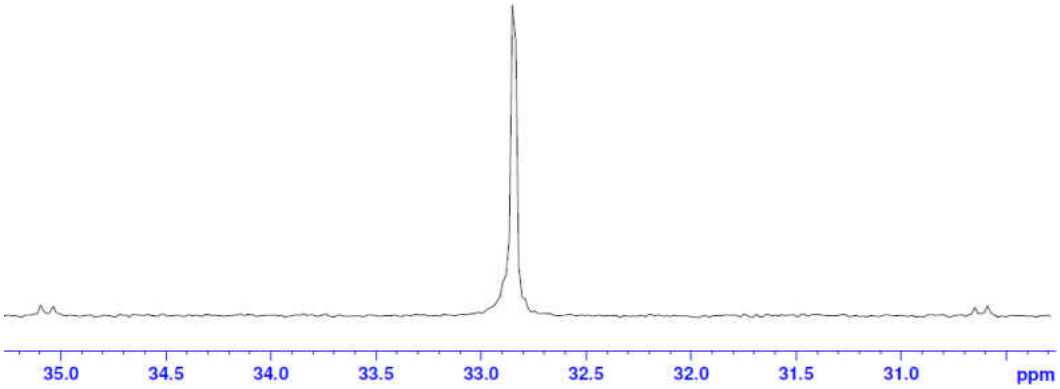

Figure 61. $^{31}P\{^{1}H\}$ NMR Spectrum for **3bSe$_2$**.

Solid-state Structure of {[(^{t}BuNP=Se)$_2$(^{t}BuN)$_2$]SbPh} 3bSe$_2$

Colorless, needle-like crystals of **3bSe$_2$**, suitable for crystallographic studies, were isolated from a cold (–6 °C) concentrated toluene solution after recrystallization. The solid-state structure of **3bSe$_2$**, with a partial numbering scheme is shown in Figure 62, while the crystal data and selected bond parameters are listed in Tables 39 and 40 below, respectively. Compound **3bSe$_2$** **(**like **3bS$_2$)** crystallized in the monoclinic space group, $P2_1/n$, with four molecules per unit cell. The P=Se bonds in **3bSe$_2$** are 2.0922(5) and 2.0758(6) Å long, identical to those in compound **3cSe$_2$** (2.0758(6) and 2.0813(6) Å). Compound **3bSe$_2$** shows great similarities to **3bS$_2$**, as such, a detailed description of **3bSe$_2$** will not be given.

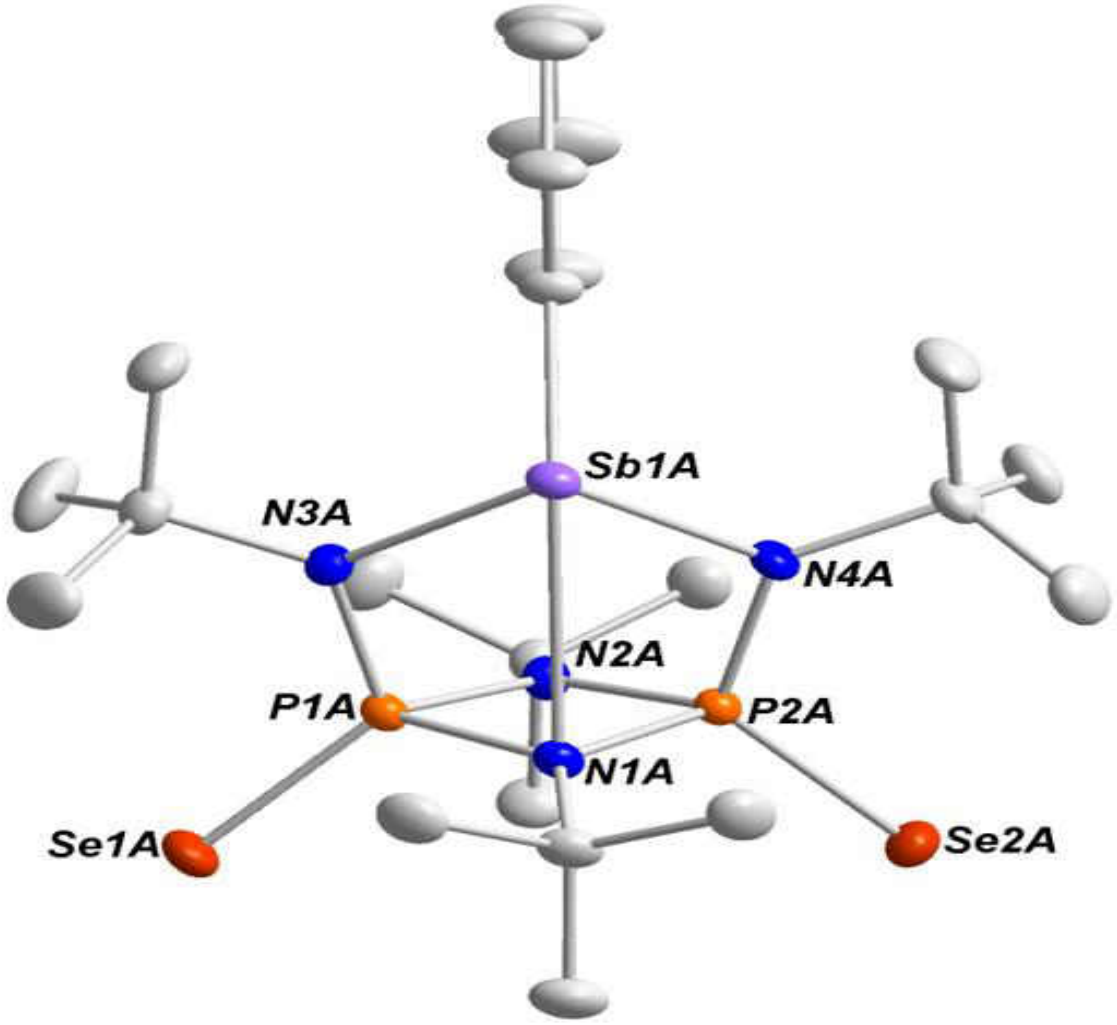

Figure 62. Solid-state structure and partial labelling scheme of **3bSe$_2$**. All atoms are drawn at the 50% probability level.

Table 39. Crystal and structure refinement data for **3bSe$_2$**.

Chemical formula	$C_{22}H_{41}N_4P_2Se_2Sb$
Fw	703.22
T/K	149.97
λ/Å	0.71073
Crystal system	*monoclinic*
Space group	$P2_1/n$
a/Å	11.6751(6)
b/Å	32.4055(19)
c/Å	15.5021(9)
α/°	90
β/°	100.812(2)
γ/°	90
V/Å^3	5760.9(6)
Z	8
ρ (calc.) g cm^{-3}	1.6215
μ/mm^{-1}	3.613
F(000)	2796.3
Reflections collected	63264
Independent reflections	21150 [R_{int} = 0.0339, R_σ = 0.0308]
$Rw(F^2)^b$ [I>2σ(I)]	R_1 = 0.0262, wR_2 = 0.0557
$R(F)^a$ (all data)	R_1 = 0.0388, wR_2 = 0.0599

[a] $R = \sum|F_o - F_c| \sum |F|_o$. [b] $R_w = \{[\sum w(F_o^2 - F_c^2)] / [\sum w(F_o^2)^2]\}^{1/2}$; $w = 1/[\sigma^2(F_o)^2 + (xP)^2 + yP]$, where $P = (F_o^2 + 2F_c^2)/3$.

Table 40. Selected bond lengths (Å) and angles (°) for **3bSe$_2$**.

Bond Lengths (Å)			
Sb1–N3	2.1504(14)	Se2–P2	2.0999(5)
Sb1–N4	2.1453(15)	N1–P1	1.7116(15)
Sb1–C10	2.1478(18)	N1–P2	1.6976(15)
Se1–P1	2.0758(6)	N2–P1	1.7060(14)
N3–P1	1.6979(15)	N4–P2	1.6930(15)
Bond Angles (°)			
N3–Sb1–N4	103.64(5)	N1–P2–Se2	120.15(5)
C10–Sb1–N4	95.16(6)	N2–P2–Se2	116.78(5)
C10–Sb1–N3	96.30(7)	Se2–P2–N2	118.66(5)
Se1–P1–N1	120.20(5)	N4–P2–Se2	119.47(6)
N2–P2–Se2	120.32(6)	N1–P2–N4	100.51(7)

5 SUMMARY AND CONCLUSIONS

The oxidations of cyclodiphosph(III/III)azane compounds of the group 15 elements with sulfur and selenium in toluene were studied. By treating **{[(^{t}BuNP)$_2$(^{t}BuN)$_2$]PCl} 1a** with selenium, the monoselenide **{[(^{t}BuNP)$_2$(^{t}BuN)$_2$Se]PCl} 1aSe** and diselenide **{[(^{t}BuNP=Se)$_2$(^{t}BuN)$_2$]PCl} 1aSe$_2$** were obtained. Compound **1aSe$_2$** crystallized in the

monoclinic space group, $P2_1/c$. While **1aSe** was obtained at 50 °C within 12 h, it took 24 h at 60 °C to obtain **1aSe$_2$** showing that the selenium atom tends to pull electrons away from the P(III) atom making further oxidation more difficult. When **{[(^{t}BuNP)$_2$(^{t}BuN)$_2$]PPh} 1b** was treated with excess selenium at RT, compound **{[(^{t}BuNP)$_2$(^{t}BuN)$_2$](P=Se)Ph} 1bSe′** was isolated in which only the central P(III) atom was oxidized. The electron withdrawing chlorine atom on the central P(III) atom in **1a** tend to direct oxidation to the P(III) atoms of the P_2N_2 heterocycle, while the electron releasing phenyl group in **1b** directs oxidation to the central P(III) atom.

The monochalcogenides **{[(^{t}BuNP)$_2$(^{t}BuN)$_2$S]AsCl} 2aS** and **{[(^{t}BuNP)$_2$(^{t}BuN)$_2$Se]AsCl} 2aSe** were obtained by treating **{[(^{t}BuNP)$_2$(^{t}BuN)$_2$]AsCl} 2a** with one equivalent of S and Se, respectively. Compound **2aSe** was isolated at 50 °C within 12 h as opposed to **2aS** which was realized at 70 °C for 24 h, suggesting that gray selenium is a better oxidizing agent than sulfur. The dichalcogenides **{[(^{t}BuNP=S)$_2$(^{t}BuN)$_2$Se]AsCl} 2aS$_2$** and **{[(^{t}BuNP=Se)$_2$(^{t}BuN)$_2$]AsCl} 2aSe$_2$** were obtained by treating the precursor **2a** with excess S_8 and Se, respectively, in toluene. Compound **2aS$_2$** was synthesized at 80 °C within 48 h, while **2aSe$_2$** was obtained upon heating a reaction mixture at 70 °C for one day. The compounds **2aS**, **2aSe**, **2aS$_2$** and **2aSe$_2$** crystallized in the space groups, $P2_1/n$, $P2_12_12_1$, *Cmca* and *Pnma*, respectively.

When **{[(^{t}BuNP)$_2$(^{t}BuN)$_2$]AsPh} 2b** was treated with excess sulfur at 70 °C for 2 days the monosulfide, **{[(^{t}BuNP)$_2$(^{t}BuN)$_2$S]AsPh} 2bS** was obtained. Similarly, the dichalcogenides, **{[(^{t}BuNP=S)$_2$(^{t}BuN)$_2$]AsPh} 2bS$_2$** and **{[(^{t}BuNP=Se)$_2$(^{t}BuN)$_2$]AsPh} 2bSe$_2$** were obtained by treating **2b** with excess S_8 and Se, respectively, in toluene. Compound **2bS$_2$** was synthesized at 75 °C for two days, while **2bSe$_2$** was obtained at 70 °C upon heating the reaction mixture for one day. Despite the presence of the electron-releasing group (Ph) on the central As(III) atom, it was not oxidized to As(V), showing that it is difficult to achieve the +5 oxidation state as we move

down the group. While compound **2bS$_2$** crystallized in the monoclinic space group, $P2_1/n$, **2bSe$_2$** crystallized in the triclinic space group, $P\bar{1}$. Meanwhile, **{[(^{t}BuNP=Se)$_2$(^{t}BuN)$_2$]AsN$_3$} 2cSe$_2$**, which crystallized in the monoclinic space group, $P2_1/n$, was synthesized by treating the precursor **{[(^{t}BuNP)$_2$(^{t}BuN)$_2$]AsN$_3$} 2c** with excess selenium in toluene at 70 °C for one day. The azide moiety in the post-oxidation compound **2cSe$_2$** points upward, compared to that of **2c** which points downward.

The disulfides, **{[(^{t}BuNP=S)$_2$(^{t}BuN)$_2$]SbCl} 3aS$_2$**, **{[(^{t}BuNP=S)$_2$(^{t}BuN)$_2$]SbPh} 3bS$_2$**, and **{[(^{t}BuNP=S)$_2$(^{t}BuN)$_2$]SbN$_3$} 3cS$_2$** were obtained by treating their respective precursors, **{[(^{t}BuNP)$_2$(^{t}BuN)$_2$]SbCl} 3a**, **{[(^{t}BuNP)$_2$(^{t}BuN)$_2$]SbPh} 3b** and **{[(^{t}BuNP)$_2$(^{t}BuN)$_2$]SbN$_3$} 3c**, with excess sulfur in toluene. Compounds **3aS$_2$** and **3bS$_2$** were obtained at 80 °C within 48 h and 36 h, respectively, while **3cS$_2$** was obtained upon stirring the reaction mixture at 75 °C for 48 h. Compounds **3aS$_2$** and **3bS$_2$** crystallized in the monoclinic space group, $P2_1/n$, while **3cS$_2$** crystallized in the orthorhombic space group, $P2_12_12_1$. Treating **3b** and **3c** with excess selenium in toluene for 24 h at 70 °C furnished the diselenides **{[(^{t}BuNP=Se)$_2$(^{t}BuN)$_2$]SbPh} 3bSe$_2$** and **{[(^{t}BuNP=Se)$_2$(^{t}BuN)$_2$]SbN$_3$} 3cSe$_2$**, respectively. These compounds, **3bSe$_2$** and **3cSe$_2$**, crystallized in the monoclinic and orthorhombic space groups, $P2_1/n$ and $P2_12_12_1$, respectively. In the compounds **3aS$_2$** and **3bS$_2$**, the Sb atom does not make bonding contacts with N1 of the P_2N_2 heterocycle, while this bonding contact is maintained in **3bSe$_2$**, **3cS$_2$** and **3cSe$_2$** as in **3a** due to the inductive effect of the ligands and Se. Unlike the azide moiety that points upward in **2cSe$_2$,** those of **3cS$_2$** and **3cSe$_2$** point downward compared to that of **3c.** Our major findings are summarized in Table 41 below.

Table 41. Summary of Crystallographic Data and Reaction Conditions.

Compound	Duration of reaction (h)	Optimum temp of reaction (°C)	Crystal system	Space group
1aSe	12	50	–	–
1aSe$_2$	24	60	monoclinic	$P2_1/c$
1bSe′	12	RT	–	–
2aS	48	70	monoclinic	$P2_1/n$
2aS$_2$	48	80	orthorhombic	*Cmca*
2aSe	12	50	orthorhombic	$P2_12_12_1$
2aSe$_2$	24	75	orthorhombic	*Pnma*
2bS	48	50	–	–
2bS$_2$	48	75	monoclinic	$P2_1/n$
2bSe$_2$	24	70	triclinic	$P\bar{1}$
2cSe$_2$	24	70	monoclinic	$P2_1/n$
3aS$_2$	48	80	monoclinic	$P2_1/n$
3bS$_2$	36	80	monoclinic	$P2_1/n$
3bSe$_2$	24	70	orthorhombic	$P2_12_12_1$
3cS$_2$	48	75	monoclinic	$P2_1/n$
3cSe$_2$	24	70	orthorhombic	$P2_12_12_1$

CHAPTER IV

OXIDATION REACTIONS WITH ELIMINATION OF CYCLODIPHOSPH(III)AZANE COMPOUNDS OF GROUP 15 ELEMENTS

1. INTRODUCTION

As noted in Chapter III, cyclodiphosph(III)azane compounds of group 15 elements can further be derivatized by oxidation with sulfur or selenium. Because the +5 oxidation state of the pnictogens is relatively difficult to achieve, as we move down the group, the oxidation in these compounds is limited to the P(III) centers, where this state is stable and easy to realize. However, when these compounds are subjected to high refluxing temperatures in toluene, those of the metalloids and metal simply crumble, while those of phosphorus undergo elimination of small molecules like ^{t}BuNCl and molecular rearrangements to form new compounds. For example, Otang *et al*. reported that when [(^{t}BuNP)$_2$(^{t}BuN)$_2$]PCl **1a** and excess sulfur are refluxed in toluene, the compound [(^{t}BuNP=S)$_3$N][99] is obtained with the probable elimination of ^{t}BuNCl. Similarly, as earlier mentioned, Garcia *et al*. reported the elimination of *tert*-butyl groups in the form of isobutene when [{P(μ-N^{t}Bu)}$_2$(μ-N^{t}Bu)$_2$]$_2$ was oxidized by selenium to P$_4$(μ-N^{t}Bu)$_6$Se$_4$ and the formation of N–H bonds.[58, 101] They attributed this observation to steric congestion from selenium. In the cyclodiphoph(III)azane compounds of phosphorus, **1a–h**, the central P(III) is capable of being oxidized to P(V) state. We, therefore, anticipate rearranged compounds with possible elimination of small molecules from the oxidation of **1a** and **1b** with selenium at high temperatures. Despite the presence of an electron donating group (phenyl) on As(III), Sb(III), and Bi(III) in **2b**, **3b,** and **4b**, respectively, these atoms are not expected to be oxidized, due to the difficulty in obtaining the +5 state in them.

Here we report on the reaction of [(^{t}BuNP)$_2$(^{t}BuN)$_2$]PCl **1a** and [(^{t}BuNP)$_2$(^{t}BuN)$_2$]PPh **1b** with excess selenium at high temperatures.

2. EXPERIMENTAL

General Procedure

All experimental procedures were performed under an atmosphere of argon using standard Schlenk techniques. Immediately before use, solvents were dried and freed of molecular oxygen by distillation under a nitrogen atmosphere from sodium- or potassium benzophenone ketyl. Selenium was purchased from Sigma Millipore or Alfa Aesar and used as obtained. The compounds, $[(^{t}BuNP)_2(^{t}BuN)_2]PCl$ **1a** and $[(^{t}BuNP)_2(^{t}BuN)_2]PPh$ **1b**, were synthesized according to published procedures.[98, 99] All fritted filter tubes used were of medium porosity.

Description of Instrumentation

NMR spectra were recorded on a Bruker AVANCE-500 NMR spectrometer. The ^{1}H and ^{13}C NMR spectra are referenced relative to C_6D_5H (7.16 ppm) and (128.39 ppm), respectively, or $CHCl_3$ (7.27 ppm) and $CDCl_3$ (77.23 ppm), respectively, as internal standards, while the $^{31}P\{^{1}H\}$ spectra are referenced relative to $P(OEt)_3$ (137.0 ppm) as an external standard in C_6D_6 or $CDCl_3$. In all cases positive chemical shift values represent higher frequencies and downfield shifts. Melting points were recorded on a Mel-Temp melting point apparatus; they are uncorrected. Elemental analyses were performed by ALS Life Sciences Division Environmental, Tucson, AZ.

X-ray Crystallography

A suitable single crystal of **1aSe$_2$Se′** was coated with Paratone oil and quickly transferred to the goniometer head of a Bruker Quest diffractometer with a fixed angle χ, a sealed fine focus X-ray tube, single crystal curved graphite incident beam monochromator, a Photon100 CMOS area detector and an Oxford Cryosystems low temperature device. Examination and data collection were performed with Mo Kα radiation (λ = 0.71073 Å) at 150 K.

Data were collected, reflections were indexed and processed, and the files scaled and corrected for absorption using APEX3.[110] The space groups were assigned and the structures were solved by direct methods using XPREP within the SHELXTL suite programs[105, 111] and refined by full matrix least squares against F^2 with all reflections using Shelxl2018[112, 113] using the graphical interface Shelxle.[114] If not specified otherwise H atoms attached to carbon and nitrogen atoms were positioned geometrically and constrained to ride on their parent atoms. C–H bond distances were constrained to 0.95 Å for aromatic and CH_2 moieties, and to 1.00, 0.99 and 0.98 Å for aliphatic C–H, CH_2 and CH_3 moieties, respectively. N–H bond distances were constrained to 0.88 Å for planar sp^2 hybridized N–H groups. Methyl (CH_3) were allowed to rotate but not to tip to best fit the experimental electron density. H atoms of pyramidalized R_2NH units were refined and the N–H distances were restrained to 0.88(2) Å.

3. SYNTHESES OF COMPOUNDS

{[(^{t}BuNP=Se)$_2$(NH)$_2$(N^{t}Bu(H)P=Se)]} 1aSe$_2$Se′

In a 100 mL two-necked flask, (0.980 g, 2.36 mmol) sample of {[(^{t}BuNP)$_2$(^{t}BuN)$_2$]PCl} **1a** and excess selenium, (0.600 g, 7.60 mmol) were combined in toluene (35 mL) and refluxed for 12 h. After the reaction mixture had been allowed to cool to RT, unreacted selenium was removed with a frit and the orange filtrate was concentrated *in vacuo* and kept at –12 °C. After one day, colorless, tiny rod-shaped crystals of **1aSe$_2$Se′** were isolated. Yield: (0.880 g, 1.58 mmol), 67%. Mp: 278–280 °C (dec). ^{1}H NMR (C_6D_6, 25 °C): 4.52 (s, 2 H, NH), 2.16 (s, H, (H)N^{t}Bu), 1.68 (s, 9 H, N^{t}Bu, amido), 1.49 (s, 9 H, N^{t}Bu, imido), 1.16 (s, 9 H, N^{t}Bu, imido). ^{13}C{^{1}H} NMR (C_6D_6, 25 °C): 59.52 (s, N*C*(CH$_3$)$_3$, amido), 58.71 (s, N*C*(CH$_3$)$_3$, imido), 53.73 (s, N*C*(CH$_3$)$_3$, imido), 30.81 (d, J_{PC} = 4.46 Hz, NC(*C*H$_3$)$_3$, amido), 30.65 (q, J_{PC} = 4.64 Hz,

NC(CH_3)$_3$, imido). $^{31}P\{^1H\}$ NMR (C_6D_6, 25 °C): 32.00 (septet, J_{PC} = 24.03 Hz, P(V)). Anal. Calcd. for $C_{12}H_{30}N_5P_3Se_3$: C, 25.87; H, 4.88; N, 10.06 %. Found: C, 25.67; H, 4.57; N 10.11%.

{[(^{t}BuNP=Se)$_2$(NH)$_2$](P=Se)Ph} 1bSe$_2$Se′

Like in the synthesis of **1aSe$_2$Se′**, [(^{t}BuNP)$_2$(^{t}BuN)$_2$]PPh **1b**, (0.970 g, 2.13 mmol) and excess selenium (0.470 g, 5.95 mmol) were combined in toluene (30 mL) and the mixture was stirred at 85 °C for 36 h and then allowed to cool. The resulting solution was kept at – 6 °C for 1 day to afford colorless, shiny, cubic crystals of **1bSe$_2$Se′**. Yield: (1.10 g, 2.00 mmol) 89%. Mp: 165–167 °C. ^1H NMR (C_6D_6, 25 °C): 7.39 (m, 3 H, Ph), 6.93 (s, 2 H, Ph, *ortho*), 4.90 (br, 2 H, NH), 1.70 (s, 9 H, N^{t}Bu), 1.13 (s, 9 H, N^{t}Bu). $^{13}C\{^1H\}$ NMR (C_6D_6, 25 °C): 142.19 (s, C_{ipso}), 141.28 (s, Ph, *ortho*), 131.77 (s, Ph, *meta*), 126.02 (s, Ph, *para*), 60.42 (s, N*C*(CH_3)$_3$), 59.04 (s, N*C*(CH_3)$_3$), 30.76 (t, J_{PC} = 6.99 Hz, NC(*C*H_3)$_3$, N^{t}Bu), 30.20 (t, J_{PC} = 4.25 Hz, N*C*(CH_3)$_3$, N^{t}Bu). $^{31}P\{^1H\}$ NMR (C_6D_6, 25 °C): 44.42 (t, J_{PP} = 42.96 Hz, J_{PSe} = 920.69 Hz, P(V)), 33.55 (d, J_{PC} = 32.62 Hz, J_{PSe} = 1051.66 Hz, P(V)). Anal. Calcd. for $C_{14}H_{25}N_4P_3Se_3$: C, 29.03; H, 4.35; N, 9.67 %. Found: C, 29.10; H, 4.38; N, 8.98 %.

4. RESULTS AND DISCUSSIONS

Synthesis and Spectroscopic Analysis of [(^{t}BuNP=Se)$_2$(^{t}BuNHP=Se)(NH)$_2$] 1aSe$_2$Se′

When **1a** and excess selenium were refluxed in toluene for 12 h, compound **1aSe$_2$Se′** was obtained (Scheme 36). After the reaction mixture had been allowed to cool to RT, unreacted selenium was removed using a frit and the resulting filtrate was concentrated to produce **1aSe$_2$Se′** with a moderate yield of 67%. Due to the high refluxing temperature, a ^{t}BuCl group was lost, causing molecular rearrangement to form compound **1aSe$_2$Se′**. Probably, due to partial hydrolysis in the course of refluxing, a ^{t}BuNH group was attached to the phosphorus atom above the P_2N_2 ring, although the mechanism of this reaction is still unclear to us.

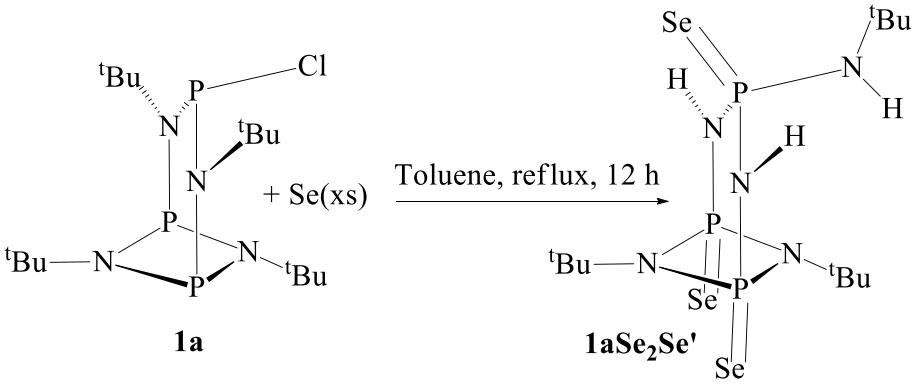

Scheme 36. Synthesis of **1aSe$_2$Se′**.

The ^{1}H NMR spectrum of **1aSe$_2$Se′** (Figure 63) depicts five signals at 4.52, 2.16, 1.68, 1.49 and 1.16 ppm. The broad singlets found at 4.52 and 2.16 ppm are assigned to the protons attached directly to nitrogen atoms. The signal at 2.16 ppm is attributable to the proton on the nitrogen which is attached a *tert*-butyl group, while the signal at 4.52 ppm is assigned to the protons on the nitrogen atoms linking the P(V) atoms of the P_2N_2 ring to the central P(V) atom of the bicycle. Similar values were reported by Chivers *et al*. for NH moieties attached to a *tert*-butyl group.[87] In the ^{13}C{^{1}H} NMR spectrum of **1aSe$_2$Se′** (Figure 64) five signals are observed between 59.52 and 30.65 ppm representing the quaternary and primary carbons of the *tert*-butyl groups. The singlet at 59.52 ppm is due to the quaternary carbon of the *tert*-butyl group attached to the *sec*-amino nitrogen at the apex of the bicycle, while the singlets at 58.71 and 53.73 ppm represent those of the *tert*-butylimino groups in the P_2N_2 ring. The doublet (J_{PC} = 4.46 Hz) at 30.81 ppm is assigned to the primary carbons of the *sec*-amino *tert*-butyl group which couples with the P(V) atom at the apex of the bicycle to generate this doublet, while the quartet at 30.65 ppm, with ^{31}P–^{13}C coupling constant, 4.64 Hz, represents the primary carbons of the *tert*-butylimino groups. The ^{31}P{^{1}H} NMR spectrum of **1aSe$_2$Se′** reveals a septet at 32.00 ppm with a P–P coupling constant of 24.03 Hz, that represents the three P(V) centers in the compound. Also associated with this spectrum are pairs of selenium–77 satellite peaks due to ^{31}P–^{77}Se coupling.

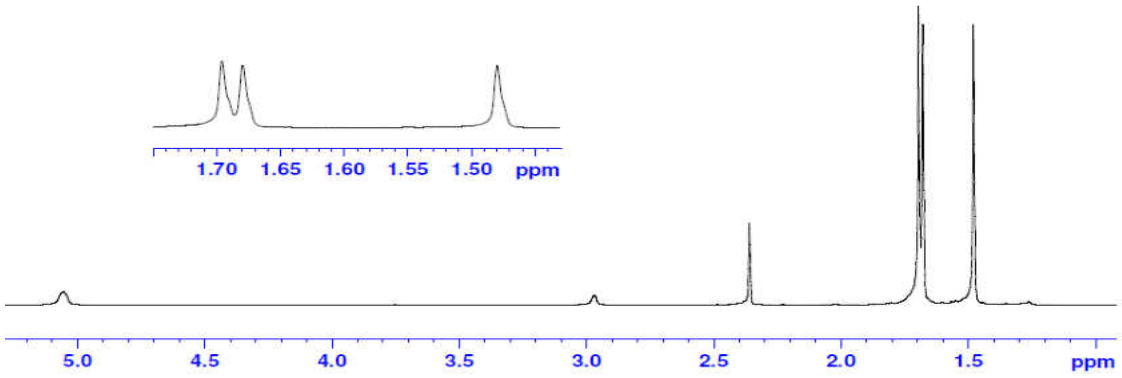

Figure 63. ^{1}H NMR Spectrum for **1aSe$_2$Se′**.

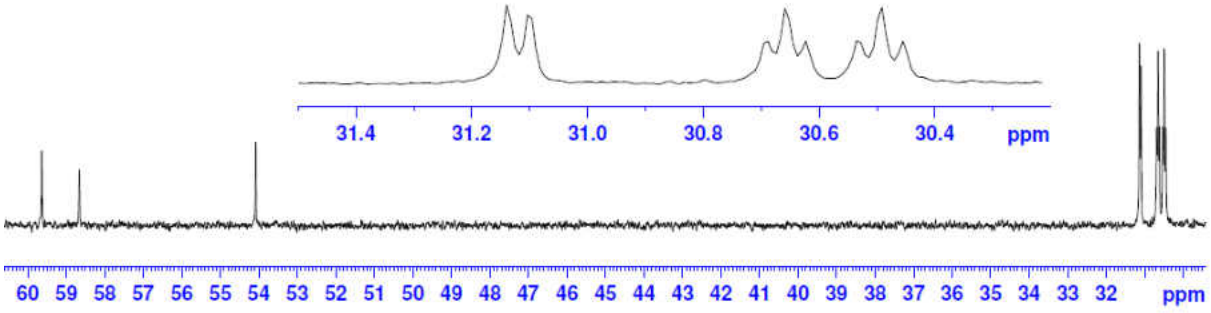

Figure 64. ^{13}C{^{1}H} NMR Spectrum for **1aSe$_2$Se′**.

Solid-state Structure of {[(^{t}BuNP=Se)$_2$(NH)$_2$(N^{t}Bu(H)P=Se)]} 1aSe$_2$Se′

Tiny, colorless, rod-shaped crystals of **1aSe$_2$Se′**, suitable for crystallographic analysis were collected from a cold (–6 °C) concentrated toluene solution after recrystallization. The solid-state structure of **1aSe$_2$Se′**, with a partial numbering scheme is shown in Figure 65, while the crystal data and selected bond parameters are listed in Tables 42 and 43 below, respectively. Compound **1aSe$_2$Se′** crystallized in the triclinic space group, $P\bar{1}$, with two molecules per unit

cell. Probably, a *tert*-butyl group was eliminated from the molecule, in the form of ^{t}BuCl, while another *tert*-butylamino group migrated to the P(V) atom above the P_2N_2 heterocycle.

The nitrogen atoms, N3, N4 and N5 are secondary amine functional groups in **1aSe$_2$Se′**. The P=Se bonds, 2.0490(7) and 2.0967(7) Å, are consistent with same bond distances in *cis*-[Ph(H)(Se=PN^{t}Bu)$_2$N(H)Ph] (2.0815(8) and 2.0826(8) Å).[64] However, the difference between the P=Se bonds in the P_2N_2 ring and that on the P(V) above the ring is remarkable (0.0477(7) Å). The mean endocyclic P–N bond in **1aSe$_2$Se′** is 1.684(2) Å, show a considerable reduction compared to those of **1a** (1.721(4) Å), while the exocyclic P–N mean distance is 1.682(2) Å compared to 1.733(4) Å. All the P–N bond distances in **1aSe2Se′** are all equidistant. The average P–N bond distances around the P(V) atom above the P_2N_2 ring is 1.673(2) Å, shorter than similar bonds in [P(BIMEt$_3$)][OTf]$_3$.[133]The sum of the N–P–Se angles around the P1 atom (340.92°) shows that phosphorus is pyramidally coordinated to the three nitrogen atoms and Se.

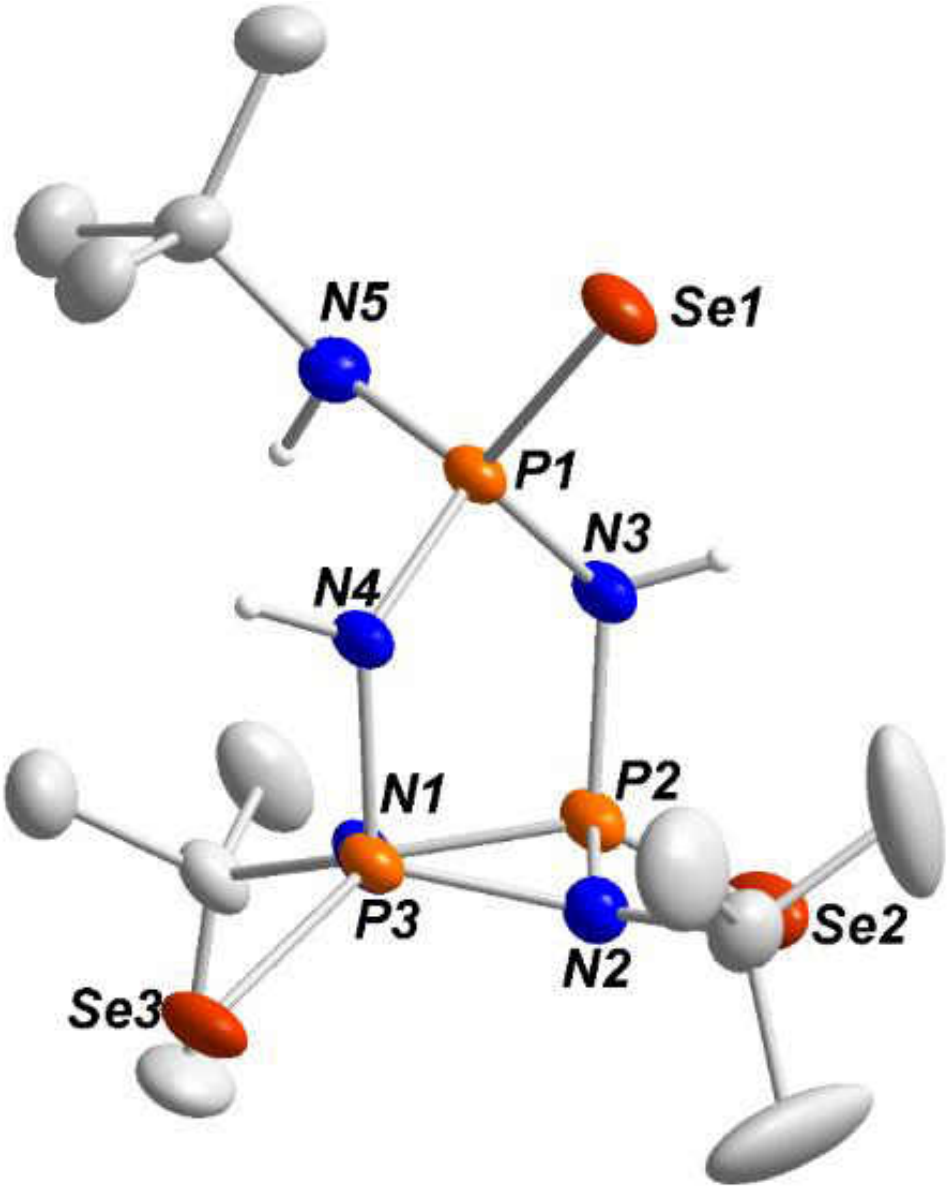

Figure 65. Solid-state structure and partial labelling scheme of **1aSe$_2$Se′**. All atoms are drawn at the 50% probability level. For clarity hydrogen atoms on carbon are omitted.

Table 42. Crystal data and structure refinement for **1aSe$_2$Se′**.

Chemical formula	$C_{12}H_{30}N_5P_3Se_3$
Fw	666.35
T/K	149.97
λ/Å	0.71073
Crystal system	*triclinic*
Space group	$P\bar{1}$
a/Å	9.9971(6)
b/Å	11.7454(8)
c/Å	12.1815(8)
α/°	93.957(3)
β/°	98.411(3)
γ/°	90.539(3)
V/Å^3	1411.32(16)
Z	2
ρ (calc.) g cm^{-3}	1.5679
μ/mm^{-1}	4.095
F(000)	668.3
Reflections collected	39890
Independent reflections	10805 [R_{int} = 0.0448, R_σ = 0.0616
$Rw(F^2)^b$ [I>2σ(I)]	R_1 =0.0436, wR_2 = 0.1094
$R(F)^a$ (all data)	R_1 = 0.0861, wR_2 = 0.1256

[a] $R = \sum|F_o - F_c| \sum |F|_o$. [b] $R_w = \{[\sum w(F_o^2 - F_c^2)] / [\sum w(F_o^2)^2]\}^{1/2}$; $w = 1/[\sigma^2(F_o)^2 + (xP)^2 + yP]$, where $P = (F_o^2 + 2F_c^2)/3$.

Table 43. Selected bond lengths (Å) and angles (°) for **1aSe$_2$Se′**.

Bond Lengths (Å)			
Se1–P1	2.0970(7)	P1–N3	1.678(2)
Se2–P2	2.0493(7)	P2–N1	1.688(2)
Se3–P3	2.0674(7)	P2–N2	1.686(2)
P3–N5	1.632(2)	P2–N4	1.684
P1–N1	1.688(2)	P3–N3	1.699(2)
P1–N2	1.672(2)	P3–N4	1.685(2)
Bond Angles (°)			
P2–P1–Se1	151.94(30	N3–P1–N2	101.73(11)
N1–P1–Se1	122.10(8)	N1–P2–Se2	122.37(8)
N2–P1–Se1	124.19(8)	N2–P2–Se2	126.45(8)
N2–P1–N1	84.03(11)	N2–P2–N1	83.63(10)
N3–P1–Se1	113.92(7)	N4–P2–Se2	112.21(7)
N3–P1–N1	105.84(11)	N4–P2–N1	105.90(11)
N4–P2–N2	101.51(11)	N4–P3–Se3	115.55(8)
N3–P3–Se3	109.25(8)	N5–P3–N3	109.50(11)

Synthesis and Spectroscopic Analysis of {[(^{t}BuNP=Se)$_2$(NH)$_2$](P=Se)Ph} 1bSe$_2$Se′

When compound **1b** was treated with excess selenium at 85 °C for 36 h, compound **1bSe$_2$Se′** was obtained in 89% yield (Scheme 37). Like in **1aSe$_2$Se′** where a ^{t}BuCl group was eliminated, all the *tert*-butyl groups attached to the amino nitrogen atoms were lost in this reaction, perhaps in the form of isobutene. This is probably caused by the steric bulk created by the phenyl ligand and the incoming selenium atoms. Compound **1bSe$_2$Se′** crystallizes readily in a cold (–6 °C) toluene solution to furnish shiny cubic crystals. The crystals were twinned. The solid-state structure of the compound was solved but refinement was problematic.

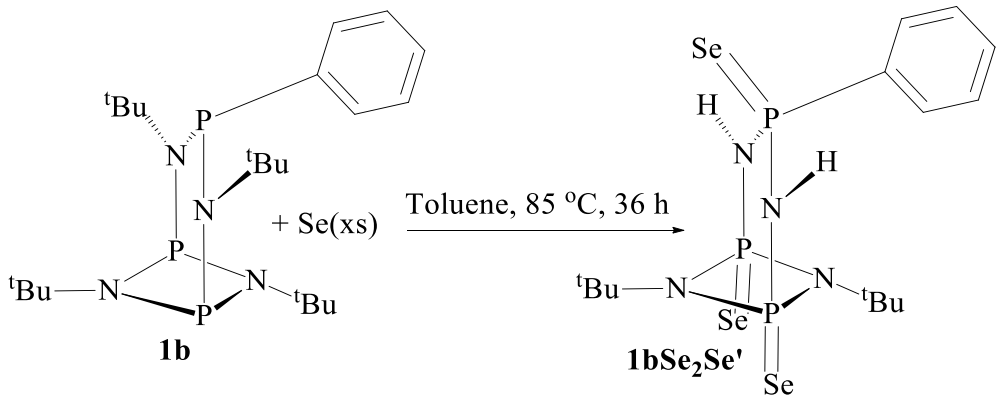

Scheme 37. Synthesis of **1bSe$_2$Se′**.

The ^{1}H NMR spectrum for **1bSe$_2$Se′** (Figure 66) depicts multiplets at 7.39 ppm assigned to the *para* and *meta* protons, and a singlet at 6.93 ppm attributable to the *ortho* protons. At 4.90 ppm, there is a broad signal, attributed to the protons attached to the *sec*-amine nitrogen atoms. The *tert*-butylimino protons are observed upfield at 1.70 and 1.13 ppm as singlets with relative intensities 1:1. The ^{13}C{^{1}H} NMR spectrum for **1bSe$_2$Se′** (Figure 68) shows singlets at 142.19, 141.28, 131.77 and 126.02 ppm assigned to the *ipso*, *ortho*, *meta* and *para* carbons of the phenyl group, respectively. The quaternary carbons of the *tert*-butylimino carbons appear as two singlets at 60.42 and 59.04 ppm. Two triplets are observed at 30.76 and 30.20 ppm, representing the

primary carbons of the *tert*-butyl groups. Shown on the $^{31}P\{^{1}H\}$ NMR spectrum for **1bSe$_2$Se′** (Figure 67) is a triplet at 44.42 ppm (J_{PP} = 42.96 Hz, J_{PSe} = 920.69 Hz) with ^{77}Se satellite peaks surrounding it, while a doublet is seen at 33.55 ppm (J_{PP} = 32.62 Hz, J_{PSe} = 1051.66 Hz) equally flanked on both sides by ^{77}Se peaks. We assigned the triplet to the central P(V) atom which couples with the P(V) atoms of the P_2N_2 heterocyclic ring, while the doublet represents the phosphorus atoms of the ring. The two J_{PSe} values (920.69 and 1051.66 Hz) confirms the presence of the P=Se bonds formed in the molecule.

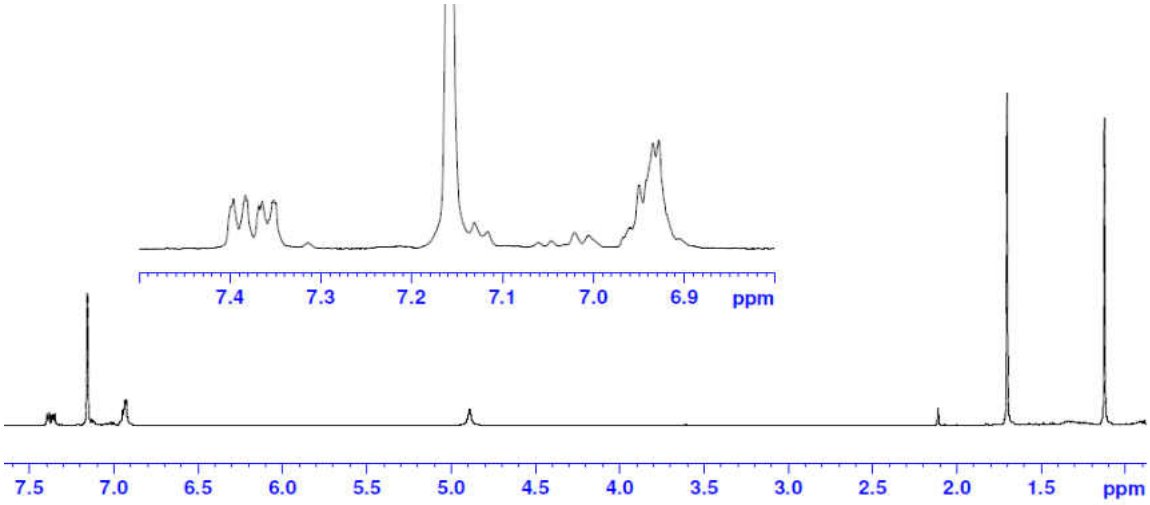

Figure 66. ^{1}H NMR Spectrum for **1bSe$_2$Se′**.

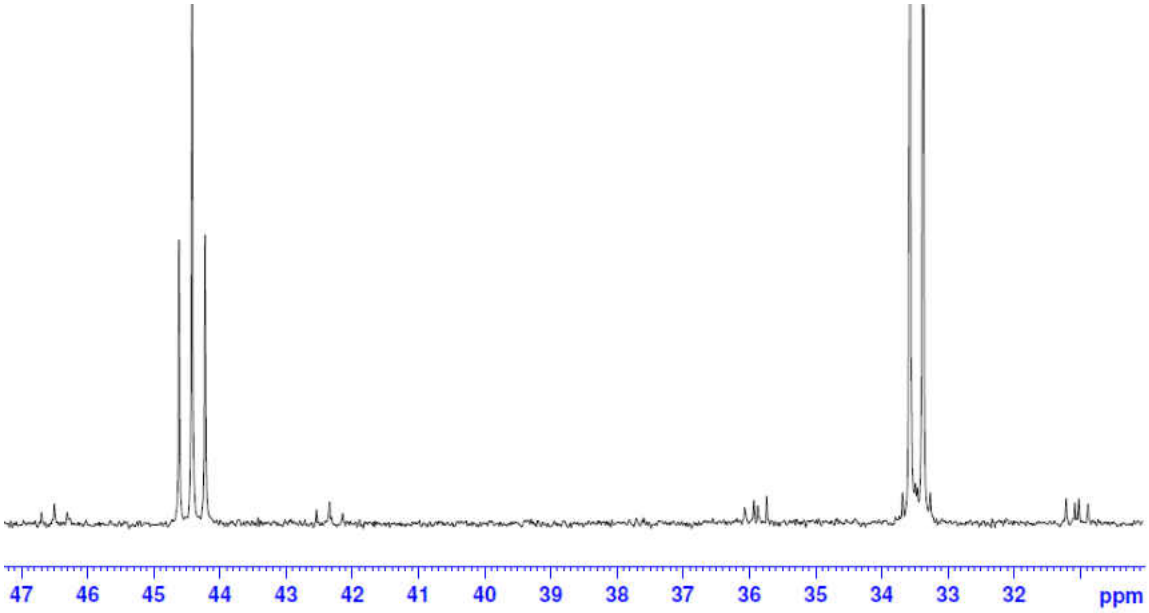

Figure 67. $^{31}P\{^{1}H\}$ NMR Spectrum for **1bSe$_2$Se′**.

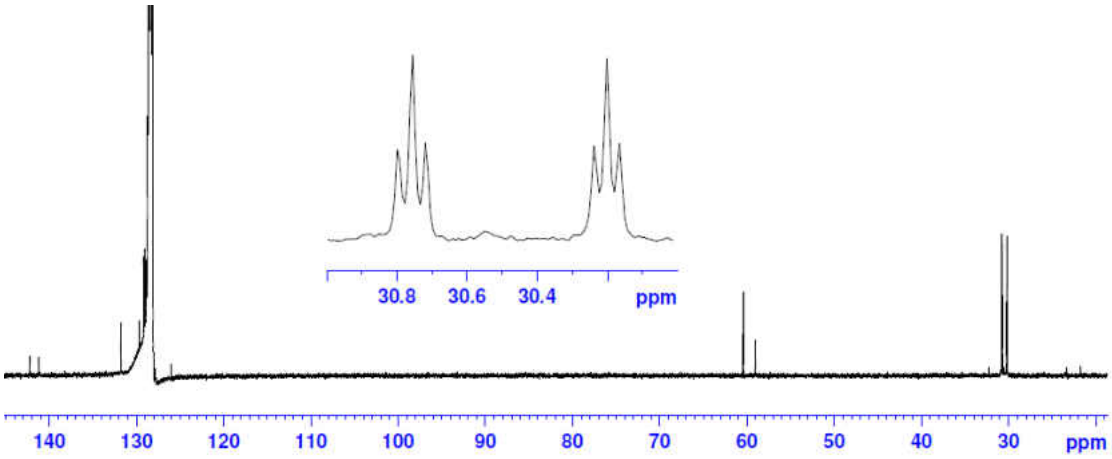

Figure 68. $^{13}C\{^{1}H\}$ NMR Spectrum for **1bSe$_2$Se′**.

SUMMARY AND CONCLUSIONS

The reaction of [(^{t}BuNP)$_2$(^{t}BuN)$_2$]PCl **1a** with excess selenium under reflux in toluene has been investigated. When a mixture of **1a** and selenium was refluxed in toluene for 12 h, a ^{t}BuCl

group was lost, while the residue underwent a molecular rearrangement to form compound **1aSe$_2$Se′** in 69 % yield. Compound **1aSe$_2$Se′** crystallized in the triclinic space group, $P\bar{1}$, with two molecules per unit cell. The P(V) atom above the P_2N_2 ring in **1aSe$_2$Se′** is tetrahedrally bonded to three *sec*-amine nitrogen atoms and a selenium atom. Meanwhile, the P=Se bond length range is 2.0490(7) to 2.0967(7) Å in the molecule.

When [(^{t}BuNP)$_2$(^{t}BuN)$_2$]PPh **1b** was treated with excess selenium for 36 h at 85 °C, the two *tert*-butyl groups attached to the amino nitrogen atoms were eliminated to form compound **1bSe$_2$Se′** with a yield of about 89%. Like in **1aSe$_2$Se′**, the three P(III) atoms in **1bSe$_2$Se′** are oxidized to P(V) atoms by selenium. The $^{31}P\{^1H\}$ NMR spectrum for **1bSe$_2$Se′** depicts a triplet at 44.42 ppm (J_{PP} = 42.96 Hz and J_{PSe} = 920.69 Hz) assigned to the central P(V) atom and a doublet at 33.55 ppm (J_{PP} = 32.62 Hz, J_{PSe} = 1051.66 Hz) representing the P(V) atoms on the P_2N_2 ring.

CHAPTER V

REACTIONS OF DIANIONIC BIS(*tert*-BUTYLAMIDO) CYCLODIPHOSPH(III)AZANES WITH DICHLOROPHENYLPHOSPHINE, ARSENIC(III) CHLORIDE AND ANTIMONY(III) CHLORIDE

1. INTRODUCTION

The *cis*-cyclodiphosph(III)azane **E**, is an easy-to-synthesize molecule with a framework made up of phosphorus and nitrogen atoms linked up by covalent bonds. Since the heterocycle is both a diamine and a bis(phosphine), it is therefore an important bifunctional building block for synthetic chemists.[1] It is also a dimeric amino(imino)phosphine, which can serve as a soft donor ligand for main group and transition metals. Another important feature of **E** is that the diamine functional groups can be deprotonated by a strong base like *n*-butyllithium to form a chelating dianion $\mathbf{E}^{2-}$ or diamide.[87, 93]

Many groups, including ours, have incorporated non-metals, metalloids and metals into the dianion, $\mathbf{E}^{2-}$, to synthesize compounds for various applications, ranging from catalysis to materials applications. The chelation of elements is achieved by the exocyclic nitrogen atoms, but additional coordination can come from the endocyclic nitrogen to give a heterocube arrangement. The possible coordination modes from $\mathbf{E}^{2-}$ chelation are bicyclic, *seco*-cubic or cubic molecules.[24, 98]

Stahl *et al*. synthesized and characterized thallium(1) and indium(III) cage complexes of $\mathbf{E}^{2-}$ and those of group 13.[45, 60] Using compound **31** and ECl_3 (E = P, As, Sb, Bi), they synthesized the compounds **1a**, **2a**, **3a** and **4a**, respectively. Our focus here is to extend the above study, by treating **31** with dichlorophenylphosphine, and to also investigate the reaction of **32** with $AsCl_3$ and $SbCl_3$. Below we present our findings in this project.

2. EXPERIMENTAL

General Procedure

All experimental procedures were performed under an atmosphere of argon using standard Schlenk techniques. Immediately before use, solvents were dried and freed of molecular oxygen by distillation under a nitrogen atmosphere from sodium- or potassium benzophenone ketyl. $PhPCl_2$, $AsCl_3$ and $SbCl_3$ were purchased from Sigma Millipore or Alfa Aesar and used as obtained. The compounds, *cis*-[(^{t}BuNP)$_2$(^{t}BuNLi·thf)$_2$] **31**,[24] and *cis*-[(^{t}BuNP)$_2$(CyNLi·thf)$_2$] **32**,[98, 99] were synthesized according to published procedures. All fritted filter tubes used were of medium porosity.

Description of Instrumentation

NMR spectra were recorded on a Bruker AVANCE-500 NMR spectrometer. The ^{1}H, ^{13}C NMR spectra are referenced relative to C_6D_5H (7.16 ppm) and (128.39 ppm), respectively, or $CHCl_3$ (7.27 ppm) and $CDCl_3$ (77.23 ppm), respectively, as internal standards, while the ^{31}P{^{1}H} spectra are referenced relative to $P(OEt)_3$ (137.0 ppm) as external standard in C_6D_6 or $CDCl_3$. In all cases positive chemical shift values represented higher frequencies and downfield shifts. Melting points were recorded on a Mel-Temp melting point apparatus; they are uncorrected. Elemental analyses were performed by ALS Life Sciences Division Environmental, Tucson, AZ.

X-ray Crystallography

Single crystals were coated with Paratone oil and quickly transferred to the goniometer head of a Bruker Quest diffractometer with a fixed angle χ, a sealed fine focus X-ray tube, single crystal curved graphite incident beam monochromator, a Photon100 CMOS area detector and an Oxford Cryosystems low temperature device. Examination and data collection were performed with Mo Kα radiation (λ = 0.71073 Å) at 150 K.

Data were collected, reflections were indexed and processed, and the files scaled and corrected for absorption using APEX3.[110] The space groups were assigned and the structures were solved by direct methods using XPREP within SHELXTL suite programs[105, 111] and refined by full matrix least squares against F^2 with all reflections using Shelxl2018[112, 113] using the graphical interface Shelxle.[114] If not specified otherwise H atoms attached to carbon and nitrogen atoms were positioned geometrically and constrained to ride on their parent atoms. C–H bond distances were constrained to 0.95 Å for aromatic and CH_2 moieties, and to 1.00, 0.99 and 0.98 Å for aliphatic C–H, CH_2 and CH_3 moieties, respectively. Methyl groups (CH_3) were allowed to rotate but not to tip to best fit the experimental electron density.

3. SYNTHESES OF COMPOUNDS

{[(^{t}BuNP)$_2$(CyN)$_2$]AsCl} 2aCy

Arsenic chloride (10.2 mL, 2.43 mmol) was cooled to 0 °C and (1.24 g, 2.24 mmol) of *cis*-[(^{t}BuNP)$_2$(CyNLi·thf)$_2$] **32** dissolved in toluene (30 mL) was added dropwise to the cooled solution, while stirring. The reaction mixture was allowed to gradually warm to RT and then stirred for 12 h. The reaction mixture was filtered using a frit and the filtrate was concentrated to about 5 mL *in vacuo* and stored at –12 °C to obtain colorless crystals of **2aCy** after several days. Yield: (1.04, 2.04 mmol), 91%. Mp: 106–108 °C (dec). ^{1}H NMR (C_6D_6, 25 °C): 3.21 (m, Cy), 2.43 (m, Cy), 1.98 (m, Cy), 1.78 (m, Cy), 1.56 (m, Cy), 1.48 (s, 9 H, N^{t}Bu), 1.39 (m, Cy), 1.26 (s, 9 H, N^{t}Bu), 1.09 (m, Cy), 0.90 (m, Cy). ^{13}C{^{1}H} NMR (C_6D_6, 25 °C): 61.82 (t, J_{PC} = 9.52 Hz, CHCy), 53.54 (t, J_{PC} = 11.41 Hz, N*C*(CH$_3$)$_3$, imido), 52.62 (t, J_{PC} = 4.01 Hz, N*C*(CH$_3$)$_3$, imido), 37.86 (t, J_{PC} = 3.52 Hz, Cy), 36.54 (t, J_{PC} = 6.19 Hz, Cy), 30.21 (t, J_{PC} = 6.45 Hz, NC(*C*H$_3$)$_3$, imido), 29.66 (t, J_{PC} = 6.45 Hz, NC(*C*H$_3$)$_3$, imido), 27.01 (d, J_{PC} = 14.74 Hz, Cy),

26.02 (s, Cy). $^{31}P\{^{1}H\}$ NMR (C_6D_6, 25 °C): 188.32 (s). Anal. Calcd. for $C_{20}H_{40}N_4P_2ClAs$: C, 47.20; H, 7.92; N, 11.01%. Found: C, 47.09; H, 8.04; N, 11.09%.

{[(^{t}BuNP)$_2$(CyN)$_2$]SbCl} 3aCy

Similar to the synthesis of **2aCy**, a crystalline sample of $SbCl_3$ (0.460 g, 2.00 mmol), dissolved in toluene (18 mL), was added to **32** (1.03 g, 1.85 mmol) dissolved in toluene (20 mL). The resulting reaction mixture was filtered using a frit and the filtrate was concentrated *in vacuo* and stored at –12 °C to obtain colorless crystals of **3aCy** after several days. Yield: (0.900 g, 1.61 mmol), 87%. Mp: 162–164°C. ^{1}H NMR (C_6D_6, 25 °C): 3.77 (s, Cy), 2.23 (m, Cy), 2.07 (m, Cy), 1.73 (m, Cy), 1.63 (m, Cy), 1.45 (m, Cy), 1.41 (s, 9 H, N^{t}Bu, imido), 1.32 (s, 9 H, N^{t}Bu, imido), 1.24 (m, Cy), 1.06 (m, Cy). $^{13}C\{^{1}H\}$ NMR (C_6D_6, 25 °C): 57.73 (t, J_{PC} = 7.97 Hz, CHCy), 54.83 (t, J_{PC} = 11.38 Hz, N*C*(CH$_3$)$_3$, imido), 52.75 (t, J_{PC} = 5.12 Hz, N*C*(CH$_3$)$_3$, imido), 38.81 (s, Cy), 37.54 (t, J_{PC} = 7.88 Hz, Cy), 31.31 (t, J_{PC} = 6.17 Hz, NC(*C*H$_3$)$_3$, imido), 26.80 (s, Cy), 26.55 (t, J_{PC} = 7.36 Hz, Cy), 26.27 (d, J_{PC} = 7.02 Hz, Cy). $^{31}P\{^{1}H\}$ NMR (C_6D_6, 25 °C): 169.33 (s). Anal. Calcd. for $C_{20}H_{40}N_4P_2ClSb$: C, 43.23; H, 7.25; N, 10.08%. Found: C, 43.68; H, 7.47; N, 10.11%.

{[(^{t}BuNP)$_2$(^{t}BuNP)$_2$]Ph$_2$Cl$_2$} 1ab

Dichlorophenylphosphine (1.77 g, 9.91 mmol) was dissolved in toluene (30 mL), and the solution was cooled to 0 °C. To this solution was added dropwise **31** (2.50 g, 4.96 mmol) while stirring. A white precipitate was formed instantly, and the reaction mixture was allowed to warm to RT and then stirred for 24 h. The precipitate, LiCl, was removed and the ensuing colorless solution was concentrated *in vacuo* and stored at –12 °C to produce colorless, cubic crystals of **1ab** after 3 days. Yield: (2.85, 4.50 mmol), 91%. Mp: 154–156 °C. ^{1}H NMR (C_6D_6, 25 °C): 7.54 (s, 4 H, Ph, *ortho*), 7.01 (m, 4 H, Ph, *meta*), 6.96 (m, 2 H, Ph, *para*), 1.68 (s, 18 H, N^{t}Bu, amido), 1.49 (s, 18 H, N^{t}Bu, imido). $^{13}C\{^{1}H\}$ NMR (C_6D_6, 25 °C): 141.40 (t, J_{PC} = 28.28 Hz, C$_{ipso}$),

130.64 (t, J_{PC} = 12.28 Hz, Ph, *ortho*), 127.35 (s, Ph, *meta*), 65.17(m, N*C*$(CH_3)_3$, amido), 54.56 (t, J_{PC} = 14.46 Hz, N*C*$(CH_3)_3$, imido), 33.78 (t, J_{PC} = 5.75 Hz, NC(*C*$H_3)_3$, amido), 32.14 (t, J_{PC} = 7.25 Hz, NC(*C*$H_3)_3$, imido). $^{31}P\{^1H\}$ NMR (C_6D_6, 25 °C): 129.39 (s), 113.75 (s). Anal. Calcd. for $C_{28}H_{46}N_4P_4Cl_2$: C, 53.09; H, 7.32; N, 8.84%. Found: C, 53.32; H, 7.30; N, 8.72%.

{[(^{t}BuNP)$_2$(^{t}BuNP)$_2$]Ph$_2$} 1bb

A 50 mL two-necked flask was charged with a sample of [(^{t}BuNP)$_2$(^{t}BuNP)$_2$]Ph$_2$Cl$_2$ **1ab** (0.24 g, 0.38 mmol) and magnesium powder (0.01 g, 0.53 mmol). Tetrahydrofuran (20 mL), was added and the mixture was refluxed for 24 h, after which time unreacted Mg and $MgCl_2$ was filtered off, and the resulting solution was concentrated *in vacuo* and stored at –12 °C to obtain colorless crystals of **1bb** after 24 h. Yield: (0.19 g, 0.34 mmol), 89%. Mp: 210–212 °C. ^1H NMR (C_6D_6, 25 °C): 8.08 (m, 4 H, Ph, *ortho*), 7.16 (m, 4 H, Ph, *meta*), 7.04 (m, 2 H, Ph, *para*), 1.50 (s, 18 H, P–P(P)N^{t}Bu), 1.22 (s, 18 H, N^{t}Bu, imido). $^{13}C\{^1H\}$ NMR (C_6D_6, 25 °C): 143.62 (t, J_{PC} = 5.34 Hz, C_{ipso}), 131.37 (t, J_{PC} = 16.32 Hz, Ph, *ortho*), 127.76 (s, Ph, *meta*), 127.20 (s, Ph, *para*), 59.62 (m, N*C*$(CH_3)_3$, amido), 55.31 (t, J_{PC} = 20.69 Hz, N*C*$(CH_3)_3$, imido), 33.85 (m, NC(*C*$H_3)_3$, amido), 31.02 (t, J_{PC} = 8.75 Hz, NC(*C*$H_3)_3$, imido). $^{31}P\{^1H\}$ NMR (C_6D_6, 25 °C): 134.29 (s, P_2N_2), 29.74 (s, P–Ph).

4. RESULTS AND DISCUSSIONS

Synthesis and Spectroscopic Analysis of {[(^{t}BuNP)$_2$(CyN)$_2$]AsCl} 2aCy

Treatment of compound **32** with arsenic(III) chloride in toluene at RT gave compound **2aCy**. The reaction was completed after 12 h, and compound **2aCy** was isolated in 91% yield (Scheme 38). Unlike PCl_3 that gave *N′,N*-bis(dichlorophosphinyl)-bis(cyclohexylamino)cyclodiphosphazane[99] when **32** was treated with one or two equivalents of the former, an attempt to synthesize a similar compound using one or two equivalents of $AsCl_3$

and $SbCl_3$ failed, and only the monochloroarsine **2aCy** and monochlorostibine **3aCy**, respectively, were obtained. This outcome is probably due to the large size of As and Sb which prevents the insertion of two atoms of the elements between the exocyclic nitrogen atoms.

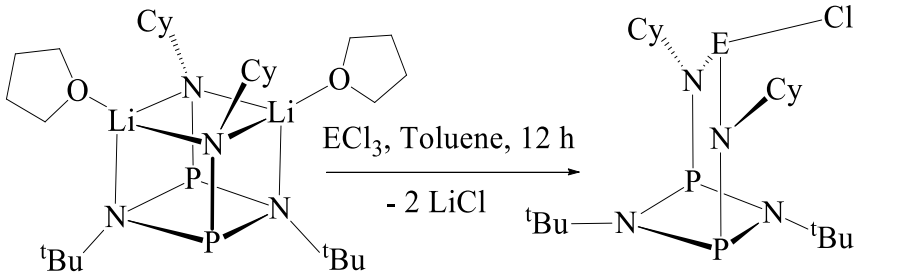

32 **2aCy**, (E = As), **3aCy** (E = Sb)

Scheme 38. Synthesis **2aCy** and **3aCy**.

The presence of the cyclohexyl substituents on the amino nitrogen atoms of **2aCy** renders its ^1H and $^{13}C\{^1H\}$ NMR somewhat complex. The ^1H NMR of **2aCy** depicts 8 signals, all appearing in the aliphatic region as expected. The *tert*-butylimino protons are diastereotopic and appear as singlets at 1.48 and 1.26 ppm. The cyclohexyl protons are observed as multiplets at 3.21, 2.43, 1.98, 1.78, 1.56, 1.39, 1.09 and 0.90 ppm. In the $^{13}C\{^1H\}$ NMR spectrum of **2aCy**, the tertiary cyclohexyl carbons attached to the amino nitrogen atoms are observed as a triplet at 61.82 ppm. The remaining cyclohexyl carbons are observed as triplets at 37.86 (J_{PC} = 3.52 Hz) and 36.54 ppm (J_{PC} = 6.19 Hz), a doublet at 27.01 ppm (J_{PC} = 14.74 Hz) and a singlet at 26.02 ppm. Meanwhile, the quaternary carbons of the *tert*-butylimino carbons are observed as triplets at 53.54 (J_{PC} = 11.41 Hz) and 52.62 ppm (J_{PC} = 4.01 Hz), while their primary carbons are seen as triplets at 30.21 (J_{PC} = 6.45 Hz) and 29.66 ppm (J_{PC} = 6.45 Hz). The $^{31}P\{H\}$ NMR of **2aCy** shows a singlet at 188.32 ppm representing the two phosphorus(III) atoms of the P_2N_2 cycle.

Solid-state Structure of {[(^{t}BuNP)$_2$(CyN)$_2$]AsCl} 2aCy

Colorless crystals of **2aCy**, suitable for single crystal analysis were collected from a cold (–12 °C) concentrated toluene solution. The solid-state structure of **2aCy**, with a partial numbering scheme is shown in Figure 69, while the crystal data and selected bond parameters are listed in Tables 44 and 45 below, respectively. Compound **2aCy** crystallized in the triclinic space group, $P\bar{1}$, with two molecules in a unit cell. The As–Cl bond distance in **2aCy** (2.2930(8) Å) is considerably shorter than that of **2a** (2.3325(11) Å) suggesting that there is little repulsive interaction between the chlorine atom and the Cy group compared to the *tert*-butyl group. Meanwhile, the mean As–N distance (1.8545(15) Å) is almost identical to those of **2a** (1.843(2).[98]The endocyclic and exocyclic P–N bond distances in **2aCy**, which range from 1.719(2) to 1.724(2) Å and from 1.722(2) to 1.725(14) Å, respectively, are quite similar to those of **2a**.

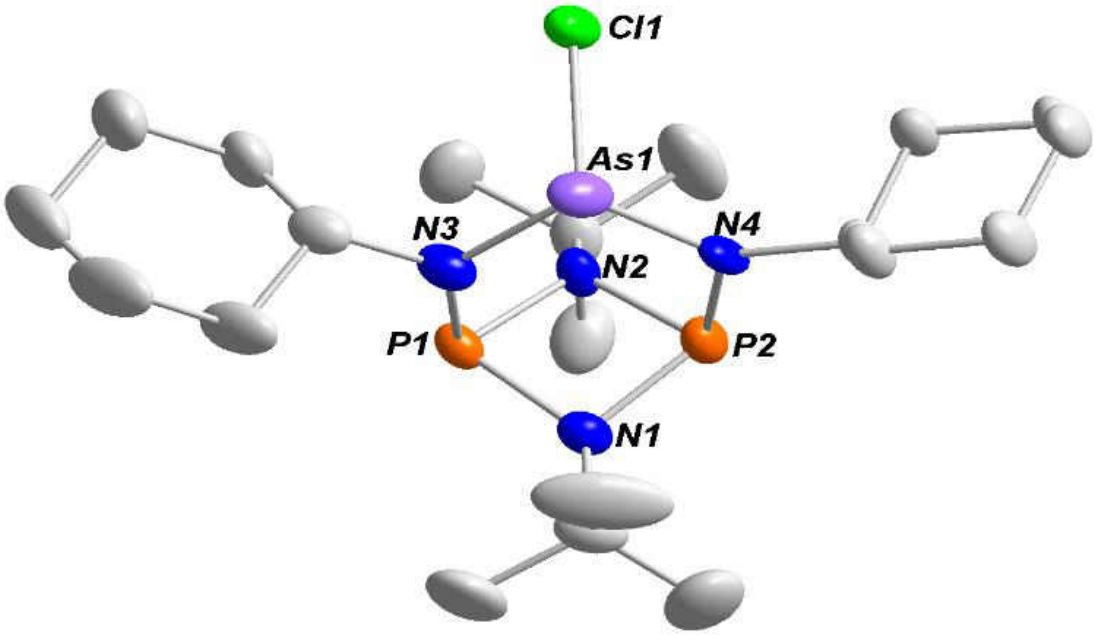

Figure 69. Solid-state structure and partial labelling scheme of **2aCy**. All atoms are drawn at the 50% probability level. Hydrogen atoms are omitted for clarity.

Table 44. Crystal data and structure refinement for **2aCy**.

Chemical formula	$C_{20}H_{40}N_4P_2ClAs$
Fw	508.89
T/K	150.0
λ/Å	0.71073
Crystal system	*triclinic*
Space group	$P\bar{1}$
a/Å	9.8082(120
b/Å	11.6112(14)
c/Å	11.8847(8)
α/°	79.212(3)
β/°	73.627(3)
γ/°	84.492(2)
V/Å^3	1274.3(2)
Z	2
ρ (calc.) g cm^{-3}	1.3262
μ/mm^{-1}	1.578
F(000)	537.0
Reflections collected	36743
Independent reflections	7159 [R_{int} = 0.0399, R_σ = 0.0358]
$Rw(F^2)^b$ [I>2σ(I)]	R_1 = 0.0435, wR_2 = 0.1034
$R(F)^a$ (all data)	R_1 = 0.0688, wR_2 = 0.1223

[a] $R = \sum|F_o - F_c| \sum |F|_o$. [b] $R_w = \{[\sum w(F_o^2 - F_c^2)] / [\sum w(F_o^2)^2]\}^{1/2}$; $w = 1/[\sigma^2(F_o)^2 + (xP)^2 + yP]$, where $P = (F_o^2 + 2F_c^2)/3$.

Table 45. Selected Bond Lengths (Å) and Bond Angles (°) for **2aCy**.

Bond Lengths (Å)			
As1–Cl1	2.2930(8)	P1–N3	1.722(20
As1–N3	1.827(2)	P2–N1	1.722
As1–N4	1.882(16)	P2–N2	1.724(2)
P1–P2	2.5546(9)	P2–N4	1.725(14)
P1–N1	1.719(2)	N1–C1	1.474(3)
P1–N2	1.723(2)	N2–C5	1.477(3)
Bond Angles (°)			
N3–As1–Cl1	100.69(7)	N3–P1–N1	102.31(11)
N1–P1–P2	42.11(7)	N3–P1–N2	98.86(10)
N2–P1–P2	42.19(7)	N1–P2–P1	42.03(8)
N2–P1–N1	82.29(10)	N2–P2–P1	42.15(7)
N3–P1–P2	94.06(8)	N2–P2–N1	82.19(10)
P2–N1–P1	95.86(11)	C9–N3–As1	112.05(17)
P1–N3–As1	124.56(13)	P2–N4–As1	120.6(9)
P2–N4–As1	127.5(13)	C9–N3–P1	121.05(18)

Synthesis and Spectroscopic Analysis of {[(^{t}BuNP)$_2$(CyN)$_2$]SbCl} 3aCy

Like in compound **2aCy**, the metathesis of **32** with antimony(III) chloride in toluene at RT for 12 h afforded compound **3aCy** in 87% yield (Scheme 38).

The ^{1}H NMR spectrum of **3aCy** depicts 8 signals for the cyclohexyl protons, resonating at 3.77 (s), 2.23 (m), 2.07 (m), 1.73 (m), 1.63 (m), 1.45 (m), 1.24 (m) and 1.06 ppm (m). The *tert*-butylimino protons appear as singlets at 1.41 and 1.32 ppm. The ^{13}C{^{1}H} NMR spectrum of **3aCy** shows a triplet (J_{PC} = 7.97 Hz) at 57.73 ppm representing the tertiary cyclohexyl carbons attached to the amino nitrogen atoms, while the signals for the quaternary *tert*-butylimino-carbons are observed as triplets at 54.8 (J_{PC} = 11.38 Hz) and 52.75 ppm (J_{PC} = 5.12 Hz). The other cyclohexyl carbons are observed at 38.81 (s), 37.54 (J_{PC} = 7.88 Hz), 26.80 (s), 26.55 (J_{PC} = 7.36 Hz) and 26.27 ppm (J_{PC} = 7.02 Hz). A triplet also appears at 31.31 ppm with a J_{PC} = 6.17 Hz, representing the primary carbons of the *tert*-butyl groups. The ^{31}P{H} NMR spectrum of **3aCy** shows a singlet at 169.33 ppm representing the two P(III) centers in the P_2N_2 heterocycle.

Solid-state Structure of {[(^{t}BuNP)$_2$(CyN)$_2$]SbCl} 3aCy

Colorless crystals of **3aCy** were obtained from a cold (–12 °C) concentrated toluene solution after recrystallization. The solid-state structure of **2aCy**, with a partial numbering scheme is shown in Figure 70, while the crystal data and selected bond parameters are listed in Tables 46 and 47 below, respectively. Compound **3aCy** crystallized in the monoclinic space group, $P2_1/n$, with four molecules per unit cell. Because of the large size of the antimony atom, bonding contacts are made between Sb atom and N1of the heterocycle P_2N_2 ring. Thus, compound **3aCy** like **3a** adopts a *seco*-cubic structure. While the Sb–N bond distance range in **3aCy** is 2.060(2) to 2.069(2) Å, that of **3a** is (2.089(4)–2.100(6) Å). However, the Sb–N1 bond distances are

identical in the two compounds, namely 2.432(2) Å in **3aCy** vs 2.431(5) Å in **3a**. The average endocyclic (1.750(2) Å) and exocyclic (1.688(2) Å) P–N bond distances in **3aCy** are almost identical to those of **3a** (endo = 1.745(6) Å, exo = 1.680(5) Å).[92]

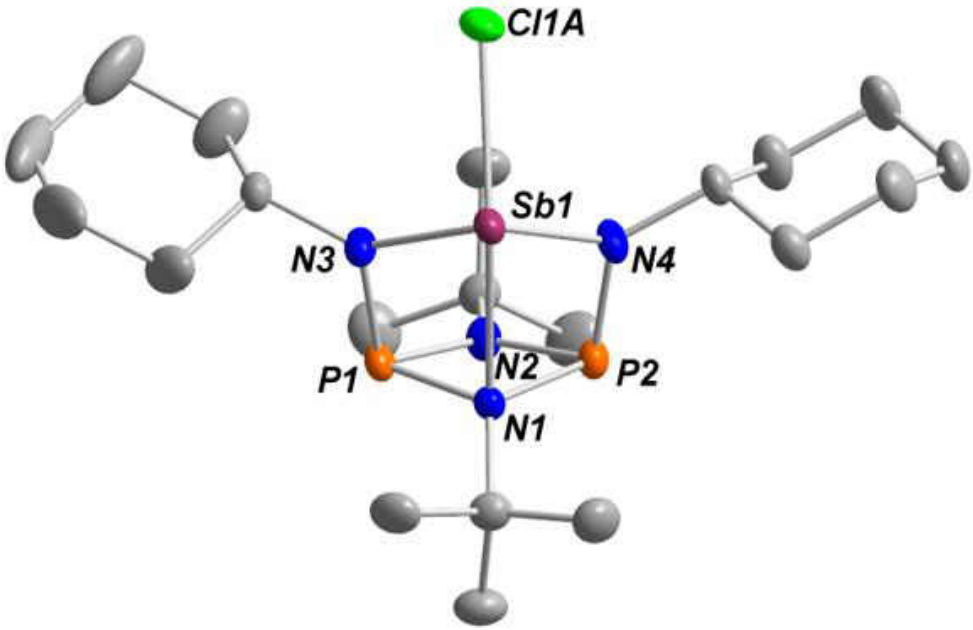

Figure 70. Solid-state structure and partial labelling scheme of **3aCy**. All atoms are drawn at the 50% probability level. Hydrogen atoms are omitted for clarity.

Table 46. Crystal data and structure refinement for **3aCy**.

Chemical formula	$C_{20}H_{40}ClN_4P_2Sb$
Fw	449.92
T/K	149.99
λ/Å	0.71073
Crystal system	*monoclinic*
Space group	$P2_1/n$
a/Å	9.7483(5)
b/Å	15.1334(8)
c/Å	18.1606(10)
α/°	90
β/°	104.7795(18)
γ/°	90
V/Å^3	2590.5(2)
Z	4
ρ (calc.) g cm^{-3}	1.1535
μ/mm^{-1}	1.009
F(000)	937.0
Reflections collected	58296
Independent reflections	9881 [R_{int} = 0.0409, R_σ = 0.0316]
$Rw(F^2)^b$ [I>2σ(I)]	R_1 = 0.0396, wR_2 = 0.0936
$R(F)^a$ (all data)	R_1 = 0.0510, wR_2 = 0.0985

[a] $R = \sum||F_o| - |F_c|| \sum |F|_o$. [b] $R_w = \{[\sum w(F_o^2 - F_c^2)] / [\sum w(F_o^2)^2]\}^{1/2}$; $w = 1/[\sigma^2(F_o)^2 + (xP)^2 + yP]$, where $P = (F_o^2 + 2F_c^2)/3$.

Table 47. Selected Bond Lengths (Å) and Bond Angles (°) for **3aCy**.

Bond Lengths (Å)			
Sb–N3	2.069(2)	N1–P2	1.784(2)
Sb–N4	2.060(2)	P2–N2	1.713(2)
Sb–N1	2.432(2)	N4–C14	1.475(3)
N1–P1	1.689(2)	N1–C10	1.501(3)
N2–P2	1.687(2)	C5–C17	1.507(4)
P1–N1	1.784(2)	C10–C13	1.515(4)
P1–N2	1.719(2)	C20–C22	1.521(5)
Bond Angles (°)			
N2–Sb–N1	98.94(9)	N2–P1–N1	80.56(10)
N1–Sb–N3	67.05(7)	P2–N1–P2	96.26(10)
N1–Sb–N4	66.71(7)	N1–P2–N4	91.61(10)
N1–P1–N3	92.26(10)	N2–P2–N4	108.14(11)
N2–P1–N3	106.95(11)	N2–P2–N1	80.73(10)

Synthesis and Spectroscopic Analysis of {[(^{t}BuNP)$_2$(^{t}BuNP)$_2$]Ph$_2$Cl$_2$} 1ab

The reaction of compound **31** with two equivalents of dichlorophenylphosphine in toluene at RT for 24 h gave compound **1ab** in 91% yield (Scheme 39). However, when one equivalent of dichlorophenylphosphine was used, **1ab** and **1bb** were formed with **1ab** as the major product.

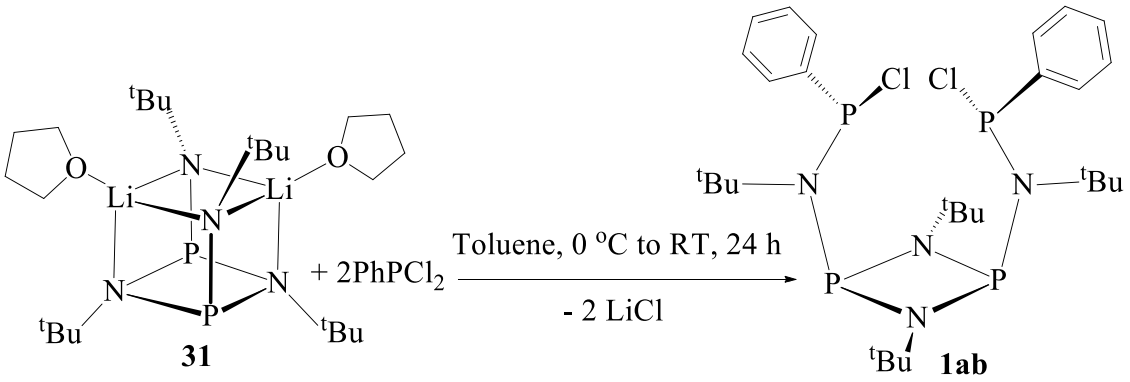

Equation 39. Synthesis of **1ab**.

The ^{1}H NMR spectrum of **1ab** shows three signals at 7.54 (s), 7.01 (m) and 6.96 ppm (m), representing the *ortho*, *meta* and *para* phenyl protons, respectively. Two singlets in the ratio 1:1 are observed at 1.68 and 1.49 ppm, corresponding to the *tert*-butylamino and *tert*-butylimino protons, respectively. The ^{13}C{^{1}H} NMR spectrum for **1ab** depicts three signals at 141.40, 130.64 and 127.35 ppm representing the respective *ipso*, *ortho* and *meta* carbons of the phenyl groups. The signals for the quaternary carbons of the *tert*-butyl groups are observed at 65.17 ppm as multiplets and 54.56 ppm as a triplet (J_{PC} = 14.46 Hz) representing the *tert*-butylamino and *tert*-butylimino carbons, respectively. Meanwhile, the primary carbons of the *tert*-butyl groups show up as triplets at 33.78 (J_{PC} = 5.75 Hz) and 32.14 ppm (J_{PC} = 7.25 Hz). The ^{31}P{^{1}H} NMR spectrum of compound **1ab** shows two singlets with relative intensities 1:1 at 129.39 and 113.75 ppm. The 129.39 ppm signal represents the two P(III) centers to which the phenyl groups are attached, while the 113.75 ppm represents the P(III) centers of the P_2N_2 heterocycle.

Solid-state Structure of {[(^{t}BuNP)$_2$(^{t}BuNP)$_2$]Ph$_2$Cl$_2$} 1ab

Colorless, cubic crystals of **1ab**, with X-ray analysis quality, were obtained from a cold (–12 °C) concentrated toluene solution. The solid-state structure of **1ab**, with a partial numbering scheme is shown in Figure 71, while the crystal data and selected bond parameters are listed in

Tables 48 and 49 below, respectively. Compound **1ab** crystallized in the monoclinic space group, $P2_1$, with two molecules per unit cell. Like stereogenic carbon centers in organic molecules that possess four different substituents, the P3 and P4 atoms in **1ab** are stereogenic. These P(III) atoms contain four different substituents: the lone pair, the phenyl group, the chlorine atom and the amino nitrogen. From the priority-sequence rules, these chiral centers are designated *S,S*. Compound **1ab** is both air- and moisture-sensitive and it can be further derivatized because of the lone pairs of electrons on the P(III) atoms and the chlorine atoms present in the molecule.

The mean P–Cl bond distances in **1ab** (2.1307(5) Å) is much shorter than the P–Cl bond in **1a** (2.244(3) Å) but slightly longer than the P–Cl bonds in *cis*-[(MeSiN^{t}Bu)$_2$(N^{t}BuPCl$_2$)$_2$)] (2.0901(4)–2.1063(4) Å) and 2.0886(2) to 2.1021(2) Å in *cis*-{[P(μ–N^{t}Bu)]$_2$(CyNPCl$_2$)$_2$}.[99] This can be explained by the fact that the *tert*-butyl groups are far apart in the open chain, as such exert little steric hindrance on the chlorine atoms compared to the closed ring in **1a**. The mean endocyclic bond length (1.7251(11) Å) is identical to those of **1a** (1.720(4) Å), **1c** (1.715(2) Å) and [(^{t}BuNP)$_2$(N^{t}Bu)$_2$]SnMe$_2$[94] (1.741(9) Å). By contrast, the mean exocyclic P–N bond lengths (1.7598(11) Å) are elongated compared to those of **1a**, **1c** and [(^{t}BuNP)$_2$(N^{t}Bu)$_2$]SnMe$_2$. Compared to the mean P3–N3 and P4–N4 bond lengths in **1ab** (1.6900(11) Å), those of *cis*-{[P(μ–N^{t}Bu)]$_2$(CyNPCl$_2$)$_2$}[99] (1.6653(6) Å) are relatively shorter. This is probably due to the steric bulk of the phenyl group that prevents the P(III) atoms from moving closer to the amino nitrogen atom. The mean P–C bond length in **1ab** (1.8368(11) Å) is identical to the P–C bond in PPh$_3$[134] (1.828(3)–1.839(5) Å) and [CH$_3$C(NH$_2$)$_2$]$^+$[C$_{10}$H$_6$P(S)(NH$_2$)SP(S)$_2$]$^-$[135] (1.820(4) Å) but slightly shorter than the two equidistant P–C bonds in [(PPh$_2$)^{t}BuNP(μ-N^{t}Bu)$_2$PN^{t}Bu(PPh$_2$)][99] (1.844(6) and 1.8457(17) Å) and tris(3,5-dimethyl-4-methoxyphenyl)phosphine[136] (1.844(6) and 1.840(5) Å).

The sum of the internal angles in the P_2N_2 heterocycle in **1ab** is 357.48(5)°, indicating a puckered structure compared to that of **1a** and **3c**.[98, 103] This is due to the relatively small phosphorus atom, which causes enough strain in the molecule, thus distorting the normally planar P_2N_2 ring. Both the nitrogen atoms of the P_2N_2 and the amino groups in **1ab** are almost perfectly trigonal planar since there are no groups interacting with the *tert*-butyl groups attached to them.

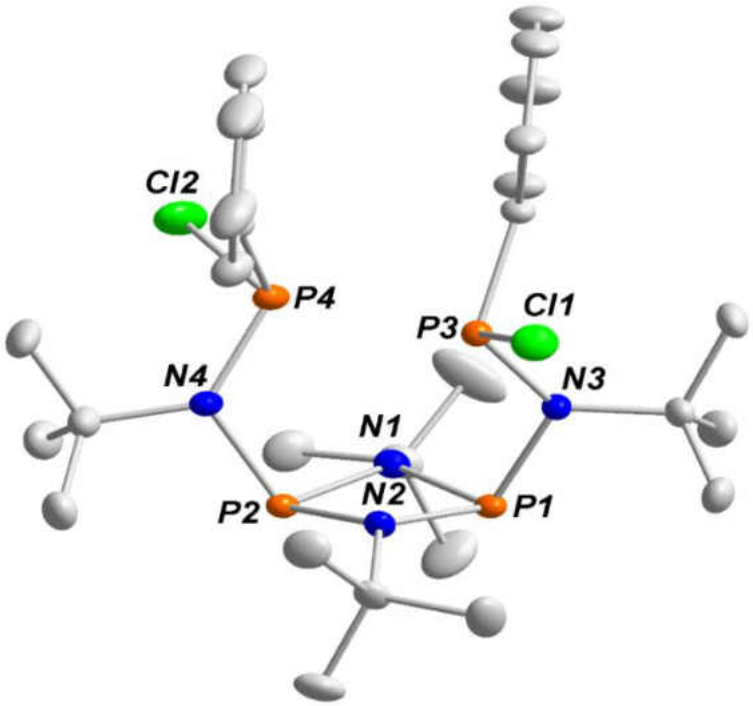

Figure 71. Solid-state structure and partial labelling scheme of **1ab**. All atoms are drawn at the 50% probability level. Hydrogen atoms are omitted for clarity.

Table 48. Crystal and structure refinement data for **1ab**.

Chemical formula	$C_{28}H_{46}N_4P_4Cl_2$
Fw	633.50
T/K	150.0
λ/Å	0.71073
Crystal system	*monoclinic*
Space group	$P2_1$
a/Å	9.8985(6)
b/Å	16.8686(10)
c/Å	11.0098(6)
α/°	90
β/°	114.4860(19)
γ/°	90
V/Å^3	1673.01(17)
Z	2
ρ (calc.) g cm^{-3}	1.2575
μ/mm^{-1}	0.410
F(000)	673.6
Reflections collected	32695
Independent reflections	12362 [R_{int} = 0.0304, R_σ = 0.0374]
$Rw(F^2)^b$ [I>2σ(I)]	R_1 = 0.0299, wR_2 = 0.0728
$R(F)^a$ (all data)	R_1 = 0.0367, wR_2 = 0.0767

[a] $R = \sum||F_o| - |F_c|| \sum |F|_o$. [b] $R_w = \{[\sum w(F_o^2 - F_c^2)] / [\sum w(F_o^2)^2]\}^{1/2}$; $w = 1/[\sigma^2(F_o)^2 + (xP)^2 + yP]$, where $P = (F_o^2 + 2F_c^2)/3$.

Table 49. Selected Bond Lengths (Å) and Angles (°) for **1ab**.

Bond Lengths (Å)			
P1–N1	1.7334(11)	P2–N4	1.7653(11)
P1–P2	2.5878	Cl2–P4	2.1481(5)
P1–N2	1.7173(10)	C2–P3	1.8345(13)
P1–N3	1.7543(11)	P3–N3	1.6860(11)
N1–P2	1.7156(11)	P4–N4	1.6940(11)
Cl1–P3	2.1132(5)	P4–C12	1.8391(15)
P2–N2	1.7342(11)	N1–C29	1.4891(17)
Bond Angles (°)			
P2–P1–N1	41.13(3)	N3–P1–N2	104.95(5)
N2–P1–N1	81.56(5)	P2–N1–P1	97.21(5)
N2–P1–P2	41.69(4)	N2–P2–N1	81.59(5)
N3–P1–N1	107.70(5)	N4–P2–N1	105.27(5)
N3–P1–P2	119.70(4)	N4–P2–N2	109.40(5)
P2–N2–P1	97.12(5)	N3–P3–Cl1	105.28(4)
C2–P3–Cl1	99.44(4)	N3–P3–C2	107.14(6)
P3–N3–P1	114.83(6)	C11–C12–P4	119.18(13)
C7–C12–P4	120.19(10)	C27–C24–N4	111.69(12)

Synthesis and Spectroscopic Analysis of {[(^{t}BuNP)$_2$(^{t}BuN)$_2$]P$_2$Ph$_2$} 1bb

The treatment of compound **1ab** with magnesium powder in THF under refluxing conditions for 24 h gave compound **1bb** in a yield of 89% (Scheme 40). Compound **1bb** was first synthesized in 1993 by Linti *et al*. with a yield of 29% using {[(^{t}BuNP)$_2$(^{t}BuN)$_2$]SnMe$_2$} and one equivalent of dichlorophenylphospine.[94]Here we present a more efficient method for the synthesis of **1bb**.

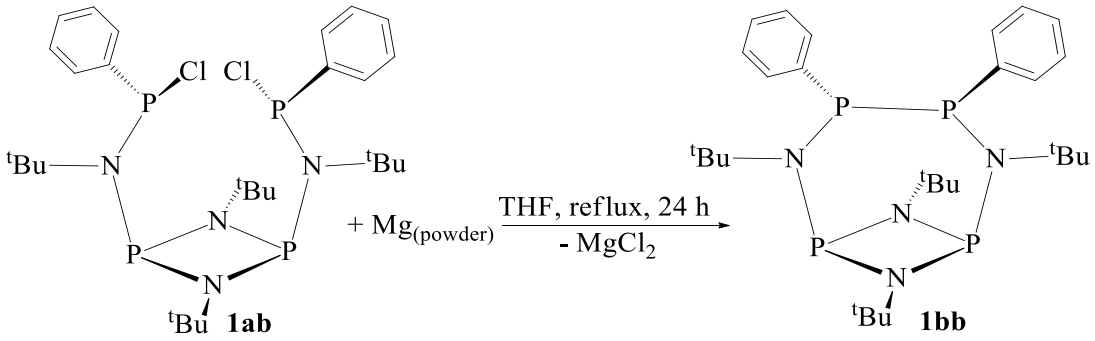

Scheme 40. Synthesis of **1bb**.

The ^{1}H NMR spectrum of **1bb** (Figure 72) shows three signals (multiplets) at 8.08, 7.15, and 7.04 ppm representing the *ortho*, *meta* and *para* phenyl protons, respectively. Two singlets are also observed at 1.50 and 1.22 ppm in the ratio 1:1, representing the *tert*-butyl protons directly linked to the P–PNC(CH$_3$)$_3$ moiety and the P$_2$N$_2$ ring, respectively. The ^{13}C{^{1}H} NMR spectrum of **1bb** reveals four signals for the phenyl carbons at 143.62, 131.37, 127.76 and 127.20 ppm representing the *ipso*, *ortho*, *meta* and *para* carbons, respectively. There are two signals at 59.62 (m) and 55.31 ppm (s) representing the quaternary carbons of the *tert*-butyl groups, while two other signals at 33.85 and 31.02 ppm were observed for the primary carbons. In the ^{31}P{^{1}H} NMR spectrum of **1bb** (Figure 73), two singlets are observed at 134.31 and 29.74 ppm. While the signal at 134.29 ppm represents the P(III) atoms on the P$_2$N$_2$ ring, the one at 29.74 ppm is

attributable to the P(III) atoms on which the phenyl groups are attached. Because of the shielding effects of the phenyl groups, the P(III) atoms move farther upfield to 29.74 ppm.

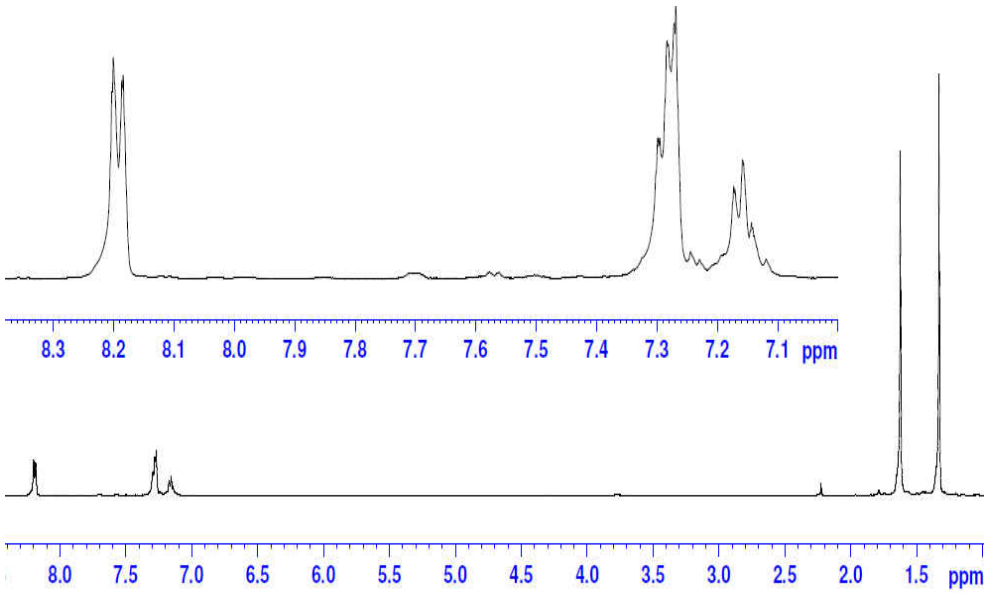

Figure 72. ^{1}H NMR Spectrum of **1bb**.

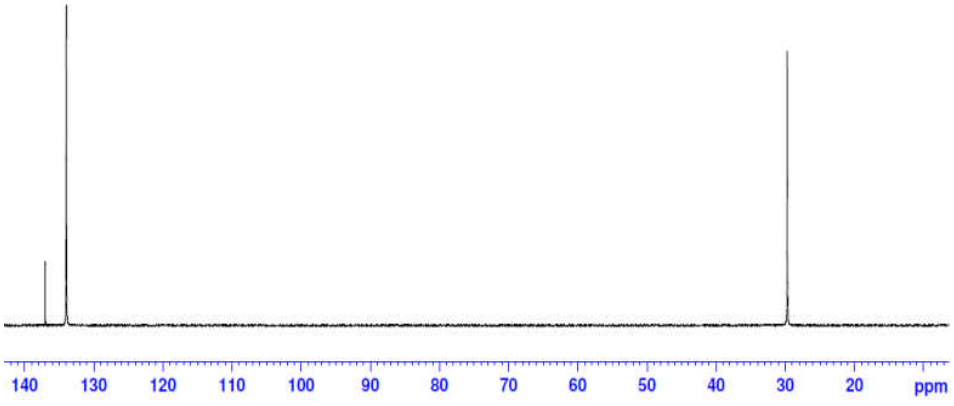

Figure 73. ^{31}P{^{1}H} NMR Spectrum for **1bb**.

5. SUMMARY AND CONCLUSIONS

The reaction of *cis*-[(^{t}BuNP)$_2$(RNLi·thf)$_2$] (R = ^{t}Bu (**31**), R = Cy (**32**)), with the electrophiles, $AsCl_3$, $SbCl_3$ and $PhPCl_2$ were investigated. When **32** was reacted with one equivalent of $AsCl_3$ in toluene for 12 h, {[(^{t}BuNP)$_2$(CyN)$_2$]AsCl} **2aCy** was obtained in good yield (91%). Compound **2aCy** formed a bicyclic cage that crystallized in the triclinic space group, $P\bar{1}$. On the other hand, compound {[(^{t}BuNP)$_2$(CyN)$_2$]SbCl} **3aCy** which was synthesized by treating **32** with $SbCl_3$ using the same solvent, crystallized in the monoclinic space group, $P2_1/n$. Compounds **2aCy** and **3aCy** are the respective analogues of **2a** and **3a** in which ^{t}Bu is replaced by Cy group. The attempted insertion of two atoms of E (E = As or Sb) between the amino nitrogen atoms of **32** failed, probably due to the large size of E.

The reaction of **31** with two equivalents of $PhPCl_2$ in toluene for 12 h gave compound {[(^{t}BuNP)$_2$(^{t}BuNP)$_2$]Ph_2Cl_2} **1ab** with a yield above 90%. However, when one equivalent of $PhPCl_2$ is used, **1ab** and {[(^{t}BuNP)$_2$(^{t}BuN)$_2$]P_2Ph_2} **1bb** are formed with **1ab** being the major product. Compound **1ab** crystallized in the monoclinic space group, $P2_1$, with the two newly introduced P(III) atoms being chiral centers, with configurations *S*, *S*. Further refluxing of **1ab** with excess magnesium metal in THF for 24 h furnished **1bb** in excellent yield. Thus, we have devised a more efficient method of synthesizing **1bb**, which was earlier synthesized with a yield of 29% using {[(^{t}BuNP)$_2$(^{t}BuN)$_2$]$SnMe_2$} and one equivalent of $PhPCl_2$.

SUMMARY

Cyclodiphosph(III)azane compounds of the group 15 elements, $[(^tBuNP)_2(^tBuNP)_2]ECl$ (E = P, As, Sb and Bi), can further be derivatized by substituting the chloride ligand with monodentate *N*- or *O*-donor ligands or by oxidizing the P(III) atoms to P(V). When a non-coordinating ligand like $CF_3SO_2O^-$ is used, cationic salts of the compounds are formed in which the triflate serves as the counterion.

The oxidation of $[(^tBuNP)_2(^tBuNP)_2]EL$ (E = P, As, Sb and Bi and L = Ph, Cl, N_3) with sulfur and selenium takes place exclusively on the P(III) atoms of the P_2N_2 heterocycle except when the element above the ring is phosphorus. The P(III) atom above the P_2N_2 heterocycle is first oxidized if it bears an electron-releasing group. But if it bears an electron withdrawing group, oxidation is orientated to the P(III) atoms of the P_2N_2 heterocycle. The elements, As, Sb, and Bi were not oxidized by S nor by Se, irrespective of whether they bear an electron releasing group or not, suggesting that the +5 oxidation state is difficult to attain as we move down the group. Elemental selenium proved to be a better oxidizing agent than S_8. In addition, selenium–77 possesses a nuclear magnetic spin enabling easy characterization of its compounds by NMR spectroscopy. The monosulfide and -selenides of the group 15 element cyclodiphosph(III/V)azanes were isolated at relatively low temperatures and shorter time periods compared to the disulfide and -selenides. The $^{31}P\{^1H\}$ NMR signal of the P(V) atom bearing a selenium atom shifts more upfield (ca. 15 Hz) than that bearing a sulfur atom.

The oxidation of $[(^tBuNP)_2(^tBuNP)_2]EL$ (E = P and L = Cl or Ph) with excess selenium at elevated temperatures resulted in the elimination of small molecules like ^{t}BuCl or isobutene and subsequent molecular rearrangements. ^{t}BuCl is eliminated when L = Cl, while isobutene is given

off when L = Ph. The *tert*-butyl groups that are lost are those attached to the amino nitrogen atoms due to steric congestion.

The ligand, *cis*-[(^{t}BuNP)$_2$(RNLi·thf)$_2$] (R = Cy), readily reacts with the electrophiles, $AsCl_3$ and $SbCl_3$, at RT to produce bicyclic cages. An attempt to insert two elements (As or Sb) between the two amino nitrogen atoms failed due to the large size of the atoms. The reaction of $PhPCl_2$ with *cis*-[(^{t}BuNP)$_2$(RNLi·thf)$_2$] (R = ^{t}Bu) produced a compound with two chiral centers on the newly introduced P(III) atoms, which further reacted with Mg to give {[(^{t}BuNP)$_2$(^{t}BuNP)$_2$]Ph_2}.

In our future projects, we intend to isolate the bis(*tert*-butylamido)cyclodiphosphazane of the group 15 compounds as the salts of PF_6^- and BF_4^- and compare their bonding behaviors with those of the triflates so far isolated. An investigation of the substitution of the chloride ligand by Br^- in [(^{t}BuNP)$_2$(^{t}BuNP)$_2$]ECl (E = P, As, Sb and Bi) will also be attempted.

The oxidation of [(^{t}BuNP)$_2$(^{t}BuNP)$_2$]PL (L = N_3, O^{t}Bu, N($SiMe_3$)$_2$) using oxygen, sulfur and selenium will be undertaken to see whether elimination will occur and to access the effect of the ligand on the oxidation. Also, the compounds oxidized in this project using S and Se will be repeated with oxygen as the oxidizing agent to see the ease and duration of the oxidation compared to that using S or Se.

The compounds {[(^{t}BuNP)$_2$(CyN)$_2$]AsCl}, {[(^{t}BuNP)$_2$(CyN)$_2$]AsCl} and {[(^{t}BuNP)$_2$(tBuNP)$_2$]Ph_2Cl_2} will be further derivatized using various reagents, like PhMgCl, $AgOSO_2CF_3$, etc.

REFERENCES

1. Otang, M. E.; Josephson, D.; Duppong, T.; Stahl, L. The Chameleonic Reactivity of Dilithio Bis(alkylamido)cyclodiphosph(III)azanes with Chlorophosphines. *Dalton Trans.* **2018**, *47*, 11625–11635.

2. Earnshaw, N. N.; Greenwood, A. *Chemistry of the Elements*. 2nd ed.; Butterwood-Heinemann: Oxford, **1998**.

3. Corbridge, D. E. C. *Phosphorus: An Outline of its Chemistry, Biochemistry and Technology*. 5th ed.; Elsevier: Amsterdam, **1995**.

4. Lappert, M. F.; Sanger, A. R.; Srivastava, R. C.; Power, P. P. *Metal and Metalloid Amides*. Ellis Horwood: Chichester, **1980**.

5. Lappert, M. F.; Power, P.; Protchenko, A.; Seeber, A. *Metal Amide Chemistry*. Wiley: Chichester, **2009**.

6. Cotton, F. A.; Wilkinson, G. *Advanced Inorganic Chemistry*. Wiley: Canada, **1988**.

7. Kamer, P.; Leeuwen, P. W. N. M. *Phosphorus(III) Ligands in Homogeneous catalysis: Design and Synthesis*. Wiley: Chichester, **2012**.

8. Thompson, M. L.; Tarassoli, A.; Haltiwanger, R. C.; Norman, A. D. Synthesis of Two New 1,3,2,4-Diazadiphosphetidine-Based Phosphazane Oligomers: $[(PhNH)P_2(NPh)_2]_2NPh$ and $[(PhNH)PNPh]_3$. *Inorg. Chem.* **1987**, *26* (*5*), 684–689.

9. Stahl, L. Bicyclic and Tricyclic Bis(amido)cyclodiphosph(III)azane Compounds of Main Group Elements. *Coord. Chem. Rev.* **2000**, 203–250.

10. Day, R. O.; Schmidpeter, A.; Holmes, R. R. A Bridgehead Pentaamino Phosphorus Atom in an Aminodiazadiphosphetospirobi[triazaphosphole]. The First PN_5 Structure. *Inorg. Chem.* **1983**, *22*, 3696–3699.

11. Barendt, J. M.; Bent, E. G.; Haltiwanger, R. C.; Norman, A. D. Skeletally Stabilized Triphosphazanes: New Classes of Linear Phosphazanes. *Inorg. Chem.* **1989**, *28*, 2334–2339.

12. Holmes, R. R.; Forstner, J. A. *Inorg. Chem.* **1963**, *2*, 380–384.

13. Spinney, H. A.; Korobkov, I.; DiLabio, G. A.; Yap, G. P. A.; Richeson, D. S. Diamidonaphthalene-Stabilized N-Heterocyclic Pnictogenium Cations and Their Cation-Cation Solid-State Interactions. *Organometallics* **2007**, *26*, 4972–4982.

14. Cowley, A. H.; Lattman, M.; Wilburn, J. C. An NMR Study of the Reactions of Phosphorus(III) Halides with Halide Ion Acceptors, Two-Coordinate Phosphorus Cations with Bulky Ligands. *Inorg. Chem.* **1981**, *20*, 2916–2919.

15. Chivers, T.; Laitinen, R. S. Insights into the Formation of Inorganic Heterocycles Via Cyclocondensation of Primary Amines with Group 15 and 16 halides. *Daltons Trans.* **2017**, *46*, 1357–1367.

16. Balakrishna, M. S. Unusual and Rare Pincer Ligands: Synthesis, Metallation, Reactivity and Catalytic Studies. *Polyhedron* **2018**, *143*, 1–10.

17. Vijjulatha, M.; Swamy, K. C. K.; Vittal, J. J.; Koh, L. L. Synthesis and Structures of New Symmetrically and Unsymmetrically Substituted Cyclodiphosphazanes. *Polyhedron* **1999**, *18*, 2249–2254.

18. Swamy, K. C. K.; Gangadhararao, G.; Suresh, R. R.; Kumar, N. N. B.; Chakravarty, M. Exploring Organic Reactions Using Simple Cyclodiphosphazanes. *J. Organomet. Chem.* **2010**, *695*, 1042–1051.

19. Suresh, D.; Balakrishna, M. S.; Rathinasamy, K.; Panda, D.; Mobin, S. M. Water-Soluble Cycodiphosphazanes: Synthesis, Gold(I) Metal Complexes and Their In Vitro Antitumor Studies. *Dalton Trans.* **2008**, 2812–2814.

20. Sim, Y.; Tan, D.; Ganguly, R.; Li, Y.; Garcia, F. Orthogonality in Main Group Compounds: A Direct One-Step Synthesis of Air- and Moisture-Stable Cyclophosphazanes by Mechanochemistry. *Chem. Commun.* **2018**, *54*, 6800–6803.

21. Siddiqui, M. M.; Mague, J. T.; Balakrishna, M. S. Diamond-Type Copper Coordination Polymers Containing Soft Cyclodiphosphazane Ligands. *Inorg. Chem.* **2015**, *54*, 6063–6065.

22. Shi, Y. X.; Liang, R. Z.; Martin, K. A.; Weston, N.; Gonzalez, -C. S.; Ganguly, R.; Li, Y.; Lu, Y.; Ribeiro, A. J. M.; Ramos, M. J.; Fernandes, P. A.; Garcia, F. Synthesis and Hydrolytic Studies on the Air-Stable [(4-CN-PhO)(E)P(μ-N^{t}Bu)]$_2$ (E = O, S, and Se) Cyclodiphosphazanes. *Inorg. Chem.* **2015**, *54*, 6423–6432.

23. Schulz, A.; Villinger, A.; Westenkirchner, A. Synthesis of 1,3-Dichloro-*cyclo*-1,3-diphosphadiazanes from Silylated Amino(dichloro)phosphanes. *Inorg. Chem.* **2013**, *52*, 11457–11468.

24. Schranz, I.; Stahl, L. Polycyclic Bis(*tert*-butylamido)cyclodiphosph(III)azane Complexes of Lithium and Magnesium: Their Syntheses, Molecular Structures, and Relationships to Isoelectronic Cyclodisilazane. *Inorg. Chem.* **1998**, *37*, 1493–1498.

25. Plajer, A. J.; Niu, H. -C.; Rizzuto, F. J.; Wright, D. S. Formation and Selection of the Macrocycle [{(^{t}BuN=)P(μ-N^{t}Bu)}$_2${P(μ-N^{t}Bu)}$_2$]$_3$. *Dalton Trans.* **2018**, *47*, 6675–6678.

26. Pandey, M. K.; Kunchur, H. S.; Ananthnag, G. S.; Mague, J. T.; Balakrishna, M. S. Cathechol and 1,2,4,5-Tetrahydroxybenzene Functionalized Cyclodiphosphazane Ligands: Synthesis, Structural Studies, and Transition Metal Complexes. *Dalton Trans.* **2019**, *48*, 3610–3624.

27. Klare, H.; Hanft, S.; Neudorfl, J. M.; Schlorer, N. E.; Griesbeck, A.; Goldfuss, B. Anion Recognition with Hydrogen-Bonding Cyclodiphosphazanes. *Chem. Eur. J.* **2014**, *20*, 11847–11855.

28. Eisler, D. J.; Chivers, T. Bis(1-amino)cyclodistib(III)azanes: The First Structural Characterization Of *Cis* and *Trans* Isomers of a Single Cyclodipnict(III)azane. *Inorg. Chem.* **2006**, *45*, 10734–10742.

29. Doyle, E. L.; Riera, L.; Wright, D. S. Toroidal Main Group Macrocycles: New Opportunites for Cation and Anion Coordination. *Eur. J. Inorg. Chem.* **2003**, 3279–3289.

30. Chandrasekaran, P.; Mague, J. T.; Balakrishna, M. S. Synthesis and Derivatization of the Bis(amino)-λ^3-cyclodiphosphazanes *cis*-[R'(H)NP(μ-NR)]$_2$, Including a Rare Example, *trans*-[^{t}Bu(H)N(Se)P(μ-NCy)]$_2$, Showing Intermolecular Se...H–O Hydrogen Bonding. *Eur. J. Inorg. Chem.* **2011**, 2264–2272.

31. Chandrasekaran, P.; Mague, J. T.; Balakrishna, M. S. Gold(I) Complexes of Cyclodiphosphazanes *cis*-{RP(μ-N^{t}Bu)}$_2$: Structure of a Novel Tetranuclear Gold(I) Macrocycle, [{Au{(*o*-MeOC$_6$H$_4$O)P(u-N^{t}Bu)}$_2$}$_4$](ClO$_4$)$_4$. *Dalton Trans.* **2009**, 5478–5486.

32. Chandrasekaran, P.; Mague, J. T.; Balakrishna, M. S. Intramolecular Amine-Induced[1,3]-Sigmatropic Rearrangement in the Reactions of Aminophosphinites or Phosphites with Elemental Sulfur or Selenium. *Inorg. Chem.* **2006**, *45*, 5893–5897.

33. Chandrasekaran, P.; Mague, J. T.; Balakrishna, M. S. Copper(I) Coordination Polymers [{Cu(μ-X)}$_2${RP(μ-N^{t}Bu)}]$_n$ (R= OC$_6$H$_4$OMe-o; X = Cl, Br, and I) and Their Reversible Conversion into Mononuclear Complexes [CuX{(RP(μ-N^{t}Bu))$_2$}$_2$]: Synthesis and Structural Characterization. *Inorg. Chem.* **2006**, 45, 6678–6683.

34. Balakrishna, M. S.; Suresh, D.; Ananthnag, G. S.; Mague, J. T. Quaternization and Oxidation Reactions of Cyclodiphosphazane Derivatives and Their Copper(I) and Gold(I) complexes. *Dalton Trans.* **2014**, *43*, 8835–8848.

35. Balakrishna, M. S.; Suresh, D.; Mague, J. T. Cyclodiphosphazane Appended with Thioether Functionality: Synthesis, Transition Metal Chemistry and Catalytic Application in Suzuki-Miyaura Cross-Coupling Reactions. *Inorg. Chim. Acta* **2011**, *372*, 259–265.

36. Balakrishna, M. S.; Mague, J. T. Synthesis and Molecular Structure of 1,3-Di-*tert*-butyl-2,4-bis(cyclopentadienyl)iron(II)1,3,2,4-diazadiphosphetidine, $[Fe(\eta^5\text{-}C_5H_4)_2(PN^tBu)_2]$. *Organometallics* **2007**, *26*, 4677–4679.

37. Balakrishna, M. S.; Eisler, D. J.; Chivers, T. Chemistry of Pnictogen(III)-Nitrogen Ring Systems. *Chem. Soc. Rev.* **2007**, *36*, 650–664.

38. Balakrishna, M. S. Cyclophosphazanes with Functionalities: Synthesis, Reactivity and Transition Metal Chemistry. *J. Organomet. Chem.* **2010**, *695*, 925–936.

39. Ananthnag, G. S.; Mague, J. T.; Balakrishna, M. S. Cyclodiphosphazane Appended with Pyridyl Functionalities: Reactivity, Transition Metal Chemistry and Structural Studies. *J. Organomet. Chem.* **2015**, *779*, 45–54.

40. Michaelis, A.; Schroeter, F. *Chem. Ber.* **1894**, *27*, 490–498.

41. Holmes, R. R. *J. Am. Chem. Soc.* **1961**, *83*, 1334–1336.

42. Muir, K. W.; Nixon, J. F. *J. Chem. Soc., Chem. Commun.* **1971**, 1405–1406.

43. Keat, R. *Top. Curr. Chem.* **1982,** *102*, 89–116.

44. Siddiqui, M. M.; Mague, J. T.; Balakrishna, M. S. *cis*-Bisphenylalkynyl Cyclodiphosphazane: Oxidation Reactions and Transition Metal Complexes. *J. Organomet. Chem.* **2015**, *794*, 81–87.

45. Schranz, I.; Moser, D. F.; Stahl, L.; Staples, R. J. Ring Opening of Dilithio Bis(amido)cyclodiphosphazanes As a Route to 1,3-Diaza-2λ^2-phosphaallyl Gallium Complexes. *Inorg. Chem.* **1999**, *38*, 5814–5819.

46. Roth, T.; Wadepohl, H.; Wright, D. S.; Gade, L. H. Chiral Ditopic Cyclodiphosphazane(CycloP) Ligands: Synthesis, Coordination Chemistry, and Application in Asymmetric Catalysis. *Chem. Eur. J.* **2013**, *19*, 13823–13837.

47. Moser, D. F.; Carrow, C. J.; Stahl, L.; Staples, R. J. Titanium Complexes of Bis(1-amido)cyclodiphosph(III)azanes and Bis(1-amido)cyclodiphosph(V)azanes: Facial and Lateral Coordination. *J. Chem. Soc., Daltons Trans.* **2001**, 1246–1252.

48. Mohanty, S.; Balakrishna, M. S. Suzuki-Miyaura, Mizoroki-Heck carbon-carbon coupling and hydrogenation reactions catalysed by Pd^{II} and Rh^{I} complexes containing cyclodiphosphazane *cis*-$\{^{t}BuNP(OC_6H_4O)\}_2$. *J. Chem. Sci.* **2010**, *122* (4), 137–142.

49. Gangadhararao, G.; Swamy, K.C.K. Cyclodiphosphazanes as Synthetic Probes: P-C/P-N Bond Formation from the Reaction with Functionalized Propargyl Alcohols and *N*-Hydroxy Substrates. *J. Chem. Sci.* **2015**, *127* (2), 197–207.

50. Chandrasekaran, P., Mague, J. T.; Balakrishna, M. S. Synthesis and Characterization of Ru^{II}/Au^{I}, Pd^{II}/Au^{I}, $Pd^{II}/2Au^{I}$, $P^{tII}/2Au^{I}$ and $Cu^{I}/2Au^{I}$ Heterometallic Complexes of Cyclodiphosphazane *cis*-$\{(o\text{-}MeOC_6H_4O)P(\mu\text{-}N^{t}Bu)\}_2$. *Polyhedron* **2008**, *27*, 80–86.

51. Chandrasekaran, P.; Mague, J. T.; Balakrishna, M. S. Cyclodiphosphazanes with Hemilabile Ponytails: Synthesis, Transition Metal Chemistry (Ru(II), Rh(II), Pd(II), Pt(II)) and Crystal and Molecular Structures of Mononuclear (Pd(II), Rh(I)) and Bi- and Tetranuclear Rhodium(I) Complexes. *Inorg. Chem.* **2005**, *44*, 7925–7932.

52. Chandrasekaran, P.; Mague, J. T.; Balakrishna, M. S. Tetranuclear Rhodium(I) macrocycle Containing Cycodiphosphazane $[Rh_2(\mu\text{-}Cl)_2(CO)_2\{(^{t}BuNP(OC_6H_4OMe\text{-}o))_2\text{-}\kappa P\}_2]$ and Its Reversible Conversion into *trans*-$[Rh(CO)Cl\{(^{t}BuNP(OC_6H_4OMe\text{-}o))_2\text{-}\kappa P\}_2]$. *Organometallics* **2005**, *24*, 3780–3783.

53. Calera, S. G.; Wright, D. S. Macrocyclic Phosphazane Ligands. *Dalton Trans.* **2010**, *39*, 5055–5065.

54. Axenov, K. V.; Leskela, M.; Repo, T. Bis(imino)cyclodiphosph(V)azane Complexes of Late Transition Metals: Efficient Catalyst Precursors for Ethene and Propene Oligomerization and Dimerization. *J. Catal.* **2006**, *238*, 196–205.

55. Axenov, K. V.; Kilpelainen, I.; Klinga, M.; Leskela, M.; Repo, T. Titanium and Zirconium Benzyl Complexes Bearing Bulky Bis(amido)cyclodiphosph(III)azanes: Synthesis, Structure, Activation, and Ethene Polymerization Studies. *Organometallics* **2006**, *25*, 463–471.

56. Axenov, K. V.; Klinga, M.; Leskela, M.; Repo, T. Bis(amido)cyclodiphosph(III)azane Hafnium Complexes and Their Activation by Tris(perfluorophenyl)borane. *Organometallics* **2005**, *24*, 1336–1343.

57. Ananthnag, G. S.; Kuntavali, S.; Mague, J. T.; Balakrishna, M. S. Resorcinol Based Acyclic Dimeric and Cyclic Di-and Tetrameric Cyclodiphosphazanes: Synthesis, Structural Studies and Transtion Metal Complexes. *Inorg. Chem.* **2012**, *51*, 5919–5930.

58. Shi, Y. X.; Liang, R. Z.; Martin, K. A.; Star, D. G.; Li, Y.; Ganguly, R.; Sim, Y.; Tan, D.; Diaz, J.; Garcia, F. Synthesis of Unique Phosphazane Macrocycles Via Steric Activation of C-N Bonds. *Inorg. Chem.* **2018**, *57*, 10993–11004.

59. Schranz, I.; Stahl, L. Synthesis of Group 14 Bis(*tert*-butylamido)cyclodiphosph(III)azane Dichlorides, and the Solid-state Structures of the Silicon and Tin Derivatives. *Inorg. Chim. Acta* **2010**, *363*, 975–980.

60. Schranz, I.; Grocholl, L.; Carrow, C. J.; Stahl, L.; Staples, R. J. Heterocarbenoids of Germanium and Tin and Their Polyhedral Oxidation Products: The Case of

Thermodynamic Product Control in Group 14 Chalcogenides. *J. Organomet. Chem.* **2008**, *693*, 1081–1095.

61. Plajer, A. J.; Garcia, -R. R.; Benson, C. G. M.; Matthews, P. D.; Bond A. D.; Singh, S.; Gade, L. H.; Wright, D. S. A Modular Approach to Inorganic Phosphazane Macrocycles. *Angew. Chem. Int. Ed.* **2017**, *56*, 9087–9090

62. Niu, H.-C.; Plajer, A. J.; Garcia,-R. R.; Singh, S.; Wright, D. S., Designing the Macrocyclic Dimension in Main Group Chemistry. *Chem. Eur. J.* **2018**, *24*, 3073–3082.

63. Moser, D. F.; Grocholl, L.; Stahl, L.; Staples, R. J. Bis(*tert*-butylamido)- and Bis(arylamido)cyclodiphosph(III)azne Complexes of Ti, V, Zr, and Hf: Ligand Substituent Effects and Coordination Number. *Dalton Trans.* **2003**, 1402–1410.

64. Lief, G. R.; Carrow, C. J.; Stahl, L. Trispirocyclic Bis(dimethylaaluminum)bis(amido)cyclodiphosph(V)azanes. *Organometallics* **2001**, *20*, 1629–1635.

65. Grocholl, L.; Stahl, L.; Staples, R. J. Syntheses and Single-crystal X-ray Structures of $[(Bu^tNP)_2(^tBuN)_2]MCl_2$ (M = Zr, Hf): The First Transition Metal Bis(alkylamido)cyclodiphosphazane Complexes. *Chem. Commun.* **1997**, 1465–1466.

66. Briand, G. G., Chivers, T.; Krahn, M. Coordination Complexes of Bis(amido)cyclodiphosph(III/V and V/V)azane Imides and Chalcogenides. *Coord. Chem. Rev.* **2002**, *233–234*, 237–254.

67. Balakrishna, M. S.; Suresh, D.; Rai, A.; Mague, J. T.; Panda, D. Dinuclear Copper(I) Complexes Containing Cyclodiphosphazane Derivatives and Pyridyl Ligands: Synthesis, Structural Studies, and Antiproliferative Activity Toward Human Cervical and Breast Cancer Cells. *Inorg. Chem.* **2010**, *49*, 8790–8801.

68. Balakrishna, M. S.; Chandrasekaran, P.; Venkateswaran, R. Functionalized Cyclodiphosphazanes *cis*-[^{t}BuNP(OR)]$_2$ (R = C_6H_4OMe-o, CH_2CH_2OMe, CH_2CH_2SMe, $CH_2CH_2NMe_2$) as Neutral 2e, 4e, or 8e Donor Ligands. *J. Organomet. Chem.* **2007**, *692*, 2642–2648.

69. Balakrishna, M. S. Cyclodiphosphazane: options are endless. *Dalton Trans.* **2016**, *45* (31), 12252–12282.

70. Axenov, K. V.; Klinga, M.; Leskela, M.; Kotov, V.; Repo, T. [Bis(amido)cyclodiphosph(III)azane]dichlorozirconium Complexes for Ethene Polymerization. *Eur. J. Inorg. Chem.* **2004**, 4702–4709.

71. Nordheider, A.; Hull, K.; Prentis, J. K. D.; Arachchige, K. S. A.; Slawin, A. M. Z.; Woollins, J. D.; Chivers, T. Main Group Tellurium Heterocycles Anchored by a $P^{V}N_2$ Scaffold and their Sulfur/Selenium Analogues. *Inorg. Chem.* **2015**, *54*, 3043–3054.

72. Nordheider, A.; Hull, K.; Arachchige, K. S. A.; Slawin, A. M. Z.; Woollins, J. D.; Thirumoorthi, R.; Chivers, T. Spirocyclic, Macrocyclic and Ladder Complexes of Coinage metals and Mercury with Dichalcogeno P_2N_2-Supported Anions. *Dalton Trans.* **2015**, *44*, 5338–5346.

73. Nordheider, A.; Chivers, T.; Thirumoorthi, R.; Vargas-Baca, I.; Woollins, J. D.; Planar P_6E_6 (E = Se, S) Macrocycles Incorporating P_2N_2 Scaffolds. *Chem. Commun.* **2012**, *48*, 6346–6348.

74. Chivers, T.; Krahn, M.; Schatte, G. Syntheses and X-ray Structures of Potassium Derivatives and a Paramagnetic Nickel(II) Complex of a Cyclodiphosph(III/V)azane Monoselenide. *Inorg. Chem.* **2002**, *41*, 4348–4354.

75. Briand, G. G.; Chivers, T.; Parvez, M.; Schatte, G. Experimental and Theoretical Investigations of Lithium and Magnesium Derivatives of Bis(*tert*-butylamido)cyclodiphosph(III/V)- and (V/V)azane Mono- and Ditellurides. *Inorg. Chem.* **2003**, *42*, 525–531.

76. Nordheider, A.; Slawin, A. M. Z.; Woollins, J. D.; Chivers, T. A Silver(I) Iodide Complex of a Tellurophosphorane. *Anorg. Allg. Chem.* **2015**, *641(2)*, 405–407.

77. Rashid, A.; Ananthnag, G. S.; Naik, S.; Mague, J. T.; Panda, D.; Balakrishna, M. S. Dinuclear Cu^{I} Complexes of Pyridyl-diazadiphosphetidines and Aminobis(phosphonite) Ligands: Synthesis, Structural Studies, and Antiproliferative Activity Towards Human Cervical, Colon Carcinoma and Breast Cancer Cells. *Dalton Trans.* **2014**, *43*, 11339–11351.

78. Siddiqui, M. M.; Mobin, S. M.; Senkovska, I.; Balakrishna, M. S. Novel Zeotype Frameworks with Soft Cyclodiphosphazane Linkers and Soft Cu_4X_4 Clusters as Nodes. *Chem. Commun.* **2014**, *50*, 12273–12276.

79. Hinz, A.; Shulz, A.; Villinger, A. Stable Heterocyclopentane-1, 3-diyls. *Angew. Chem. Int. Ed.* **2015**, *54*, 2776–2779.

80. Hinz, A.; Schulz, A.; Villinger, A. Tunable Cyclopentane-1,3-diyls Generated by Insertion of Isonitriles into Diphosphadiazanediyls. *J. Am. Chem. Soc.* **2015**, *137*, 9953–9962.

81. Beweries, T.; Kuzora, R.; Rosenthal, U.; Schulz, A.; Villinger, A. $[P(\mu\text{-NTer})]_2$: A Biradicaloid That is Stable at High Temperature. *Angew. Chem. Int. Ed.* **2011**, *50*, 8974–8978.

82. Roth, T.; Vasilenko, V.; Benson, C. G. M.; Wadepohl, H.; Wright, D. S.; Gade, L. H. Extending *N*-Heterocyclic Carbene Ligands into The Third Dimension : A New Type of Hybrid Phosphazane/NHC System. *Chem. Sci.* **2015**, *6*, 2506–2510.

83. Roth, T.; Vasilenko, V.; Wadepohl, H.; Wright, D. S.; Gade, L. H. Structures, Electronics, and Reactivity of Strained Phosphazane Cages: A combined Experimental and Computational Study. *Inorg. Chem.* **2015**, *54*, 7636–7644.

84. Chen, H.-J.; Haltiwanger, R. C.; Hill, T. G.; Thompson, M. L.; Coons, D. E.; Norman, A. D. Synthesis and Structural Study of 2,4-Disubstituted 1,3-Diaryl-1,3,2,4-diazadiphosphetidines. *Inorg. Chem.* **1985**, *24*, 4725–4730.

85. Haagenson, D. C.; Moser, D. F.; Stahl, L.; Staples, R. J. Syntheses and Structures of P-Anilino-P-Chalcogeno-and P-Anilino-P-iminodiazasilaphosphetidines and Their Group 12 and 13 Metal Compounds. *Inorg. Chem.* **2002**, *41*, 1245–1253.

86. Haagenson, D. C.; Lief, G. R.; Stahl, L.; Staples, R. J. *N*-versus *O*-Silylation in *cis*-[(^{t}BuHN)O=P(μ-N^{t}Bu)$_2$P=O(NH^{t}Bu)] and [Me$_2$Si(μ-N^{t}Bu)$_2$P=O(NHPh)]. Solid-State Structures of Their Silylation Products, of Co-Crystalline cis-[(^{t}BuHN)O=P(μ-N^{t}Bu)$_2$P=O(NH^{t}Bu)], and of {[Me$_2$Si(μ-N^{t}Bu)$_2$P=O(N(SiMe$_3$)Ph)]VCl$_3$}. *J. Organomet. Chem.* **2008**, *693*, 2748–2754.

87. Chivers, T.; Fedorchuk, C.; Krahn, M.; Parvez, M.; Schatte, G. Preparation and X-ray Structures of Cu(I), Ni(II), and Pd(II) (N,S) Complexes of the Monoanion [(^{t}BuN)(S)P(μ-N^{t}Bu)$_2$P(S)(NH^{t}Bu)]$^-$ and a Pt(II) (S,S') Complex of the Dianion [(^{t}BuN)(S)P(μ-N^{t}Bu)$_2$P(S)(N^{t}Bu)]$^{2-}$. *Inorg. Chem.* **2001**, *40*, 1936–1942.

88. Briand, G. G.; Chivers, T.; Schatte, G. Redox Chemistry of Tellurium Bis(*tert*-butylamido)cyclodiphosph(V)azane Disufide and Diselenide Systems: A Spectroscopic and Structural Study. *Inorg. Chem.* **2002**, *41*, 1958–1965.

89. Keat, R.; Rycroft, D. S.; Thompson, D. G. *J. Chem. Soc., Daltons Trans.* **1979**, 1224–1230.

90. Hill, T. G.; Haltiwanger, R. C.; Thompson, M. L.; Katz, S. A.; Norman, A. D. *Cis*/*Trans* Isomerization and Conformational Properties of 2,4-Bis(primary amino)-1,3,2,4-Diazadiphosphetidines. *Inorg. Chem.* **1994**, *33*, 1770–1777.

91. Hursthouse, M. B.; Parkes, H. G.; Shaw, L. S.; Shaw, R. A.; Watkins, D. A. *Phosphorus, Sulfur, Rel. Elts.* **1986**, *28*, 221–227.

92. Moser, D. F.; Schranz, I.; Gerrety, M. C.; Stahl, L.; Staples, R. J. *J. Chem. Soc. Dalton Trans.* **1999**, 751–757.

93. Otang, M. E.; Lief, G. R.; Stahl, L. Alkoxido-, Amido-, and Chlorido- Derivatives of Zirconium- and Hafnium Bis(amido)cyclodiphosph(V)azanes: Ligand Ambidenticity and Catalytic Productivity. *J. Organomet. chem.* **2016**, *820*, 98–110.

94. Linti, G.; Nöth, H.; Schneider, E.; Storch, W. Tetraaza-λ^3-diphospha-stanna-bicyclo[3.1.1]heptane: Reaktive Vorstufen Neuer Heterobicyclen. *Chem. Ber.* **1993**, *126*, 619–629.

95. Axenov, K. V.; Kotov, V. V.; Klinga, M.; Leskela, M.; Repo, T. New bulky Bis(amido)cyclodiphosph(III)azanes and Their Titanium Complexes: Synthesis, Structures, and Ethene Polymerization Studies. *Eur. J. Inorg. Chem.* **2004**, 695–706.

96. Bashall, A.; Bond, D. A.; Doyle, L. E.; Garcia, F.; Kidd, S.; Lawson, T. G.; Parry, C. M.; McPartlin, M.; Woods, D. A.; Wright, S. D. Templating and Selection in the Formation of

Macrocycles Containing [{P(μ-N^{t}Bu)$_2$}(μ-NH)]$_n$ Frameworks: Observation of Halide Ion Coordination. *Chem. Eur. J.* **2002**, *8*, 3377–3385.

97. Gonzalez, -C. S.; Eisler, D. J.; Morey, J. V.; McPartlin, M.; Singh, S.; Wright, D. S. The Selenium-Bsed Hexameric Macrocycle [(Se=)P(μ-N^{t}Bu)$_2$P(μ-Se)]$_6$. *Angew. Chem. Int. Ed.* **2008**, *47*, 1111–1114.

98. Schranz, I.; Grocholl, L.; Stahl, L. Syntheses and Structures of Heterobicyclic Bis(*tert*-butylamido)cyclodiphosph(III)azane Compounds Having Phosphorus(III) and Arsenic(III) Centers. *Inorg. Chem.* **2000**, *39*, 3037–3041.

99. Otang, M. E. Syntheses and Characterization of Bis(amino)cyclodiphosphazane Complexes of Group 4 and 15 Elements, Dissertation. **2015**.

100. Shi, Y. X.; Liang, R. Z.; Martin, K. A.; Star, D. G.; Li, Y.; Ganguly, R.; Sim, Y.; Tan, D.; Diaz, J.; Garcia, F. Synthesis of Unique phosphazane Macrocycles via Steric Activation of C-N Bonds. *Inorg. Chem.* **2018**, *57*, 10993–11004.

101. Shi, Y. X.; Liang, R. Z.; Martin, K. A.; Star, D. G.; Li, Y.; Ganguly, R.; Sim, Y.; Tan, D.; Diaz, J.; Garcia, F. Steric C-N Bond Activation on The Dimeric Macrocycle, [{P(μ-N^{t}Bu)}$_2$(μ-NR)]$_2$. *Chem. Commun.* **2015**, *51*, 16468–16471.

102. Schranz, I.; Lief, G. R.; Carrow, C. J.; Haagenson, D. C.; Grocholl, L.; Stahl, L.; Staples, R. J.; Boomishankar, R.; Steiner, A. Reversal of Polarization in Amidophosphines: Neutral- and Anionic-κ*P* Coordination vs. Anionic-κ*P*, N Coordination and The Formation of Nickelaazaphosphiranes. *Dalton Trans.* **2005**, 3307–3318.

103. Moser, D. F.; Schranz, I.; Gerrety, M. C.; Stahl, L.; Staples, R. J. Polycyclic Bis(amido)cyclodiphosphazane Complexes of Antimony(III) and Bismuth(III): Syntheses, Molecular Structures and Solution Behaviour. *J. Chem. Soc., Dalton Trans.* **1999**, 751–757.

104. SMART Version 4.053, Siemens Analytical X-ray Systems. Madison, WI, **1995**.

105. Sheldrick, G. M. *Acta. Cryst.* **2008**, (A64), 112–122.

106. SADABS Program for Absorption Corrections Using the Bruker CCD Detector System. Based on: Blessing, R. H. *Acta Cryst. C.* **1995**, *A51*, 33–38.

107. Sheldrick, G. M., SHELXS-90, Program for the Solution of Crystal Structures. University of Göttingen, Göttingen, Germany, **1990**.

108. SHELXTL 5.10 (PC-Version), Siemens Analytical X-Ray Instruments, Inc. Madison, WI, **1998**.

109. SHELXTL NT Version 5.10, Program Library for Structure Solution and Molecular Graphics, Bruker Analytical X-ray Systems. Madison, WI, **1999**.

110. Bruker, Apex3 V 2016.9-0, Saint V8.34A, SAINTV8.37A, Bruker AXS Inc. Madison, WI, USA, **2016**.

111. SHELXTL, Suite of programs, Version 6.14, Bruker Advanced X-ray Solutions, Bruker AXS Inc., Madison, WI, USA, **2000–2003**.

112. Sheldrick, G. M., Crystal Structure Refinement with SHELXL. *Acta Cryst. Sec C Struct. Chem.* **2015**, *71(1)*, 3–8.

113. Sheldrick, M. G. SHELXS-2018, Program for the Solution of Crystal Structures. University of Göttingen, Göttingen, Germany, **2018**.

114. Hubschle, C. B.; Sheldrick, G. M.; Dittrich, B. ShelXle: A Qt Graphical User Interface for SHELXL. *J. Appl. Crystallogr.* **2011**, *44(6)*, 1281–1284.

115. Pyykko, P. Additive Covalent Radii for Single-, Double-, and Triple-Bonded Molecules and Tetrahedrally Bonded Crystals: A Summary. *J. Phys. Chem. A* **2015**, *119*, 2326–2337.

116. Hinz, A.; Goicoechea, J. M. The 2-Arsaethynolate Anion: Synthesis and Reactivity. *Angew. Chem.* **2016**, *128*, 8678–8683.

117. Tamm, M.; Doddi, A.; Bockfeld, D.; Zaretzke, M. -K.; Bannenberg, T. Isolation of Carbene-Stabilized Arsenic Monophosphide [AsP] and Its Radical Cation $[AsP]^{+}$ and Dication $[AsP]^{2+}$. *Chem. Eur. J.* **2019**, *25*, 13119–13123.

118. Gupta, A. K.; Green, J. P.; Orthaber, A. Rearrangements and Redistribution Reaction of Ph_2PCH_2TMS with $PhAsCl_2$ or $AsCl_3$. *Phosphorus, Sulfur, and Silicon and the Rel. Elts.* **2019**, 1563–5325.

119. Dori, Z.; Zoilo, R. The Chemistry of Coordinated Azides. *Chem. Rev.* **1972**, *73*, 247–254.

120. Schulz, J.; Cisarova, I.; Stepnicka, P. Phosphinoferrocene Amidosulfonates: Synthesis, Palladium Complexes, and Catalytic Use in Pd-Catalyzed Cyanation Of Arylbromides in an Aqueous Reaction Medium. *Organometallics* **2012**, *31*, 729–738.

121. Schulz, S.; Lyhs, B.; Jansen, G.; Blaser, D.; Wolper, C. Syntheses and Structures of Triazides of Heavy Group 15 Elements. *Chem. Commun.* **2011**, *47*, 3401–3403.

122. Palenik, R. C.; Abboud, K. A.; Palenik, G. J. Bond Valence Sums and Structural Studies of Antimony Complexes Containing Sb Bonded only to O Ligands. *Inorg. Chim. Acta* **2005**, *358*, 1034–1040.

123. Lance, E. T.; Haschke, J. M.; Peacor, D. R. Crystal and Molecular Structure of Phosphorus Triiodide. *Inorg. Chem.* **1976**, *15*, 780–781.

124. Xu, Y.; Huang, J.; Gabidullin, B.; Bryce, D. L. A Rare Example of Phosphine as a Halogen Bond Acceptor. *Chem. Commun.* **2018**, *54*, 11041–11043.

125. Ozturk, I. I.; Yarar, S.; Gurgan, M.; Ceyhan, D.; Banti, C. N.; Hadjikakou, S. K.; Manoli, M.; Moushi, E.; Tasiopoulos, A. J. Synthesis, Characterization and Biological Evaluation

of Novel Antimony(III) Iodide Complexes with Tetramethylthiourea and *N*-Ethylthiourea. *Inorg. Chim. Acta* **2019**, *491*, 14–24.

126. Housecroft, C. E.; Sharpe, A. G. *Inorganic Chemistry*. 3rd ed.; Prentice Hall: Pearson Educational Limited, **2008**.

127. Kerr, J. A. *Chem. Rev.* **1966**, *66*, 465.

128. Darwent, B. D. National Standard Reference Data Series. In *National Bureau of Standards*, Washington, **1970**.

129. Cottrell, T. L. *The Strengths of Chemical Bonds*. 2nd ed.; Butterworth: London, **1958**.

130. Benson, S. W. *J. Chem. Educ.* **1965**, *42*, 502.

131. Keat, R.; Thompson, D. G. *J. Chem. Soc. Dalton Trans* **1980**, 928.

132. Chang, C.-C.; Haltiwanger, R. C.; Thompson, M. L.; Chen, H.-J.; Norman, A. D. Structural Characterization of *trans*-2,4-Dithio-2,4-dianilino-1,3-diphenyl-1,3,2,4-diazadiphosphetidine, $[(C_6H_5NH)P(S)NC_6H_5]_2$. *Inorg. Chem.* **1979**, *18(7)*, 1899–1904.

133. Swidan, A.; Suter, R.; Macdonald, C. L. B.; Burford, N. Tris(benzoimidazol)amine(L) Complexes of Pnictogen(III) and Pnictogen(V) Cations and Assessment of the $[LP]^{3+}/[LPF_2]^{3+}$. *Chem. Sci.* **2018**, *9*, 5837–5841.

134. Kooijman, H.; Spek, A. L.; Bommel, K. J. C.; Verboom, W.; Reinhoudt, D. N. *Acta Cryst. C.* **1996**, *54*, 1695–1698.

135. Kilian, P.; Pazdera, P.; Marek, J.; Novosad, J.; Touzin, J. New Heterocyclic Organophosphorus-Sulfur-Nitrogen Compounds, Syntheses and Structures. *Z. anorg. allg. Chem.* **1998**, *624*, 1497–1502.

136. Kadish, K. M.; Autret, M.; Ou, Z.; Akiba, K.-Y.; Masumoto, S.; Wada, R.; Yamamoto, Y. *Inorg. Chem.* **1996**, *35*, 3564–3569.